

Computational approaches to dissect immunotherapy response in breast cancer

Isaeva, O.

DOI

[10.4233/uuid:d3c9c56b-ccc5-4cd6-9052-d5b75bfc40b1](https://doi.org/10.4233/uuid:d3c9c56b-ccc5-4cd6-9052-d5b75bfc40b1)

Publication date

2025

Document Version

Final published version

Citation (APA)

Isaeva, O. (2025). *Computational approaches to dissect immunotherapy response in breast cancer*. [Dissertation (TU Delft), Delft University of Technology]. PrintSupport4U. <https://doi.org/10.4233/uuid:d3c9c56b-ccc5-4cd6-9052-d5b75bfc40b1>

Important note

To cite this publication, please use the final published version (if applicable).
Please check the document version above.

Copyright

Other than for strictly personal use, it is not permitted to download, forward or distribute the text or part of it, without the consent of the author(s) and/or copyright holder(s), unless the work is under an open content license such as Creative Commons.

Takedown policy

Please contact us and provide details if you believe this document breaches copyrights.
We will remove access to the work immediately and investigate your claim.

Computational approaches to dissect immunotherapy response in breast cancer

Isaeva, O.

Publication date
2025


Document Version
Final published version

Citation (APA)
Isaeva, O. (2025). *Computational approaches to dissect immunotherapy response in breast cancer*. [Dissertation (TU Delft), Delft University of Technology]. PrintSupport4U.

Important note
To cite this publication, please use the final published version (if applicable).
Please check the document version above.

Copyright
Other than for strictly personal use, it is not permitted to download, forward or distribute the text or part of it, without the consent of the author(s) and/or copyright holder(s), unless the work is under an open content license such as Creative Commons.

Takedown policy
Please contact us and provide details if you believe this document breaches copyrights.
We will remove access to the work immediately and investigate your claim.

A watercolor illustration of a hedgehog looking up at a butterfly. The hedgehog is on the left, its body covered in dark, spiky quills. It has a light-colored face with small eyes and a small nose. A butterfly with white wings and black spots is flying in front of it. The background is a textured, light-colored wash with some dark, vertical lines suggesting grass or reeds on the right side.

Computational approaches to dissect immunotherapy response in breast cancer

**Computational
approaches
to dissect
immunotherapy
response
in breast cancer**

*Public Doctoral
Thesis Defense*

10 November 2025

12:30

Senaatszaal Aula
Delft University
of Technology

At 12:00 there would
be a short
presentation
about my
dissertation.

Olga Igorevna
Isaeva

Computational approaches to dissect immunotherapy response in breast cancer

Computational approaches to dissect immunotherapy response in breast cancer

Dissertation

for the purpose of obtaining the degree of doctor

at Delft University of Technology

by the authority of the Rector Magnificus,

Prof.Dr.Ir T.H.J.J. van der Hagen,

chair of the Board for Doctorates

to be defended publicly on

Monday 10 November 2025 at 12:30 o'clock

by

Olga Igorevna ISAEVA

Master of Science in Biotechnology, Skolkovo Institute of Science and
Technology, Moscow

born in Khimki, Russia.

This dissertation has been approved by the promotor.

Composition of the doctoral committee:

Rector Magnificus	chairperson
Prof. dr. L.F.A. Wessels	Delft University of Technology, <i>promotor</i>
Dr. M. Kok	Netherlands Cancer Institute, <i>copromotor</i>

Independent members:

Prof. dr. ir. M.J.T. Reinders	Delft University of Technology
Dr. H. Jacobs	Netherlands Cancer Institute
Prof. dr. ir. M.K. Schmidt	Leiden University
Prof. dr. C.L. Zuur	Leiden University Medical Center
Dr. D. S. Thommen	Netherlands Cancer Institute

Reserve members:

Prof. dr. ir. B. Rieger	Delft University of Technology
-------------------------	--------------------------------

Dr. Pia Kvistborg has contributed substantially to the research described in this dissertation.



Keywords: cancer, breast cancer, TNBC, immunotherapy, checkpoint blockade, clinical trials, biomarkers, tumor microenvironment, bioinformatics, RNA-Seq, ctDNA, SARS-CoV-2

Cover art by: Alexander Hazen, Serhii Volosheniuk

Layout by: Serhii Volosheniuk, Olga Isaeva

Copyright © 2025 by O.I. Isaeva

ISBN: 9789463848534

An electronic copy of this dissertation is available at

<https://repository.tudelft.nl/>.

*To all women and girls who did not have the opportunity to obtain the
level of education they would want.*

Contents

Summary	ix
Samenvatting	xi
1 Introduction	1
1.1 Part 1. COVID-19 & SARS-CoV-2	2
1.2 Part 2. Breast cancer	2
1.3 Immunotherapy	3
1.4 High-throughput sequencing in cancer immunotherapy . . .	4
1.5 Thesis outline	5
Part 1	
2 In silico analysis predicts a limited impact of SARS-CoV-2 variants on CD8 T cell recognition	11
2.1 Introduction	13
2.2 Results	16
2.3 Discussion	24
2.4 Materials and Methods	26
2.5 Author Contributions	28
2.6 Funding	28
2.7 Conflict of Interest	28
2.8 Data Availability Statement	28
2.9 Supplementary Information	28
Part 2	
3 PD-L1 blockade in combination with carboplatin as immune induction in metastatic lobular breast cancer: the GELATO trial	39
3.1 Introduction	42
3.2 Results	43
3.3 Discussion	53
3.4 Methods	57
3.5 Data availability	65
3.6 Acknowledgments	65
3.7 Author Contributions	66
3.8 Competing Interests	66
3.9 Supplementary Information	67

4	ctDNA-based copy number dynamics during anti-PD-1 treatment in metastatic triple negative breast cancer	91
4.1	Introduction	93
4.2	Results	94
4.3	Discussion	97
4.4	Methods	100
4.5	Acknowledgements	103
4.6	Author contributions	103
4.7	Declaration of interests	103
4.8	Supplementary Information	104
5	Neoadjuvant nivolumab or nivolumab plus ipilimumab in early-stage triple negative breast cancer: a phase 2 adaptive BELLINI trial	117
5.1	Introduction	120
5.2	Results	121
5.3	Discussion	132
5.4	Methods	137
5.5	Data availability	147
5.6	Acknowledgements	147
5.7	Author Contributions	148
5.8	Competing interests	149
5.9	Supplementary Information	150
6	Discussion	171
6.1	Breast cancer immunotherapy: successes and challenges	173
6.2	Biomarkers for breast cancer immunotherapy	173
6.3	Combining treatments for breast cancer immunotherapy	175
6.4	Treating particular breast cancer patient populations	176
6.5	Limitations of the studies presented in the thesis	178
6.6	Improving biomarkers in breast cancer	179
6.7	Outlook	180
	Curriculum Vitæ	189
	List of Publications	191
	Acknowledgements	195

Summary

This thesis is dedicated to applications of high-throughput sequencing data analysis in immunology. Initially, the project included the part focusing on the T cell biology in the context of cancer, supervised by Dr. Pia Kvistborg, and the part focusing on the translational analysis of the breast cancer clinical trials, supervised by Dr. Marleen Kok, both under the general supervision of Dr. Lodewyk Wessels. Because of the COVID-19 pandemic, Part 1 of this work focused instead on the T cell functionality in the context of COVID-19. As Dr. Kvistborg resigned in 2022, the larger part of the thesis, Part 2, was completed under the supervision of Dr. Kok and Dr. Wessels, the copromotor and promotor of this work.

Thus, this thesis describes bioinformatics approaches to the translational studies in immunology in the context of COVID-19 disease and breast cancer. We demonstrate that the use of genomic and transcriptomic data, including whole-exome and shallow whole-genome DNA sequencing and single-cell and bulk RNA sequencing, allows us to make conclusions about the underlying biology of the disease and identify biomarkers related to disease outcomes and response to treatment.

In particular, in **Chapter 2** we used the publicly available SARS-CoV-2 genomic data and determined that vaccination or infection by the original SARS-CoV-2 strain is likely to provide sufficient T cell protection against novel SARS-CoV-2 variants most prevalent until early 2022.

In **Chapter 3**, we explored the tumor microenvironment of metastatic lobular breast tumors upon anti-PDL1 blockade in combination with carboplatin in the context of the GELATO trial. We described an increase in T cell infiltration and checkpoint molecule upon treatment which indicated the biological activity of the treatment, even though only a subset of patients reached a clinical response.

In **Chapter 4**, we demonstrated that it is possible to use a ctDNA-based copy number alteration score to predict responses to checkpoint blockade treatment in metastatic triple-negative breast cancer.

Finally, in **Chapter 5**, we analysed the biology of the tumor microenvironment in early triple-negative breast cancer upon treatment with anti-PD1 +/- anti-CTLA4 checkpoint blockade in context of the BELLINI trial. We showed that the tumor microenvironment of responders to checkpoint blockade is more inflamed both before and after therapy, and that

responders have higher fractions of pre-existing tumor-reactive CD8+ T cells than non-responders.

Samenvatting

Dit proefschrift is gewijd aan toepassingen van high-throughput sequencing data-analyse in immunologie. Aanvankelijk omvatte het project een deel gericht op de T-celbiologie in de context van kanker, onder supervisie van Dr. Pia Kvistborg, en een deel gericht op de translationele analyse van klinische studies naar borstkanker, onder supervisie van Dr. Marleen Kok, beide onder algemene supervisie van Dr. Lodewyk Wessels. Vanwege de COVID-19-pandemie richtte deel 1 van dit werk zich in plaats daarvan op de functionaliteit van T-cellen in de context van COVID-19. Toen Dr. Kvistborg in 2022 aftrad, werd het grootste deel van het proefschrift, deel 2, voltooid onder supervisie van Dr. Kok en Dr. Wessels, de copromotor en promotor van dit werk.

Dit proefschrift beschrijft dus bioinformatica-benaderingen voor translationele studies in de immunologie in de context van COVID-19 en borstkanker. Wij tonen aan dat we met behulp van genomische en transcriptoomgegevens, waaronder DNA-sequenties van het hele exoom en ondiepe genoom, en sequenties van individuele cellen en bulk-RNA, conclusies kunnen trekken over de onderliggende biologie van de ziekte en biomarkers kunnen identificeren die verband houden met de uitkomsten van de ziekte en de reactie op behandeling.

In het bijzonder hebben we in **Hoofdstuk 2** de openbaar beschikbare SARS-CoV-2-genomische gegevens gebruikt en vastgesteld dat vaccinatie of infectie door de oorspronkelijke SARS-CoV-2-stam waarschijnlijk voldoende T-celbescherming biedt tegen nieuwe SARS-CoV-2-varianten die het meest voorkomen tot begin 2022.

In **Hoofdstuk 3** hebben we de tumormicro-omgeving van gemetastaseerde lobulaire borsttumoren onderzocht bij anti-PDL1-blokkade in combinatie met carboplatine in de context van de GELATO-studie. We beschreven een toename in T-celinfiltratie en checkpointmolecuul na behandeling, wat de biologische activiteit van de behandeling aangaf, ook al bereikte slechts een subgroep van patiënten een klinische respons.

In **Hoofdstuk 4** hebben we aangetoond dat het mogelijk is om een op ctDNA gebaseerde kopie-aantal-alteratiescore te gebruiken om responsen op checkpointblokkadebehandeling bij gemetastaseerde triple-negatieve borstkanker te voorspellen.

Tot slot hebben we in **Hoofdstuk 5** de biologie van de tumormicro-

omgeving bij vroege triple-negatieve borstkanker geanalyseerd na behandeling met anti-PD1 +/- anti-CTLA4 checkpointblokkade in de context van de BELLINI-studie. We hebben aangetoond dat de tumormicro-omgeving van respondenten op checkpointblokkade zowel voor als na de therapie meer ontstoken is, en dat respondenten hogere fracties van reeds bestaande tumorreactieve CD8+ T-cellen hebben dan niet-respondenten.

1

Introduction

1.1. Part 1. COVID-19 & SARS-CoV-2

C OVID-19 pandemic was a global healthcare emergency caused by SARS-CoV-2 virus [1]. It was officially recognized as a pandemic on March 11, 2020, and continued to be recognized as a public health emergency of international concern until May 5, 2023 [2]. It caused more than 775 million cases and 7 million deaths [3]. Unprecedented international efforts directed to the development of a SARS-CoV-2 vaccine allowed for fast development of vaccines [4] which became available for the general public in 2021 [5]. SARS-CoV-2 vaccines were highly effective in preventing critical disease and death [6], and have been estimated to prevent at least 14 million deaths [5].

SARS-CoV-2, the pathogen that caused the pandemic, is a coronavirus, a member of the group of RNA-based viruses [7]. It consists of a lipid membrane encapsulating the membrane (M), envelope (E) and spike (S) proteins [8]. The spike protein is particularly relevant as it is involved in interaction with the host cells enabling infection of the host [9]. SARS-CoV-2 vaccines have mostly targeted spike protein epitopes, as spike protein tends to be quite conserved during the SARS-CoV-2 evolution [10]. Several thousands of SARS-CoV-2 variants have been described, however, some of them (e.g. Alpha, Beta, Gamma, Delta, Omicron, etc) had particular epidemiological significance [11]. Since these variants differed from the original SARS-CoV-2 variant that many people have been infected with and that had been used for the vaccine development, it was important to investigate whether immune protection offered by prior infection or vaccination persisted for infections with these later variants.

1.2. Part 2. Breast cancer

Cancer is a major cause of death worldwide [12]. It is frequently associated with a challenging and painful end of life [13], and it is getting increasingly common [14]: as a British study put it, “more common than marriage” [15]. We all know people who have cancer, and the majority of us will also get cancer during our lifetime [16]. Therefore, it is crucially important to learn more about cancer biology to allow for better treatments and outcomes.

Breast cancer is the most common type of cancer diagnosed in the world [17]. The patient prognosis depends on the disease stage at diagnosis and on the disease subtype [18]. These subtypes may be differentiated by the expression status of the estrogen and progesterone receptors and the expression and amplification of the HER2 receptor. Tumors that are negative for all three receptors are

assigned to the triple-negative breast cancer subtype (TNBC) [19]. Molecular subtypes of breast cancer also have different prognosis and are treated differently. TNBC has a particularly challenging prognosis at the metastatic stage, with median overall survival in the metastatic setting being approximately 1-1,5 years [20], highlighting the high need for improving the treatment landscape for TNBC tumors.

The heterogeneity explained by the molecular subtypes of breast cancer does not cover the whole heterogeneity of breast tumors. Breast tumors can be also divided in histological subtypes, with most cases belonging to the ductal subtype and lobular being the second most common histological breast cancer subtype. It accounts for 10-15% of all breast cancer cases and has distinct morphology and prognosis [21]. In 85-95% of cases, lobular breast cancer is associated with the loss of E cadherin expression, which drives the discohesive morphology of the disease [22]. The distinct biology associated with special histological breast cancer subtypes makes it important to include histology of the tumor into consideration when developing treatment regimens.

In breast cancer, as well as in other malignancies, tumors are comprised not only of transformed cells, but also of the components of the tumor microenvironment: immune cells, stromal cells, intracellular matrix, blood and lymphatic vessels, etc [23]. The tumor microenvironment composition and activity is important for the development and prognosis of the disease [24]. The transformed cells employ different strategies to reprogram the components of the tumor microenvironment to a “pro-tumor” state, in which they would functionally support the tumor and prevent its recognition and destruction by the immune system [25].

1.3. Immunotherapy

In the last decade, immunotherapy changed the treatment landscape of many cancers [26], including metastatic TNBC [27]. This form of treatment is working through activating the patient’s own immune system to fight cancer, and it can lead to profound and durable responses [28]. Immunotherapy generally influences the tumor microenvironment, facilitating its reprogramming to an “anti-tumor” state. However, not all patients respond to these therapies, which understrikes the importance of better understanding of the tumor biology [29].

One of the ways employed by the transformed cells to avoid immune responses is expression of immune checkpoint ligands on the cell surface [30]. These molecules can bind to the immune checkpoint receptors on the surface of T cells, and this interaction prevents T cells

from destroying the cells expressing the ligands. Some of the most common immunotherapies are immune checkpoint inhibitors that inhibit interaction between immune checkpoint molecules on the surface of T cells and their partner proteins on the surface of tumor cells and components of the tumor microenvironment [28]. They lead to profound and durable responses in some patients across a range of malignancies [31].

Monoclonal antibodies against PD1 and PDL1 are among the most commonly used checkpoint inhibitors [32]. Anti-PD1 therapy was approved by the FDA for all microsatellite instability-high (MSI-H) or mismatch repair deficient (dMMR) solid tumors [33], which was a remarkable change in FDA practices, previously focused on making recommendations within cancer types. It is also widely used in treatment of multiple early and metastatic cancers without mismatch repair deficiency, including early and metastatic TNBC [31]. These therapies work through removing the tolerance induced by the interaction between PD1 receptor on T cells and PDL1 ligand on the tumor surface and reinstates the ability of T cells to recognize and kill tumor cells [28].

Anti-PD1 checkpoint blockade in combination with chemotherapy is the standard of care for PDL1+ metastatic TNBC [34]. For early, stage II/III, TNBC, anti-PD1 in combination with neoadjuvant chemotherapy was approved by FDA and EMA and is currently the standard of care in the Netherlands [35].

Other immune checkpoint-targeting therapies include monoclonal antibodies against CTLA4, LAG3, and other molecules such as VISTA and TIM3 [28]. Anti-CTLA4 therapy is approved for use in combination with anti-PD1/anti-PDL1 in metastatic melanoma, non-small cell lung cancer, hepatocellular carcinoma and other malignancies [36].

1.4. High-throughput sequencing in cancer immunotherapy

In the last decade, the development of high-throughput sequencing technologies allowed the use of DNA and RNA sequencing data in translational research and in clinical trials [37]. New technologies, such as single-cell RNA sequencing or spatial transcriptomics, allow the study of the tumor microenvironment on single-cell resolution [38]. Liquid biopsy technologies, such as analysis of circulating tumor DNA, are also a powerful innovation that allows to gain insights into the real-time biology of the tumor without performing an invasive traditional biopsy [39].

As many patients still do not respond to modern immunotherapy regimens, it becomes attractive to leverage the data generated by high-throughput sequencing methods in clinical and translational research [40]. It requires a multidisciplinary team effort, with clinicians joining forces with bioinformaticians and wet lab scientists.

In this thesis, we will demonstrate how using high-throughput sequencing data such as bulk and single-cell RNA-Seq, whole exome sequencing and shallow whole genome sequencing can provide insights into which patients could benefit from immune checkpoint blockade in breast cancer. Additionally, the skills and technologies acquired for cancer research may be directed to other needs if necessary. In particular, during the COVID-19 pandemic, the bioinformatic skills of the author were leveraged to gain understanding of the degree of protection offered by SARS-CoV-2 infection or vaccination in case of infection by new variants of the virus.

1.5. Thesis outline

We will start this thesis with exploring the ability of different SARS-CoV-2 variants to escape memory CD8 T cell responses raised by vaccination or prior infection with SARS-CoV-2 early in the pandemic in **Chapter 2**. For this chapter, O.I. Isaeva shared the first authorship in the manuscript with S.L.C. Ketelaars. O.I. Isaeva and S.L.C. Ketelaars performed the experiments, analyzed the data and wrote the manuscript together.

In **Chapter 3**, we will discuss the effects of PD-L1 blockade in combination with carboplatin as immune induction in metastatic lobular breast cancer in the context of the GELATO clinical trial. For this chapter, O.I. Isaeva shared the first authorship in the manuscript with L. Voorwerk. O.I. Isaeva was the leading bioinformatician in the study and performed and interpreted computational analyses of the DNA and RNA sequencing data.

In **Chapter 4**, we will discuss the use of circulating tumor DNA-based copy number dynamics during anti-PD-1 treatment in metastatic triple negative breast cancer. For this chapter, O.I. Isaeva shared the first authorship in the manuscript with A.Y. Lin and conceptualized the study together with M. Kok. O.I. Isaeva also supervised A.Y. Lin, and they performed and interpreted computational analyses and wrote the manuscript together.

In **Chapter 5**, we will proceed to the early TNBC setting and discuss the effects of neoadjuvant nivolumab or nivolumab plus ipilimumab treatment in early triple negative breast cancer with higher levels of tumor infiltrating lymphocytes in the context of the BELLINI trial. For

this chapter, O.I. Isaeva shared the first authorship in the manuscript with I. Nederlof. O.I. Isaeva was the leading bioinformatician in the study, designed, performed and interpreted computational analyses of the DNA, bulk and single-cell RNA sequencing data, analyzed and interpreted translational data and wrote the paper together with I. Nederlof and M. Kok.

References

- [1] C. A. Pollard, M. P. Morran, and A. L. Nestor-Kalinoski. “The COVID-19 pandemic: a global health crisis”. en. *Physiol. Genomics* 52.11 (Nov. 2020), pp. 549–557.
- [2] World Health Organization. *Director-General’s opening remarks at the media briefing – 5 May 2023*. <https://www.who.int/director-general/speeches/detail/who-director-general-s-opening-remarks-at-the-media-briefing---5-may-2023>. 2023.
- [3] World Health Organization. *COVID-19 epidemiological update – 15 July 2024*. <https://www.who.int/publications/m/item/covid-19-epidemiological-update-edition-169>. 2024.
- [4] V. P. Chavda, Q. Yao, L. K. Vora, V. Apostolopoulos, C. A. Patel, R. Bezbaruah, A. B. Patel, and Z.-S. Chen. “Fast-track development of vaccines for SARS-CoV-2: The shots that saved the world”. *Front. Immunol.* 13 (Oct. 2022), p. 961198.
- [5] O. J. Watson, G. Barnsley, J. Toor, A. B. Hogan, P. Winskill, and A. C. Ghani. “Global impact of the first year of COVID-19 vaccination: a mathematical modelling study”. *Lancet Infect. Dis.* 22.9 (Sept. 2022), pp. 1293–1302.
- [6] G. E. Calabrò, C. Pappalardo, F. D’Ambrosio, M. Vece, C. Lupi, A. Lontano, M. Di Russo, R. Ricciardi, and C. de Waure. “The impact of vaccination on COVID-19 burden of disease in the adult and elderly population: A systematic review of Italian evidence”. *Vaccines (Basel)* 11.5 (May 2023).
- [7] J. F.-W. Chan, S. Yuan, K.-H. Kok, K. K.-W. To, H. Chu, J. Yang, F. Xing, J. Liu, C. C.-Y. Yip, R. W.-S. Poon, H.-W. Tsoi, S. K.-F. Lo, K.-H. Chan, V. K.-M. Poon, W.-M. Chan, J. D. Ip, J.-P. Cai, V. C.-C. Cheng, H. Chen, C. K.-M. Hui, and K.-Y. Yuen. “A familial cluster of pneumonia associated with the 2019 novel coronavirus indicating person-to-person transmission: a study of a family cluster”. *Lancet* 395.10223 (Feb. 2020), pp. 514–523.
- [8] H. Yang and Z. Rao. “Structural biology of SARS-CoV-2 and implications for therapeutic development”. *Nat. Rev. Microbiol.* 19.11 (Nov. 2021), pp. 685–700.
- [9] Y. Huang, C. Yang, X.-F. Xu, W. Xu, and S.-W. Liu. “Structural and functional properties of SARS-CoV-2 spike protein: potential antiviral drug development for COVID-19”. *Acta Pharmacol. Sin.* 41.9 (Sept. 2020), pp. 1141–1149.

- [10] M. A. Islam. "A review of SARS-CoV-2 variants and vaccines: Viral properties, mutations, vaccine efficacy, and safety". *Infect. Med. (Beijing)* 2.4 (Dec. 2023), pp. 247–261.
- [11] W. T. Harvey, A. M. Carabelli, B. Jackson, R. K. Gupta, E. C. Thomson, E. M. Harrison, C. Ludden, R. Reeve, A. Rambaut, COVID-19 Genomics UK (COG-UK) Consortium, S. J. Peacock, and D. L. Robertson. "SARS-CoV-2 variants, spike mutations and immune escape". *Nat. Rev. Microbiol.* 19.7 (July 2021), pp. 409–424.
- [12] GBD 2015 Mortality and Causes of Death Collaborators. "Global, regional, and national life expectancy, all-cause mortality, and cause-specific mortality for 249 causes of death, 1980-2015: a systematic analysis for the Global Burden of Disease Study 2015". *Lancet* 388.10053 (Oct. 2016), pp. 1459–1544.
- [13] C. D. Ruijs, A. J. Kerkhof, G. van der Wal, and B. D. Onwuteaka-Philipsen. "The broad spectrum of unbearable suffering in end-of-life cancer studied in dutch primary care". *BMC Palliat. Care* 11.1 (Aug. 2012), p. 12.
- [14] W. You and M. Henneberg. "Cancer incidence increasing globally: The role of relaxed natural selection". *Evol. Appl.* 11.2 (Feb. 2018), pp. 140–152.
- [15] Macmillan press releases and statements. *Cancer diagnosis now as common a 'life milestone' as marriage or getting a degree*. <https://medium.com/macmillan-press-releases-and-statements/cancer-diagnosis-now-as-common-a-life-milestone-as-marriage-or-getting-a-degree-f145cd53ab94>. (2018).
- [16] A. S. Ahmad, N. Ormiston-Smith, and P. D. Sasieni. "Trends in the lifetime risk of developing cancer in Great Britain: comparison of risk for those born from 1930 to 1960". *Br. J. Cancer* 112.5 (Mar. 2015), pp. 943–947.
- [17] L. Wilkinson and T. Gathani. "Understanding breast cancer as a global health concern". *Br. J. Radiol.* 95.1130 (Feb. 2022), p. 20211033.
- [18] T. Zuo, H. Zeng, H. Li, S. Liu, L. Yang, C. Xia, R. Zheng, F. Ma, L. Liu, N. Wang, L. Xuan, and W. Chen. "The influence of stage at diagnosis and molecular subtype on breast cancer patient survival: a hospital-based multi-center study". *Chin. J. Cancer* 36.1 (Dec. 2017).
- [19] E. Orrantia-Borunda, P. Anchondo-Nuñez, L. E. Acuña-Aguilar, F. O. Gómez-Valles, and C. A. Ramírez-Valdespino. "Subtypes of Breast Cancer". *Breast Cancer*. Exon Publications, Aug. 2022, pp. 31–42.
- [20] F. Kassam, K. Enright, R. Dent, G. Dranitsaris, J. Myers, C. Flynn, M. Fralick, R. Kumar, and M. Clemons. "Survival outcomes for patients with metastatic triple-negative breast cancer: implications for clinical practice and trial design". *Clin. Breast Cancer* 9.1 (Feb. 2009), pp. 29–33.
- [21] J. A. Mouabbi, A. Hassan, B. Lim, G. N. Hortobagyi, D. Tripathy, and R. M. Layman. "Invasive lobular carcinoma: an understudied emergent subtype of breast cancer". *Breast Cancer Res. Treat.* 193.2 (June 2022), pp. 253–264.

- [22] E. A. Rakha, A. Patel, D. G. Powe, A. Benhasouna, A. R. Green, M. B. Lambros, J. S. Reis-Filho, and I. O. Ellis. "Clinical and biological significance of E-cadherin protein expression in invasive lobular carcinoma of the breast". *Am. J. Surg. Pathol.* 34.10 (Oct. 2010), pp. 1472–1479.
- [23] J. J. Li, J. Y. Tsang, and G. M. Tse. "Tumor microenvironment in breast cancer-updates on therapeutic implications and pathologic assessment". *Cancers (Basel)* 13.16 (Aug. 2021), p. 4233.
- [24] M. A. Domínguez-Cejudo, A. Gil-Torralvo, M. Cejuela, S. Molina-Pinelo, and J. Salvador Bofill. "Targeting the tumor microenvironment in breast cancer: Prognostic and predictive significance and therapeutic opportunities". *Int. J. Mol. Sci.* 24.23 (Nov. 2023).
- [25] K. E. de Visser and J. A. Joyce. "The evolving tumor microenvironment: From cancer initiation to metastatic outgrowth". *Cancer Cell* 41.3 (Mar. 2023), pp. 374–403.
- [26] C. Liu, M. Yang, D. Zhang, M. Chen, and D. Zhu. "Clinical cancer immunotherapy: Current progress and prospects". *Front. Immunol.* 13 (Oct. 2022), p. 961805.
- [27] C. Valenza, G. Rizzo, M. I. Passalacqua, L. Boldrini, C. Corti, D. Trapani, and G. Curigliano. "Evolving treatment landscape of immunotherapy in breast cancer: current issues and future perspectives". *Ther. Adv. Med. Oncol.* 15 (Jan. 2023), p. 17588359221146129.
- [28] A. D. Waldman, J. M. Fritz, and M. J. Lenardo. "A guide to cancer immunotherapy: from T cell basic science to clinical practice". *Nat. Rev. Immunol.* 20.11 (Nov. 2020), pp. 651–668.
- [29] P. Sharma, S. Hu-Lieskovan, J. A. Wargo, and A. Ribas. "Primary, adaptive, and acquired resistance to cancer immunotherapy". *Cell* 168.4 (Feb. 2017), pp. 707–723.
- [30] G. L. Beatty and W. L. Gladney. "Immune escape mechanisms as a guide for cancer immunotherapy". *Clin. Cancer Res.* 21.4 (Feb. 2015), pp. 687–692.
- [31] Y. Shiravand, F. Khodadadi, S. M. A. Kashani, S. R. Hosseini-Fard, S. Hosseini, H. Sadeghirad, R. Ladwa, K. O'Byrne, and A. Kulasinghe. "Immune checkpoint inhibitors in cancer therapy". *Curr. Oncol.* 29.5 (Apr. 2022), pp. 3044–3060.
- [32] S. Tan, C. W.-H. Zhang, and G. F. Gao. "Seeing is believing: anti-PD-1/PD-L1 monoclonal antibodies in action for checkpoint blockade tumor immunotherapy". *Signal Transduct. Target. Ther.* 1.1 (Nov. 2016).
- [33] U.S. Food and Drug Administration. *Office of the Commissioner. FDA approves first cancer treatment for any solid tumor with a specific genetic feature.* <https://www.fda.gov/news-events/press-announcements/fda-approves-first-cancer-treatment-any-solid-tumor-specific-genetic-feature>. (2020).

- [34] J. Cortes, D. W. Cescon, H. S. Rugo, Z. Nowecki, S.-A. Im, M. M. Yusof, C. Gallardo, O. Lipatov, C. H. Barrios, E. Holgado, H. Iwata, N. Masuda, M. T. Otero, E. Gokmen, S. Loi, Z. Guo, J. Zhao, G. Aktan, V. Karantza, P. Schmid, and KEYNOTE-355 Investigators. "Pembrolizumab plus chemotherapy versus placebo plus chemotherapy for previously untreated locally recurrent inoperable or metastatic triple-negative breast cancer (KEYNOTE-355): a randomised, placebo-controlled, double-blind, phase 3 clinical trial". *Lancet* 396.10265 (Dec. 2020), pp. 1817–1828.
- [35] P. Schmid, J. Cortes, L. Pusztai, H. McArthur, S. Kümmel, J. Bergh, C. Denkert, Y. H. Park, R. Hui, N. Harbeck, M. Takahashi, T. Foukakis, P. A. Fasching, F. Cardoso, M. Untch, L. Jia, V. Karantza, J. Zhao, G. Aktan, R. Dent, J. O'Shaughnessy, and KEYNOTE-522 Investigators. "Pembrolizumab for early triple-negative breast cancer". *N. Engl. J. Med.* 382.9 (Feb. 2020), pp. 810–821.
- [36] P. Saad and A. Kasi. "Ipilimumab". *StatPearls [Internet]*. Treasure Island (FL): StatPearls Publishing, (2023). url: <https://www.ncbi.nlm.nih.gov/books/NBK557795/>.
- [37] H. Satam, K. Joshi, U. Mangrolia, S. Waghoo, G. Zaidi, S. Rawool, R. P. Thakare, S. Banday, A. K. Mishra, G. Das, and S. K. Malonia. "Next-generation sequencing technology: Current trends and advancements". *Biology (Basel)* 12.7 (July 2023), p. 997.
- [38] S. Chen, Z. Zhou, Y. Li, Y. Du, and G. Chen. "Application of single-cell sequencing to the research of tumor microenvironment". *Front. Immunol.* 14 (Oct. 2023), p. 1285540.
- [39] G. Alexandrou, K.-T. Mantikas, R. Allsopp, C. A. Yapeter, M. Jahin, T. Melnick, S. Ali, R. C. Coombes, C. Toumazou, J. A. Shaw, and M. Kalofonou. "The evolution of affordable technologies in liquid biopsy diagnostics: The key to clinical implementation". *Cancers (Basel)* 15.22 (Nov. 2023), p. 5434.
- [40] G. Lightbody, V. Haberland, F. Browne, L. Taggart, H. Zheng, E. Parkes, and J. K. Blayney. "Review of applications of high-throughput sequencing in personalized medicine: barriers and facilitators of future progress in research and clinical application". *Brief. Bioinform.* 20.5 (Sept. 2019), pp. 1795–1811.

Part 1.

2

In silico analysis predicts a limited impact of SARS-CoV-2 variants on CD8 T cell recognition

Published in: *Frontiers in Immunology*, 13:891524, 2022.
DOI: 10.3389/fimmu.2022.891524

Olga I. Isaeva^{#1,2,3}, Steven Ketelaars^{#1}, Pia Kvistborg¹

[#]These authors have contributed equally to this work, share first authorship, and are listed in alphabetical order.

¹ Department of Molecular Oncology and Immunology, Netherlands Cancer Institute, Amsterdam, the Netherlands.

² Department of Tumor Biology and Immunology, Netherlands Cancer Institute, Amsterdam, the Netherlands.

³ Onco Institute, Utrecht, the Netherlands.

Since the start of the COVID-19 pandemic, mutations have led to the emergence of new SARS-CoV-2 variants, and some of these have become prominent or dominant variants of concern. This natural course of development can have an impact on how protective the previously naturally or vaccine induced immunity is. Therefore, it is crucial to understand whether and how variant specific mutations influence host immunity. To address this, we have investigated how mutations in the recent SARS-CoV-2 variants of interest and concern influence epitope sequence similarity, predicted binding affinity to HLA, and immunogenicity of previously reported SARS-CoV-2 CD8 T cell epitopes. Our data suggests that the vast majority of SARS-CoV-2 CD8 T cell recognized epitopes are not altered by variant specific mutations. Interestingly, for the CD8 T cell epitopes that are altered due to variant specific mutations, our analyses show there is a high degree

of sequence similarity between mutated and reference SARS-CoV-2 CD8 T cell epitopes. However, mutated epitopes, primarily derived from the spike protein, in SARS-CoV-2 variants Delta, AY.4.2 and Mu display reduced predicted binding affinity to their restriction element. These findings indicate that the recent SARS-CoV-2 variants of interest and concern have limited ability to escape memory CD8 T cell responses raised by vaccination or prior infection with SARS-CoV-2 early in the pandemic. The overall low impact of the mutations on CD8 T cell cross-recognition is in accordance with the notion that mutations in SARS-CoV-2 are primarily the result of receptor binding affinity and antibody selection pressures exerted on the spike protein, unrelated to T cell immunity.

2.1. Introduction

The COVID-19 pandemic caused by SARS-CoV-2 is having a global catastrophic impact on public health and social economy [1, 2]. SARS-CoV-2 was first identified in humans in late 2019 in Wuhan, China, and the outbreak was designated as a pandemic by the WHO on March 11th, 2020 [3, 4]. The early variant of SARS-CoV-2 (also known as lineage B or Wuhan-Hu-1; UniProt: UP000464024; Genome accession: MN908947) is hereafter referred to as 'reference SARS-CoV-2'.

SARS-CoV-2 is a single-stranded RNA virus characterized by an inherently high mutation rate, short replication time and high virion yield [5–8]. As the virus spreads, this leads to a high genetic diversity and allows the virus to evolve rapidly as a result of natural selection pressures, including those originating from the host immune system. Mutations accumulate over time and result in amino acid changes that decrease the antigenicity of immune targeted proteins. This gradual change in antigenicity of viral proteins, driven by selective immune pressure, is known as antigenic drift [9]. Antigenic drift allows viruses to continuously evade host immunity, facilitating recurrent viral outbreaks. In acute infectious disease, antigenic drift is primarily driven by antibody responses leading to selection of escape mutants [9]. In accordance with this, many of the amino acid changes in SARS-CoV-2 variants are located in the spike protein, the main target of neutralizing antibodies [10]. These antibodies form the only immune mechanism that is able to provide sterilizing immunity, preventing host cells from being infected. The rate of evolution of the SARS-CoV-2 spike protein is much higher than that of similar proteins in other known viruses that cause acute infectious disease in humans. For example, its rate of evolution is approximately 10-fold higher than the evolution rate of the influenza A hemagglutinin and neuraminidase proteins [9]. In addition, a large number of amino acid changes have accumulated in SARS-CoV-2 proteins that are not known antibody targets [11]. These amino acid changes may have conferred a fitness advantage to the virus unrelated to antibody immunity, as antigenic drift is primarily driven by antibody responses in acute viral infections [6, 9, 12, 13].

Even though T cells are unlikely to be a main source to antigenic drift, there is ample evidence for the importance of these cells in protection against severe and critical COVID-19 and re-infections: 1) Depletion of CD8 T cells led to impaired clearance of SARS-CoV-2 in a COVID-19 mouse model [14] and breakthrough infections in a rhesus macaque model upon rechallenge; 2) Lower baseline peripheral blood CD8 T cell counts have been shown to correlate with decreased patient survival [15, 16]; and 3) CD8 T cells have also been shown to impact COVID-19 disease severity: high percentages of HLA-DR+CD38hi CD8+ T cells in

peripheral blood of COVID-19 patients were demonstrated to correlate with disease severity [17], and early bystander CD8 T cell activation combined with absence of systemic inflammation was shown to predict asymptomatic or mild disease [18]. Combined, these observations suggest that CD8 T cell immunity is important for protection against reinfection and severe COVID-19 disease [19].

As a direct consequence of antigenic drift, several SARS-CoV-2 variants defined by amino acid changes that directly impact virus transmissibility, pathogenicity, infectivity and/or antigenicity have emerged [20]. The most prominent SARS-CoV-2 variants in Europe were designated as variants of concern (VOC) (Alpha, B.1.1.7; Beta, B.1.351; Gamma, P.1; Delta, B.1.617.2; Omicron, B.1.1.529) and variants of interest (VOI) (Lambda, C.37; Mu, B.1.621; “Delta Plus”, AY.4.2), according to the European Centre for Disease Prevention and Control (ECDC) designation [21]. All VOC and VOI except AY.4.2 were also designated as VOC or VOI by the World Health Organization at the moment of this investigation [20]. SARS-CoV-2 variant Alpha was the dominant variant in circulation starting in late 2020 and was subsequently replaced by SARS-CoV-2 variant Delta which accounted for 90% of the infections worldwide by August 2021. In November 2021, SARS-CoV-2 variant Omicron was first detected. It was responsible for at least 92% of global SARS-CoV-2 infections by February 2022 [22](**Figure 2.1A**). There is accumulating evidence that recent SARS-CoV-2 variants including Beta, Delta and Omicron, are less efficiently neutralized by vaccine recipients’ sera [23, 24]. In terms of T cell immunity, there is experimental data by other groups showing that T cell responses induced by reference SARS-CoV-2 generally cross-recognize SARS-CoV-2 variants Alpha, Beta, Gamma, Delta and Omicron [25–29]. However, these papers do not include systematic data regarding the effect of SARS-CoV-2 variant-specific amino acid changes on the properties of previously recognized CD8 T cell epitopes.

In this work, we investigate the potential consequences of variant-specific mutations on the SARS-CoV-2-specific CD8 T cell responses raised by either natural infection or vaccination based on *in silico* analysis. In particular, we explore changes in predicted binding affinity of the epitopes to their HLA restriction elements, predicted immunogenicity and likelihood of CD8 T cell receptor cross-recognition of epitopes between the reference SARS-CoV-2 strain and SARS-CoV-2 variants of interest and concern (**Figure 2.1B**). We perform these analyses pan-proteome to identify the degree of protection after a natural infection. Furthermore, the vaccines currently approved by WHO are limited to the spike protein [30]. Therefore, we have also conducted the analyses focused on CD8 T cell recognized epitopes derived from the spike protein only to determine the degree of the vaccine-mediated

2.1. Introduction

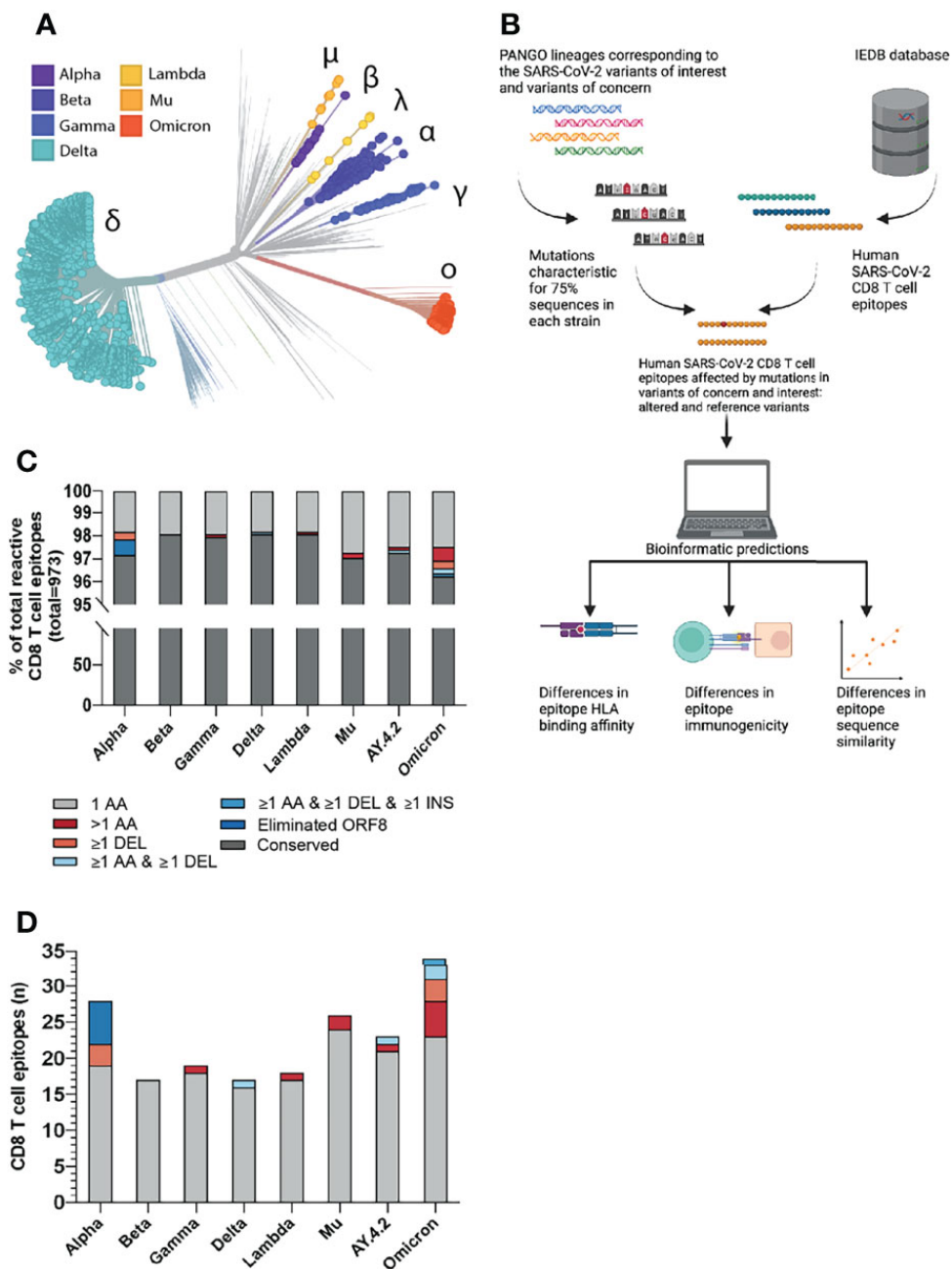


Figure 2.1: Overview of the investigated SARS-CoV-2 CD8 T cell reactive epitopes. (A) Phylogenetic tree where isolates originating from variants of concern (VOCs) Alpha, Beta, Gamma, Delta and Omicron are highlighted, as well as variants of interest (VOIs) Lambda and Mu. AY.4.2 is a subvariant of Delta and overlaps with the Delta branch. The length of the branches reflects the time of emergence. Visualization generated using the Nextstrain platform [22]. (B) Depiction of the project workflow. Created with Biorender. (C) Stacked bar graph indicating the percentages of CD8 T cell recognized epitopes per variant that are conserved or harbor the indicated types of mutations. (D) Numbers of CD8 T cell recognized epitopes per variant that harbor the indicated types of mutations.

protection.

2.2. Results

A Minor Fraction of SARS-CoV-2 Derived CD8 T Cell Recognized Epitopes Are Mutated in Variants of Concern and Interest

We focused our analysis on the current SARS-CoV-2 variants of concern (VOC) (Alpha, B.1.1.7; Beta, B.1.351; Gamma, P.1; Delta, B.1.617.2; Omicron, B.1.1.529) and variants of interest (VOI) (Lambda, C.37; Mu, B.1.621; “Delta Plus”, AY.4.2). First, we identified the non-synonymous amino acid substitutions, insertions and deletions that were present in at least 75% of total virus isolates for each variant in the GISAID database [31, 32] (per December 6th, 2021; as compared to the reference SARS-CoV-2 variant (**Supplementary Table 1**). Next, we parsed all 973 unique experimentally validated CD8 T cell recognized reference SARS-CoV-2 derived epitopes identified in patients with COVID-19, per December 8th 2021, from the Immune Epitope Database [33, 34] (IEDB) and aligned these with the sequences spanning the identified non-synonymous mutations in the investigated SARS-CoV-2 variants (**Figure 2.1B**). Specifically, all SARS-CoV-2 CD8 T cell epitopes detected in patients with COVID-19 were included. Epitopes deduced from peptide pools, in which the exact reactive peptide is not validated, were filtered out. In addition, studies conducted in the adoptive transfer setting were filtered out. Subsequently, we proceeded with the bioinformatic analysis of differences in HLA binding affinity, immunogenicity and sequence similarity between altered and reference epitopes (**Figure 2.1B**).

The vast majority of the 973 included CD8 T cell recognized epitopes was found to be conserved across the different variants (median: 97.8%, range: 96.5-98.3%): we identified a total of 93 unique epitopes that harbored one or more mutations (**Figure 2.1C**). Specifically, between 17 and 34 unique epitopes per variant (median: 21) overlap with one or more amino acid substitutions, deletions and/or insertions (**Figure 2.1D** and **Supplementary Tables 2, 3**). Six CD8 T cell recognized epitopes were considered eliminated in SARS-CoV-2 variant Alpha as they were located downstream of a stop-codon mutation (ORF8 Q27*); three additional epitopes contain a deletion (SΔ69/70 or Δ144/144). In SARS-CoV-2 variant Beta, the identified CD8 T cell recognized epitopes only contain single amino acid substitutions. Altered CD8 T cell recognized epitopes in the more recent Gamma, Delta, Lambda, Mu and AY.4.2 SARS-CoV-2 variants do not harbor single deletions but harbor other types of mutations, for example, epitopes with mutations consisting of more than one amino acid substitution (Gamma, Lambda, Mu and AY.4.2; n = 1, 1, 2 and 1, respectively) or an epitope with a

deletion (Δ 157-158) together with an amino acid substitution (Delta and AY.4.2). The recently emerged SARS-CoV-2 Omicron variant harbors the largest number of CD8 T cell recognized epitopes that overlap with non-synonymous mutations ($n=34$). These mutations result in epitopes with single ($n=23$), double ($n=2$) and triple ($n=3$) amino acid substitutions; single deletions ($n=3$); a combined amino acid substitution and deletion ($n=2$), and even a combined substitution, deletion and insertion ($n=1$) (**Figure 2.1D** and **Supplementary Tables 2, 3**).

To be able to investigate the potential consequences of the variant specific mutations on T cell recognition, we made a list of all variant specific CD8 T cell epitopes based on the variant specific mutations. For the analyses investigating the likelihood of T cell receptor cross-recognition and epitope immunogenicity of the altered epitopes, we included the 93 unique CD8 T cell recognized epitopes with variant specific mutations. For the prediction of HLA binding affinity, we limited the analysis to the 74 of the 93 epitopes for which HLA restriction elements had been experimentally determined by the scientific community (**Supplementary Tables 2, 3**). In total, these epitopes bind 27 HLA alleles, with between 1 and 14 epitopes per allele (median: 3, **Supplementary Figure 2.5A**).

Properties of Altered Epitopes Are Highly Conserved Between Variants and Reference SARS-CoV-2 CD8 T Cell Recognized Epitopes

Amino acid changes in SARS-CoV-2-derived CD8 T cell epitopes can reduce the sequence similarity to the reference epitope. The more distinct the biochemical properties of an amino acid substitution are compared to the reference amino acid, the greater the dissimilarity. This could lead to reduced or abrogated activation of memory CD8 T cells reacting to the altered epitope. The epitope sequence similarity of the altered epitope to the reference epitope can therefore be used as an *in silico* proxy for likelihood of T cell receptor cross-recognition.

To test the epitope sequence similarity between the variant-specific and matched reference epitopes, we conducted two analyses: 1) We compared the sequence similarity between the reference and the altered epitopes using a previously published method ([35]). Importantly, this method incorporates the biochemical properties of amino acid substitutes to score the epitope sequence similarity, which is crucial in epitope cross-recognition by CD8 T cell receptors. Experimental data demonstrate that CD8 T cell receptor recognition drops to 50% if peptide similarity drops below 85% [36]. We found that the vast majority (median: 90%, range: 65-100%) of the reference and the matched variant specific CD8 T cell epitopes share over 85% sequence similarity (**Figure 2.2A** and **Supplementary Figure 2.6A**).

2) In addition, we measured the degree of sequence similarity between the pairs of epitopes using the IEDB clustering tool which performs a local alignment [37]. In contrast to the first method, the IEDB clustering tool allows comparison of epitopes of differing lengths (e.g. due to insertions/deletions). Data from our previous experiments in the tumor setting suggests that a sequence similarity above 80% could serve as an indicator of potential TCR cross-reactivity [38, 39]. The majority (median: 93%, range: 73-100%) of reference SARS-CoV-2 epitopes and variant derived epitopes share at least 80% similarity (**Supplementary Figure 2.6B**). Taken together, these in silico analyses suggest that the ability of memory CD8 T cells, induced by natural infection with the reference virus, to respond to the included variants is not significantly impaired.

The likelihood that a certain peptide is immunogenic can be predicted based on the presence and, importantly, positioning of amino acids with certain biochemical properties [40]. To investigate whether a SARS-CoV-2 CD8 T cell recognized epitope is predicted to be more or less immunogenic as a result of an amino acid change, we applied the IEDB T cell class I pMHC immunogenicity prediction tool to the set of reference SARS-CoV-2 CD8 T cell recognized epitopes and variant derived epitopes. This tool uses a large set of known peptide immunogenicity values to computationally predict whether CD8 T cell epitopes are immunogenic (i.e., likelihood for T cell recognition) or not [40]. Surprisingly, the epitopes derived from the Omicron and Lambda variants were predicted to be significantly more and less immunogenic, respectively (Omicron: $p=0.0042$, (Lambda: $p=0.03$; **Figure 2.2B**). For all included SARS-CoV-2 variants, a large fraction of mutated epitopes was predicted to be either more immunogenic (median: 47%, range: 11-57%) or unchanged in immunogenicity (median: 28%, range: 19-44%). Between 6% and 44% (median: 24%) of variant specific CD8 T cell recognized epitopes were predicted to be less immunogenic as a result of the mutation (**Supplementary Figure 2.7A**). Taken together, these analyses indicate that there is a high degree of sequence similarity between altered and reference epitopes in all analyzed SARS-CoV-2 variants, which is likely to result in a high degree of CD8 T cell cross-reactivity between these epitopes.

A Minor Fraction of Mutated Epitopes From Delta and AY.4.2 Exhibit Reduced Predicted Binding Affinity to MHC Class I

Amino acid changes in CD8 T cell recognized epitopes may result in altered binding affinity to the corresponding HLA restriction elements. This may result in altered presentation of the epitope on the surface of SARS-CoV-2 infected cells, making the infected cells less visible to T cell recognition. To estimate the changes in binding affinity of the altered epitopes, we used the 74 unique SARS-CoV-2 CD8 T

2.2. Results

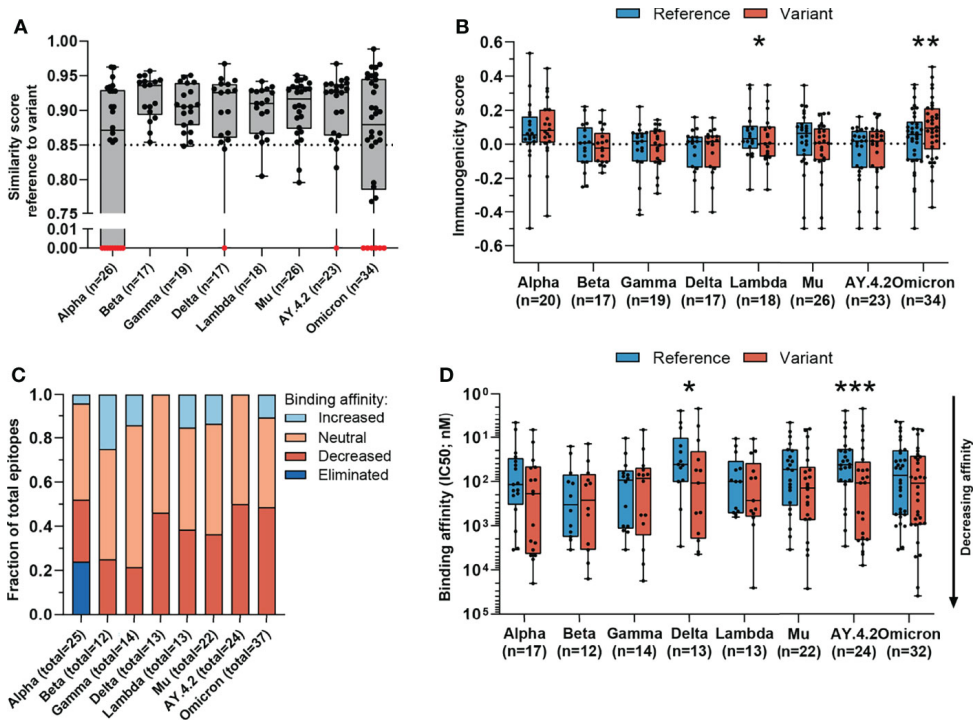


Figure 2.2: Sequence similarity and predicted binding affinity of mutated CD8 T cell recognized epitopes. **(A)** Sequence similarity scores between the reference SARS-CoV-2 CD8 T cell recognized epitopes and the altered epitopes. Sequence similarity of epitopes in red is set to zero as a result of one or more deletions/insertions in the epitope sequence (Alpha, n = 3; Delta, n = 2; AY.4.2, n = 2; Omicron, n = 13) or due to the ORF8 Q27* stop codon mutation (Alpha, n = 6). **(B)** Box plot indicating the predicted immunogenicity of the reference SARS-CoV-2 CD8 T cell recognized epitopes and the altered epitopes according to the IEDB T cell class I pMHC immunogenicity prediction tool. **(C)** Fractions of total altered CD8 T cell recognized epitopes where the predicted binding affinity of the epitope to the corresponding HLA restriction element was increased (≤ 0.5 -fold change in IC₅₀), remained neutral ($0.5 < \text{fold change in IC}_{50} < 2$) or was decreased (≥ 2 -fold change in IC₅₀) as a result of the mutation. Epitopes were considered eliminated as a result of the ORF8 Q27* stop codon mutation (Alpha variant). **(D)** Box plot indicating the predicted binding affinity IC₅₀ (nM) of the reference and altered CD8 T cell recognized epitope to the corresponding HLA restriction element. Box plots indicate the median (line), 25th and 75th percentile (box), min and max (whiskers), and all data points (single circles). Statistical significance was tested with a two-tailed Wilcoxon matched-pairs signed rank test. Variation in numbers of epitopes in the analyses are due to inclusion of epitopes binding one or more HLA restriction elements. *P < 0.05, **P < 0.01, ***P < 0.001. n indicates the number of epitopes analyzed per group.

cell recognized epitopes with previously experimentally validated HLA restriction elements. We used the NetMHCpan-4.1 tool to predict the binding affinity of each reference and variant specific CD8 T cell epitope to the matched HLA restriction element [41]. In this analysis, epitopes that can bind to more than one HLA allele were included for each of the HLA allele they bind to.

For each included SARS-CoV-2 variant, we observed decreased binding

affinity, defined as a ≥ 2 -fold change in IC50 value for a subset of the variant specific epitopes (median 37% of epitopes, range: 21%-50%) (**Figure 2.2C**). Between 41% and 64% (median: 50%) of variant specific epitopes retained their predicted binding affinity (neutral; $0.5 < \text{fold change in IC50} < 2$), and for between 0% and 25% (median: 12%) of altered epitopes an increased binding affinity was predicted (≤ 0.5 -fold change in IC50 value). Following a comparison of the difference in predicted binding affinity of the paired reference SARS-CoV-2 CD8 T cell recognized epitopes and mutated epitopes, the small set of epitopes of the Delta variant and its subvariant AY.4.2 were predicted to have a significantly reduced binding affinity to the HLA as a result of their mutations (Delta: $p=0.01$, AY.4.2: $p=0.0002$; **Figure 2.2D**). Importantly, despite these statistically significant differences, these results are derived from a highly limited number of epitopes (12 and 18 altered epitopes derived from Delta and AY.4.2, respectively, out of a total of 973 CD8 T cell recognized epitopes per variant).

A Larger Fraction of Spike Derived CD8 T Cell Epitopes Are Affected by Variant Specific Mutations Compared to Pan Proteome Derived Epitopes

To date, it is estimated that since the start of the pandemic there have been more than 400 million COVID-19 cases [42]. This translates to approximately 5% of the world population, however, many cases were never included in the official statistics. In contrast, it is estimated that over half of the world population (62.6% on February 25, 2022) has received at least one dose of a COVID-19 vaccine based on the reference SARS-CoV-2 sequence of the spike protein [43]. Of all the proteins encoded by SARS-CoV-2, the spike protein is subject to the highest rate of evolution [10]. As a consequence, spike protein-derived CD8 T cell recognized epitopes are inherently the least conserved T cell epitopes of the SARS-CoV-2 proteome. Therefore, individuals that have not been infected but have only received the vaccine may have a lower level of protective CD8 T cell immunity as their T cell immunity is limited to epitopes from the spike protein.

We performed our analysis on spike protein-derived epitopes only. The SARS-CoV-2 spike protein encodes 263 previously identified CD8 T cell recognized epitopes. The majority of these 263 CD8 T cell recognized epitopes is conserved across the variants included in our analysis (median: 95.1%, range: 92.0-96.6%) corresponding to between 9 and 21 (median: 13) epitopes per variant which have alterations in the amino acid sequence (**Figure 2.3A**, **Supplementary Figure 2.5C**, **Supplementary Tables 2, 3**). The majority (median 84%, range: 52-100%) of these mutated variant specific epitopes share at least 85% similarity with the corresponding references epitopes (**Figure 2.3B** and **Supplementary Figure 2.6C**) based on the IEDB epitope clustering

tool (median 89%, range: 71-100%; **Supplementary Figure 2.6D**).

Interestingly, the mutated spike protein-derived epitopes from the Alpha, AY.4.2 and Omicron variants are predicted to be significantly more immunogenic compared to reference (Alpha: $p=0.0034$, AY.4.2: $p=0.031$, Omicron: $p=0.0065$; **Figure 2.3C**). A large fraction of mutated epitopes was predicted to be either more immunogenic (median: 63%, range: 22-79%) or unchanged in immunogenicity (median: 20%, range: 11-31%). Between 6% and 67% (median: 15%) of variant specific CD8 T cell recognized epitopes were predicted to be less immunogenic as a result of the mutation (**Supplementary Figure 2.7B**). Furthermore, for each included SARS-CoV-2 variant, decreased binding affinity is predicted (≥ 2 -fold change in IC50 value; **Figure 2.3D**) for a subset of the altered epitopes (median 48% of epitopes, range: 22%-75%). Between 25% and 59% (median: 44%) of altered epitopes retained their predicted binding affinity (neutral; $0.5 < \text{fold change in IC50} < 2$), and between 0% and 25% (median: 6%) of altered epitopes had an increased predicted binding affinity (≤ 0.5 -fold change in IC50 value). Spike protein-derived CD8 T cell recognized epitopes of the Delta, Mu and AY.4.2 variants were predicted to have a significantly reduced binding affinity to the HLA as a result of their mutations (Delta: $p=0.016$, Mu: $p=0.017$, AY.4.2: $p=0.0002$; **Figure 2.3E**). Importantly, despite these statistically significant differences, these results are derived from only 8 to 14 (median: 12) unique CD8 T cell recognized epitopes that are mutated per variant, out of a total of 263 unique epitopes per variant.

Next, we tested whether variant-specific mutations may have a more profound effect on spike protein-derived CD8 T cell recognized epitopes compared to non-spike. We performed the analysis on non-spike protein-derived epitopes and compared these to the results above. As expected, a smaller fraction of CD8 T cell recognized epitopes in the SARS-CoV-2 spike protein were found to be conserved compared to those in non-spike proteins (median: 95.1%, range: 92.0-96.6%; versus median: 98.9%, range: 98.0-99.2%; **Supplementary Figures 2.5C, D**). All epitopes overlapping with multi-amino acid substitutions, deletions and/or insertions except one were located in the SARS-CoV-2 spike protein (**Supplementary Figures 2.5F, G**). Such multi-amino acid changes are expected to lead to a lower sequence similarity between altered and reference epitopes. In line with this, there was a significantly lower sequence similarity between mutated and reference CD8 T cell recognized epitopes in the spike protein, compared to the single-amino acid mutations in non-spike proteins (in variants Delta, $p=0.043$; AY.4.2, $p=0.047$; Omicron, $p=0.028$; **Figure 2.4A**).

Across the investigated SARS-CoV-2 variants, the fraction of CD8 T cell recognized epitopes with low ($<85\%$) sequence similarity to reference epitopes was significantly higher in spike versus non-spike protein-

2. In silico analysis predicts a limited impact of SARS-CoV-2 variants on CD8 T cell recognition

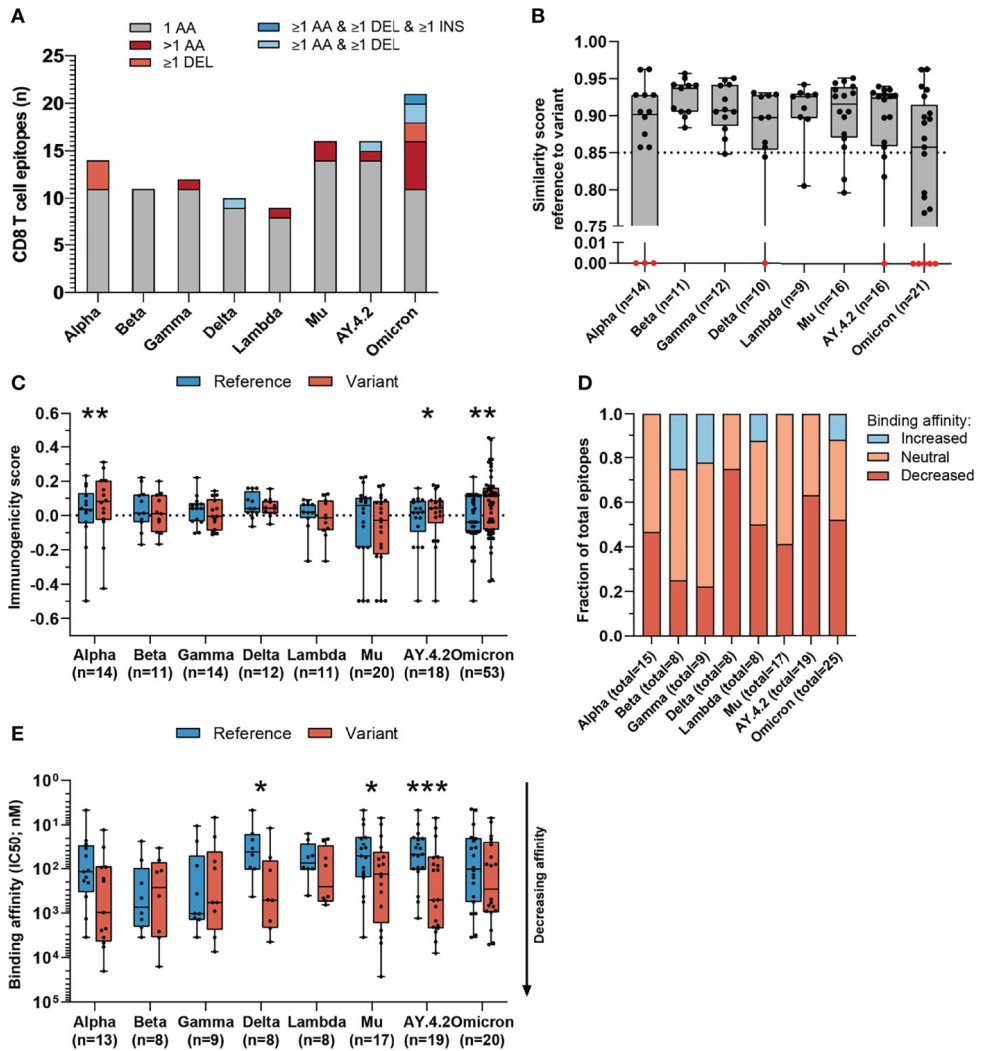


Figure 2.3: Sequence similarity and predicted binding affinity of mutated CD8 T cell recognized epitopes derived from the spike protein. (A) Numbers of spike protein-derived CD8 T cell recognized epitopes per variant that harbor the indicated categories of mutations. (B) Sequence similarity scores between the spike protein-derived reference SARS-CoV-2 CD8 T cell recognized epitopes and the matched variant epitopes. Sequence similarity of epitopes in red is set to zero as a result of one or more deletions/insertions in the epitope sequence (Alpha, n = 3; Delta, n = 2; AY.4.2, n = 2; Omicron, n = 12). (C) Box plot indicating the predicted immunogenicity of the spike protein-derived reference SARS-CoV-2 CD8 T cell recognized epitopes and the altered epitopes according to the IEDB T cell class I pMHC immunogenicity prediction tool. (D) Fractions of total altered spike protein-derived CD8 T cell recognized epitopes where the predicted binding affinity of the epitope to the corresponding HLA restriction element was increased (≤ 0.5 -fold change in IC₅₀), remained neutral ($0.5 < \text{fold change in IC}_{50} > 2$) or was decreased (≥ 2 -fold change in IC₅₀) as a result of the mutation. (E) Box plot indicating the predicted binding affinity IC₅₀ (nM) of the reference and altered spike protein-derived CD8 T cell recognized epitope to the corresponding HLA restriction element. Box plots indicate the median (line), 25th and 75th percentile (box), min and max (whiskers), and all data points (single circles). Statistical significance was tested with a two-tailed Wilcoxon matched-pairs signed rank test. Variation in numbers of epitopes in the analyses are due to inclusion of epitopes binding one or more HLA restriction elements. AA, amino acid; DEL, deletion; INS, insertion. *P < 0.05, **P < 0.01, ***P < 0.001. n indicates the number of epitopes analyzed per group.

2.2. Results

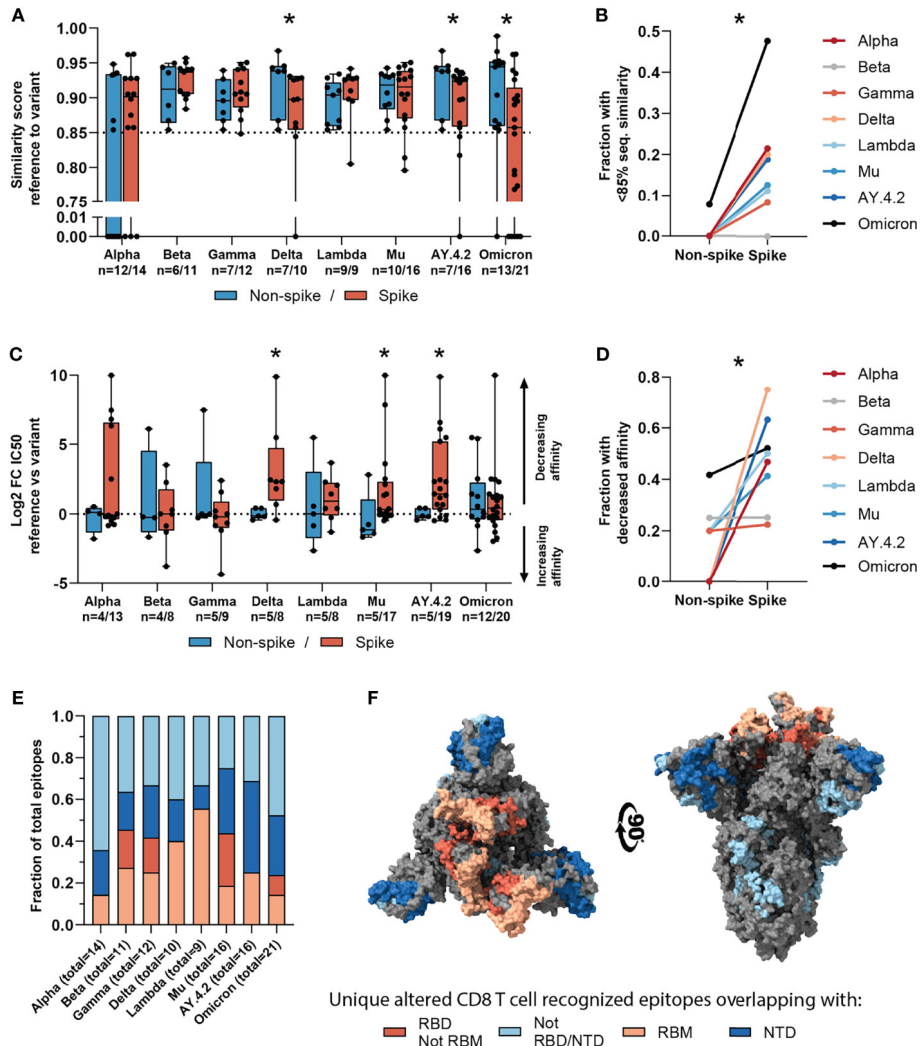


Figure 2.4: Sequence similarity and predicted binding affinity of spike- versus non-spike-derived mutated CD8 T cell recognized epitopes. (A) Box plot comparing the sequence similarity of the altered spike and non-spike protein-derived CD8 T cell recognized epitopes, to the reference epitopes. Sequence similarity of indicated epitopes is set to zero as a result of one or more deletions/insertions in the epitope sequence (Alpha, $n = 6/3$; Delta, $n = 0/2$; AY.4.2, $n = 0/2$; Omicron, $n = 1/12$). (B) Fraction of spike versus non-spike protein-derived epitopes where the sequence similarity of the epitope to the reference epitope dropped below 85% as a result of the mutation. (C) Box plot comparing the log2 fold change in predicting binding affinity of spike and non-spike protein-derived CD8 T cell recognized epitopes to the corresponding HLA restriction element, as a result of the mutation. (D) Fraction of spike versus non-spike protein-derived CD8 T cell recognized epitopes where the predicted binding affinity of the epitope to the corresponding HLA restriction element was decreased (≥ 2 -fold change in IC50) as a result of the mutation. (E) Fractions of unique spike protein-derived CD8 T cell recognized epitopes overlapping with a mutation located in the N-terminal domain (NTD), receptor-binding domain (RBD), receptor-binding motif (RBM) or a mutation located outside of these domains. (F) SARS-CoV-2 spike trimer in the open conformation with one erect RBD. Colors represent unique altered CD8 T cell recognized epitopes overlapping with the indicated domains. Image produced with ChimeraX using PDB accession: 6ZGG. Box plots indicate the median (line), 25th and 75th percentile (box), min and max (whiskers), and all data points (single circles). Statistical significance was tested with a two-tailed Mann-Whitney U test (A, C) or with a two-tailed Wilcoxon matched-pairs signed rank test (B, D). Variation in numbers of epitopes in the analyses are due to inclusion of epitopes binding one or more HLA restriction elements. * $P < 0.05$. n indicates the number of epitopes analyzed per group.

derived epitopes ($p=0.016$, **Figure 2.4B**). Additionally, mutations in the spike protein of the Delta, Mu and AY.4.2 variants were more detrimental to predicted HLA binding affinity compared to non-spike protein mutations (Delta: $p=0.019$, Mu: $p=0.025$, AY.4.2: $p=0.030$; **Figure 2.4C**). In accordance with this, the fraction of CD8 T cell recognized epitopes with decreased predicted binding affinity was significantly higher in spike versus non-spike protein-derived epitopes across the variants ($p=0.016$, **Figure 2.4D**). However, despite these statistically significant differences, these results are derived from a limited number of unique mutated CD8 T cell recognized epitopes per variant.

The overrepresentation of altered CD8 T cell recognized epitopes with multiple amino acid changes, insertions and deletions in the spike protein is clearly pronounced. Accordingly, these epitopes are more profoundly affected in terms of epitope sequence similarity, predicted binding affinity and immunogenicity compared to non-spike protein derived epitopes. These results may be unrelated to T cell immunity and may be explained for example by the high rate of evolution of the spike protein due to natural selection pressure by antibody responses. In line with this, a substantial part (median: 65%, range: 36-75%) of the unique spike protein-derived CD8 T cell recognized epitopes that overlap mutations were located in key domains that are associated with cell attachment and are antibody targets (N-terminal domain, NTD; receptor-binding domain, RBD; receptor-binding motif, RBM; **Figure 2.4E**). Moreover, they are primarily present on the surface of the spike protein, making them accessible to host antibodies (**Figure 2.4F**).

2.3. Discussion

After the initial SARS-CoV-2 outbreak, SARS-CoV-2 variants Alpha, Delta and Omicron have replaced the previous variant as the globally dominant SARS-CoV-2 variant [31, 44]. This is the result of accumulated mutations resulting in amino acid changes that have allowed these variants to evade immunity in the general population. This notion is supported by for example data showing that serum from vaccine-recipients is less effective at neutralizing SARS-CoV-2 variants Delta and Omicron [23, 24]. The mutations do not appear to prevent general cross-recognition of SARS-CoV-2 variants by T cells induced by reference SARS-CoV-2 [25–29]. However, systematic data regarding the effect of SARS-CoV-2 variant-specific amino acid changes on the properties of the previously recognized CD8 T cell epitopes has been lacking.

Our analyses revealed that the vast majority of both the spike (median:

95.1%, range: 92.0-96.6%) and pan-proteome (median: 98.9%, range: 98.0-99.2%) derived CD8 T cell recognized epitopes were conserved in the investigated SARS-CoV-2 variants. In accordance with the experimental data described above, this suggests that memory T cell responses are not likely to be diminished upon re-infection by a different SARS-CoV-2 variant, or upon infection by one of the SARS-CoV-2 variants after vaccination. In addition, for the minority of presented CD8 T cell recognized epitopes that is altered by mutations, the high degree of sequence similarity to the reference epitopes will likely also not prevent cross-recognition by memory CD8 T cells.

The finding that CD8 T cell epitopes from SARS-CoV-2 were generally conserved is in accordance with the concept of antigenic drift. Antigenic drift driven by selective pressure from T cells is largely irrelevant in acute viral infections such as SARS-CoV-2 due to the huge polymorphism of HLA loci in a population and the diverse antigen repertoire these complexes present to T cells [9]. Antigenic drift is likely to have a stochastic influence on T cell epitopes - a 'bystander effect'. Our observations are in line with this notion. First, for the minority of CD8 T cell recognized epitopes that overlap with mutations, epitope sequences are generally conserved in terms of sequence similarity to the reference sequence. Second, the majority (median: 55.6%, range: 46.2-78.6%) of these CD8 T cell recognized epitopes are predicted to possess unchanged or even increased binding affinity to the HLA allele as a result of the mutation. Third, the mutations in the CD8 T cell recognized epitopes in SARS-CoV-2 variants AY.4.2 and Omicron are predicted to result in more immunogenic, rather than less immunogenic T cell epitopes. Fourth, many of the observed changes in predicted binding affinity and sequence similarity of mutated CD8 T cell recognized epitopes in comparison to the reference epitopes, are indeed driven by mutations in the spike protein. Finally, the majority (median: 65%, range: 36-75%) of spike protein-derived CD8 T cell recognized epitopes that overlap with a mutation are located in key domains that are frequently recognized by antibody responses and/or are involved in cell attachment [10]. Therefore, on the basis of our analysis and as expected, there is no indication of T cell based selective pressure on SARS-CoV-2 leading to alteration of the CD8 T cell recognized epitopes.

As SARS-CoV-2 derived T cell epitopes are not subject to substantial antigenic drift, T cells are likely to remain consistent in their recognition of infected cells. However, the stochastic influence by the mutations focused on the spike protein affects the ability of spike protein-derived T cell epitopes to be presented to the immune system or to be recognized by previously induced T cell responses. This is most pronounced for the SARS-CoV-2 variants Delta, AY.4.2 and Omicron, which are also most efficient at escaping humoral immunity as a result of numerous

mutations in the spike protein. These variants also have the largest, albeit overall minor, negative effect on epitope presentation relative to the other SARS-CoV-2 variants. By only targeting the spike protein, the vaccine induced immunity is limited to SARS-CoV-2 T cell epitopes which are most prone to a ‘bystander’ effect as a result of the high mutation rate of the spike protein. Even though the currently approved vaccines only include the spike protein, our data suggest that T cell immunity can protect against severe COVID-19. However, it does seem like a logical approach to develop next generation vaccines incorporating other parts of the SARS-CoV-2 proteome which can lead to a broader T cell response providing protection should the spike protein undergo further changes over time.

2.4. Materials and Methods

Identification of Dominant Non-Synonymous Mutations in SARS-CoV-2 Variants

The list of SARS-CoV-2 variants of interest and variants of concern has been compiled according to the WHO and ECDC designations as of December 10, 2021. For each of the variants, a list of mutations present in 75% of the GISAID sequences for the corresponding PANGO lineage was compiled via the outbreak.info API. The lists of mutations per lineage [31, 44] can be found in **Supplementary Table 1**.

Parsing of CD8 T Cell Recognized SARS-CoV-2 Epitopes Using IEDB

The table of T cell assay results was downloaded from the IEDB website [33, 45] on December 8, 2021. The table was filtered to include only linear SARS-CoV-2 epitopes in humans, presented in context of the MHC class I. Only epitopes from patients with infectious disease were included. Only positive assays with negative adoptive flag field were included. The tables of variant mutations and SARS-CoV-2 CD8 T cell recognized epitopes were subsequently intersected. CD8 T cell recognized epitopes that were deduced from reactive overlapping peptide pools were filtered from the list. Epitopes with published HLA restriction elements were manually curated. The final list of epitopes and corresponding HLA alleles is shown in the **Supplementary Tables 2, 3**.

Epitope Analysis

The normalized epitope similarity score between the altered and reference SARS-CoV-2 CD8 T cell recognized epitope was calculated as described by Frankild et al. [35]. This method does not allow the

calculation of the similarity score between two sequences of differing lengths. For this reason, we have set the sequence similarity score of CD8 T cell recognized epitopes harboring deletions and/or insertions to 0. IEDB's epitope cluster analysis tool [37] was additionally used on each reference and altered epitope to determine if the epitope pairs share a sequence identity of 80%, 80-90% or more than 90%. The parameters used were: minimum sequence identity threshold: 80%, 90%. Minimum/Maximum peptide length: NA. Clustering method: fully interconnected clusters (cliques).

IEDB's T cell class I pMHC immunogenicity prediction tool [40] was used to compare the immunogenicity of the altered and reference SARS-CoV-2 CD8 T cell recognized epitopes. The default setting was used, masking the 1st, 2nd and C-terminus amino acids of the epitopes in the analysis.

For all parsed reference SARS-CoV-2 CD8 T cell recognized epitopes with experimentally validated HLA restriction information, the predicted binding affinity to the given HLA was calculated for both the reference and altered epitope using NetMHCpan-4.1 [41]. The predicted binding affinity is expressed as the half-maximal inhibitory concentration IC50 nM. For each paired reference and altered epitope, the fold change in predicted binding affinity as a result of the mutation(s) was calculated. A 2-fold change in predicted binding affinity was defined as a decrease in predicted binding affinity, a fold change below 0.5 as an increase in predicted binding affinity and a fold change between 0.5 and 2 was conservatively defined as neutral. CD8 T cell recognized epitopes overlapping with a deletion and/or insertion and not predicted to bind to the HLA as a result of the mutation were defined as decreased in predicted binding affinity.

Statistical Analysis

For all analyzed SARS-CoV-2 CD8 T cell recognized reference and altered epitope pairs, differences in predicted immunogenicity and predicted binding affinity were assessed using a two-tailed Wilcoxon matched-pairs signed rank test. The increase in fractions of CD8 T cell recognized epitopes with decreased binding affinity and/or an epitope sequence similarity <85% was also assessed using a two-tailed Wilcoxon matched-pairs signed rank test. Comparisons in log2 fold change predicted binding affinity and/or epitope sequence similarity between spike and non-spike protein-derived mutated CD8 T cell recognized epitopes were assessed using a two-tailed Mann-Whitney U test. Differences were considered significant if $P < 0.05$. Statistical analysis was performed with GraphPad Prism [version: 8.4.2, for Windows, GraphPad Software, San Diego, California USA] [46].

2.5. Author Contributions

OI and SK performed the experiments, analyzed the data and wrote the manuscript. PK obtained the funding and supervised the study. All authors contributed to the article and approved the submitted version.

2.6. Funding

The project was funded with the Netherlands Cancer Institute Kvistborg group start-up funding.

2.7. Conflict of Interest

The authors declare that the research was conducted in the absence of any commercial or financial relationships that could be construed as a potential conflict of interest.

2.8. Data Availability Statement

The original contributions presented in the study are included in the article/Supplementary Material. Further inquiries can be directed to the corresponding author.

2.9. Supplementary Information

Supplementary Tables 1, 2 and 3 are available via the link: <https://www.frontiersin.org/articles/10.3389/fimmu.2022.891524/full#supplementary-material>

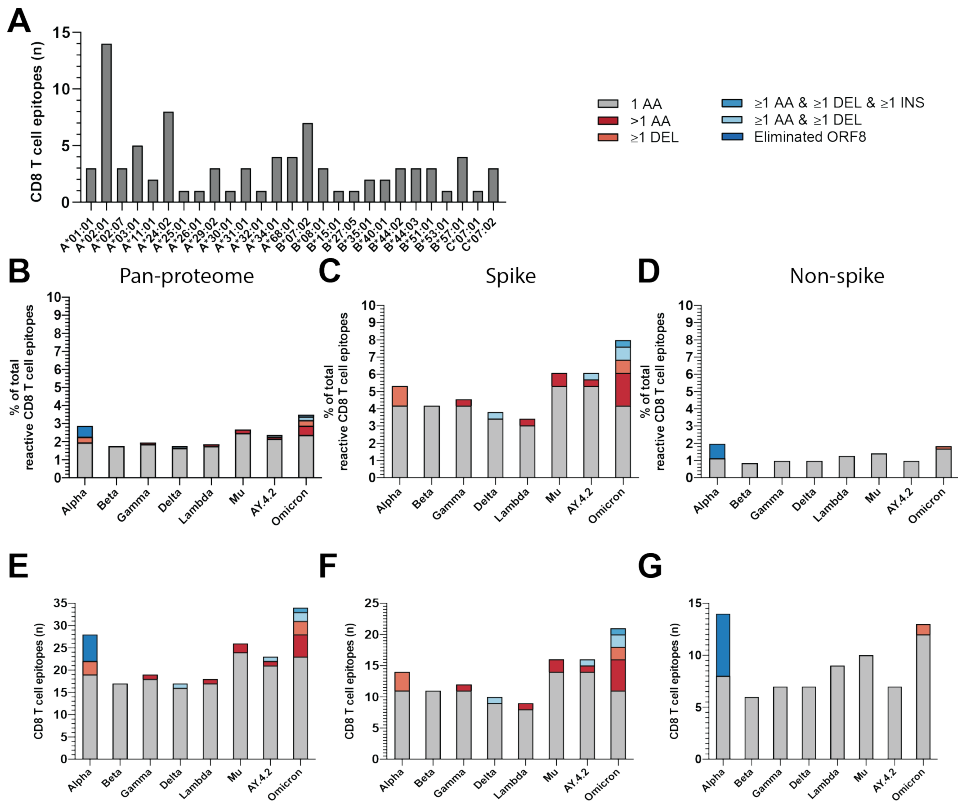


Figure 2.5: CD8 T cell recognized epitopes that overlap with a mutation. (A) Numbers of unique CD8 T cell recognized epitopes included in this study that bind the indicated HLA restriction elements, based on literature. (B) Percentage of pan-proteome, spike (C), non-spike (D) CD8 T cell recognized epitopes per variant that harbor the indicated types of mutations. Total epitope numbers are 973, 263 and 710, respectively. (E) Numbers of pan-proteome, (F) spike, (G) non-spike CD8 T cell recognized epitopes per variant that harbor the indicated categories of mutations.

2. In silico analysis predicts a limited impact of SARS-CoV-2 variants on CD8 T cell recognition

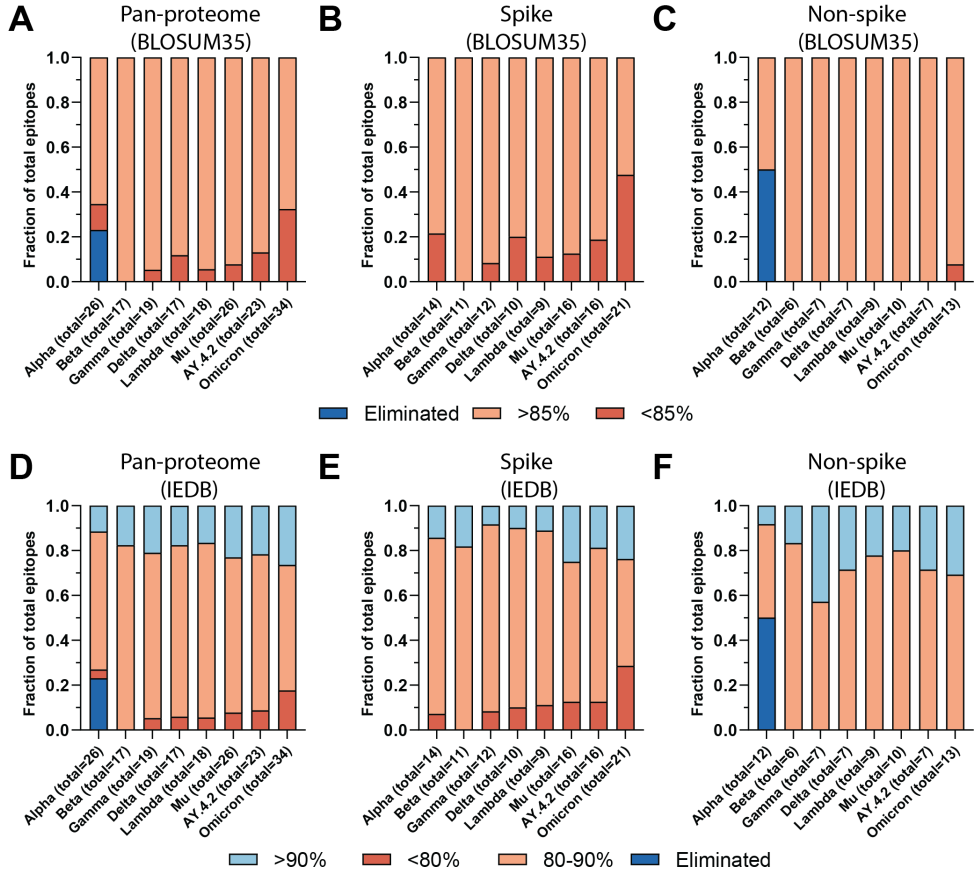


Figure 2.6: Mutant epitope sequence similarity to reference epitope sequence. (A) Fractions of pan-proteome, spike (B), non-spike (C) CD8 T cell recognized epitopes where the sequence similarity of the altered epitope to the reference epitope was below or above 85%, using the method by Frankild et al. described in the text. (D) Fractions of pan-proteome, spike (E), non-spike (F) CD8 T cell recognized epitopes where the sequence similarity of the altered epitope to the reference epitope was below 80%, above 90% or between 80-90%, using the IEDB epitope clustering tool described in the text. Epitopes were considered eliminated as a result of the ORF8 Q27* stop codon mutation (Alpha, n = 6).

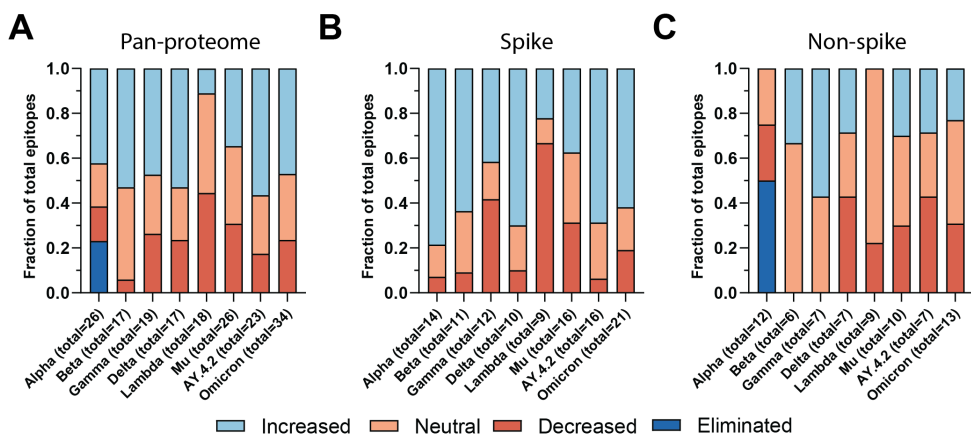


Figure 2.7: Fraction of altered CD8 T cell recognized epitopes with a change in predicted immunogenicity. (A) Fractions of pan-proteome, spike (B), non-spike (C) CD8 T cell recognized epitopes where the predicted immunogenicity increased, decreased or was unchanged as a result of the overlapping mutation.

References

- [1] M. E. Lam. "United by the global COVID-19 pandemic: divided by our values and viral identities". *Humanit. Soc. Sci. Commun.* 8.1 (Jan. 2021).
- [2] H. Lambert, J. Gupte, H. Fletcher, L. Hammond, N. Lowe, M. Pelling, N. Raina, T. Shahid, and K. Shanks. "COVID-19 as a global challenge: towards an inclusive and sustainable future". *Lancet Planet. Health* 4.8 (Aug. 2020), e312–e314.
- [3] D. L. Roberts, J. S. Rossman, and I. Jarić. "Dating first cases of COVID-19". *PLoS Pathog.* 17.6 (June 2021), e1009620.
- [4] M. Worobey. "Dissecting the early COVID-19 cases in Wuhan". *Science* 374.6572 (Dec. 2021), pp. 1202–1204.
- [5] M. Amicone, V. Borges, M. J. Alves, J. Isidro, L. Zé-Zé, S. Duarte, L. Vieira, R. Guiomar, J. P. Gomes, and I. Gordo. "Mutation rate of SARS-CoV-2 and emergence of mutators during experimental evolution". May 2021.
- [6] E. Domingo and J. J. Holland. "RNA virus mutations and fitness for survival". *Annu. Rev. Microbiol.* 51.1 (1997), pp. 151–178.
- [7] R. Sanjuán and P. Domingo-Calap. "Mechanisms of viral mutation". *Cell. Mol. Life Sci.* 73.23 (Dec. 2016), pp. 4433–4448.
- [8] S. Duffy, L. A. Shackelton, and E. C. Holmes. "Rates of evolutionary change in viruses: patterns and determinants". *Nat. Rev. Genet.* 9.4 (Apr. 2008), pp. 267–276.
- [9] J. W. Yewdell. "Antigenic drift: Understanding COVID-19". *Immunity* 54.12 (Dec. 2021), pp. 2681–2687.
- [10] W. T. Harvey, A. M. Carabelli, B. Jackson, R. K. Gupta, E. C. Thomson, E. M. Harrison, C. Ludden, R. Reeve, A. Rambaut, COVID-19 Genomics UK (COG-UK) Consortium, S. J. Peacock, and D. L. Robertson. "SARS-CoV-2 variants, spike mutations and immune escape". *Nat. Rev. Microbiol.* 19.7 (July 2021), pp. 409–424.
- [11] D. P. Martin, S. Weaver, H. Tegally, J. E. San, S. D. Shank, E. Wilkinson, A. G. Lucaci, J. Giandhari, S. Naidoo, Y. Pillay, L. Singh, R. J. Lessells, NGS-SA, COVID-19 Genomics UK (COG-UK), R. K. Gupta, J. O. Wertheim, A. Nekturenko, B. Murrell, G. W. Harkins, P. Lemey, O. A. MacLean, D. L. Robertson, T. de Oliveira, and S. L. Kosakovsky Pond. "The emergence and ongoing convergent evolution of the SARS-CoV-2 N501Y lineages". *Cell* 184.20 (Sept. 2021), 5189–5200.e7.
- [12] K.-Y. A. Huang, P. Rijal, L. Schimanski, T. J. Powell, T.-Y. Lin, J. W. McCauley, R. S. Daniels, and A. R. Townsend. "Focused antibody response to influenza linked to antigenic drift". *J. Clin. Invest.* 125.7 (July 2015), pp. 2631–2645.

- [13] S. R. Das, S. E. Hensley, W. L. Ince, C. B. Brooke, A. Subba, M. G. Delboy, G. Russ, J. S. Gibbs, J. R. Bennink, and J. W. Yewdell. "Defining influenza A virus hemagglutinin antigenic drift by sequential monoclonal antibody selection". *Cell Host Microbe* 13.3 (Mar. 2013), pp. 314–323.
- [14] J. Sun, Z. Zhuang, J. Zheng, K. Li, R. L.-Y. Wong, D. Liu, J. Huang, J. He, A. Zhu, J. Zhao, X. Li, Y. Xi, R. Chen, A. N. Alshukairi, Z. Chen, Z. Zhang, C. Chen, X. Huang, F. Li, X. Lai, D. Chen, L. Wen, J. Zhuo, Y. Zhang, Y. Wang, S. Huang, J. Dai, Y. Shi, K. Zheng, M. R. Leidinger, J. Chen, Y. Li, N. Zhong, D. K. Meyerholz, P. B. McCray Jr, S. Perlman, and J. Zhao. "Generation of a broadly useful model for COVID-19 pathogenesis, vaccination, and treatment". *Cell* 182.3 (Aug. 2020), 734–743.e5.
- [15] M. Luo, J. Liu, W. Jiang, S. Yue, H. Liu, and S. Wei. "IL-6 and CD8+ T cell counts combined are an early predictor of in-hospital mortality of patients with COVID-19". *JCI Insight* 5.13 (July 2020).
- [16] Q. Liu, X. Fang, S. Tokuno, U. Chung, X. Chen, X. Dai, X. Liu, F. Xu, B. Wang, and P. Peng. "Prediction of the clinical outcome of COVID-19 patients using T lymphocyte subsets with 340 cases from Wuhan, China: A retrospective cohort study and a web visualization tool". *SSRN Electron. J.* (2020).
- [17] J. Du, L. Wei, G. Li, M. Hua, Y. Sun, D. Wang, K. Han, Y. Yan, C. Song, R. Song, H. Zhang, J. Han, J. Liu, and Y. Kong. "Persistent high percentage of HLA-DR+CD38high CD8+ T cells associated with immune disorder and disease severity of COVID-19". *Front. Immunol.* 12 (Sept. 2021), p. 735125.
- [18] L. Bergamaschi, F. Mescia, L. Turner, A. L. Hanson, P. Kotagiri, B. J. Dunmore, H. Ruffieux, A. De Sa, O. Huhn, M. D. Morgan, P. P. Gerber, M. R. Wills, S. Baker, F. J. Calero-Nieto, R. Doffinger, G. Dougan, A. Elmer, I. G. Goodfellow, R. K. Gupta, M. Hosmillo, K. Hunter, N. Kingston, P. J. Lehner, N. J. Matheson, J. K. Nicholson, A. M. Petrunkina, S. Richardson, C. Saunders, J. E. D. Thaventhiran, E. J. M. Toonen, M. P. Weekes, Cambridge Institute of Therapeutic Immunology and Infectious Disease-National Institute of Health Research (CITIID-NIHR) COVID BioResource Collaboration, B. Göttgens, M. Toshner, C. Hess, J. R. Bradley, P. A. Lyons, and K. G. C. Smith. "Longitudinal analysis reveals that delayed bystander CD8+ T cell activation and early immune pathology distinguish severe COVID-19 from mild disease". *Immunity* 54.6 (June 2021), 1257–1275.e8.
- [19] K. McMahan, J. Yu, N. B. Mercado, C. Loos, L. H. Tostanoski, A. Chandrashekar, J. Liu, L. Peter, C. Atyeo, A. Zhu, E. A. Bondzie, G. Dagotto, M. S. Gebre, C. Jacob-Dolan, Z. Li, F. Nampanya, S. Patel, L. Pessaint, A. Van Ry, K. Blade, J. Yalley-Ogunro, M. Cabus, R. Brown, A. Cook, E. Teow, H. Andersen, M. G. Lewis, D. A. Lauffenburger, G. Alter, and D. H. Barouch. "Correlates of protection against SARS-CoV-2 in rhesus macaques". *Nature* 590.7847 (Feb. 2021), pp. 630–634.
- [20] World Health Organization. *Tracking SARS-CoV-2 Variants*. <https://www.who.int/activities/tracking-SARS-CoV-2-variants> (Accessed March 2, 2022).

- [21] European Centre for Disease Prevention and Control. *SARS-CoV-2 Variants of Concern as of 24 February 2022*. <https://www.ecdc.europa.eu/en/covid-19/variants-concern> (Accessed March 2, 2022).
- [22] J. Hadfield, C. Megill, S. M. Bell, J. Huddleston, B. Potter, C. Callender, P. Sagulenko, T. Bedford, and R. A. Neher. "Nextstrain: real-time tracking of pathogen evolution". *Bioinformatics* 34.23 (Dec. 2018), pp. 4121–4123.
- [23] C. Davis, N. Logan, G. Tyson, R. Orton, W. T. Harvey, J. S. Perkins, G. Mollett, R. M. Blacow, COVID-19 Genomics UK (COG-UK) Consortium, T. P. Peacock, W. S. Barclay, P. Cherepanov, M. Palmarini, P. R. Murcia, A. H. Patel, D. L. Robertson, J. Haughney, E. C. Thomson, B. J. Willett, and COVID-19 DeplOyed VaccinE (DOVE) Cohort Study investigators. "Reduced neutralisation of the Delta (B.1.617.2) SARS-CoV-2 variant of concern following vaccination". *PLoS Pathog.* 17.12 (Dec. 2021), e1010022.
- [24] D. Planas, N. Saunders, P. Maes, F. Guivel-Benhassine, C. Planchais, J. Buchrieser, W.-H. Bolland, F. Porrot, I. Staropoli, F. Lemoine, H. Péré, D. Veyer, J. Puech, J. Rodary, G. Baele, S. Dellicour, J. Raymenants, S. Gorissen, C. Geenen, B. Vanmechelen, T. Wawina-Bokalanga, J. Martí-Carreras, L. Cuypers, A. Sève, L. Hocqueloux, T. Prazuck, F. A. Rey, E. Simon-Loriere, T. Bruel, H. Mouquet, E. André, and O. Schwartz. "Considerable escape of SARS-CoV-2 Omicron to antibody neutralization". *Nature* 602.7898 (Feb. 2022), pp. 671–675.
- [25] S. C. Jordan, B.-H. Shin, T.-A. M. Gadsden, M. Chu, A. Petrosyan, C. N. Le, R. Zabner, J. Oft, I. Pedraza, S. Cheng, A. Vo, N. Ammerman, J. Plummer, S. Ge, M. Froch, A. Berg, M. Toyoda, and R. Zhang. "T cell immune responses to SARS-CoV-2 and variants of concern (Alpha and Delta) in infected and vaccinated individuals". *Cell. Mol. Immunol.* 18.11 (Nov. 2021), pp. 2554–2556.
- [26] A. Tarke, J. Sidney, N. Methot, E. D. Yu, Y. Zhang, J. M. Dan, B. Goodwin, P. Rubiro, A. Sutherland, E. Wang, A. Frazier, S. I. Ramirez, S. A. Rawlings, D. M. Smith, R. da Silva Antunes, B. Peters, R. H. Scheuermann, D. Weiskopf, S. Crotty, A. Grifoni, and A. Sette. "Impact of SARS-CoV-2 variants on the total CD4+ and CD8+ T cell reactivity in infected or vaccinated individuals". *Cell Rep. Med.* 2.7 (July 2021), p. 100355.
- [27] F. Melo-González, J. A. Soto, L. A. González, J. Fernández, L. F. Duarte, B. M. Schultz, N. M. S. Gálvez, G. A. Pacheco, M. Ríos, Y. Vázquez, D. Rivera-Pérez, D. Moreno-Tapia, C. Iturriaga, O. P. Vallejos, R. V. Berríos-Rojas, G. Hoppe-Elsholz, M. Urzúa, N. Bruneau, R. A. Fasce, J. Mora, A. Grifoni, A. Sette, D. Weiskopf, G. Zeng, W. Meng, J. V. González-Aramundiz, P. A. González, K. Abarca, E. Ramírez, A. M. Kalergis, and S. M. Bueno. "Recognition of variants of concern by antibodies and T cells induced by a SARS-CoV-2 inactivated vaccine". *Front. Immunol.* 12 (Nov. 2021), p. 747830.
- [28] R. Thiruvengadam, A. Awasthi, G. Medigeshi, S. Bhattacharya, S. Mani, S. Sivasubbu, T. Shrivastava, S. Samal, D. Rathna Murugesan, B. Koundinya Desiraju, P. Kshetrapal, R. Pandey, V. Scaria, P. Kumar Malik,

- J. Taneja, A. Binayke, T. Vohra, A. Zaheer, D. Rathore, N. Ahmad Khan, H. Shaman, S. Ahmed, R. Kumar, S. Deshpande, C. Subramani, N. Wadhwa, N. Gupta, A. K. Pandey, J. Bhattacharya, A. Agrawal, S. Vrati, S. Bhatnagar, P. K. Garg, and Department of Biotechnology India Consortium for COVID-19 research. "Effectiveness of ChAdOx1 nCoV-19 vaccine against SARS-CoV-2 infection during the delta (B.1.617.2) variant surge in India: a test-negative, case-control study and a mechanistic study of post-vaccination immune responses". *Lancet Infect. Dis.* 22.4 (Apr. 2022), pp. 473–482.
- [29] R. Keeton, M. B. Tincho, A. Ngomti, R. Baguma, N. Benede, A. Suzuki, K. Khan, S. Cele, M. Bernstein, F. Karim, S. V. Madzorera, T. Moyo-Gwete, M. Mennen, S. Skelem, M. Adriaanse, D. Mutithu, O. Aremu, C. Stek, E. du Bruyn, M. A. Van Der Mescht, Z. de Beer, T. R. de Villiers, A. Bodenstein, G. van den Berg, A. Mendes, A. Strydom, M. Venter, J. Giandhari, Y. Naidoo, S. Pillay, H. Tegally, A. Grifoni, D. Weiskopf, A. Sette, R. J. Wilkinson, T. de Oliveira, L.-G. Bekker, G. Gray, V. Ueckermann, T. Rossouw, M. T. Boswell, J. N. Bhiman, P. L. Moore, A. Sigal, N. A. B. Ntusi, W. A. Burgers, and C. Riou. "T cell responses to SARS-CoV-2 spike cross-recognize Omicron". *Nature* 603.7901 (Mar. 2022), pp. 488–492.
- [30] D. Martínez-Flores, J. Zepeda-Cervantes, A. Cruz-Reséndiz, S. Aguirre-Sampieri, A. Sampieri, and L. Vaca. "SARS-CoV-2 vaccines based on the Spike glycoprotein and implications of new viral variants". *Front. Immunol.* 12 (July 2021), p. 701501.
- [31] S. Elbe and G. Buckland-Merrett. "Data, disease and diplomacy: GISAID's innovative contribution to global health". *Global Chall.* 1.1 (Jan. 2017), pp. 33–46.
- [32] Y. Shu and J. McCauley. "GISAID: Global initiative on sharing all influenza data - from vision to reality". *Euro Surveill.* 22.13 (Mar. 2017).
- [33] R. Vita, S. Mahajan, J. A. Overton, S. K. Dhanda, S. Martini, J. R. Cantrell, D. K. Wheeler, A. Sette, and B. Peters. "The Immune Epitope Database (IEDB): 2018 update". *Nucleic Acids Res.* 47.D1 (Jan. 2019), pp. D339–D343.
- [34] IEDB.org. *Free Epitope Database and Prediction Resource*. <http://www.iedb.org>.
- [35] S. Frankild, R. J. de Boer, O. Lund, M. Nielsen, and C. Kesmir. "Amino acid similarity accounts for T cell cross-reactivity and for "holes" in the T cell repertoire". *PLoS One* 3.3 (Mar. 2008), e1831.
- [36] J. K. Lee, G. Stewart-Jones, T. Dong, K. Harlos, K. Di Gleria, L. Dorrell, D. C. Douek, P. A. van der Merwe, E. Y. Jones, and A. J. McMichael. "T cell cross-reactivity and conformational changes during TCR engagement". *J. Exp. Med.* 200.11 (Dec. 2004), pp. 1455–1466.
- [37] S. K. Dhanda, K. Vaughan, V. Schulten, A. Grifoni, D. Weiskopf, J. Sidney, B. Peters, and A. Sette. "Development of a novel clustering tool for linear peptide sequences". *Immunology* 155.3 (Nov. 2018), pp. 331–345.
- [38] P. Kvistborg, D. Philips, S. Kelderman, L. Hageman, C. Ottensmeier, D. Joseph-Pietras, M. J. P. Welters, S. van der Burg, E. Kapiteijn, O. Michielin,

- E. Romano, C. Linnemann, D. Speiser, C. Blank, J. B. Haanen, and T. N. Schumacher. "Anti-CTLA-4 therapy broadens the melanoma-reactive CD8+ T cell response". *Sci. Transl. Med.* 6.254 (Sept. 2014), 254ra128.
- [39] A. Gangaev, S. L. C. Ketelaars, O. I. Isaeva, S. Patiwaal, A. Dopler, K. Hoefakker, S. De Biasi, L. Gibellini, C. Mussini, G. Guaraldi, M. Girardis, C. M. P. T. Ormeno, P. J. M. Hekking, N. M. Lardy, M. Toebes, R. Balderas, T. N. Schumacher, H. Ovaa, A. Cossarizza, and P. Kvistborg. "Identification and characterization of a SARS-CoV-2 specific CD8+ T cell response with immunodominant features". *Nat. Commun.* 12.1 (May 2021), p. 2593.
- [40] J. J. A. Calis, M. Maybeno, J. A. Greenbaum, D. Weiskopf, A. D. De Silva, A. Sette, C. Keşmir, and B. Peters. "Properties of MHC class I presented peptides that enhance immunogenicity". *PLoS Comput. Biol.* 9.10 (Oct. 2013), e1003266.
- [41] B. Reynisson, B. Alvarez, S. Paul, B. Peters, and M. Nielsen. "NetMHCpan-4.1 and NetMHCIIpan-4.0: improved predictions of MHC antigen presentation by concurrent motif deconvolution and integration of MS MHC eluted ligand data". *Nucleic Acids Res.* 48.W1 (July 2020), W449–W454.
- [42] European Centre for Disease Prevention and Control. *COVID-19 Situation Update Worldwide, as of Week 7, Updated 24 February 2022*. <https://www.ecdc.europa.eu/en/geographical-distribution-2019-ncov-cases> (Accessed March 2, 2022).
- [43] E. Mathieu, H. Ritchie, L. Rodés-Guirao, C. Appel, D. Gavrilov, C. Giattino, J. Hasell, B. Macdonald, S. Dattani, D. Beltekian, E. Ortiz-Ospina, and M. Roser. "COVID-19 Pandemic". *Our World in Data* (2020). <https://ourworldindata.org/coronavirus>.
- [44] Outbreak.Info. <https://outbreak.info/> (Accessed March 2, 2022).
- [45] IEDB.org. *Free Epitope Database and Prediction Resource*. <http://www.iedb.org> (Accessed March 2, 2022).
- [46] GraphPad. www.graphpad.com (Accessed March 2, 2022).

Part 2.

3

PD-L1 blockade in combination with carboplatin as immune induction in metastatic lobular breast cancer: the GELATO trial

Published in: *Nature Cancer*, 4(4):535-549, 2023.

DOI: 10.1038/s43018-023-00542-x

Leonie Voorwerk^{1,*}, **Olga I. Isaeva^{1,*}**, Hugo M. Horlings², Sara Balduzzi³, Maksim Chelushkin^{1,4}, Noor A.M. Bakker^{1,5}, Elisa Champanhet¹, Hannah Garner^{1,5}, Karolina Sikorska³, Claudette E. Loo⁶, Inge Kemper⁷, Ingrid A.M. Mandjes³, Michiel de Maaker⁸, Jasper J.L. van Geel⁹, Jorianne Boers⁹, Maaïke de Boer¹⁰, Roberto Salgado^{11,12}, Marloes G.J. van Dongen⁷, Gabe S. Sonke⁷, Karin E. de Visser^{1,5,13}, Ton N. Schumacher^{5,14,15}, Christian U. Blank^{7,14}, Lodewyk F.A. Wessels^{4,5}, Agnes Jager¹⁶, Vivianne C.G. Tjan-Heijnen¹⁰, Carolien P. Schröder^{7,9}, Sabine C. Linn^{7,8,17}, Marleen Kok^{1,7}

*These authors contributed equally

3. PD-L1 blockade in combination with carboplatin as immune induction in metastatic lobular breast cancer: the GELATO trial

- 1 Division of Tumor Biology & Immunology, The Netherlands Cancer Institute, Amsterdam, the Netherlands.
- 2 Department of Pathology, The Netherlands Cancer Institute, Amsterdam, the Netherlands.
- 3 Department of Biometrics, The Netherlands Cancer Institute, Amsterdam, the Netherlands.
- 4 Division of Molecular Carcinogenesis, The Netherlands Cancer Institute, Amsterdam, the Netherlands.
- 5 Oncode Institute, Utrecht, the Netherlands.
- 6 Department of Radiology, The Netherlands Cancer Institute, Amsterdam, the Netherlands.
- 7 Department of Medical Oncology, The Netherlands Cancer Institute, Amsterdam, the Netherlands.
- 8 Division of Molecular Pathology, The Netherlands Cancer Institute, Amsterdam, the Netherlands.
- 9 Department of Medical Oncology, University Medical Center Groningen, Groningen, the Netherlands.
- 10 Department of Medical Oncology, GROW, Maastricht University Medical Center, Maastricht, the Netherlands.
- 11 Department of Pathology, GZA-ZNA hospitals, Antwerp, Belgium.
- 12 Division of Research, Peter Mac Callum Cancer Centre, Melbourne, Australia.
- 13 Department of Immunology, Leiden University Medical Center, Leiden, the Netherlands.
- 14 Division of Molecular Oncology & Immunology, The Netherlands Cancer Institute, Amsterdam, the Netherlands.
- 15 Department of Hematology, Leiden University Medical Center, Leiden, the Netherlands.
- 16 Department of Medical Oncology, Erasmus Medical Center, Rotterdam, the Netherlands.
- 17 Department of Pathology, University Medical Center Utrecht, Utrecht, The Netherlands.

Invasive lobular breast cancer (ILC) is the second most common histological breast cancer subtype, but ILC-specific trials are so far lacking. Translational research revealed an immune-related ILC subset and in murine ILC models, synergy between immune checkpoint blockade and platinum was observed. In the phase II, GELATO-trial (NCT03147040), patients with metastatic ILC were treated with weekly carboplatin (AUC1.5) as immune induction for 12 weeks and atezolizumab (PD-L1 blockade; triweekly) from the third week until progression. Four of 23 evaluable patients had a partial response (17%) and two had stable disease, resulting in a clinical benefit rate of 26%. From these six patients, four had triple-negative ILC (TN-ILC). We observed higher CD8 T-cell infiltration, immune checkpoint expression, and exhausted T cells upon treatment. GELATO is an ILC-specific clinical trial. We demonstrate promising anti-tumor activity of atezolizumab

with carboplatin, particularly for TN-ILC, and provide insights for design of highly needed ILC-specific trials.

3.1. Introduction

Invasive lobular breast cancer (ILC) is the second most common histological breast cancer subtype, comprising approximately 10-15% of cases [1-3]. The non-cohesive and single file or targetoid pattern observed on routine histology is characteristic for the morphological diagnosis of ILC and loss or aberrant expression of E-cadherin supports the diagnosis of ILC [4]. Approximately 80-90% of primary ILCs express estrogen receptor (ER), have a luminal A phenotype and can be considered classic ILC [5, 6]. Approximately 5% of ILC are triple-negative (TN) and frequently exhibit a luminal phenotype implying that this subtype has a different biology compared to the majority of triple-negative breast cancer (TNBC) that is dominated by basal-like tumors [1, 7, 8].

Patients with ER+ metastatic ILC have preferred metastatic spread to the gastrointestinal tract and bone [2, 6] and a worse overall survival as compared to patients with ER+ metastatic breast cancer of no special type (NST) [1], highlighting the need for new treatment modalities. CDK4/6 inhibitors combined with endocrine treatment are an effective treatment option for patients with metastatic ER+ ILC [9], but no other highly effective treatment options have been defined once patients become resistant to endocrine treatment. Although ILCs are a different disease entity as compared to NST, so far patients with ILC have been underrepresented in clinical trials for breast cancer [10] and reports of clinical trials specifically for ILC are lacking.

Several groups have shown that based on transcriptomic profiling a subgroup of ILCs can be characterized as immune-related (IR) with high levels of immune-related genes, expression of immune checkpoints and lymphocytic infiltration [5, 11, 12]. This suggests that a subset of ILCs might benefit from immune checkpoint blockade (ICB). While ICB in combination with chemotherapy has become standard of care in PD-L1 positive metastatic TNBC [13], in patients with ER+ breast cancer only a small subgroup of patients benefits from ICB. Objective response rates (ORR) to ICB monotherapy in metastatic ER+ breast cancer (including all histological subtypes) range from 3%-12% [14, 15] to 27%-41% in combination with eribulin [16, 17]. Notably, in the KEYNOTE-028 for patients with metastatic PD-L1 positive ER+ breast cancer, two out of three responders were ILC patients [15]. Rational treatment combinations are needed to improve responses to ICB in ER+ breast cancer and in ILC specifically.

Previous data indicates synergy between platinum compounds and ICB in genetically engineered mouse models for ILC [18]. Of note, while these models strongly resemble human ILC, the field traditionally lacks models for endocrine-sensitive ILC [19, 20]. Additionally, immune-

related ILCs, characterized by expression of immune-related genes, were responsive to DNA damaging agents, such as platinum, *in vitro* [11]. Mechanistically, platinum agents have been shown to trigger the cyclic GMP-AMP synthase (cGAS) - stimulator of interferon (IFN) genes (STING) pathway by increasing the amounts of cytosolic DNA [21] and to increase MHC class I expression [22]. Based on these data, we hypothesize that the combination of platinum-based chemotherapy and ICB could be effective in patients with ILC.

Here, we report the clinical and translational results of stage I of the GELATO-trial, in which patients with metastatic ILC were treated with anti-PD-L1 until disease progression, combined with low-dose carboplatin as immune induction. To dissect the immunomodulatory effects of carboplatin alone and in combination with anti-PD-L1, we profiled immune cells in the circulation and in the tumor microenvironment of longitudinal biopsies of metastatic lesions. Besides PD-L1 expression, stromal tumor-infiltrating lymphocyte (sTIL) and CD8+ T-cell levels, deconvolution algorithms and specific immune-related gene signatures were used to dissect the effect on the various T-cell populations as well as on other elements of the cancer-immunity cycle. In addition, we studied paired primary tumors and metastatic lesions to unravel differences in the immune landscape during ILC disease progression. Finally, we studied whether carboplatin is able to modulate PD-L1 expression patterns across different metastatic lesions, using molecular imaging (^{89}Zr -atezolizumab-PET [23]). The GELATO-trial is the earliest reported clinical trial specifically conducted in patients with ILC, and our results provide insights in the biology of metastatic ILC.

3.2. Results

Inclusion and patient demographics

In the GELATO-trial, patients with metastatic ILC (based on morphology and a negative or aberrant E-cadherin staining) were treated with weekly carboplatin (area under the curve (AUC) 1.5) for the first 12 weeks and atezolizumab (anti-PD-L1) every three weeks starting from the third cycle of carboplatin onwards (**Figure 3.1A**). The purpose of this short-term platinum-based regimen was to exploit the immunological effects of carboplatin and potentially synergize with PD-L1 blockade, and not to induce direct cytotoxic effects. The low and weekly dosing was chosen to minimize the risk of hematological toxicity in this heavily pretreated patient population [24, 25]. Following a Simon's two-stage design, 22 patients had to be accrued in the first stage of the trial. Based on a null hypothesis of 10% of patients being progression-free at 24 weeks and an alternative hypothesis of 25%, three out of 22 patients had to

be progression-free at 24 weeks to allow continuation of accrual in the second stage of the trial. Between November 2017 and January 2021, 26 female patients with metastatic ILC were registered in the trial, of which 23 patients started anti-PD-L1 treatment (**Supplementary Figure 3.5**) with the last two patients being registered simultaneously. Eighteen patients had ER+HER2- metastatic disease, whereas five patients had triple-negative disease (**Table 3.1**). Four out of five patients with TN-ILC had ER+ primary ILC. Six patients had non-classical ILC based on morphological assessment of a metastatic lesion biopsy. Seventy-eight percent (n=18) of patients had visceral metastases, with 52% (n=12) of patients having liver metastases and 48% (n=11) having three or more metastatic sites, all higher compared to other studies [1, 6] and inherent to our eligibility criteria for biopsy site availability. Seventy-eight percent (n=18) of patients received prior chemotherapy, with 52% (n=12) of patients receiving prior palliative chemotherapy. Ninety-four percent (n=17) of patients with ER+ disease received prior CDK4/6 inhibitors and 40% (n=2) of patients with TN-ILC received prior platinum. Patients received a median of nine cycles of weekly carboplatin and five cycles of anti-PD-L1.

Efficacy

Four patients out of the 23 evaluable patients (per protocol population) had a partial response (PR), leading to an objective response rate (ORR) of 17% (95% CI 5-39%) with two responses being short-lived. The median duration of response was 14.9 weeks. Two additional patients had stable disease (SD) or non-complete response (non-CR)/non-progressive disease (non-PD) for at least 24 weeks, resulting in a clinical benefit rate of 26% (95% CI 10-48%, **Table 3.2, Figures 3.1B-D**). Remarkably, four out of these six patients with clinical benefit had TN-ILC (**Figure 3.1B**). Four out of the first 22 patients were free of progression at 24 weeks, meeting the primary endpoint of the first stage of the trial for which at least three responders were needed. However, as responses were generally short-lived and observed mainly in patients with TN-ILC, the trial stopped accrual after the first stage was completed. One patient has an ongoing partial response even after PD-L1 blockade was stopped due to toxicity (**Figure 3.1B**). With a median follow-up of 23.8 months, we observed a median overall survival of 54.4 weeks. Patients with clinical benefit had numerical favorable survival as compared to patients with no clinical benefit, either upon analyzing patients alive after 24 weeks (**Figure 3.1E**, HR 0.13, p = 0.07) or using a time-dependent Cox model (HR 0.26, p = 0.108).

Toxicity

Carboplatin and anti-PD-L1 were generally well tolerated, with 26% and 48% of patients, respectively, not experiencing any treatment-related

3.2. Results

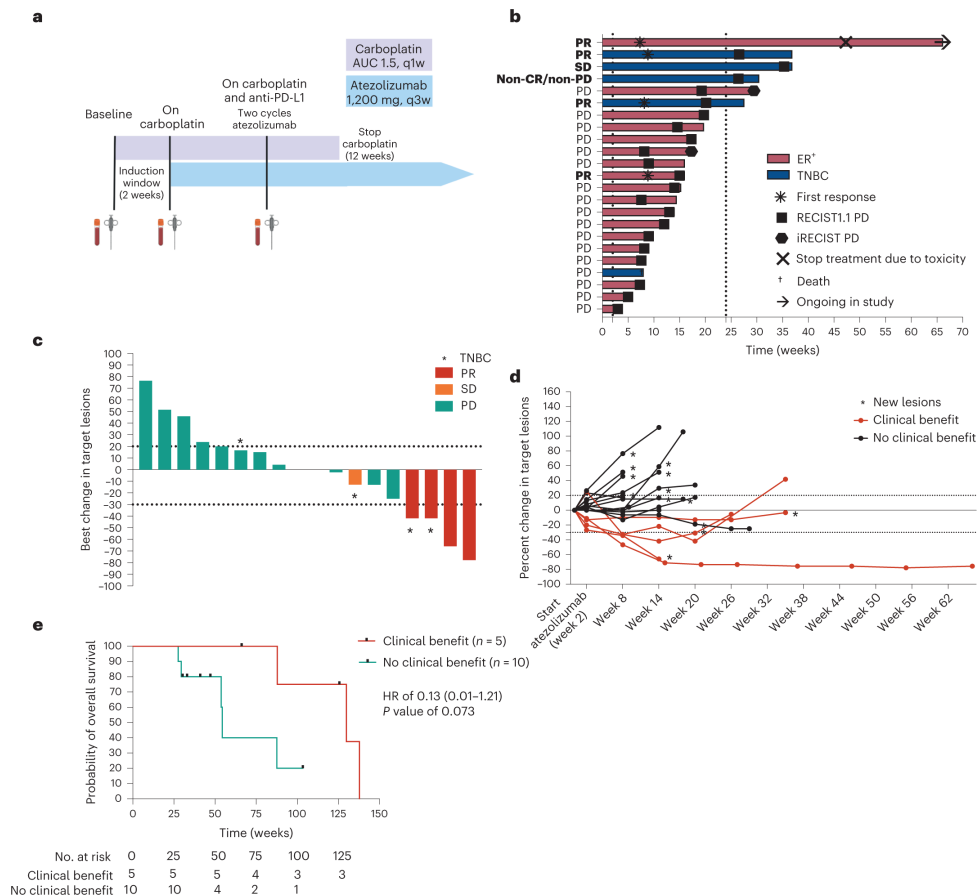


Figure 3.1: Design of GELATO-trial and efficacy data. (A) GELATO-trial setup. Patients were treated with 12 cycles of low-dose carboplatin. Atezolizumab (anti-PD-L1) was added from the third cycle onwards until disease progression or toxicity. Biopsies and blood were taken at baseline, before the start of anti-PD-L1 and during carboplatin+anti-PD-L1. Created with BioRender.com. (B) Swimmer's plot of all included patients. N = 23 patients. Each bar reflects one patient and is annotated with events indicated by the legend and clinical response according to RECISTv1.1. The dotted lines indicate the start of anti-PD-L1 at two weeks and the 24-week landmark of the primary endpoint. (C) Waterfall plot of patients with measurable disease. N = 18 patients. (D) Change in target lesions of patients with measurable disease. N as in (C). (E) Kaplan-Meier curve of overall survival with a 24-week landmark in patients with clinical benefit versus no clinical benefit. N = 15 patients. The table lists numbers at risk at indicated timepoints. A 24-week landmark was used, causing 8 patients to be removed from the analysis (1 patient with clinical benefit and 7 patients with progressive disease). Hazard ratio (HR) calculated with Cox regression analysis on the patients alive at 24 weeks, including the 95% confidence interval and p-value.

3. PD-L1 blockade in combination with carboplatin as immune induction in metastatic lobular breast cancer: the GELATO trial

Table 3.1: Baseline characteristics of evaluable patients in the per protocol population.

N = 23 evaluable patients		No. (%)
Age at inclusion, years	median (range)	60 (45-69)
WHO performance status	WHO 0	12 (52)
	WHO 1	11 (48)
Histological subtype (assessed on metastatic lesion)*	ER+HER2-	18 (78)
	TNBC	5 (22)
	HER2+	0 (0)
ILC subtype (assessed on metastatic lesion)	Classic	17 (74)
	Pleiomorphic^	4 (17)
	Alveolar	2 (9)
Germline BRCA1/2 mutations	gBRCA1 mutation	1 (4)
	No mutation	4 (17)
	Unknown	18 (78)
Visceral metastasis		18 (78)
Liver metastasis		12 (52)
No. of metastatic sites	1-2 metastatic sites	12 (52)
	≥ 3 metastatic sites	11 (48)
LDH	LDH ≤ ULN	15 (65)
	LDH ≤ 2x ULN	8 (35)
Previous chemotherapy exposure	Chemotherapy naive	5 (22)
	(Neo)-adjuvant	15 (65)
	Palliative	12 (52)
Previous platinum treatment	ER+	0 (0)
Previous exposure to CDK4/6 inhibitors	TNBC	2 (40% of TNBC)
	ER+	17 (94% of ER+)
Disease-free interval	TNBC	0 (0)
	De novo M1	5 (22)
	DFI ≤ 5 years	12 (52)
	DFI >5 years	6 (26)
No. of cycles carboplatin	median (range)	9 (3-12)
No. of cycles atezolizumab (anti-PD-L1)	median (range)	5 (1-16)

* ER+ ≥10% expression, TNBC defined as having ER and PR <10% and HER2-. 4/5 patients with triple-negative metastases had a primary ER+ tumor.

^ Two of the patients had TNBC. World Health Organization (WHO), lactate dehydrogenase (LDH).

Table 3.2: Efficacy analysis of evaluable patients in the per protocol population.

N = 23 evaluable patients	Best overall response (RECIST1.1), no (%)
Complete response (CR)	0 (0)
Partial response (PR)	4 (17)^
Stable disease (SD) or non-CR/non-PD >24 weeks*	2 (9)
Progressive disease (PD)	17 (74)
Objective response rate (CR+PR)^	17% (95%CI: 5-39%)
Clinical benefit rate (CR+PR+SD>24 weeks)	26% (95%CI: 10-48%)
Median duration of response	14.9 weeks (95%CI: 6.1 weeks – not reached)
Median progression-free survival according to RECIST1.1 (22 events)	13 weeks (95%CI: 8.1 – 19.7 weeks)
Median progression-free survival according to iRECIST (22 events)	14 weeks (95%CI: 9.0 – 20.14 weeks)
Median overall survival (16 events)	54.4 weeks (95%CI: 23.6 weeks – not reached)

* 1 patient had stable disease of 24 weeks according to iRECIST. Confidence interval (CI).

^ one partial response was unconfirmed.

adverse events (**Table 3.3**). The most commonly observed adverse event induced by carboplatin was neutropenia, which occurred in 48% of patients (**Table 3.4**). Anti-PD-L1 caused an increase in aspartate aminotransferase (ASAT) in 17% of patients, with only one patient having a grade 4 increase requiring corticosteroid treatment (**Table 3.5**). Other relevant immune-related events were hypophysitis and colitis, occurring in two patients and one patient, respectively (**Table 3.5**). No other endocrinopathies, such as thyroid dysfunction, were reported. One patient experienced immune-related myalgia and an immune-related sarcoid-like reaction of the mediastinal lymph nodes, cytologically confirmed granulomatous inflammation, and subsequent hoarseness. This patient stopped anti-PD-L1, was treated with steroids and had an ongoing response at the time of data cut-off.

Exploratory associations with clinical benefit

Patients with TN-ILC had a significantly higher clinical benefit rate as compared to patients with ER+ILC ($p=0.008$, **Figure 3.2A**). We observed a non-significant higher clinical benefit rate in patients without liver metastases ($p=0.07$), in line with previous findings that liver metastases might have detrimental effects on immunotherapy efficacy [26]. Looking into immune features of the metastatic lesions, we observed low baseline stromal tumor-infiltrating lymphocytes (sTILs, median 1%) and stromal CD8 T-cell levels (median 1.5%), and no association between sTILs

or CD8+ T cells and clinical benefit (**Figure 3.2B**, **Supplementary Figure 3.6A**). A higher clinical benefit rate was observed in patients with PD-L1 positive tumors ($\geq 1\%$ expression on immune cells, SP142, **Figure 3.2C**), but this was not statistically significant. Using RNA sequencing, we assessed previously established gene signatures of response to ICB. An IFN γ signature [27], exhausted T-cell signature [28], tertiary lymphoid structure (TLS) signature [29] and a signature capturing immune checkpoint molecules [30], were all not significantly associated with clinical outcome (**Supplementary Figures 3.6B-E**). Of note, the patient with an ongoing durable response at data cut-off had high levels of stromal CD8+ cells (50%) and relatively high expression of immune-related genes, suggesting that, although rare in ILC, patients with high immune infiltration can benefit from ICB. We observed several genomic alterations in metastatic lesions with a well described role in metastatic ILC [31–33], with PIK3CA being the most frequently mutated gene (**Figure 3.2D**). There was a non-significantly higher total tumor mutational burden (TMB) in responders ($p=0.15$; **Figure 3.2E**) and in patients with TN-ILC ($p=0.10$, **Supplementary Figure 3.6F**). Additionally, 41% of the lesions demonstrated an APOBEC enrichment profile (**Figure 3.2D**) [31], and APOBEC and cytosine deamination comprised the most prominent mutational signatures enriched in the data (**Supplementary Figure 3.6G**).

Tumor-immune evolution of primary tumors to metastasis

To study the evolution of the immune landscape between matched primary lesions and metastases in ILC, we collected archival primary tumors and local recurrences (characteristics of this patient subset in **Table 3.6**). We observed slightly higher sTIL levels ($p=0.03$) in metastases compared to primary tumors, while this was not accompanied by a significant increase in PD-L1 and CD8 T cells (**Supplementary Figures 3.3A-C**). Using CIBERSORTx immune cell deconvolution [34] on gene expression data, we observed little immune infiltration across tumors and across timepoints, with M2 macrophages being the most abundant cell type (**Supplementary Figures 3.8A-B**), and confirmed that CD8 T-cell levels did not differ between paired primary and metastatic lesions (**Figure 3.3A**). Resting mast cells and memory B cells were the only immune cell populations that were significantly lower in metastases (**Figures 3.3B-C**). Furthermore, we applied the four previously assessed immune-related signatures and found no significant changes in expression of IFN γ -related genes, exhausted T cells, TLS or immune checkpoints (**Supplementary Figures 3.7D-G**). Looking at differences in genomic profiles, we found non-significantly higher TMB in metastases as previously described [31, 32] (**Figure 3.3D**). To assess other biological differences between paired primary tumors and metastases, we performed a gene set enrichment analysis (GSEA)

3.2. Results

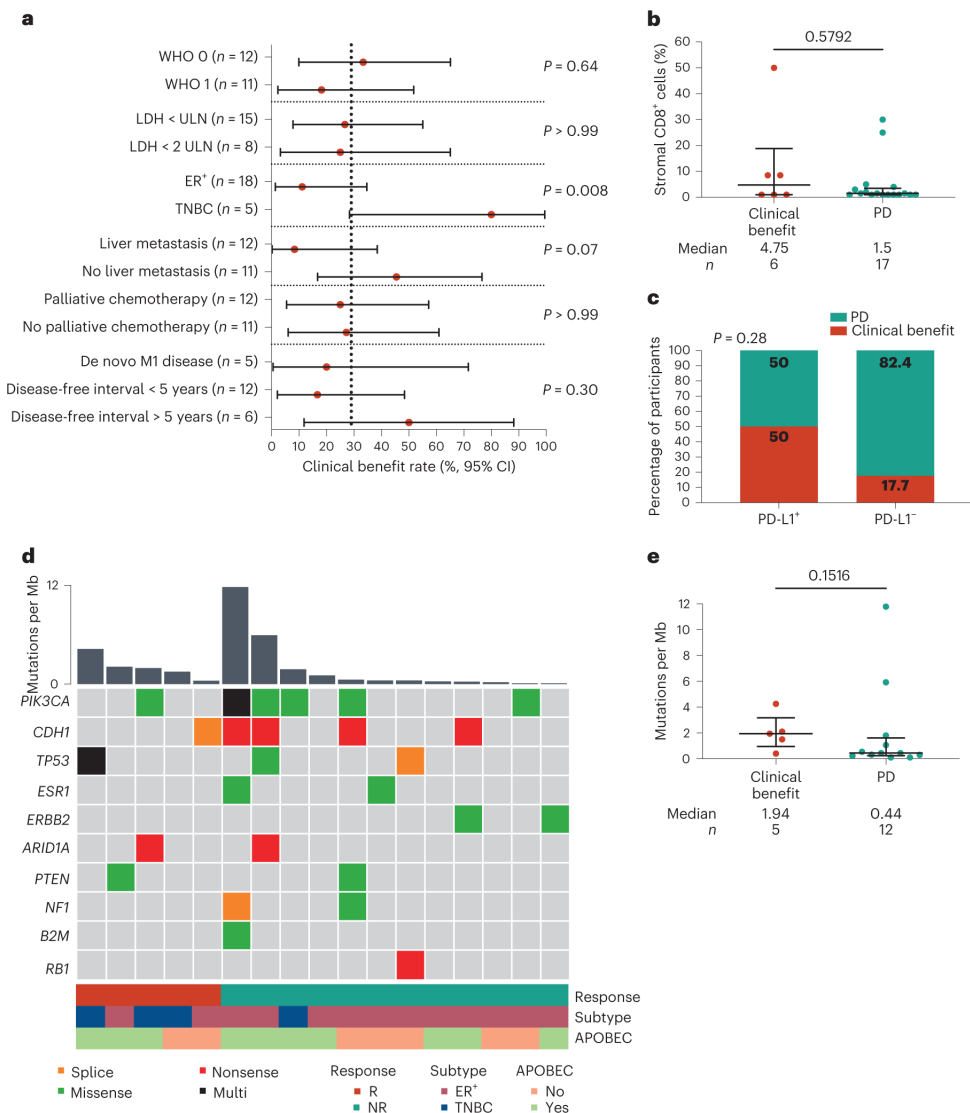


Figure 3.2: Association of baseline clinical features and characteristics of the tumor microenvironment with clinical benefit. (A) Clinical benefit rate with 95% confidence interval (shown as error bars) per indicated subgroup. N = 23 patients. Statistics by two-sided Fisher's exact test (two groups) or Chi-square test (multiple groups). (B) Percentage of CD8⁺ cells in the stromal area of a metastatic lesion (immunohistochemistry). Median with interquartile range, statistics by two-sided Mann-Whitney-U test. N as in (A). (C) Percentage of patients with clinical benefit and PD-L1 expression (clone SP142). A cut-off of 1% expression on immune cells for PD-L1 positivity was used. Numbers in the graph indicate percentages, statistics by two-sided Fisher's exact test. N as in (A). (D) OncoPrint of tumor mutational burden (TMB, mutations per Mb) and selected genes frequently altered in metastatic ILC [31–33], assessed in biopsies of metastatic lesions. Data was available for 17 patients. Each column represents one patient and is annotated by response, subtype and enrichment of the APOBEC mutational signature. (E) TMB of metastatic lesions in relation to response. N as in (D). Median with interquartile range, Statistics as in (B). (B)-(E) Baseline metastatic lesions correspond to metastases presented in Figure 3.3 and Supplementary Figures 3.7 and 3.8.

of the Hallmark gene sets [35] (**Supplementary Figures 3.8C-D**). In metastases, we observed enrichment of glycolysis and oxidative phosphorylation gene sets (**Supplementary Figures 3.7H-I**), indicative of increased cellular respiration, and enrichment of MYC targets and mTOR signaling (**Supplementary Figures 3.7J-K**), suggestive of acquired signaling pathway alterations. Altogether, we observed subtle differences between primary and metastatic lesions but the immune landscape remained largely unaffected.

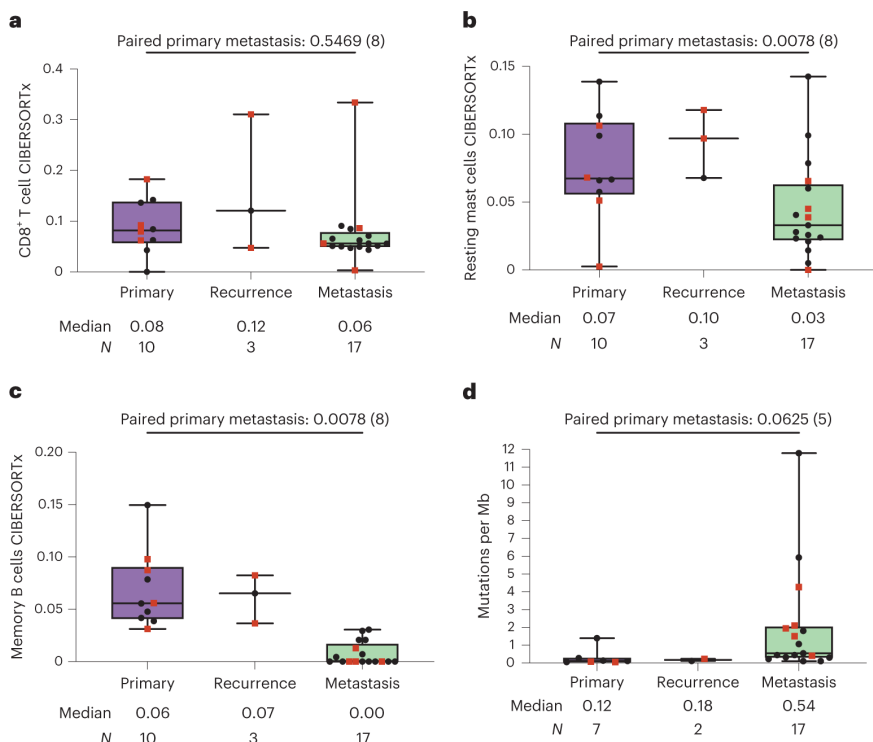


Figure 3.3: Tumor-immune evolution in paired primary tumors, local recurrences and metastasis. (A) Gene set expression score of CD8 T cells according to CIBERSORTx in paired primary tumors, recurrences, and metastasis. N = 30 samples. (B) Gene set expression score of resting mast cells according to CIBERSORTx in paired primary tumors, recurrences, and metastasis. N as in (A). (C) Gene set expression score of memory B cells according to CIBERSORTx in paired primary tumors, recurrences, and metastasis. N as in (A). (D) TMB in paired primary tumors, recurrences, and metastases. N = 26 samples. (A)-(D). Boxplots display a minimum (Q0), a maximum (Q4), a median (Q2) and the interquartile range. Statistics by two-sided Wilcoxon-signed-rank test on paired primary tumors and metastases, the number of patients in each analysis are listed between brackets behind the p-value. Red squares indicate patients with clinical benefit, black dots patients with no clinical benefit. Metastatic lesions correspond with baseline samples presented in **Figure 3.2**, **Figure 3.4**, **Supplementary Figures 3.6**, **3.8** and **3.10**.

Treatment-mediated changes in circulating immune cells

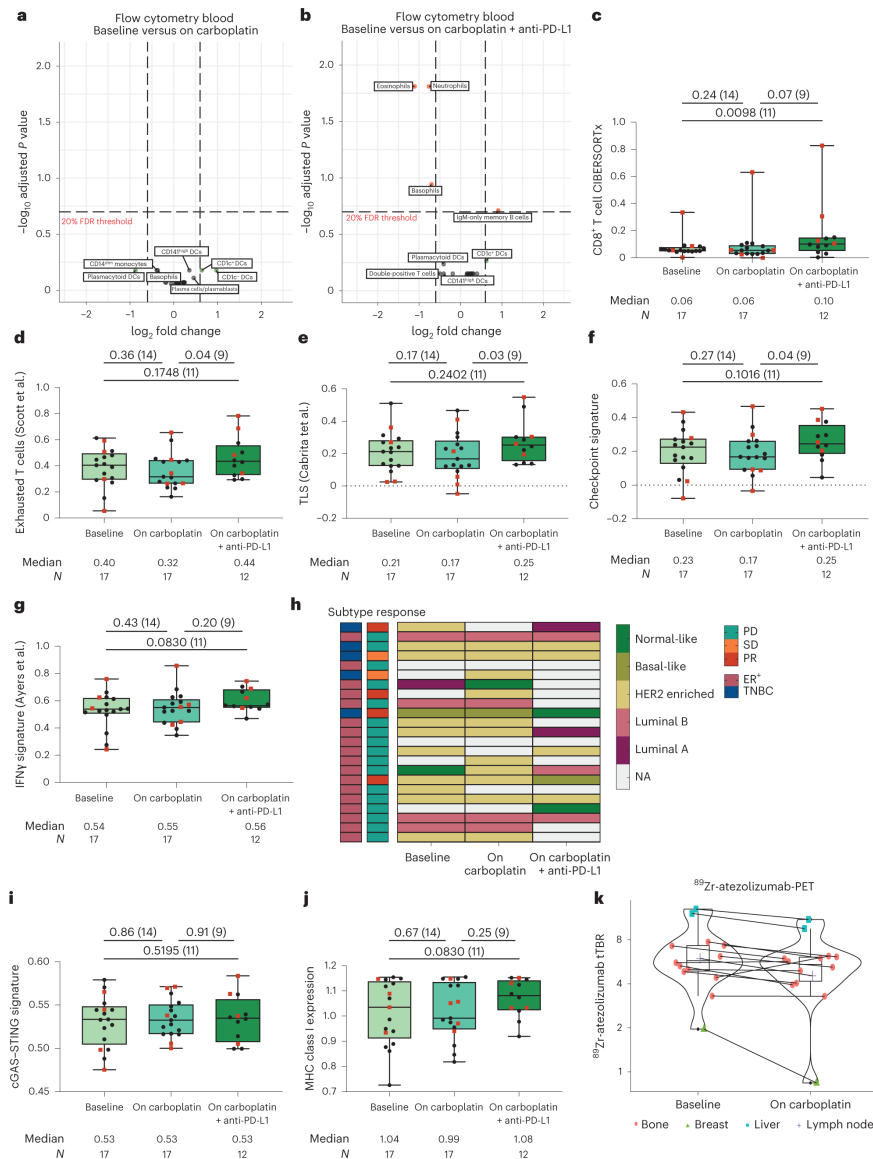
Several circulating immune cell populations can be affected by ICB, resulting in increased exhausted T cells, eosinophils or a decreased

neutrophil-to-lymphocyte ratio (NLR) [36–38]. To investigate this in ILC, we characterized absolute counts of immune cell populations in fresh blood by flow cytometry at baseline, during carboplatin, and during carboplatin+anti-PD-L1 (**Table 3.7**). After two cycles of carboplatin, no major changes were observed in circulating immune cells (**Figure 3.4A**), but after carboplatin and anti-PD-L1 we observed a significant decrease in neutrophils, basophils, eosinophils and the NLR, probably related to the cumulative carboplatin effect (**Figure 3.4B**, **Supplementary Figures 3.9A–B**). Circulating total T cells, CD4+ and CD8+ T cell levels remained unaffected (**Supplementary Figures 3.9C–E**) but we observed a significant increase upon carboplatin and anti-PD-L1 in circulating PD-1+CTLA4+ CD8+ T cells (**Supplementary Figures 3.9F–G**). This suggests systemic reinvigoration of a dysfunctional or exhausted T cell population that is frequently used as a proxy for the presence of a tumor-reactive T-cell compartment [39].

Treatment-induced changes in the tumor microenvironment

Next, we assessed treatment-induced changes by carboplatin and anti-PD-L1 within the tumor microenvironment (TME) of ILC metastases. Using CIBERSORTx immune cell deconvolution [34], we observed increased CD8 T cells during anti-PD-L1, most notably in the patient with a durable response (**Figure 3.4C**), and the same pattern was seen when analyzing CD8 using immunohistochemistry (IHC) (**Supplementary Figure 3.10A**). sTIL levels remained largely unaffected (**Supplementary Figure 3.10B**). Interestingly, while mast cells decreased during ILC disease progression (**Figure 3.3B**), resting mast cells increased during carboplatin (**Supplementary Figure 3.10C**). Next, we assessed immune-related gene signatures and observed a significant increase after carboplatin and anti-PD-L1 in exhausted T cells [28], TLSs [29] and immune checkpoint expression [30], and a trend towards a higher IFN γ signature score, but only when compared to the on-carboplatin timepoint (before the start of anti-PD-L1) indicating a subtle decrease of these signatures upon carboplatin alone (**Figures 3.4D–G**). Next, we investigated changes in PAM50 molecular subtype during treatment in the metastatic setting. We observed that the majority of tumors (59%, 10 out of 17) were classified as HER2-enriched at baseline (**Figure 3.4H**), while patients had no HER2-overexpression or amplification. Notably, we observed that the PAM50 subtype changed in six out of 16 patients during treatment with carboplatin with or without anti-PD-L1, of which three were responders. High proportions of HER2-enriched metastases have been observed before in breast cancer, possibly due to disease progression in a more aggressive phenotype [41, 42]. Finally, we tested our preclinical hypotheses on immunogenic effects of carboplatin and, surprisingly, did not see alterations in gene signatures for cGAS-STING [40], immunogenic cell death [43], MHC class I or MHC class

3. PD-L1 blockade in combination with carboplatin as immune induction in metastatic lobular breast cancer: the GELATO trial



II (**Figures 3.4I-J, Supplementary Figures 3.10D-E**). In conclusion, induction with two cycles of carboplatin did not lead to major changes in the TME, but the combination of carboplatin and anti-PD-L1 was able to induce immune infiltration by CD8 T cells and increased expression of immune-related genes.

PD-L1 uptake after carboplatin by ^{89}Zr -atezolizumab-PET

To investigate the effect of carboplatin on the TME in a non-invasive fashion, which could be particularly attractive for ILC where biopsies can be challenging to obtain, we explored the use of ^{89}Zr -atezolizumab-PET. Repeated ^{89}Zr -atezolizumab-PET could be performed in one patient, who had two measurable lesions on computed tomography (CT) scan (breast, liver), and twelve other lesions on FDG-PET at baseline (**Supplementary Figure 3.11**). Heterogeneous ^{89}Zr -atezolizumab uptake between the lesions was observed, at baseline and after two cycles of carboplatin. Contrary to the hypothesis of PD-L1 induction by carboplatin, but in line with lack of clinical treatment benefit in this patient, the median tumor-to-blood ratio (TBR) decreased after induction treatment ($p=0.01$; **Figure 3.4K**) particularly in the index breast lesion. Meanwhile the maximal standardized uptake value (SUVmax) of this lesion remained low (2.13 and 1.2 respectively), in line with its negative PD-L1 IHC (0% in immune cells) at baseline and after carboplatin. Concluding, repeated ^{89}Zr -atezolizumab-PET showed heterogeneity in dynamics of tracer uptake in tumor lesions and background during carboplatin treatment.

3.3. Discussion

To our knowledge, the GELATO-trial is the earliest reported clinical trial conducted specifically in ILC patients based on a hypothesis founded on preclinical and translational data. While carboplatin alone neither led to significant changes in immune cell composition nor in an increase in cGAS-STING signaling or MHC class I expression, the addition of anti-PD-L1 caused an increase in CD8 T-cell infiltration and higher expression of immune-related gene signatures. Four out of the first 22 patients were progression-free at 24 weeks in the first stage of the trial, warranting expansion of the trial according to the Simon's two-stage design. However, responses were mainly observed in patients with TN-ILC and responses were not durable. This suggests that most responses could have been mainly induced by carboplatin and to a lesser extent by anti-PD-L1, since carboplatin monotherapy is effective in approximately 30% of patients with metastatic TNBC [24]. Since ICB plus chemotherapy is now standard of care for patients with PD-L1 positive ($\geq 10\%$ combined positive score, 22C3) metastatic TNBC [13], regardless of histological subtype, the study team decided, despite

meeting the success criteria for stage I, not to proceed to the next stage of the GELATO-trial. The lack of responses to anti-PD-L1 in ER+ ILC could be partially explained by not pre-selecting patients based on a pre-existing anti-tumor immune phenotype. Important in this context is that in prior studies, the vast majority of immune-related ILCs was ER-positive. We illustrate this by one ER+ ILC patient with a clear durable response of over one year, with a TME characterized by high sTILs, CD8+ T-cell levels and positive PD-L1 expression at baseline. This indicates that, although rare, ILC patients with an immunogenic phenotype might benefit from ICB.

Recent research has suggested that TN-ILCs have different biological characteristics as compared to TN-NST and ER+ ILC, with increased androgen receptor (AR) signaling and a higher frequency of HER2 mutations [8, 44]. Though approximately 2% of patients with primary ILC and 12-15% of patients with metastatic ILC harbor a HER2 mutation and 90% of primary ILCs are considered AR-positive [45], among TN-ILC 20% of the tumors harbor a HER2 mutation and 74%-94% of tumors express AR [8, 44]. In GELATO, four out of five patients with TN-ILC had ER+ primary tumors, and all patients with TN-ILC had positive AR IHC expression ($\geq 10\%$ of tumor cells). Recently, it has been shown that AR inhibition and ICB synergize in vivo, by reduced suppression of $\text{Ifn}\gamma$ via AR signaling in CD8+ T cells [46]. Also, estrogen signaling has been negatively associated with response to ICB and chemotherapy in metastatic TNBC [47] and metastatic ER+ breast cancer [48]. Recently, it has been shown that estrogen might polarize tumor-associated macrophages towards an immunosuppressive state in melanoma models [49]. Polarized tumor-associated macrophages have been associated with residual disease post-chemotherapy in ER+ breast cancer [50] and with poor survival in ILC patients [51]. In our CIBERSORTx analysis, we indeed found M2 macrophages as the most abundant cell type across samples (**Supplementary Figures 3.8A-B**). Therefore, targeting AR or macrophages might help to overcome ICB resistance in ILC.

Only one patient with TN-ILC was classified as basal-like by PAM50 in the metastatic setting and four out of five patients with TN-ILCs had ER+ primary tumors. This implicates that although ER expression was lost during disease progression, TN-ILCs do not exhibit a clear basal-like phenotype. A basal-like phenotype has been associated with response to ICB and chemotherapy in early-stage high-risk ER+ breast cancer [52] and a basal-like immune-activated phenotype in metastatic TNBC [47].

Interestingly, most metastases were classified as HER2-enriched. This might be an artefact of PAM50 assessment on metastatic lesions and/or fresh-frozen material. However, also in paired lesions of the AURORA program for metastatic breast cancer and another retrospective series,

a particular high proportion of HER2-enriched tumors was observed [41, 42]. The high level of HER2-enriched lesions might be due to the more aggressive features of metastatic disease, and endocrine treatment refractory disease potentially losing its luminal features upon disease progression [41]. Furthermore, in the recent BioPER trial, after treatment with a CDK4/6-inhibitor, 37.5% of the samples showed an HER2-enriched subtype [53], suggesting that HER2-enriched tumors are prominent in patients that are heavily pretreated and/or have been exposed to CDK4/6 inhibition, as was the case for 94% of ER-positive GELATO patients. Interestingly, in GELATO 90% of primary tumors were classified as either luminal A or luminal B (**Supplementary Table 3.6**), suggestive of an acquired HER2-enriched phenotype later in the disease course.

During treatment with carboplatin with or without anti-PD-L1, we also observed PAM50 subtype switching in 6/16 patients of which 5 switched towards a luminal or normal-like phenotype. Since we studied serial biopsies of the same lesions, this suggests that treatment modified the tumor-intrinsic characteristics of these lesions towards a less proliferative phenotype. Most notably, the baseline metastatic lesion of the patient with a durable response was characterized as HER2-enriched but switched to a basal-like phenotype during anti-PDL1, suggesting increased susceptibility to ICB.

On the immune cell level, we observed higher levels of CD8+ T cells in the stroma as compared to stromal TILs. As CD8+ T cells comprise the most prevalent immune cell type captured by the sTILs readout [54], this is surprising. Since both sTILs and CD8+ counts were scored by the same independent expert pathologists, it is unlikely that interrater variability played a major role here. Alternatively, we hypothesize that based on its morphology, sTILs can be easily misunderstood for tumor cells in ILC, and sTILs might therefore not be the appropriate read-out for anti-tumor immunity in ILC. Research comparing sTILs in ILC with other subtypes might have underestimated sTILs scores in ILC and incorporating a CD8 staining may improve immune assessment in patients with ILC.

Our trial is limited by a small sample size and lack of a control arm. Of note, the inclusion of a relatively small number of patients (n=23) in high-volume breast cancer centers took approximately 3.5 years. In view of the priority for translational research, patients with bone-only disease or only small lesions in, for example, the peritoneum could not participate due to the lack of an available biopsy site, which might have slowed down inclusion. Since serial biopsies were mandatory in the trial, we included a relatively high proportion of ILC patients with visceral metastasis (18 out of 23), higher as compared to the general ILC population [1], making our cohort not fully representative of the general ILC population. Additionally, the included patients comprise a

heterogenous group characterized by different pre-treatment regimens, biopsy locations and hormone receptor status. Due to the small number of patients, our translational analyses should be considered exploratory. However, given the strong preclinical rationale behind the GELATO-trial, we would like to highlight the importance of the validation of preclinical findings in patients which was the main reason to execute the GELATO-trial.

Although ILCs comprise a separate disease entity within the breast cancer subtypes, so far reports of clinical trials specific for patients with ILC were lacking [55] and patients with metastatic ILC are often underrepresented because of a lack of measurable disease [10]. In our experience, several patients stopped treatment early due to rapid clinical progression (**Supplementary Figure 3.5**). These aspects of the disease complicate the inclusion of ILC patients in clinical trials. Moreover, to our knowledge only two reports of recent randomized trials for novel treatment options in ER+ metastatic breast cancer have presented prespecified subgroup analysis in ILC patients, namely benefit from CDK4/6 inhibition to endocrine treatment in patients with metastatic ER+ILC [9] and more recently a high clinical benefit rate was observed to neratinib and fulvestrant in HER2-mutated ILC in the phase II MutHER trial [56]. Targetable features of ILC are for example: high expression of ER/luminal A phenotype, synthetic lethal deficiency of ROS1/E-cadherin [57], high tumor-mutational burden [31, 32], high T-cell infiltration [5, 11, 12] and downstream activation of the PI3K-AKT-mTOR pathway via activating PIK3CA mutations [5, 31], activating HER2 mutations [31, 33] or activation via the insulin-like growth factor 1 receptor (IGF1R) [58]. Some of these concepts are currently under investigation in ILC-specific clinical trials, such as inducing synthetic lethality with ROS1 inhibitors in E-cadherin negative cells in both early-stage and metastatic ILC (NCT04551495, NCT03620643); exploiting sensitivity to neo-adjuvant endocrine treatment in early-stage ILC (NCT02206984, NCT01953588) or in combination with CDK4/6 inhibition (NCT02764541); and targeting activating HER2-mutations in metastatic ILC with neratinib and fulvestrant in a basket of the SUMMIT-trial (NCT01953926). Additionally, based on preclinical data and our work presented here, targeting the PI3K-AKT-mTOR pathway [59] or macrophages [60] in combination with ICB and/or chemotherapy might be promising treatment strategies for ILC patients. Besides trials specific for ILC, subgroup analyses of ILC patients in randomized clinical trials are of vital importance to inform treatment decisions for ILC patients and thereby improve outcome for this difficult-to-treat breast cancer subtype.

In conclusion, this is the earliest report on a clinical trial specific for metastatic ILC representing a difficult-to-treat breast cancer subtype

and we demonstrate that the combination of carboplatin and anti-PD-L1 induces clinical and immunological responses in a subset of ILC patients. Most of the responses were observed in patients with TN-ILC, highlighting that patients with TNBC should be considered for ICB regardless of histological subtype. Our work provides hypotheses and paves the way for highly needed ILC-specific clinical trials.

3.4. Methods

Study design

The GELATO trial was conducted in accordance with Good Clinical Practice guidelines and the Declaration of Helsinki. All patients provided written informed consent. The trial protocol, informed consent form and amendments were approved by the medical-ethical committee of the Netherlands Cancer Institute. GELATO is a phase-II, single-arm, multicenter clinical trial, conducted at four centers in the Netherlands (NCT03147040) to evaluate the efficacy of carboplatin and atezolizumab (anti-PD-L1) in patients with metastatic ILC. Lobular histology needed to be confirmed on a biopsy of a metastatic lesion with a negative or aberrant E-cadherin immunohistochemistry (IHC) staining. Eligible patients were treated with 12 cycles of weekly carboplatin (AUC of 1.5 mg/ml x min) and atezolizumab (anti-PD-L1; 1200 mg flat-dose) every three weeks starting from the third cycle of carboplatin onwards (**Figure 3.1A**). The purpose of this short-term, low-dose platinum regimen was to exploit the immunological effects of carboplatin instead of establishing a direct cytotoxic effect and avoid potential prolonged bone marrow suppression (**Supplementary Note**). As responses to immunotherapy in the metastatic breast cancer setting are predominantly observed within 12 weeks [15], the duration of carboplatin induction treatment was limited to 12 weeks (**Supplementary Note**).

Anti-PD-L1 was continued until disease progression according to RECISTv1.1 [61], clinical progression or unacceptable toxicity. Before the start of carboplatin, after two cycles of carboplatin (two weeks from baseline) and after two cycles of anti-PD-L1 (+ 6 weekly administrations of carboplatin, 8 weeks from baseline), blood was drawn and sequential biopsies from a metastatic lesion were taken. The first six patients were included in a 3+3 phase Ib safety run-in part, with the same treatment schedule, and were included in the total number of patients. This investigator-initiated trial was sponsored by the Netherlands Cancer Institute, atezolizumab was provided by Roche. Participants were not financially compensated for their involvement in the study.

Eligibility criteria GELATO-trial

Eligible patients had metastatic or incurable locally advanced ILC. Non-female patients were also eligible for the trial. Sex of the participants was determined based on ID check upon hospital administration. Median age of the patients in the study was 60 years, ranging from 45 to 69 years. Patients were not preselected based on PD-L1 expression. Patients had to have a metastatic lesion or recurrence available for sequential biopsies (bone lesions were not allowed) and had to have evaluable disease according to RECISTv1.1 [61]. In case of Estrogen Receptor (ER+) disease, patients had to have progression after endocrine treatment in the advanced setting and had to have received an anti-estrogen and an aromatase inhibitor in the early-stage or for advanced setting. A maximum of two lines of palliative chemotherapy was allowed. Patients had to have a WHO performance status of 0 or 1, and normal bone marrow, kidney and liver functions with a Lactate Dehydrogenase (LDH) below 500 U/L (2 times upper limit of normal). Exclusion criteria were bone-only disease, symptomatic brain metastasis (stable and treated brain metastases were allowed), leptomeningeal disease localization, previous treatment with immune checkpoint inhibitors and/or a history of autoimmune disorders requiring immunosuppressive treatment. At the start of the trial, patients were eligible regardless of their receptor status. Since we aimed for a representative patient population for ILC with 10-20% ER- patients [1, 2], inclusion of patients with triple-negative (TN)-ILC (ER and PR expression <10%, HER2-negative) was stopped after reaching 20% of total patients.

Trial procedures

Clinically stable patients with disease progression according to RECISTv1.1 were permitted to continue anti-PD-L1 until confirmation of progression on a subsequent CT scan according to iRECIST guidelines [62]. Response evaluation was performed by a CT-scan of the neck (if applicable), thorax and abdomen (including pelvis) at baseline (four weeks prior to start), before the start of anti-PD-L1, and every six weeks during treatment (every nine weeks after 24 weeks). RECISTv1.1 measurements were done by experienced breast cancer radiologists and in case of inconsistencies revised by one dedicated radiologist. Carboplatin treatment was withheld in case of hematological toxicity, such as anemia or neutropenia. Dose modification of atezolizumab was not allowed, but treatment interruptions were allowed in case of toxicity or suspicion thereof. Adverse events (AEs) were monitored every three weeks (weekly during carboplatin treatment) by laboratory assessments, vital signs and physical examinations. Grading of AEs was done per National Cancer Institute's Common Terminology Criteria for Adverse Events (NCI-CTCAE) v4.03. Supportive treatment with antiemetics, bisphosphonates, and palliative radiation (only if response could still

be evaluated) was allowed. Archival formalin-fixed paraffin-embedded (FFPE) blocks of primary tumors (biopsies in case of neo-adjuvant chemotherapy or resection material) were collected via PALGA (the nationwide network and registry of histo- and cytopathology in the Netherlands) [63]. The study protocol is included as a **Supplementary Note**.

Trial objectives and endpoints

The primary endpoint of the trial was progression-free survival (PFS) rate at six months (24 weeks), assessed from date of registration to date of progression according to RECISTv1.1 or death from any cause. Secondary endpoints were progression-free survival (PFS) rate at six months in patients with immune-related ILC, PFS rate at 12 months, PFS according to iRECIST, overall survival (OS), objective response rate (ORR) and safety. The clinical benefit rate (CBR) comprised complete responses (CR), partial responses (PR) and stable disease (SD) for at least 24 weeks. PFS was calculated from date of registration to date of progression according to RECIST1.1 or date of death, whichever occurred earlier. OS was calculated from date of registration to date of death or last date of follow-up. Patients were censored in case of no event at the last assessment before the data cut-off of 1 October 2021. Duration of response was calculated from the first date of an objective response to date of progression according to RECIST1.1. Translational endpoints were the assessment of immunogenic effects of carboplatin on the TME and in the circulation using immunohistochemistry, next-generation sequencing and flow cytometry; the additive effect of anti-PD-L1 on these changes; and exploration of predictive biomarkers.

Statistics & reproducibility

A Simon's two-stage [64] design was used to determine the sample size. The median PFS of palliative chemotherapy regimens in patients with endocrine-treatment refractory breast cancer typically lies within 2-4 months (**Supplementary Note**). If 25% of patients were free of progression at 6 months (24 weeks) in the GELATO-trial, this would warrant further investigation of the treatment regimen. The null hypothesis that the true proportion of patients progression-free at six months is 10% or lower was tested against a one-sided alternative of at least 25%. In the first stage of the trial, 22 patients had to be accrued. If two or fewer patients were progression-free at six months, the study would be stopped, otherwise 18 additional patients could be included. This design yields a type one error rate of 0.04 and power of 0.80 when the true proportion of patients progression-free at six months is 25%. The last two patients were registered in the same week and therefore both included in the trial, leading to a total inclusion of 23 patients. Primary endpoint analysis for Simon's two-stage

was therefore performed separately for the first included 22 patients. Secondary and translational endpoint analyses were performed in the per protocol population (n=23, patients who received at least one dose of anti-PD-L1, **Supplementary Figure 3.5**). The data cut-off for follow-up was 1 October 2021. No data was excluded from the analyses. Data collection and analysis were not performed blind to the conditions of the experiments. The investigators were not blinded to the outcome assessment. Since the study included one experimental group, randomization and allocation procedures were not applicable. Further information on research design is available in the Nature Research Reporting Summary linked to this article.

Flow cytometry fresh blood

Peripheral blood was collected in an K2EDTA vacutainer (BD) and processed within 24 hours. Three panels spanning T-cell, B-cell and myeloid cell biology were used (**Table 3.7** for all assessed immune cell populations, **Table 3.8** for antibodies, gating strategy in **Supplementary Figure 3.12**) as described before [65]. Red blood cells were lysed (lysis buffer: dH₂O, NH₄Cl, NaHCO₃, EDTA) and cells were resuspended in PBS containing 0.5% BSA and 2mM EDTA. For surface antigen staining, cells were first incubated with human FcR Blocking Reagent (1:100 Miltenyi) for 15 min at 4°C and then incubated with fluorochrome-conjugated antibodies for 30 min at 4°C, in the dark. For intracellular antigen staining, cells were fixed with Fixation/Permeabilization solution 1X (Foxp3/Transcription Factor Staining Buffer Set, eBioscience) for 30 min at 4°C and stained with fluorochrome-conjugated antibodies in Permeabilization buffer 1X (eBioscience) for 30 min at room temperature. Viability was assessed by staining with either 7AAD staining solution (1:20; eBioscience) or Zombie Red Fixable Viability Kit (1:800 BioLegend). Data acquisition was performed on BD LSRII flow cytometer using Diva software (BD Biosciences) and data analysis was performed using FlowJo software version 10.6.2. To obtain absolute white blood cell counts per mL of human blood, the total post-lysis cell count was obtained using the NucleoCounter NC-200 (Chemometec) automated cell counter. To assess dynamics in each cell population with cell count/mL, linear modeling was performed using limma R package v3.46.0 (<https://kasperdanielhansen.github.io/genbioconductor/html/limma.html>). Predicting log₂ transformed cell counts per mL for the same patient at different time points was done as following: log₂(cell counts/mL) time point + patient ID. The modeling was performed independently for paired samples of baseline versus post-induction (**Figure 3.4A**) and baseline versus carboplatin+anti-PD-L1 (**Figure 3.4B**). Sample pair dynamics was assessed analogously to the paired t-test. For visualization purposes, Benjamini-Hochberg corrected p-values were plotted against the corresponding log₂ fold changes: the log₂ fold change from

baseline to pre-atezo ($\log_2(\text{pre-atezo}) - \log_2(\text{baseline})$) and the \log_2 fold change from baseline to on-atezo ($\log_2(\text{on-atezo}) - \log_2(\text{baseline})$) (**Figures 3.4A-B**). The plots were made by EnhancedVolcano R package v1.12.0 (<https://github.com/kevinblighe/EnhancedVolcano>).

TILs and immunohistochemistry

Formalin-fixed paraffin-embedded (FFPE) tumor blocks of archived primary tumor blocks and newly collected biopsies of metastatic lesions were used for sTIL assessment and CD8 and PD-L1 (SP142) immunohistochemistry staining. IHC of formalin-fixed paraffin-embedded FFPE tumor samples was performed on a BenchMark Ultra autostainer (Ventana Medical Systems). Briefly, paraffin sections were cut at 3 μm , heated at 75°C for 28 minutes and deparaffinized in the instrument with EZ prep solution (Ventana Medical Systems). Heat-induced antigen retrieval was carried out using Cell Conditioning 1 (CC1, Ventana Medical Systems) for 32 minutes at 95°C (CD8) or 48 minutes at 95°C (PD-L1). CD8 was detected using clone C8/144B (1/200 dilution, 32 minutes at 37°C, Agilent / DAKO) and PD-L1 using clone SP142 (Ready-to-Use dispenser, 16 minutes at 37°C, Roche / Ventana). Bound antibodies were detected using the OptiView DAB Detection Kit (Ventana Medical Systems). Slides were counterstained with Hematoxylin and Bluing Reagent (Ventana Medical Systems). A PANNORAMIC®1000 scanner from 3DHISTECH was used to scan the slides at a 40x magnification. Scans of all stainings were uploaded on Slide Score (www.slidescore.com). Stromal tumor-infiltrating lymphocytes (sTILs) were assessed on an H&E slide according to international standard from the International Immuno-Oncology Biomarker Working Group (www.tilsinbreastcancer.org) [66]. CD8 was assessed as percentage of positive cells in the tumor-associated stromal area, and PD-L1 as percentage of positive immune cells in the tumor and stromal area. Two expert pathologists (H.M.H. and R.S.) independently evaluated the stainings digitally and the average of scores was taken.

DNA and RNA sequencing

DNA and RNA material was isolated from FFPE sections of primary tumors or fresh-frozen (FF) tissue sections of biopsies of metastatic lesions, containing at least 30% tumor cells. DNA and RNA isolation was done simultaneously using the Qiagen AllPrep DNA/RNA FF kit for FF tissue and the Qiagen AllPrep DNA/RNA FFPE kit for FFPE blocks, according to manufacturer's instructions. Germline DNA was isolated from peripheral blood using the QIAasympphony DSP DNA midi kit. The total amount of DNA was quantified on the Nanodrop 2000 (ThermoFisher). The amount of double stranded DNA in the genomic DNA samples was quantified using the Invitrogen Qubit®dsDNA HS Assay Kit. Maximum 2000 ng of double stranded genomic DNA was fragmented by Covaris shearing. Samples were purified using 2X Agencourt AMPure XP PCR Purification

beads according to Beckman Coulter manufacturer's instructions. The sheared DNA samples were quantified and qualified on a BioAnalyzer system using the Agilent Technologies DNA7500 assay kit. With an input of maximum 1 μ g sheared DNA, library preparation for Illumina sequencing was performed using the KAPA HTP Prep Kit for FF DNA (KAPA Biosystems, KK8234) or KAPA Hyper prep kit (KAPA Biosystems, KK8504) for FFPE DNA. Libraries were amplified with 4 (FF) or 6 (FFPE) PCR cycles and cleaned with 1X AMPure XP beads. Concentrations were measured with DNA7500 chips on a BioAnalyzer system. 6 pools of 6 to 7 samples were created using 500 ng of each indexed sample of FF DNA. 2 pools of 6 to 7 samples were created using 65 ng of each indexed sample of FFPE DNA. 2 μ l of IDT TS-mix universal blockers and 5 μ l Invitrogen Human Cot-1 DNA was added to each pool. Each pool was dried with a concentrator (Eppendorf). To each dried pool 8.5 μ l of hybridization buffer, 3.4 μ l Hybridization component A (SeqCap Hybridization and wash kit, Roche) and 1.1 μ l nuclease-free water was added to rehydrate the pool. Each pool was incubated at room temperature for 10 minutes, followed by an incubation at 96 degrees Celsius for 10 minutes. Samples were hybridized with the IDT xGen Exome Research Panel v1.0. The pool was captured and washed following the IDT protocol and amplified using 10 PCR cycles. The amplified pool was purified using AMPure®XP beads (Beckman Coulter). The purified pools were quantified on the Agilent Bioanalyzer 7500 system and one sequence pool was made by equimolar pooling. The sequence pool was diluted to a final concentration of 10nM and subjected to sequencing on an Illumina Novaseq 6000 machine with a SP 2 300 cycle kit for a paired end 150 bp run for FF samples and with a SP 200 cycle kit for a paired-end 100 bp run for FFPE samples, according to manufacturer's instructions.

Quality and quantity of the total RNA from was assessed by the 2100 Bioanalyzer using a Nano chip (Agilent, Santa Clara, CA). The percentage of RNA fragments > 200nt fragment distribution values (DV200) were determined using the region analysis method according to the manufacturer's instructions (Illumina, technical-note-470-2014-001). Strand-specific libraries were generated using the TruSeq RNA Exome Library Prep Kit (Illumina Inc., San Diego) according to the manufacturer's instructions (Illumina, # 1000000039582v01). Briefly, total RNA was fragmented (only for FF material), random primed and reverse transcribed using SuperScript II Reverse Transcriptase (Invitrogen, part # 18064-014) with the addition of Actinomycin D. Second strand synthesis was performed using Polymerase I and RNaseH with replacement of dTTP for dUTP. The generated cDNA fragments were 3' end adenylated and ligated to Illumina Paired-end sequencing adapters and subsequently amplified by 15 cycles of PCR. The libraries were validated on a 2100 Bioanalyzer using a 7500 chip (Agilent, Santa Clara, CA) followed by a 1-4 plex library pooling containing up to 200ng

of each sample. The pooled libraries were enriched for target regions using the probe Coding Exome Oligos set (CEX, 45MB) according to the manufacturer's instructions (Illumina, # 1000000039582v01). Briefly, cDNA libraries and biotin- labeled capture probes were combined and hybridized using a denaturation step of 95°C for 10 minutes and an incubation step from 94°C to 58°C having a ramp of 18 cycles with 1 minute incubation and 2°C per cycle. The hybridized target regions were captured using streptavidin magnetic beads and subjected to two stringency washes, an elution step and a second round of enrichment followed by a cleanup using AMPure XP beads (Beckman, A63881) and PCR amplification of 10 cycles. The target enriched pools were analyzed on a 2100 Bioanalyzer using a 7500 chip (Agilent, Santa Clara, CA), diluted and subsequently pooled equimolar into a multi-plex sequencing pool. The libraries were sequenced with 54 paired-end reads on a NovaSeq6000 using a SP Reagent Kit v1.5 (100 cycles) (Illumina Inc., San Diego).

DNA Sequencing data analysis

DNA Sequencing data was aligned to GRCh38 reference genome with bwa aligner 0.7.17 [67] using the bwa-mem algorithm. Samtools fixmate 1.13 (<https://github.com/samtools/>) was used to correct mate information, and duplicate reads were marked with Picard MarkDuplicates. Next, base quality scores were recalibrated with GATK BaseRecalibrator [68], and Mutect2 2.2 [69] was used to perform variant calling. The data that passed all Mutect2 filters was subsequently filtered with fings 1.7.1 [70] and vcf2maf 1.6.21 (<https://github.com/mskcc/vcf2maf>) was used to run VEP annotation of the variants and to produce a maf file. Variants with a variant allele frequency (VAF) >0.2 were included in final analysis. TMB was calculated with maftools 2.10.5 [71] tmb function. VAF plots, mutational signature plots and oncoplot were created with maftools 2.10.5. Data was analyzed with Python 3.7.6 and R 4.1.1. Pandas 1.3.3 (<https://pandas.pydata.org/>) was used for data handling.

RNA sequencing data analysis

RNA sequencing data has been aligned to GRCh38 with STAR 2.7.1a, with twopassMode option set to "Basic" [72]. Gene counts were obtained with STAR quantMode option set to "GeneCounts". Data quality was assessed with FastQC 0.11.5 [73], FastQ Screen 0.14.0 [74], Picard CollectRnaSeqMetrics tool (<https://broadinstitute.github.io/picard/>) and RSeQC read_distribution.py and read_duplication.py tools 4.0.0 [75] and found to be suitable for the downstream analysis. Data was subsequently normalised to TPM. For cell deconvolution, CIBERSORTx was run in absolute mode with LM22 Source GEP, performing the batch correction [76]. Differential expression analysis was performed with DESeq2 1.34.0 [77]. PAM50 classification was performed with

genefu R package 2.26.0 [78]. Gseapy 0.9.18 ssgsea tool [79] with sample_norm_method option set to "rank" was used for gene set signature scoring. Data was analyzed with Python 3.7.6 and R 4.1.1. Pandas 1.3.38 (<https://pandas.pydata.org/>) and NumPy 1.18.1 (<https://numpy.org/>) were used for data handling. Seaborn 0.10.0 (<https://seaborn.pydata.org/>), Matplotlib 3.1.3 (<https://matplotlib.org/>) and statannotations 0.4.3 (<https://github.com/trevismd/statannotations>) have been used for plotting.

⁸⁹Zr-atezolizumab PET/CT imaging

Based on previous work showing superior correlation of zirconium-89 (⁸⁹Zr)-atezolizumab uptake on positron emission tomography/computerized tomography (PET/CT) with clinical response to atezolizumab, compared to immunohistochemistry- or RNA-sequencing-based predictive biomarkers [23], an imaging biomarker side study was performed in the University Medical Center Groningen (NCT04222426). At baseline and after two cycles of carboplatin, a whole body (⁸⁹Zr)-atezolizumab PET/CT was performed on a Biograph mcT 40 or 64-slice PET/CT (Siemens/CTI, Knoxville, TN), as previously described [23]. Tumor lesions were identified on standard baseline FDG-PET/CT, with a minimum width of 10mm. ⁸⁹Zr-atezolizumab-uptake was quantified in all lesions, with a maximum of 10 lesions per organ. Quantification of the ⁸⁹Zr-atezolizumab- and FDG uptake was performed using the Accurate tool [80] and Syngo.via imaging software VB20/30 (Siemens), respectively. A spherical volume-of-interest (VOI) was drawn closely around all metastases. Maximum standardized uptake values (SUVmax) were calculated, as well as background mean SUV (SUVmean). Tumor-to-blood ratio's (TBR) were calculated by dividing the SUVmax by the thoracic aorta SUVmean. Change in tumor uptake between ⁸⁹Zr-atezolizumab-PET at baseline and after two cycles of carboplatin was assessed as percentage TBR change. In addition, we calculated the median and range of the ⁸⁹Zr-atezolizumab uptake (TBR), and natural-log-transformed ⁸⁹Zr-atezolizumab uptake to obtain approximate normal distributions, yielding estimates of geometric means following back-transformation of the results.

Statistical analysis

Median time to event was calculated for PFS, OS and duration of response was calculated with the Kaplan-Meier method. The impact of clinical benefit on OS was assessed with a 24-week landmark analysis in which only patients alive after 24 weeks were considered. Additionally, a time-dependent Cox analysis was performed, with clinical benefit (on the date of first partial response or at 24 weeks in case of stable disease) as time-dependent variable. Frequencies, such as response rate and clinical benefit rate, were estimated with corresponding two-sided 95% confidence intervals (Clopper-Pearson) and comparisons between

frequencies were performed using Fisher's exact test. Two-sided non-parametric tests were used for translational analyses: Mann-Whitney U for two independent groups and Wilcoxon's signed-rank for paired data. The data met the assumptions of the statistical tests used. Data was analyzed with GraphPad Prism v9.0, IBM SPSS statistics 24, SAS v9.4, Python 3.7.6 and R 4.1.1. Reported p-values are two-sided and unadjusted unless stated otherwise.

3.5. Data availability

DNA and RNA sequencing data are stored in the European Genome-Phenome Archive (EGA) under the accession code EGAS00001006902. Sequencing data and source data supporting the findings of this study are not publicly available due to the clinical trial agreements and will be made available from the corresponding author upon reasonable request. Data requests will be reviewed by the corresponding author and Institutional Review Board of the NKI and after approval applying researchers have to sign a data transfer agreement with the NKI.

3.6. Acknowledgments

We are grateful to the patients and their families for participating in the trial. We thank all supporting clinical trial staff, in particular Myra Jansen, Greetje de Vries and the departments of Medical Oncology, Radiology, Pathology and Dermatology of participating centers. We thank the triallab of the Netherlands Cancer Institute (NKI) for handling incoming blood samples. We acknowledge the Scientific Administration departments of participating centers, particularly Abi Jayakkumaran and Michiel Sondermeijer. We thank Marjo Holtkamp and Kim Kersten for patient visits and supporting the scheduling of patients. We are grateful to the Core Facility of Molecular Pathology & Biobanking for the storage and handling of human tumor material and to the Genomics Core Facility, in particular Roel Kluin, Wim Brugman and Charline van Steenis, for DNA and RNA sequencing. We thank Marieke Bruggeman, Maxime Duijst and Chris Klaver for blood sample experiments and the Flow Cytometry Facility for support in these experiments. We acknowledge PALGA, the Dutch Pathology Registry, for enabling collection of archived material. We thank Ruud Meijer and Jeroen Paardekooper Overman from Roche for enabling the trial and arranging supply of atezolizumab. R.S. is supported by the Breast Cancer Research Foundation (BCRF, grant nr. 17-194). Research at the Netherlands Cancer Institute is supported by institutional grants of the Dutch Cancer Society and of the Dutch Ministry of Health, Welfare and Sport. Research in the Kok

group is funded by the Netherlands Organization for Scientific Research (NWO-VIDI 09150172010043) and the Hendrika Roet fund. This work was supported by F. Hoffmann-La Roche Ltd, Basel, Switzerland (no grant numbers apply). The funders had no role in study design, data collection and analysis, decision to publish or preparation of the manuscript.

3.7. Author Contributions

L.V. coordinated trial procedures, analyzed and interpreted clinical and translational data of the trial, and wrote the manuscript with O.I.I. and M.K. O.I.I. performed and interpreted computational analyses of the DNA and RNA sequencing data. H.M.H. and R.S. performed the histological scoring of the pathology slides. S.B. and K.S. performed the statistical analysis of the trial data. M.C. performed computational analyses of the flow cytometry data. N.A.M.B., E.C. and H.C.G. were responsible for blood sample processing and analysis, supervised by K.E.d.V. and M.K. and H.C.G. designed the flow cytometry panel. C.E.L. revised RECIST1.1 measurements and was together with colleagues involved in taking biopsies. I.K. was responsible for patient care. I.A.M.M. was the clinical projects manager. M.d.M. performed DNA/RNA isolations. J.J.L.v.G. and J.B. coordinated trial procedures in one participating center including the ImaGelato case. M.d.B., M.G.J.v.D., G.S.S., V.C.G.T.H., C.P.S., S.C.L. and M.K. were the main treating physicians. G.S.S., K.E.d.V., T.N.S., C.U.B., S.C.L. and M.K. wrote the trial protocol. L.F.A.W. supervised computational analyses. A.J., V.C.G.T.H., C.P.S., and M.K. were the principal investigators of the trial. All authors edited and approved the manuscript.

3.8. Competing Interests

L.V., O.I.I., S.B., M.C., N.A.M.B., E.C., H.G., K.S., C.E.L., I.K., I.A.M.M., M.d.M., J.J.L.v.G., J.B., M.G.J.v.D. and A.J. have no competing interests to declare. H.M.H. reports consultancy fees from Roche Diagnostics paid to the institute, and is advisor for SlideScore and Ellogon from Roche Diagnostics, outside the submitted work. M.d.B. received funding from Roche, AstraZeneca, Novartis, Pfizer, Eisai and Eli Lilly, outside the submitted work. R.S. reports non-financial support from Merck and Bristol Myers Squibb (BMS), research support from Merck, Puma Biotechnology and Roche, and personal fees from Roche, BMS and Exact Sciences for advisory boards, all outside the scope of this manuscript. G.S.S. reports research funding to the institute from Merck, Agendia, AstraZeneca, Roche and Novartis and a consulting role for Novartis, Seattle Genetics, Biovica, outside the submitted work. K.E.d.V. reports

research funding from Roche and is consultant for Macomics, outside the scope of this work. T.N.S. is consultant for Third Rock Ventures and is stockholder and advisor in Allogene Therapeutics, Asher Bio, Celsius, Merus, Scenic Biotech and Neogene Therapeutics, outside this work. C.U.B. has received research grants from Novartis, BMS and NanoString, is a paid advisory board member for BMS, MSD, Roche, Novartis, GlaxoSmithKline, AstraZeneca, Pfizer, Lilly, GenMab and Pierre Fabre, and holds ownership interest in Uniti Card, Neon Therapeutics and Forty Seven, all outside this submitted work. L.F.A.W. reports funding to the institute from Genmab BV. V.C.G.T.-H. reports research funding to the institute from Roche, Eisai, Pfizer, Novartis, Lilly, Daiichi Sankyo/AstraZeneca and Gilead Sciences, a consulting role from Pfizer, Lilly, Accord Healthcare and Novartis and honoraria from Novartis, Roche, Lilly and AstraZeneca, all outside this submitted work. C.P.S. has received research funding to the institute from Pfizer, Roche, Genentech, SNS Oncology, G1 Therapeutics, Abbvie, Synthon and CytoMx Therapeutics, outside this work. S.C.L. reports research funding to the institute from Roche/Genentech, AstraZeneca, BMS, Tesaro, Merck, Immunomedics, Eurocept Pharmaceuticals, Agendia and Novartis and a consulting role and travel grant from Daiichi Sankyo, outside this work. M.K. reports funding to the institute from BMS, Roche, AstraZeneca/MedImmune and an advisory role for BMS, Roche, MSD and Daiichi Sankyo, outside the submitted work.

3.9. Supplementary Information

Supplementary Note is available via the link: https://static-content.springer.com/esm/art%3A10.1038%2Fs43018-023-00542-x/MediaObjects/43018_2023_542_MOESM1_ESM.pdf.

Table 3.3: Worst grade of any treatment-related adverse event. Immune-related events are a selection of all reported atezolizumab-related events.

Worse grade of any adverse event, no. of patients (%)	No AE reported	Grade 1-2	Grade 3	Grade 4
Carboplatin-related	6 (26)	7 (30)	9 (39)	1 (4)
Atezolizumab-related	11 (48)	5 (22)	5 (22)	2 (9)
Immune-related event of interest	13 (57)	4 (17)	5 (22)	1 (4)

Only grade 2 events or higher or grade 1 immune-related events were reported. 1 patient died during treatment of disease progression.

3. PD-L1 blockade in combination with carboplatin as immune induction in metastatic lobular breast cancer: the GELATO trial

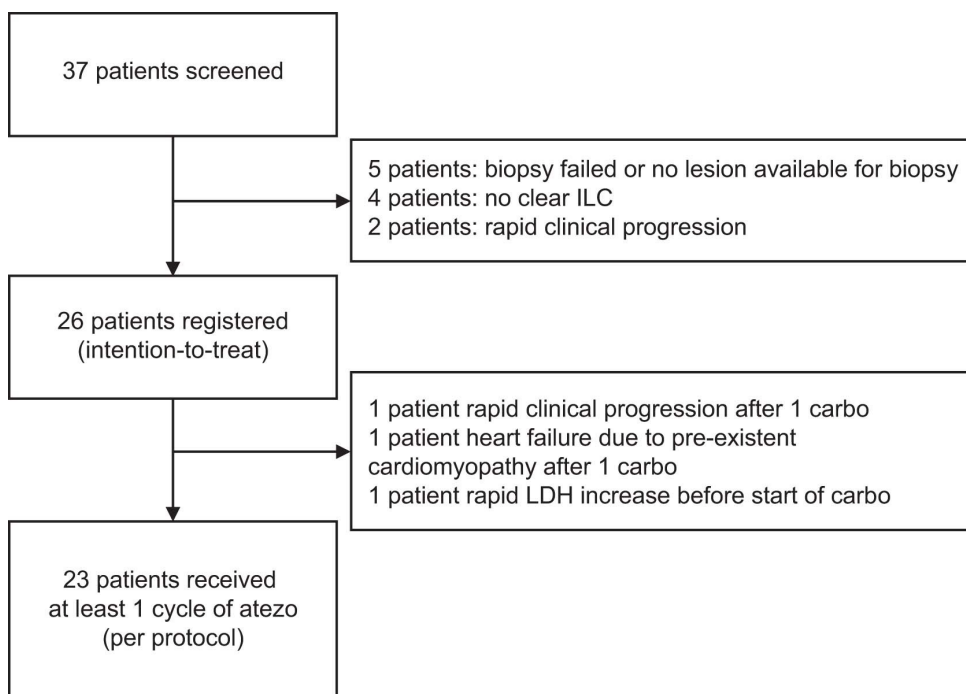


Figure 3.5: Flow chart of patient inclusion in the GELATO-trial.

Table 3.4: All reported carboplatin-related toxicity.

Carboplatin-related adverse event, no. of patients (%)	Any grade	Grade 3	Grade 4
Neutrophil count decreased	11 (48)	3 (13)	1 (4)
Anemia	5 (22)	2 (9)	0 (0)
Platelet count decreased	3 (13)	2 (9)	0 (0)
Nausea	3 (13)	0 (0)	0 (0)
Fatigue	2 (9)	0 (0)	0 (0)
Abdominal pain	1 (4)	1 (4)	0 (0)
ALAT increased	1 (4)	1 (4)	0 (0)
Dehydration	1 (4)	1 (4)	0 (0)
Flu-like symptoms	1 (4)	0 (0)	0 (0)
Gastro-esophageal reflux	1 (4)	0 (0)	0 (0)
Hyperkalemia	1 (4)	0 (0)	0 (0)
Hyponatremia	1 (4)	1 (4)	0 (0)
Infusion-related reaction	1 (4)	0 (0)	0 (0)
Increased lipase	1 (4)	0 (0)	0 (0)
Obstipation	1 (4)	0 (0)	0 (0)
Peripheral neuropathy	1 (4)	0 (0)	0 (0)

Only grade 2 events or higher were reported. Alanine aminotransferase (ALAT).

3.9. Supplementary Information

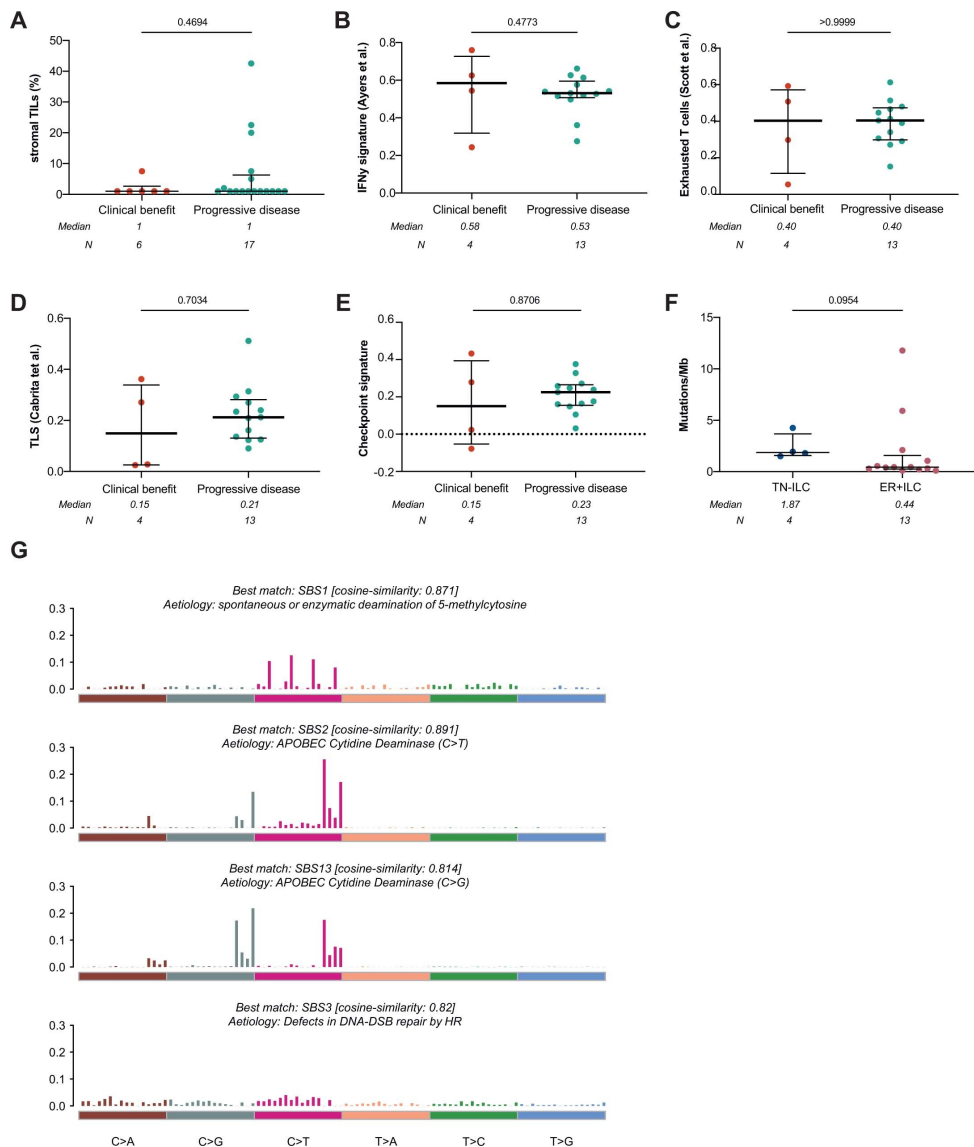


Figure 3.6: Additional baseline tumor microenvironment features associated with clinical outcome. (A) Percentage of stromal tumor-infiltrating lymphocytes (STILs). N = 23 samples. (B) Gene expression of an IFN γ signature [27]. N = 17 samples. (C) Gene expression of an exhausted T-cell signature [28]. N as in (B). (D) Gene expression of a tertiary lymphoid structure (TLS) signature [29]. N as in (B). (E) Gene expression of an immune checkpoint signature [30]. N as in (B). (F) Tumor mutational burden (TMB, mutations per MB) in ER+ vs triple-negative ILC. N as in (B). (G) Mutational signatures enriched in metastatic lesions. N as in (B). (A)–(F) Median with interquartile range, statistics by two-sided Mann-Whitney-U test. Baseline metastatic lesions correspond to metastases presented in **Figure 3.3** and **Supplementary Figures 3.7** and **3.8**.

3. PD-L1 blockade in combination with carboplatin as immune induction in metastatic lobular breast cancer: the GELATO trial

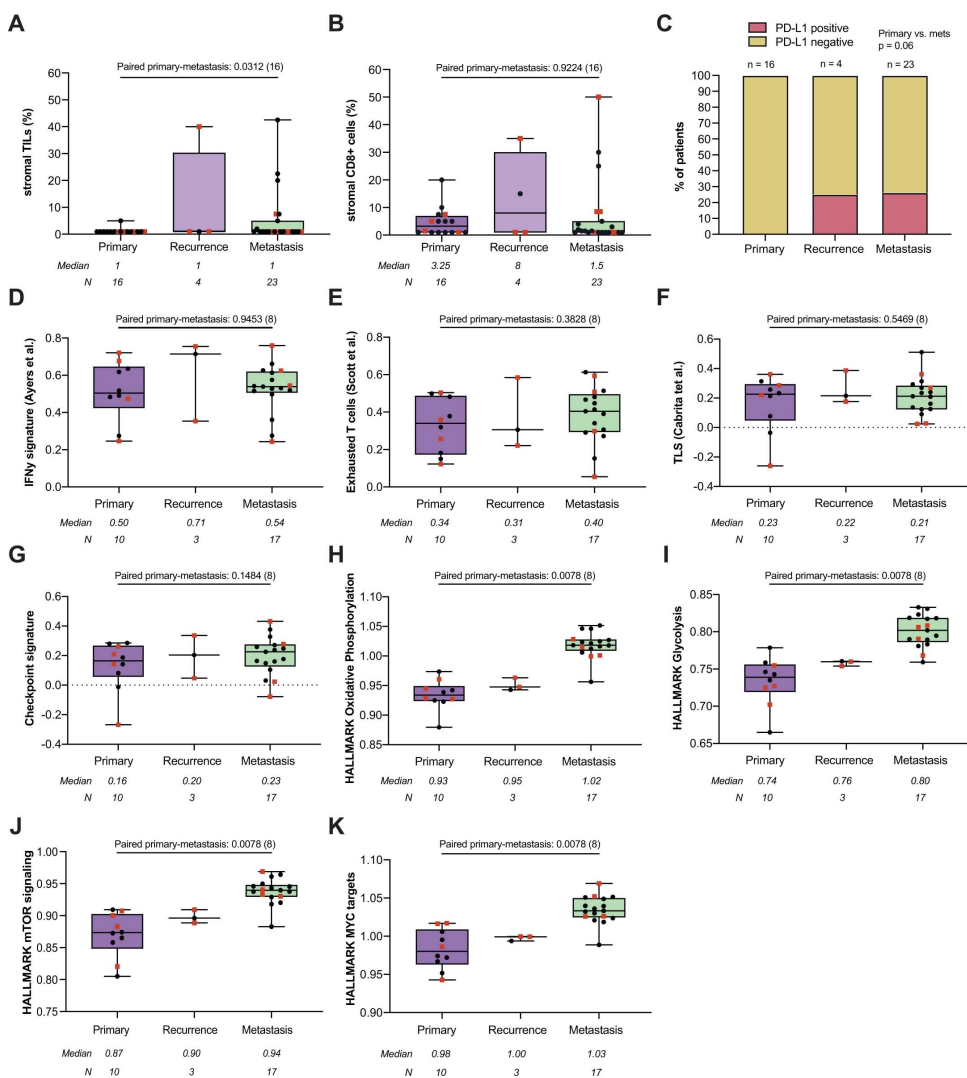


Figure 3.7: Evolution of sTILs, stromal CD8+ cells, PD-L1 expression and immune-related gene sets from paired primary tumors, local recurrences and metastasis. (A) Percentage of stromal tumor-infiltrating lymphocytes (sTILs) in paired primary tumors, recurrences, and metastases. N = 43 samples. **(B)** Percentage of CD8+ T cells in the stromal area (immunohistochemistry). N as in **(A)**. **(C)** Percentage of patients with clinical benefit and PD-L1 expression (clone SP142) in metastatic lesions. A cut-off of 1% expression on immune cells was used to determine PD-L1 positivity. Statistics by Fisher's exact test (primary versus metastasis) for proportions. N as in **(A)**. **(D)** Gene expression of an IFN γ signature [27]. N = 30 samples. **(E)** Gene expression of an exhausted T-cell signature [28]. N as in **(D)**. **(F)** Gene expression of a tertiary lymphoid structure (TLS) signature [29]. N as in **(D)**. **(G)** Gene expression of an immune checkpoint signature [30]. N as in **(D)**. **(H)** Gene set enrichment score of the HALLMARK Oxidative Phosphorylation gene set. N as in **(D)**. **(I)** Gene set enrichment score of the HALLMARK Glycolysis gene set. N as in **(D)**. **(J)** Gene set enrichment score of HALLMARK mTOR signaling gene set. N as in **(D)**. **(K)** Gene set enrichment score of HALLMARK MYC targets gene set. N as in **(D)**. **(A)-(B), (D)-(K)** Boxplots display a minimum (Q0), a maximum (Q4), a median (Q2) and the interquartile range. Statistics with two-sided Wilcoxon-signed-rank on paired primary tumors and metastasis; the number of patients in each analysis are listed between brackets behind the p-value. Red squares indicate patients with clinical benefit, black dots patients with no clinical benefit. Metastatic lesions correspond with baseline samples presented in **Figure 3.2, Figure 3.4, Supplementary Figures 3.6, 3.8 and 3.10**.

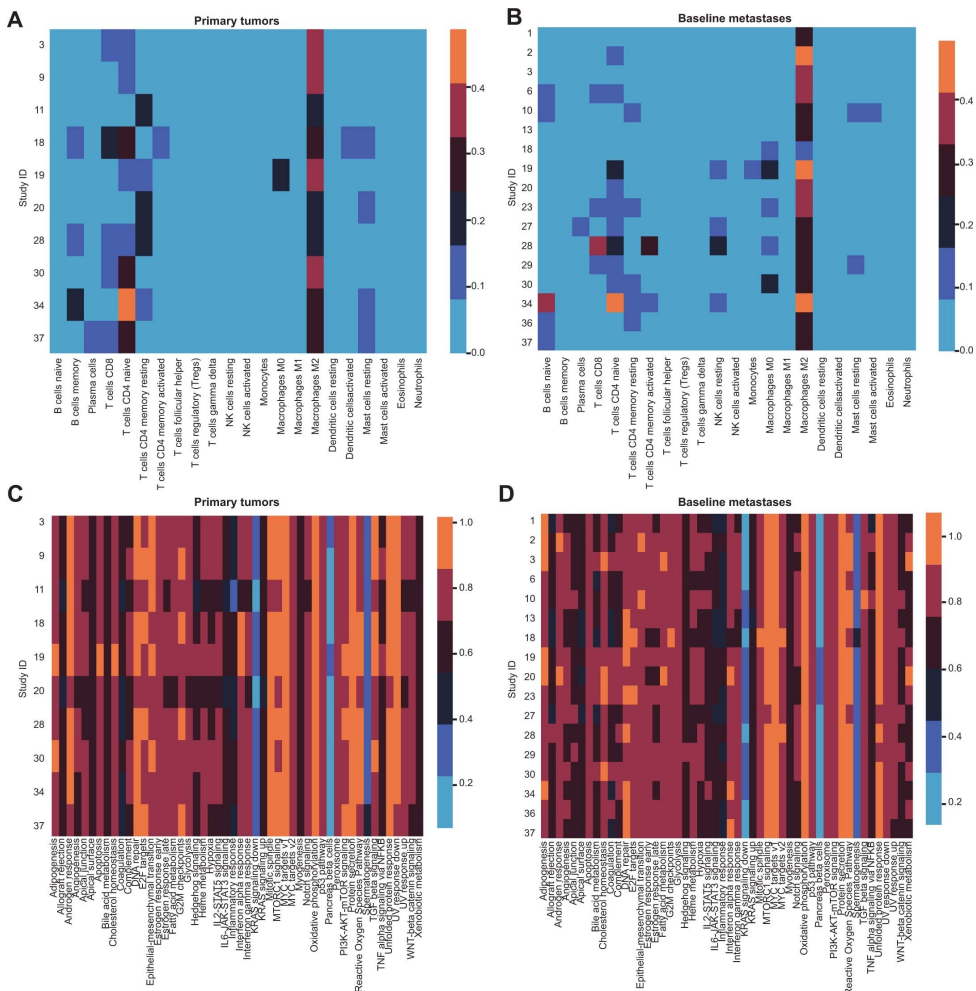


Figure 3.8: Unbiased analysis of treatment-related changes in gene expression. (A) Heatmap of CIBERSORTx immune cell deconvolution [34] across all primary tumor samples (FFPE). Rows correspond to one sample and are annotated with patient ID. N = 10 samples. **(B)** Heatmap of CIBERSORTx immune cell deconvolution [34] across all baseline metastases (FF). Rows correspond to one sample and are annotated with patient ID. N = 17 samples. **(C)** Heatmap of gene-set enrichment analysis of Hallmark gene sets [35] across all across all primary tumor samples (FFPE). Rows correspond to one sample and are annotated with patient ID. N as in **(A)**. **(D)** Heatmap of gene-set enrichment analysis of Hallmark gene sets [35] across all across all baseline metastases (FF). Rows correspond to one sample and are annotated with patient ID. N as in **(B)**.

3. PD-L1 blockade in combination with carboplatin as immune induction in metastatic lobular breast cancer: the GELATO trial

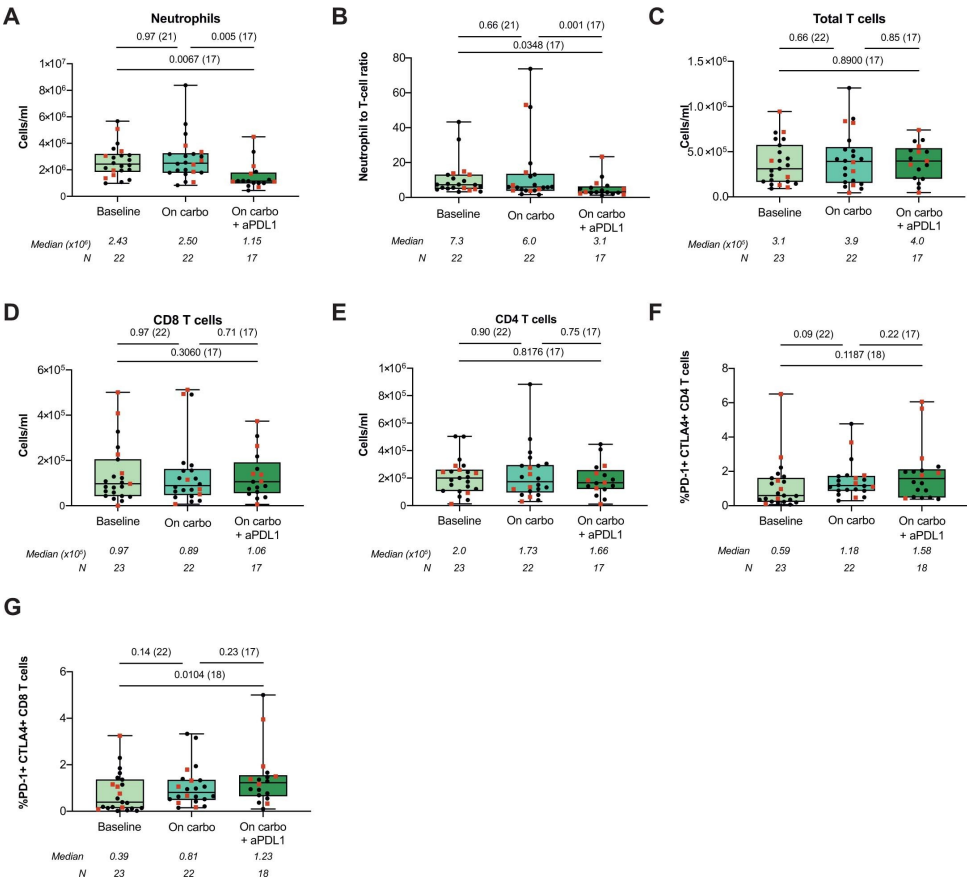


Figure 3.9: Flow cytometry-based assessment of circulating immune cell populations in paired blood samples at baseline, on carboplatin and during carboplatin/anti-PD-L1. (A) Absolute circulating neutrophil counts by flow cytometry. N = 61 sample. (B) Neutrophil-to-lymphocyte ratio (total T cell count). N as in (A). (C) Absolute circulating total T-cell counts. N = 62 samples. (D) Absolute circulating CD8+ T-cell counts. N as in (C). (E) Absolute circulating CD4+ T-cell counts. N as in (C). (F) Percentage of circulating PD-1+CTLA-4+ CD4+ T cells. N as in (C). (G) Percentage of circulating PD-1+CTLA-4+ CD8+ T cells. N as in (C). (A)-(G) Boxplots display a minimum (Q0), a maximum (Q4), a median (Q2) and the interquartile range. Statistics with two-sided Wilcoxon-signed-rank on paired samples, the number of patients in each analysis are listed between brackets behind the p-value. Red squares indicate patients with clinical benefit, black dots patients with no clinical benefit.

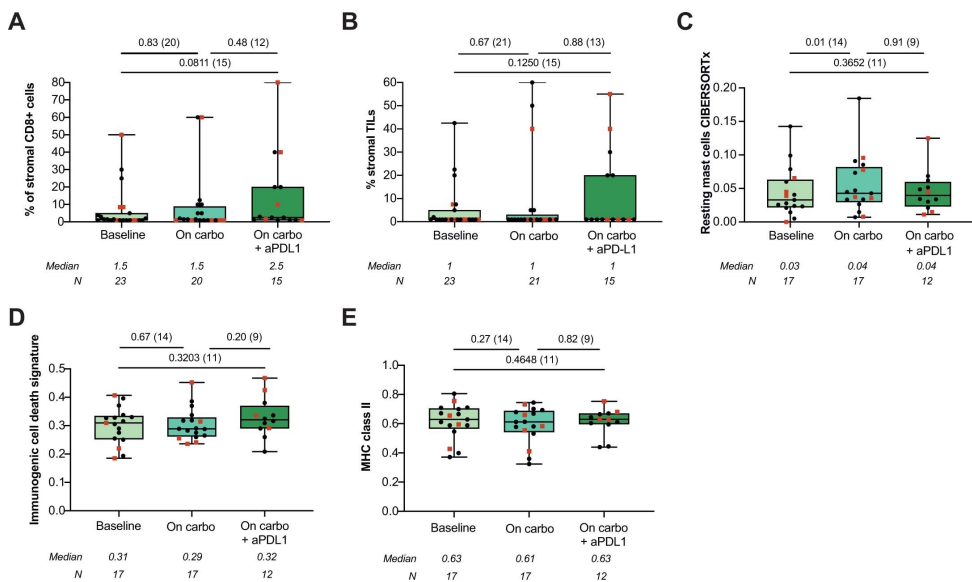


Figure 3.10: Changes in sTILs, stromal CD8+ cells and immune-related gene sets in serial biopsies of a metastatic lesion. **(A)** Percentage of CD8+ T cells (immunohistochemistry) in the stromal area in serial biopsies of metastatic lesions measured at baseline, after two cycles of carboplatin and after two cycles of anti-PD-L1 plus carboplatin. N = 58 samples. **(B)** Percentage of stromal tumor-infiltrating lymphocytes (sTILs) in serial biopsies of metastatic lesions. N = 57 samples. **(C)** Gene set expression score of resting mast cells according to CIBERSORTx in serial biopsies of metastatic lesions. N = 46 samples. **(D)** Gene expression of an immunogenic cell death signature [45] in serial biopsies of metastatic lesions. N as in **(C)**. **(E)** Gene expression score of MHC class II related genes (HLA-DRA, HLA-DRB1, HLA-DOB, HLA-DPB2, HLA-DMA, HLA-DOA, HLA-DPA1, HLA-DPB1, HLA-DMB, HLA-DQB1, HLA-DRB5, HLA-DQA2, HLA-DQB2, HLA-DRB6). N as in **(C)**. **(A)-(E)** Boxplots display a minimum (Q0), a maximum (Q4), a median (Q2) and the interquartile range. Statistics with two-sided Wilcoxon-signed-rank on paired samples, the number of patients in each analysis are listed between brackets behind the p-value. Red squares indicate patients with clinical benefit, black dots patients with no clinical benefit. Baseline metastatic lesions correspond to metastases presented in **Figure 3.3** and **Supplementary Figures 3.7** and **3.8**.

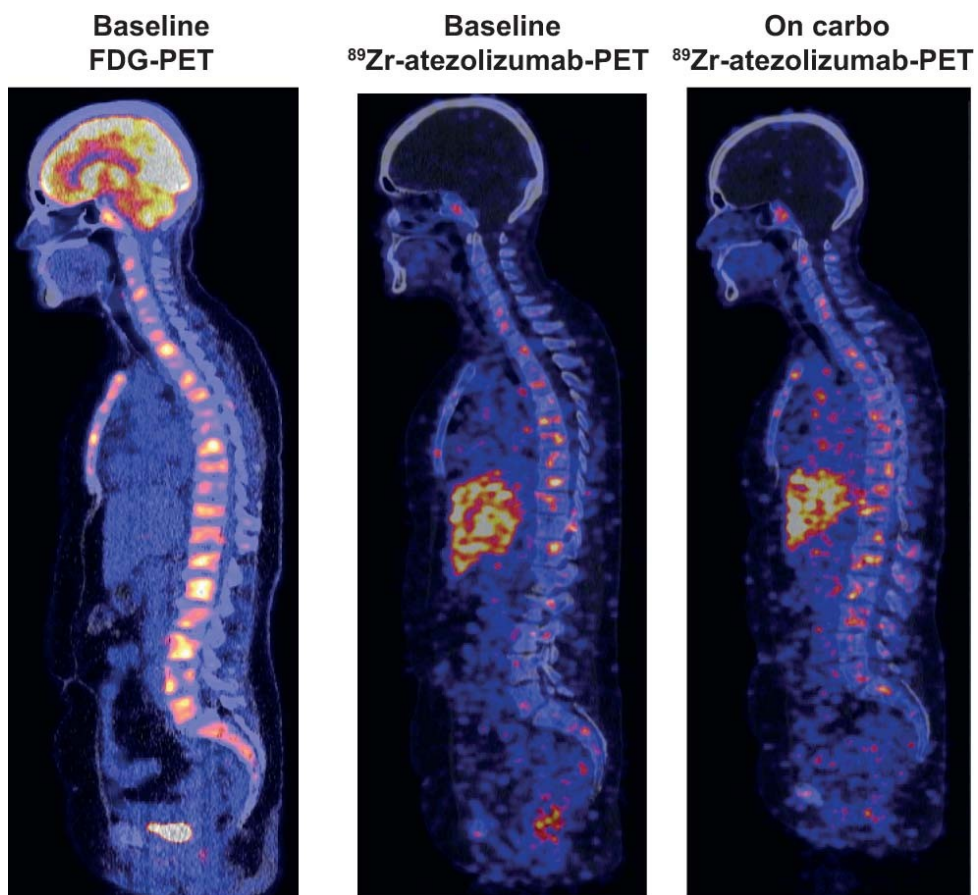


Figure 3.11: Exploratory analysis of the use ^{89}Zr -atezolizumab-PET to evaluate PD-L1 distribution in ILC patients. Representative images of one patient imaged with FDG-PET and ^{89}Zr -atezolizumab-PET. Left panel represents lateral view of baseline FDG-PET, the middle panel represents the lateral view of baseline ^{89}Zr -atezolizumab-PET and the right panel ^{89}Zr -atezolizumab-PET after two cycles of carboplatin.

3.9. Supplementary Information

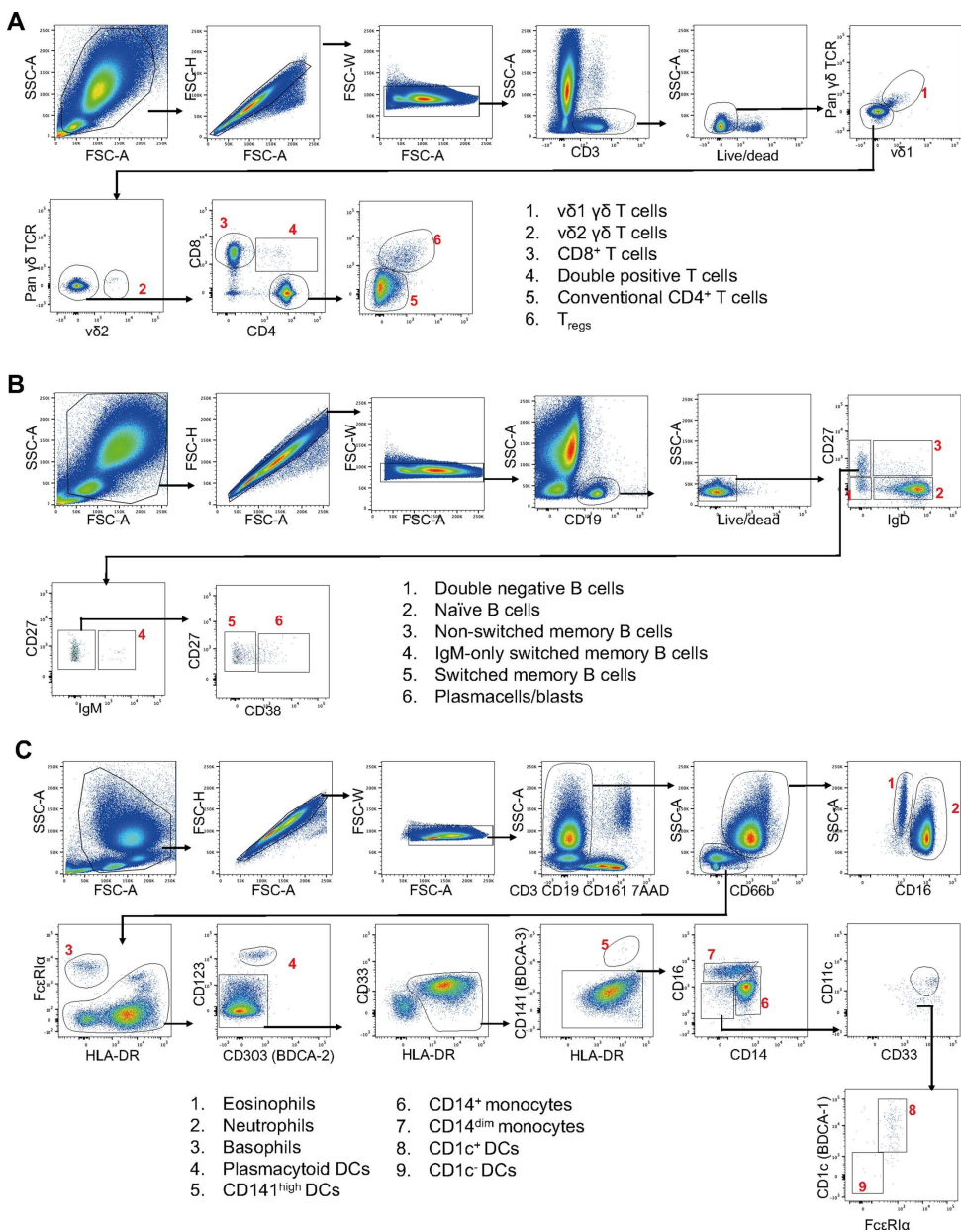


Figure 3.12: Gating strategies for flow cytometry analysis of peripheral blood immune populations. (A) T cell panel gating strategy identifying $v\delta 1$ $\gamma\delta$ T cells ($CD3^+$, $v\delta 1^+$, pan $\gamma\delta$ TCR $^+$), $v\delta 2$ $\gamma\delta$ T cells ($CD3^+$, $v\delta 2^+$), double positive T cells ($CD3^+$, $v\delta 1^-$, pan $\gamma\delta$ TCR $^-$, $v\delta 2^-$, $CD8^+$, $CD4^+$), $CD8$ T cells ($CD3^+$, $v\delta 1^-$, pan $\gamma\delta$ TCR $^-$, $v\delta 2^-$, $CD8^+$, $CD4^-$), conventional $CD4$ T cells ($CD3^+$, $v\delta 1^-$, pan $\gamma\delta$ TCR $^-$, $v\delta 2^-$, $CD8^-$, $CD4^+$, FoxP3 $^-$) and Tregs ($CD3^+$, $v\delta 1^-$, pan $\gamma\delta$ TCR $^-$, $v\delta 2^-$, $CD8^-$, $CD4^+$, FoxP3 $^+$, $CD25^{high}$). (B) Gating strategy to identify B cell subsets identifying double negative B cells ($CD19^+$, $CD27^-$, IgD $^-$), naïve B cells ($CD19^+$, $CD27^-$, IgD $^+$), non-switched memory B cells ($CD19^+$, $CD27^+$, IgD $^+$), IgM-only memory B cells ($CD19^+$, $CD27^+$, IgD $^-$, IgM $^+$), switched memory B cells ($CD19^+$, $CD27^+$, IgD $^-$, IgM $^-$, $CD38^-/+$), and plasmacells/blasts ($CD19^+$, $CD27^+$, IgD $^-$, IgM $^-$, $CD38^{high}$). (C) Myeloid panel gating strategy identifying eosinophils (lineage $^-$, high side scatter, $CD66b^+$ $CD16^-$), neutrophils (lineage $^-$, high side scatter, $CD66b^+$ $CD16^+$), basophils (lineage $^-$, FcεRIα $^+$, HLA-DR $^-$), plasmacytoid DCs (lineage $^-$, HLA-DR $^+$, $CD303^+$, $CD123^+$), $CD141^{high}$ DCs (lineage $^-$, HLA-DR $^+$, $CD33^+$, $CD141^+$), $CD14^+$ monocytes (lineage $^-$, HLA-DR $^+$, $CD33^+$, $CD14^+$, $CD16^-/+$), $CD14^{dim}$ monocytes (lineage $^-$, HLA-DR $^+$, $CD33^+$, $CD14^{dim}$, $CD16^-/+$), $CD1c^+$ DCs (lineage $^-$, HLA-DR $^+$, $CD33^+$, $CD14^-$, $CD16^-$, $CD1c^+$, FcεRIα $^+$) and $CD1c^-$ DCs (lineage $^-$, HLA-DR $^+$, $CD33^+$, $CD14^-$, $CD16^-$, $CD1c^-$, FcεRIα $^-$).

Table 3.5: Immune-related adverse events of special interest.

Immune-related adverse event, no. of patients (%)	Any grade	Grade 3	Grade 4
ASAT increased	4 (17)	2 (9)	1 (4)
ALAT increased	2 (9)	2 (9)	0 (0)
Flu-like symptoms	2 (9)	0 (0)	0 (0)
Hypophysitis*	2 (9)	1 (4)	0 (0)
Lipase increased^	2 (9)	1 (4)	0 (0)
Colitis	1 (4)	1 (4)	0 (0)
Dry mouth	1 (4)	0 (0)	0 (0)
Dry skin	1 (4)	0 (0)	0 (0)
Myalgia	1 (4)	0 (0)	0 (0)
Sarcoid-like reaction	1 (4)	1 (4)	0 (0)

Alanine aminotransferase (ALAT); aspartate aminotransferase (ASAT).

* 1 patient developed a grade 3 hypophysitis two months after stopping atezolizumab.

^ Asymptomatic without signs of (immune-related) pancreatitis.

Table 3.6: Characteristics of patients with collected primary tumors.

Characteristic		No. (%)
Age at diagnosis, years	Median (range)	51 (33-65)
Histological subtype (assessed on primary tumor ^{1,2})	ER+HER2-	16 (94)
	ER+HER2+	1 (6)
Molecular subtype (assessed on primary tumor, n=10)	Luminal A	4 (40)
	Luminal B	5 (50)
	HER2-enriched	1 (10)
Histological grade primary tumor	Grade 1	2 (12)
	Grade 2	9 (53)
	Grade 3	3 (18)
	Unknown	3 (18)
Tumor stage at diagnosis	T1	4 (24)
	T2	8 (47)
	T3	5 (29)
Nodal stage at diagnosis	N0	5 (29)
	N1	5 (29)
	N2	2 (12)
	N3	5 (29)
Neo-adjuvant chemotherapy		6 (35)
Response to neo-adjuvant chemotherapy	pCR	0 (0)
	pPR (1-50% tumor-rest)	1 (17)
	pNR (>50% tumor-rest or no response)	5 (83)
Disease course	Primary-metastasis	10 (59)
	Primary-local recurrence-metastasis ⁴	3 (18)
	De novo M1 ⁵	2 (12)
	Primary-2 nd primary-metastasis	1 (6)
	Primary-contralateral recurrence-metastasis	1 (6)
Biopsy site GELATO-trial	Liver	7 (41)
	Lymph node	4 (24)
	Peritoneum	3 (18)
	Cervix	1 (6)
	Skin	1 (6)
	Thoracal wall	1 (6)

¹ For 1 patient with a secondary primary tumor, only the second tumor was collected (first tumor was not ILC). For 1 patient with an isolated contralateral recurrence, the first primary tumor and contralateral recurrence were collected.

² 4/5 patients with a triple-negative metastasis had a primary ER+ tumor. 1 of these patients had a triple-negative contralateral recurrence. Two out of 17 patients with de novo metastatic disease had ER+ disease.

³ including mixed classical and pleomorphic.

⁴ Local recurrence including recurrence in skin. 1 patient had a local ILC recurrence and contralateral breast cancer of no special type simultaneously.

⁵ Breast lesions are compared with synchronous distant metastasis.

Table 3.7: List of measured circulating immune cell populations

Circulating immune cell populations
Eosinophils
Basophils
Neutrophils
CD141 ^{high} dendritic cells (DCs)
CD1c ⁺ DCs
CD1c ⁻ DCs
Plasmacytoid DCs
CD14 ⁺ CD16 ⁻ monocytes
CD14 ^{dim} monocytes
Total T cells
Conventional CD4 ⁺ T cells (within total T cells)
CD8 ⁺ T cells (within total T cells)
Regulatory T cells (within total T cells)
Double positive T cells (within total T cells)
v1 T cells (within total T cells)
v2 T cells (within total T cells)
Total B cells
Double negative B cells (within total B cells)
Non-switched memory B cells (within total B cells)
IgM-only memory B cells (within total B cells)
Switched memory B cells (within total B cells)
Plasmacells/blasts (within total B cells)
Naïve B cells (within total B cells)

Table 3.8: List of antibodies used for flow cytometry.

Antigen	Fluorochrome	Clone	Dilution	Company	Catalogue number
CD3	BUV496	UCHT1	1:100	1	612940
CD4	BV421	RPA-T4	1:100	1	562424
CD8	BUV805	SK1	1:200	1	612754
Pan TCR	PE	11F2	1:100	1	555717
FoxP3	PE Cy5.5	FJK-16s	1:50	2	35-5773-82
CCR7	APC R700	150503	1:50	1	565868
CD45RA	BUV737	HI100	1:400	1	612846
CD25	AF647	BC96	1:100	3	302618
PD-1	APC Cy7	EH12.2H7	1:100	3	329922
CTLA-4	PE CF594	BNI3	1:200	1	562742
v1	FITC	TS8.2	1:100	4	TCR2730
v2	BUV395	B6	1:100	1	748582
CD19	PE Cy5	HIB19	1:200	1	555414
CD3	PE Cy5	UCHT1	1:200	1	555334
CD56	PE Cy5	B159	1:100	1	555517
CD161	PE Cy5	DX12	1:100	1	551138
HLA-DR	BUV661	G46-6	1:100	1	612980
CD14	BUV737	M5E2	1:100	1	612763
CD16	BUV496	3G8	1:100	1	612944
CD11c	BV785	3.9	1:100	3	301644
CD1c	PE Cy7	L161	1:100	3	331516
CD141	BV711	1A4	1:100	1	563155
CD123	PE	6H6	1:200	3	396604
CD66b	AF647	G10F5	1:200	1	561645
CD33	PerCP Cy5.5	WM53	1:100	3	303414
CD303	APC vio770	REA693	1:100	5	130-114-178
CD41a	BUV395	HIP8	1:400	1	740295
FcRI	PE Dazzle 594	AER-37(CRA-1)	1:200	3	334634
CD34	FITC	581	1:100	1	555821
CD19	BUV395	SJ25C1	1:50	1	563549
IgD	APC	IA6-2	1:100	1	561303
CD20	BUV805	2H7	1:200	1	612905
CD27	PE	M-T271	1:200	1	555441
CD10	AF700	HI10a	1:200	1	563509
CD24	BB515	ML5	1:200	1	564521
IgM	APC Cy7	MHM-88	1:100	3	314520
CD38	BUV737	HIT2	1:400	1	741837
CD5	PE Dazzle 594	L17F12	1:400	3	364012
CD1d	BV786	42.1	1:200	1	743608
CD138	BV711	MI15	1:200	3	563184

Company: 1 BD Bioscience; 2 eBioscience/Thermofisher; 3 BioLegend; 4 Thermofisher; 5 Miltenyi Biotec.

References

- [1] F. Dalenc, A. Lusque, T. De La Motte Rouge, B. Pistilli, E. Brain, D. Pasquier, M. Debled, J.-C. Thery, A. Gonçalves, I. Desmoulins, C. Levy, L. Uwer, J.-M. Ferrero, J.-C. Eymard, M.-A. Mouret-Reynier, A. Patsouris, J.-S. Frenel, T. Petit, M. Chevrot, T. Bachelot, and S. Guiu. "Impact of lobular versus ductal histology on overall survival in metastatic breast cancer: a French retrospective multicentre cohort study". *Eur. J. Cancer* 164 (Mar. 2022), pp. 70–79.
- [2] B. C. Pestalozzi, D. Zahrieh, E. Mallon, B. A. Gusterson, K. N. Price, R. D. Gelber, S. B. Holmberg, J. Lindtner, R. Snyder, B. Thürlimann, E. Murray, G. Viale, M. Castiglione-Gertsch, A. S. Coates, A. Goldhirsch, and International Breast Cancer Study Group. "Distinct clinical and prognostic features of infiltrating lobular carcinoma of the breast: combined results of 15 International Breast Cancer Study Group clinical trials". *J. Clin. Oncol.* 26.18 (June 2008), pp. 3006–3014.
- [3] G. W. Sledge, A. Chagpar, and C. Perou. "Collective wisdom: Lobular carcinoma of the breast". *Am. Soc. Clin. Oncol. Educ. Book* 35.36 (2016), pp. 18–21.
- [4] World Health Organization. *WHO Classification of Tumours of the Breast, 5th Edition, Volume 2*. 2019.
- [5] G. Ciriello *et al.* "Comprehensive molecular portraits of invasive lobular breast cancer". *Cell* 163.2 (Oct. 2015), pp. 506–519.
- [6] G. Arpino, V. J. Bardou, G. M. Clark, and R. M. Elledge. "Infiltrating lobular carcinoma of the breast: tumor characteristics and clinical outcome". *Breast Cancer Res.* 6.3 (Feb. 2004), R149–56.
- [7] A. Okines, T. Irfan, B. Asare, K. Mohammed, P. Osin, A. Nerurkar, I. E. Smith, M. Parton, A. Ring, S. Johnston, and N. C. Turner. "Clinical outcomes in patients with triple negative or HER2 positive lobular breast cancer: a single institution experience". *Breast Cancer Res. Treat.* 192.3 (Apr. 2022), pp. 563–571.
- [8] A. Bergeron, G. MacGrogan, A. Bertaut, S. Ladoire, P. Arveux, I. Desmoulins, H. Bonnefoi, C. Loustalot, S. Auriol, F. Beltjens, E. Degrolard-Courcet, C. Charon-Barra, C. Richard, R. Boidot, and L. Arnould. "Triple-negative breast lobular carcinoma: a luminal androgen receptor carcinoma with specific ESRRA mutations". *Mod. Pathol.* 34.7 (July 2021), pp. 1282–1296.
- [9] J. J. Gao, J. Cheng, E. Bloomquist, J. Sanchez, S. B. Wedam, H. Singh, L. Amiri-Kordestani, A. Ibrahim, R. Sridhara, K. B. Goldberg, M. R. Theoret,

- P. G. Kluetz, G. M. Blumenthal, R. Pazdur, J. A. Beaver, and T. M. Prowell. "CDK4/6 inhibitor treatment for patients with hormone receptor-positive, HER2-negative, advanced or metastatic breast cancer: a US Food and Drug Administration pooled analysis". *Lancet Oncol.* 21.2 (Feb. 2020), pp. 250–260.
- [10] M. K. Abel, M. E. Melisko, H. S. Rugo, A. J. Chien, I. Diaz, J. K. Levine, A. Griffin, J. McGuire, L. J. Esserman, H. T. Borno, and R. A. Mukhtar. "Decreased enrollment in breast cancer trials by histologic subtype: does invasive lobular carcinoma resist RECIST?" *NPJ Breast Cancer* 7.1 (Oct. 2021), p. 139.
- [11] M. Michaut, S.-F. Chin, I. Majewski, T. M. Severson, T. Bismeyer, L. de Koning, J. K. Peeters, P. C. Schouten, O. M. Rueda, A. J. Bosma, F. Tarrant, Y. Fan, B. He, Z. Xue, L. Mittempergher, R. J. C. Kluin, J. Heijmans, M. Snel, B. Pereira, A. Schlicker, E. Provenzano, H. R. Ali, A. Gaber, G. O'Hurley, S. Lehn, J. J. F. Muris, J. Wesseling, E. Kay, S. J. Sammut, H. A. Bardwell, A. S. Barbet, F. Bard, C. Lecerf, D. P. O'Connor, D. J. Vis, C. H. Benes, U. McDermott, M. J. Garnett, I. M. Simon, K. Jirstrom, T. Dubois, S. C. Linn, W. M. Gallagher, L. F. A. Wessels, C. Caldas, and R. Bernards. "Integration of genomic, transcriptomic and proteomic data identifies two biologically distinct subtypes of invasive lobular breast cancer". *Sci. Rep.* 6.1 (Jan. 2016), p. 18517.
- [12] T. Du, L. Zhu, K. M. Levine, N. Tasdemir, A. V. Lee, D. A. A. Vignali, B. Van Houten, G. C. Tseng, and S. Oesterreich. "Invasive lobular and ductal breast carcinoma differ in immune response, protein translation efficiency and metabolism". *Sci. Rep.* 8.1 (May 2018), p. 7205.
- [13] J. Cortes, D. W. Cescon, H. S. Rugo, Z. Nowecki, S.-A. Im, M. M. Yusof, C. Gallardo, O. Lipatov, C. H. Barrios, E. Holgado, H. Iwata, N. Masuda, M. T. Otero, E. Gokmen, S. Loi, Z. Guo, J. Zhao, G. Aktan, V. Karantza, P. Schmid, and KEYNOTE-355 Investigators. "Pembrolizumab plus chemotherapy versus placebo plus chemotherapy for previously untreated locally recurrent inoperable or metastatic triple-negative breast cancer (KEYNOTE-355): a randomised, placebo-controlled, double-blind, phase 3 clinical trial". *Lancet* 396.10265 (Dec. 2020), pp. 1817–1828.
- [14] L. Y. Dirix, I. Takacs, G. Jerusalem, P. Nikolinakos, H.-T. Arkenau, A. Forero-Torres, R. Boccia, M. E. Lippman, R. Somer, M. Smakal, L. A. Emens, B. Hinczenko, W. Edenfield, J. Gurtler, A. von Heydebreck, H. J. Grote, K. Chin, and E. P. Hamilton. "Avelumab, an anti-PD-L1 antibody, in patients with locally advanced or metastatic breast cancer: a phase 1b JAVELIN Solid Tumor study". *Breast Cancer Res. Treat.* 167.3 (Feb. 2018), pp. 671–686.
- [15] H. S. Rugo, J.-P. Delord, S.-A. Im, P. A. Ott, S. A. Piha-Paul, P. L. Bedard, J. Sachdev, C. L. Tourneau, E. M. J. van Brummelen, A. Varga, R. Salgado, S. Loi, S. Saraf, D. Pietrangeli, V. Karantza, and A. R. Tan. "Safety and antitumor activity of pembrolizumab in patients with estrogen receptor-positive/human epidermal growth factor receptor 2-negative advanced breast cancer". *Clin. Cancer Res.* 24.12 (June 2018), pp. 2804–2811.

- [16] S. M. Tolaney, R. Barroso-Sousa, T. Keenan, T. Li, L. Trippa, I. Vaz-Luis, G. Wulf, L. Spring, N. F. Sinclair, C. Andrews, J. Pittenger, E. T. Richardson 3rd, D. Dillon, N. U. Lin, B. Overmoyer, A. H. Partridge, E. Van Allen, E. A. Mittendorf, E. P. Winer, and I. E. Krop. "Effect of eribulin with or without pembrolizumab on progression-free survival for patients with hormone receptor-positive, ERBB2-negative metastatic breast cancer: A randomized clinical trial". *JAMA Oncol.* 6.10 (Oct. 2020), pp. 1598–1605.
- [17] J. M. Pérez-García, A. Llombart-Cussac, M. G. Cortés, G. Curigliano, E. López-Miranda, J. L. Alonso, B. Bermejo, L. Calvo, V. Carañana, S. de la Cruz Sánchez, R. M. Vázquez, A. Prat, M. R. Borrego, M. Sampayo-Cordero, M. Á. Seguí-Palmer, J. Soberino, A. Malfettone, P. Schmid, and J. Cortés. "Pembrolizumab plus eribulin in hormone-receptor-positive, HER2-negative, locally recurrent or metastatic breast cancer (KELLY): An open-label, multicentre, single-arm, phase II trial". *Eur. J. Cancer* 148 (May 2021), pp. 382–394.
- [18] L. Spagnuolo, K. Kersten, O. S. Blomberg, C. S. Hau, K. Kos, K. Vrijland, and K. E. D. Visser. "PO-365 Dissecting the synergistic effect of chemotherapy and immunotherapy on anti-tumoral T cell functions in breast cancer". *Poster Presentation*. BMJ Publishing Group Ltd, July 2018.
- [19] G. Sflomos, K. Schipper, T. Koorman, A. Fitzpatrick, S. Oesterreich, A. V. Lee, J. Jonkers, V. G. Brunton, M. Christgen, C. Isacke, P. W. B. Derksen, and C. Briskin. "Atlas of lobular breast cancer models: Challenges and strategic directions". *Cancers (Basel)* 13.21 (Oct. 2021), p. 5396.
- [20] P. W. B. Derksen, X. Liu, F. Saridin, H. van der Gulden, J. Zevenhoven, B. Evers, J. R. van Beijnum, A. W. Griffioen, J. Vink, P. Krimpenfort, J. L. Peterse, R. D. Cardiff, A. Berns, and J. Jonkers. "Somatic inactivation of E-cadherin and p53 in mice leads to metastatic lobular mammary carcinoma through induction of anoikis resistance and angiogenesis". *Cancer Cell* 10.5 (Nov. 2006), pp. 437–449.
- [21] L. Schadt, C. Sparano, N. A. Schweiger, K. Silina, V. Cecconi, G. Lucchiari, H. Yagita, E. Guggisberg, S. Saba, Z. Nascakova, W. Barchet, and M. van den Broek. "Cancer-cell-intrinsic cGAS expression mediates tumor immunogenicity". *Cell Rep.* 29.5 (Oct. 2019), 1236–1248.e7.
- [22] S. Wan, S. Pestka, R. G. Jubin, Y. L. Lyu, Y.-C. Tsai, and L. F. Liu. "Chemotherapeutics and radiation stimulate MHC class I expression through elevated interferon-beta signaling in breast cancer cells". *PLoS One* 7.3 (Mar. 2012), e32542.
- [23] F. Bensch, E. L. van der Veen, M. N. Lub-de Hooge, A. Jorritsma-Smit, R. Boellaard, I. C. Kok, S. F. Oosting, C. P. Schröder, T. J. N. Hiltermann, A. J. van der Wekken, H. J. M. Groen, T. C. Kwee, S. G. Elias, J. A. Gietema, S. S. Bohorquez, A. de Crespigny, S.-P. Williams, C. Mancao, A. H. Brouwers, B. M. Fine, and E. G. E. de Vries. "89Zr-atezolizumab imaging as a non-invasive approach to assess clinical response to PD-L1 blockade in cancer". *Nat. Med.* 24.12 (Dec. 2018), pp. 1852–1858.
- [24] A. Tutt, H. Tovey, M. C. U. Cheang, S. Kernaghan, L. Kilburn, P. Gazinska, J. Owen, J. Abraham, S. Barrett, P. Barrett-Lee, R. Brown, S. Chan, M.

- Dowsett, J. M. Flanagan, L. Fox, A. Grigoriadis, A. Gutin, C. Harper-Wynne, M. Q. Hatton, K. A. Hoadley, J. Parikh, P. Parker, C. M. Perou, R. Roylance, V. Shah, A. Shaw, I. E. Smith, K. M. Timms, A. M. Wardley, G. Wilson, C. Gillett, J. S. Lanchbury, A. Ashworth, N. Rahman, M. Harries, P. Ellis, S. E. Pinder, and J. M. Bliss. "Carboplatin in BRCA1/2-mutated and triple-negative breast cancer BRCAness subgroups: the TNT Trial". *Nat. Med.* 24.5 (May 2018), pp. 628–637.
- [25] S. Loibl, J. O'Shaughnessy, M. Untch, W. M. Sikov, H. S. Rugo, M. D. McKee, J. Huober, M. Golshan, G. von Minckwitz, D. Maag, D. Sullivan, N. Wolmark, K. McIntyre, J. J. Ponce Lorenzo, O. Metzger Filho, P. Rastogi, W. F. Symmans, X. Liu, and C. E. Geyer Jr. "Addition of the PARP inhibitor veliparib plus carboplatin or carboplatin alone to standard neoadjuvant chemotherapy in triple-negative breast cancer (BrightTNess): a randomised, phase 3 trial". *Lancet Oncol.* 19.4 (Apr. 2018), pp. 497–509.
- [26] J. Yu, M. D. Green, S. Li, Y. Sun, S. N. Journey, J. E. Choi, S. M. Rizvi, A. Qin, J. J. Waninger, X. Lang, Z. Chopra, I. El Naqa, J. Zhou, Y. Bian, L. Jiang, A. Tezel, J. Skvarce, R. K. Achar, M. Sitto, B. S. Rosen, F. Su, S. P. Narayanan, X. Cao, S. Wei, W. Szeliga, L. Vatan, C. Mayo, M. A. Morgan, C. A. Schonewolf, K. Cuneo, I. Kryczek, V. T. Ma, C. D. Lao, T. S. Lawrence, N. Ramnath, F. Wen, A. M. Chinnaiyan, M. Cieslik, A. Alva, and W. Zou. "Liver metastasis restrains immunotherapy efficacy via macrophage-mediated T cell elimination". *Nat. Med.* 27.1 (Jan. 2021), pp. 152–164.
- [27] M. Ayers, J. Lunceford, M. Nebozhyn, E. Murphy, A. Loboda, D. R. Kaufman, A. Albright, J. D. Cheng, S. P. Kang, V. Shankaran, S. A. Piha-Paul, J. Yearley, T. Y. Seiwert, A. Ribas, and T. K. McClanahan. "IFN- γ -related mRNA profile predicts clinical response to PD-1 blockade". *J. Clin. Invest.* 127.8 (Aug. 2017), pp. 2930–2940.
- [28] A. C. Scott, F. Dündar, P. Zumbo, S. S. Chandran, C. A. Klebanoff, M. Shakiba, P. Trivedi, L. Menocal, H. Appleby, S. Camara, D. Zamarin, T. Walther, A. Snyder, M. R. Femia, E. A. Comen, H. Y. Wen, M. D. Hellmann, N. Anandasabapathy, Y. Liu, N. K. Altorki, P. Lauer, O. Levy, M. S. Glickman, J. Kaye, D. Betel, M. Philip, and A. Schietinger. "TOX is a critical regulator of tumour-specific T cell differentiation". *Nature* 571.7764 (July 2019), pp. 270–274.
- [29] R. Cabrita, M. Lauss, A. Sanna, M. Donia, M. Skaarup Larsen, S. Mitra, I. Johansson, B. Phung, K. Harbst, J. Vallon-Christersson, A. van Schoiack, K. Lövgren, S. Warren, K. Jirström, H. Olsson, K. Pietras, C. Ingvar, K. Isaksson, D. Schadendorf, H. Schmidt, L. Bastholt, A. Carneiro, J. A. Wargo, I. M. Svane, and G. Jönsson. "Tertiary lymphoid structures improve immunotherapy and survival in melanoma". *Nature* 577.7791 (Jan. 2020), pp. 561–565.
- [30] A. Bagaev, N. Kotlov, K. Nomie, V. Svelkolkin, A. Gafurov, O. Isaeva, N. Osokin, I. Kozlov, F. Frenkel, O. Gancharova, N. Almog, M. Tsiper, R. Ataullakhanov, and N. Fowler. "Conserved pan-cancer microenvironment

- subtypes predict response to immunotherapy". *Cancer Cell* 39.6 (June 2021), 845–865.e7.
- [31] F. Pareja, L. Ferrando, S. S. K. Lee, F. Beca, P. Selenica, D. N. Brown, A. Farmanbar, A. Da Cruz Paula, M. Vahdatinia, H. Zhang, G. Zoppoli, H. Y. Wen, E. Brogi, M. E. Robson, P. Razavi, S. Chandarlapaty, B. Weigelt, and J. S. Reis-Filho. "The genomic landscape of metastatic histologic special types of invasive breast cancer". *NPJ Breast Cancer* 6.1 (Oct. 2020), p. 53.
 - [32] E. S. Sokol, Y. X. Feng, D. X. Jin, A. Basudan, A. V. Lee, J. M. Atkinson, J. Chen, P. J. Stephens, G. M. Frampton, P. B. Gupta, J. S. Ross, J. H. Chung, S. Oesterreich, S. M. Ali, and R. J. Hartmaier. "Loss of function of NF1 is a mechanism of acquired resistance to endocrine therapy in lobular breast cancer". *Ann. Oncol.* 30.1 (Jan. 2019), pp. 115–123.
 - [33] F. Richard, S. Majjaj, D. Venet, F. Rothé, J. Pingitore, B. Boeckx, C. Marchio, F. Clatot, F. Bertucci, O. Mariani, C. Galant, G. van den Eynden, R. Salgado, E. Biganzoli, D. Lambrechts, A. Vincent-Salomon, G. Pruneri, D. Larsimont, C. Sotiriou, and C. Desmedt. "Characterization of stromal tumor-infiltrating lymphocytes and genomic alterations in metastatic lobular breast cancer". *Clin. Cancer Res.* 26.23 (Dec. 2020), pp. 6254–6265.
 - [34] A. M. Newman, C. B. Steen, C. L. Liu, A. J. Gentles, A. A. Chaudhuri, F. Scherer, M. S. Khodadoust, M. S. Esfahani, B. A. Luca, D. Steiner, M. Diehn, and A. A. Alizadeh. "Determining cell type abundance and expression from bulk tissues with digital cytometry". *Nat. Biotechnol.* 37.7 (July 2019), pp. 773–782.
 - [35] A. Liberzon, C. Birger, H. Thorvaldsdóttir, M. Ghandi, J. P. Mesirov, and P. Tamayo. "The Molecular Signatures Database (MSigDB) hallmark gene set collection". *Cell Syst.* 1.6 (Dec. 2015), pp. 417–425.
 - [36] A. C. Huang, R. J. Orlowski, X. Xu, R. Mick, S. M. George, P. K. Yan, S. Manne, A. A. Kraya, B. Wubbenhorst, L. Dorfman, K. D'Andrea, B. M. Wenz, S. Liu, L. Chilukuri, A. Kozlov, M. Carberry, L. Giles, M. W. Kier, F. Quagliarello, S. McGettigan, K. Kreider, L. Annamalai, Q. Zhao, R. Mogg, W. Xu, W. M. Blumenschein, J. H. Yearley, G. P. Linette, R. K. Amaravadi, L. M. Schuchter, R. S. Herati, B. Bengsch, K. L. Nathanson, M. D. Farwell, G. C. Karakousis, E. J. Wherry, and T. C. Mitchell. "A single dose of neoadjuvant PD-1 blockade predicts clinical outcomes in resectable melanoma". *Nat. Med.* 25.3 (Mar. 2019), pp. 454–461.
 - [37] S. C. S. Simon, X. Hu, J. Panten, M. Grees, S. Renders, D. Thomas, R. Weber, T. J. Schulze, J. Utikal, and V. Umansky. "Eosinophil accumulation predicts response to melanoma treatment with immune checkpoint inhibitors". *Oncoimmunology* 9.1 (Feb. 2020), p. 1727116.
 - [38] A.-K. A. Lalani, W. Xie, D. J. Martini, J. A. Steinharter, C. K. Norton, K. M. Krajewski, A. Duquette, D. Bossé, J. Bellmunt, E. M. Van Allen, B. A. McGregor, C. J. Creighton, L. C. Harshman, and T. K. Choueiri. "Change in neutrophil-to-lymphocyte ratio (NLR) in response to immune

- checkpoint blockade for metastatic renal cell carcinoma". *J. Immunother. Cancer* 6.1 (Dec. 2018).
- [39] D. S. Thommen, V. H. Koelzer, P. Herzig, A. Roller, M. Trefny, S. Dimeloe, A. Kiialainen, J. Hanhart, C. Schill, C. Hess, S. Savic Prince, M. Wiese, D. Lardinois, P.-C. Ho, C. Klein, V. Karanikas, K. D. Mertz, T. N. Schumacher, and A. Zippelius. "A transcriptionally and functionally distinct PD-1+ CD8+ T cell pool with predictive potential in non-small-cell lung cancer treated with PD-1 blockade". *Nat. Med.* 24.7 (July 2018), pp. 994–1004.
- [40] X. An, Y. Zhu, T. Zheng, G. Wang, M. Zhang, J. Li, H. Ji, S. Li, S. Yang, D. Xu, Z. Li, T. Wang, Y. He, L. Zhang, W. Yang, R. Zhao, D. Hao, and X. Li. "An analysis of the expression and association with immune cell infiltration of the cGAS/STING pathway in pan-cancer". *Mol. Ther. Nucleic Acids* 14 (Mar. 2019), pp. 80–89.
- [41] P. Aftimos, M. Oliveira, A. Irrthum, D. Fumagalli, C. Sotiriou, E. N. Gal-Yam, M. E. Robson, J. Ndozen, A. Di Leo, E. M. Ciruelos, E. de Azambuja, G. Viale, E. D. Scheepers, G. Curigliano, J. M. Bliss, J. S. Reis-Filho, M. Colleoni, M. Balic, F. Cardoso, J. Albanell, C. Duhem, S. Marreaud, D. Romagnoli, B. Rojas, A. Gombos, H. Wildiers, A. Guerrero-Zotano, P. Hall, A. Bonetti, K. F. Larsson, M. Degiorgis, S. Khodaverdi, R. Greil, Á. Sverrisdóttir, M. Paoli, E. Seyll, S. Loibl, B. Linderholm, G. Zoppoli, N. E. Davidson, O. T. Johannsson, P. L. Bedard, S. Loi, S. Knox, D. A. Cameron, N. Harbeck, M. L. Montoya, M. Brandão, A. Vingiani, C. Caballero, F. S. Hilbers, L. R. Yates, M. Benelli, D. Venet, and M. J. Piccart. "Genomic and transcriptomic analyses of breast cancer primaries and matched metastases in AURORA, the breast international group (BIG) molecular screening initiative". *Cancer Discov.* 11.11 (Nov. 2021), pp. 2796–2811.
- [42] C. L. T. Jørgensen, A.-M. Larsson, C. Forsare, K. Aaltonen, S. Jansson, R. Bradshaw, P.-O. Bendahl, and L. Rydén. "PAM50 intrinsic subtype profiles in primary and metastatic Breast Cancer show a significant shift toward more aggressive subtypes with prognostic implications". *Cancers (Basel)* 13.7 (Mar. 2021), p. 1592.
- [43] A. D. Garg, D. De Ruyscher, and P. Agostinis. "Immunological metagene signatures derived from immunogenic cancer cell death associate with improved survival of patients with lung, breast or ovarian malignancies: A large-scale meta-analysis". *Oncoimmunology* 5.2 (Feb. 2016), e1069938.
- [44] F. Conforti, L. Pala, E. Pagan, E. G. Rocco, V. Bagnardi, E. Montagna, G. Peruzzotti, T. De Pas, C. Fumagalli, S. Pileggi, C. Pesenti, S. Marchini, G. Corso, C. Marchio', A. Sapino, R. Graffeo, L. Collet, P. Aftimos, C. Sotiriou, M. Piccart, R. D. Gelber, G. Viale, M. Colleoni, and A. Goldhirsch. "Biological and clinical features of triple negative Invasive Lobular Carcinomas of the breast. Clinical outcome and actionable molecular alterations". *Breast* 59 (Oct. 2021), pp. 94–101.
- [45] J. A. Mouabbi, A. Hassan, B. Lim, G. N. Hortobagyi, D. Tripathy, and R. M. Layman. "Invasive lobular carcinoma: an understudied emergent subtype of breast cancer". *Breast Cancer Res. Treat.* 193.2 (June 2022), pp. 253–264.

- [46] X. Guan, F. Polesso, C. Wang, A. Sehrawat, R. M. Hawkins, S. E. Murray, G. V. Thomas, B. Caruso, R. F. Thompson, M. A. Wood, C. Hipfinger, S. A. Hammond, J. N. Graff, Z. Xia, and A. E. Moran. "Androgen receptor activity in T cells limits checkpoint blockade efficacy". *Nature* 606.7915 (June 2022), pp. 791–796.
- [47] L. A. Emens, L. D. Goldstein, P. Schmid, H. S. Rugo, S. Adams, C. H. Barrios, A. Schneeweiss, V. Dieras, H. Iwata, C.-W. Chang, H. Koeppen, S. Y. Chui, S. Loi, and L. Molinero. "The tumor microenvironment (TME) and atezolizumab + nab-paclitaxel (A+nP) activity in metastatic triple-negative breast cancer (mTNBC): IMpassion130". *J. Clin. Oncol.* 39.15_suppl (May 2021), pp. 1006–1006.
- [48] T. E. Keenan, J. L. Guerriero, R. Barroso-Sousa, T. Li, T. O'Meara, A. Giobbie-Hurder, N. Tayob, J. Hu, M. Severgnini, J. Agudo, I. Vaz-Luis, L. Anderson, V. Attaya, J. Park, J. Conway, M. X. He, B. Reardon, E. Shannon, G. Wulf, L. M. Spring, R. Jeselsohn, I. Krop, N. U. Lin, A. Partridge, E. P. Winer, E. A. Mittendorf, D. Liu, E. M. Van Allen, and S. M. Tolaney. "Molecular correlates of response to eribulin and pembrolizumab in hormone receptor-positive metastatic breast cancer". *Nat. Commun.* 12.1 (Sept. 2021), p. 5563.
- [49] B. Chakraborty, J. Byemerwa, J. Shepherd, C. N. Haines, R. Baldi, W. Gong, W. Liu, D. Mukherjee, S. Artham, F. Lim, Y. Bae, O. Brueckner, K. Tavares, S. E. Wardell, B. A. Hanks, C. M. Perou, C.-Y. Chang, and D. P. McDonnell. "Inhibition of estrogen signaling in myeloid cells increases tumor immunity in melanoma". *J. Clin. Invest.* 131.23 (Dec. 2021).
- [50] A. G. Waks, D. G. Stover, J. L. Guerriero, D. Dillon, W. T. Barry, E. Gjini, C. Hartl, W. Lo, J. Savoie, J. Brock, R. Wesolowski, Z. Li, A. Damicis, A. V. Philips, Y. Wu, F. Yang, A. Sullivan, P. Danaher, H. A. Brauer, W. Osmani, M. Lipschitz, K. A. Hoadley, M. Goldberg, C. M. Perou, S. Rodig, E. P. Winer, I. E. Krop, E. A. Mittendorf, and S. M. Tolaney. "The immune microenvironment in hormone receptor-positive breast cancer before and after preoperative chemotherapy". *Clin. Cancer Res.* 25.15 (Aug. 2019), pp. 4644–4655.
- [51] S. Tuit, C. Salvagno, T. S. Kapellos, C.-S. Hau, L. Seep, M. Oestreich, K. Klee, K. E. de Visser, T. Ulas, and J. L. Schultze. "Transcriptional signature derived from Murine tumor-associated macrophages correlates with poor outcome in breast cancer patients". *Cell Rep.* 29.5 (Oct. 2019), 1221–1235.e5.
- [52] M. V. Dieci, V. Guarneri, A. Tosi, G. Bisagni, A. Musolino, S. Spazzapan, G. Moretti, G. M. Vernaci, G. Griguolo, T. Giarratano, L. Urso, F. Schiavi, C. Pinato, G. Magni, M. Lo Mele, G. L. De Salvo, A. Rosato, and P. Conte. "Neoadjuvant chemotherapy and immunotherapy in Luminal B-like breast cancer: Results of the phase II GIADA trial". *Clin. Cancer Res.* 28.2 (Jan. 2022), pp. 308–317.
- [53] J. Albanell, J. M. Pérez-García, M. Gil-Gil, G. Curigliano, M. Ruíz-Borrego, L. Comerma, J. Gibert, M. Bellet, B. Bermejo, L. Calvo, J. de la Haba, E. Espinosa, A. M. Minisini, V. Quiroga, A. Santaballa Bertran, L. Mina,

- B. Bellosillo, F. Rojo, S. Menéndez, M. Sampayo-Cordero, C. Popa, A. Malfettone, J. Cortés, and A. Llombart-Cussac. "Palbociclib rechallenge for hormone receptor-positive/HER-negative advanced breast cancer: Findings from the phase II BioPER trial". *Clin. Cancer Res.* 29.1 (Jan. 2023), pp. 67–80.
- [54] P. Savas, Kathleen Cuninghame Foundation Consortium for Research into Familial Breast Cancer (kConFab), B. Virassamy, C. Ye, A. Salim, C. P. Mintoff, F. Caramia, R. Salgado, D. J. Byrne, Z. L. Teo, S. Dushyanthen, A. Byrne, L. Wein, S. J. Luen, C. Poliness, S. S. Nightingale, A. S. Skandarajah, D. E. Gyorki, C. M. Thornton, P. A. Beavis, S. B. Fox, P. K. Darcy, T. P. Speed, L. K. Mackay, P. J. Neeson, and S. Loi. "Single-cell profiling of breast cancer T cells reveals a tissue-resident memory subset associated with improved prognosis". *Nat. Med.* 24.7 (July 2018), pp. 986–993.
- [55] K. Van Baelen, T. Geukens, M. Maetens, V. Tjan-Heijnen, C. J. Lord, S. Linn, F.-C. Bidard, F. Richard, W. W. Yang, R. E. Steele, S. J. Pettitt, C. Van Ongeval, M. De Schepper, E. Isnaldi, I. Nevelsteen, A. Smeets, K. Punie, L. Voorwerk, H. Wildiers, G. Floris, A. Vincent-Salomon, P. W. B. Derksen, P. Neven, E. Senkus, E. Sawyer, M. Kok, and C. Desmedt. "Current and future diagnostic and treatment strategies for patients with invasive lobular breast cancer". *Ann. Oncol.* 33.8 (Aug. 2022), pp. 769–785.
- [56] C. X. Ma, J. Luo, R. A. Freedman, T. J. Pluard, J. R. Nangia, J. Lu, F. Valdez-Albini, M. Cobleigh, J. M. Jones, N. U. Lin, E. P. Winer, P. K. Marcom, S. Thomas, J. Anderson, B. Haas, L. Bucheit, R. Bryce, A. S. Lalani, L. A. Carey, M. P. Goetz, F. Gao, G. Kimmick, M. D. Pegram, M. J. Ellis, and R. Bose. "The phase II MuthER study of neratinib alone and in combination with fulvestrant in HER2-mutated, non-amplified metastatic breast cancer". *Clin. Cancer Res.* 28.7 (Apr. 2022), pp. 1258–1267.
- [57] I. Bajrami, R. Marlow, M. van de Ven, R. Brough, H. N. Pemberton, J. Frankum, F. Song, R. Rafiq, A. Konde, D. B. Krastev, M. Menon, J. Campbell, A. Gulati, R. Kumar, S. J. Pettitt, M. D. Gurden, M. L. Cardenosa, I. Chong, P. Gazinska, F. Wallberg, E. J. Sawyer, L.-A. Martin, M. Dowsett, S. Linardopoulos, R. Natrajan, C. J. Ryan, P. W. B. Derksen, J. Jonkers, A. N. J. Tutt, A. Ashworth, and C. J. Lord. "E-cadherin/ROS1 inhibitor synthetic lethality in breast cancer". *Cancer Discov.* 8.4 (Apr. 2018), pp. 498–515.
- [58] A. M. Nagle, K. M. Levine, N. Tasdemir, J. A. Scott, K. Burlbaugh, J. Kehm, T. A. Katz, D. N. Boone, B. M. Jacobsen, J. M. Atkinson, S. Oesterreich, and A. V. Lee. "Loss of E-cadherin enhances IGF1-IGF1R pathway activation and sensitizes breast cancers to anti-IGF1R/InsR inhibitors". *Clin. Cancer Res.* 24.20 (Oct. 2018), pp. 5165–5177.
- [59] Y. An, J. R. Adams, D. P. Hollern, A. Zhao, S. G. Chang, M. S. Gams, P. E. D. Chung, X. He, R. Jangra, J. S. Shah, J. Yang, L. A. Beck, N. Raghuram, K. J. Kozma, A. J. Loch, W. Wang, C. Fan, S. J. Done, E. Zacksenhaus, C. J. Guidos, C. M. Perou, and S. E. Egan. "Cdh1 and Pik3ca mutations cooperate to induce immune-related invasive lobular carcinoma of the breast". *Cell Rep.* 25.3 (Oct. 2018), 702–714.e6.

- [60] C. Salvagno, M. Ciampricotti, S. Tuit, C.-S. Hau, A. van Weverwijk, S. B. Coffelt, K. Kersten, K. Vrijland, K. Kos, T. Ulas, J.-Y. Song, C.-H. Ooi, D. Rüttinger, P. A. Cassier, J. Jonkers, J. L. Schultze, C. H. Ries, and K. E. de Visser. "Therapeutic targeting of macrophages enhances chemotherapy efficacy by unleashing type I interferon response". *Nat. Cell Biol.* 21.4 (Apr. 2019), pp. 511–521.
- [61] E. A. Eisenhauer, P. Therasse, J. Bogaerts, L. H. Schwartz, D. Sargent, R. Ford, J. Dancey, S. Arbuck, S. Gwyther, M. Mooney, L. Rubinstein, L. Shankar, L. Dodd, R. Kaplan, D. Lacombe, and J. Verweij. "New response evaluation criteria in solid tumours: revised RECIST guideline (version 1.1)". *Eur. J. Cancer* 45.2 (Jan. 2009), pp. 228–247.
- [62] L. Seymour, J. Bogaerts, A. Perrone, R. Ford, L. H. Schwartz, S. Mandrekar, N. U. Lin, S. Litière, J. Dancey, A. Chen, F. S. Hodi, P. Therasse, O. S. Hoekstra, L. K. Shankar, J. D. Wolchok, M. Ballinger, C. Caramella, E. G. E. de Vries, and RECIST working group. "iRECIST: guidelines for response criteria for use in trials testing immunotherapeutics". *Lancet Oncol.* 18.3 (Mar. 2017), e143–e152.
- [63] M. Casparie, A. T. M. G. Tiebosch, G. Burger, H. Blauwgeers, A. van de Pol, J. H. J. M. van Krieken, and G. A. Meijer. "Pathology databanking and biobanking in The Netherlands, a central role for PALGA, the nationwide histopathology and cytopathology data network and archive". *Cell. Oncol.* 29.1 (2007), pp. 19–24.
- [64] R. Simon. "Optimal two-stage designs for phase II clinical trials". *Control. Clin. Trials* 10.1 (Mar. 1989), pp. 1–10.
- [65] L. Voorwerk, H. Garner, O. S. Blomberg, L. Spagnuolo, M. Chalabi, E. van Dyk, O. I. Isaeva, N. Bakker, C. Klaver, M. Duijst, K. Kersten, L. R. Hoes, J. van Dorp, M. S. van der Heijden, W. S. M. E. Theelen, E. E. Voest, L. F. Wessels, K. E. de Visser, and M. Kok. "LBA10 Critical role of eosinophils during response to immune checkpoint blockade in breast cancer and other cancer types". *Ann. Oncol.* 31 (Sept. 2020), S1142.
- [66] R. Salgado, C. Denkert, S. Demaria, N. Sirtaine, F. Klauschen, G. Pruneri, S. Wienert, G. Van den Eynden, F. L. Baehner, F. Penault-Llorca, E. A. Perez, E. A. Thompson, W. F. Symmans, A. L. Richardson, J. Brock, C. Criscitiello, H. Bailey, M. Ignatiadis, G. Floris, J. Sparano, Z. Kos, T. Nielsen, D. L. Rimm, K. H. Allison, J. S. Reis-Filho, S. Loibl, C. Sotiriou, G. Viale, S. Badve, S. Adams, K. Willard-Gallo, and S. Loi. "The evaluation of tumor-infiltrating lymphocytes (TILs) in breast cancer: recommendations by an International TILs Working Group 2014". *Ann. Oncol.* 26.2 (Feb. 2015), pp. 259–271.
- [67] H. Li. "Aligning sequence reads, clone sequences and assembly contigs with BWA-MEM". 2013. eprint: 1303.3997 (q-bio.GN).
- [68] A. McKenna, M. Hanna, E. Banks, A. Sivachenko, K. Cibulskis, A. Kernysky, K. Garimella, D. Altshuler, S. Gabriel, M. Daly, and M. A. DePristo. "The Genome Analysis Toolkit: a MapReduce framework for analyzing next-generation DNA sequencing data". *Genome Res.* 20.9 (Sept. 2010), pp. 1297–1303.

- [69] D. Benjamin, T. Sato, K. Cibulskis, G. Getz, C. Stewart, and L. Lichtenstein. "Calling Somatic SNVs and Indels with Mutect2". Dec. 2019.
- [70] C. P. Wardell, C. Ashby, and M. A. Bauer. "FiNGS: high quality somatic mutations using filters for next generation sequencing". *BMC Bioinformatics* 22.1 (Feb. 2021), p. 77.
- [71] A. Mayakonda, D.-C. Lin, Y. Assenov, C. Plass, and H. P. Koeffler. "Maftools: efficient and comprehensive analysis of somatic variants in cancer". *Genome Res.* 28.11 (Nov. 2018), pp. 1747–1756.
- [72] A. Dobin, C. A. Davis, F. Schlesinger, J. Drenkow, C. Zaleski, S. Jha, P. Batut, M. Chaisson, and T. R. Gingeras. "STAR: ultrafast universal RNA-seq aligner". *Bioinformatics* 29.1 (Jan. 2013), pp. 15–21.
- [73] Andrews, Simon. *A quality control tool for high throughput sequence data*. 2016.
- [74] S. W. Wingett and S. Andrews. "FastQ Screen: A tool for multi-genome mapping and quality control". *F1000Res.* 7 (Aug. 2018), p. 1338.
- [75] L. Wang, S. Wang, and W. Li. "RSeQC: quality control of RNA-seq experiments". *Bioinformatics* 28.16 (Aug. 2012), pp. 2184–2185.
- [76] C. B. Steen, C. L. Liu, A. A. Alizadeh, and A. M. Newman. "Profiling cell type abundance and expression in bulk tissues with CIBERSORTx". *Methods Mol. Biol.* 2117 (2020), pp. 135–157.
- [77] M. I. Love, W. Huber, and S. Anders. "Moderated estimation of fold change and dispersion for RNA-seq data with DESeq2". *Genome Biol.* 15.12 (2014), p. 550.
- [78] D. M. A. Gendoo, N. Ratanasirigulchai, M. S. Schröder, L. Paré, J. S. Parker, A. Prat, and B. Haibe-Kains. "Genefu: an R/Bioconductor package for computation of gene expression-based signatures in breast cancer". *Bioinformatics* 32.7 (Apr. 2016), pp. 1097–1099.
- [79] Z. Fang, X. Liu, and G. Peltz. "GSEAPy: a comprehensive package for performing gene set enrichment analysis in Python". *Bioinformatics* 39.1 (Jan. 2023).
- [80] R. Boellaard. "Quantitative oncology molecular analysis suite: ACCURATE". *Journal of Nuclear Medicine* 59.supplement 1 (2018), p. 1753.

4

ctDNA-based copy number dynamics during anti-PD-1 treatment in metastatic triple negative breast cancer

A modified version of this chapter is accepted to be published in *Cell Reports Medicine*, 2025.

Aaron Y. Lin^{1,*}, **Olga I. Isaeva^{1,*}**, Teoman Deger², Veerle C.M. Geurts¹, Daan C.L. Vessies³, Leonie Voorwerk^{1,4}, Maarten Slagter^{5,6}, Kat Moore^{1,6}, Paul van der Leest³, Lodewyk F. A. Wessels⁶, John Martens², Daan van den Broek³, Marleen Kok^{1,7}

*These authors contributed equally

- ¹ Division of Tumor Biology & Immunology, The Netherlands Cancer Institute, Amsterdam, the Netherlands
- ² Department of Medical Oncology, Erasmus University Medical Center, Rotterdam, the Netherlands
- ³ Department of Laboratory Medicine, Netherlands Cancer Institute, Amsterdam, the Netherlands
- ⁴ Department of Internal Medicine, Groene Hart Ziekenhuis, Gouda, the Netherlands
- ⁵ Department of Molecular Oncology & Immunology, Netherlands Cancer Institute, Amsterdam, the Netherlands
- ⁶ Division of Molecular Carcinogenesis, Netherlands Cancer Institute, Amsterdam, the Netherlands
- ⁷ Department of Medical Oncology, Netherlands Cancer Institute, Amsterdam, the Netherlands

Circulating tumor DNA (ctDNA) is an emerging technology to predict and monitor responses to cancer treatment, including immune checkpoint blockade (ICB). However, data on ctDNA dynamics during ICB in metastatic triple negative breast cancer (mTNBC) are limited. While most ctDNA assays focus on mutation detection, mTNBC and multiple other cancer types are driven by copy number alterations (CNAs). In

this study, we explore the potential utility of ctDNA-based copy number abnormality (CPA) scores from 30 patients with mTNBC treated with ICB in a phase II clinical trial (TONIC trial, NCT02499367). We found significant concordance between ctDNA-based and tissue-based CNA profiles. CPA scores decreased in responders during ICB, while ctDNA levels increased in non-responders. These findings suggest ctDNA-based CNAs could serve as a non-invasive biomarker, complementing ctDNA levels, for early response assessment in patients with mTNBC receiving ICB.

4.1. Introduction

Triple-negative breast cancer (TNBC) accounts for 10-15% of all breast cancer cases and is characterized by the absence of estrogen receptor (ER) and progesterone receptor (PR), and lack of overexpression or amplification of human epidermal growth factor receptor 2 (HER2) [1, 2]. Over 30% of patients with TNBC develop distant metastases [1], and metastatic TNBC (mTNBC) has a poor prognosis with a median overall survival (OS) of approximately 1.5 years [3, 4].

Immunotherapy has revolutionized cancer treatment, including for mTNBC [5]. The IMpassion1306 and KEYNOTE-3557 trials showed that adding programmed death (ligand) 1 blockade (anti-PD-(L)1) to chemotherapy improved progression-free survival (PFS) and OS in PD-(L)1 positive population, leading to approval for the use of anti-PD-(L)1 in PD-L1 positive mTNBC [6, 7]. Although a subset of patients has long-term benefit with very durable responses, most do not benefit from ICB while being subjected to treatment-related adverse effects [8], suggesting that the accuracy of the tissue-based biomarker PD-L1 is suboptimal [9–11]. This underscores the need for more precise biomarkers to guide more personalized treatment approaches.

Liquid biopsies have become a significant focus in biomarker research. They offer distinct advantages over tissue biopsies, such as providing sequential dynamics due to their less invasive nature and capturing the tumor heterogeneity from various regions and metastatic sites [12, 13]. Recent studies demonstrated a consistent relationship between ctDNA levels and prognosis in early TNBC [14, 15]. Prior studies showed that early changes in ctDNA levels are associated with response to immune checkpoint blockade (ICB) and prognosis across a range of advanced solid tumors [16, 17]. However, for mTNBC data are limited so far. These findings highlight the potential of tracking ctDNA dynamics as a potential approach for predicting outcomes and monitoring response to ICB in TNBC.

Beyond tracking ctDNA dynamics, detecting copy number alterations (CNAs) from ctDNA could be of interest for tumors exhibiting higher CNAs and relatively lower mutation abundance including TNBC [12, 18]. Interestingly, CNA levels are linked to immune evasion in multiple cancer types, including breast cancer [19, 20]. Stover et al. and Prat et al. found a concordance between ctDNA-derived and tumor-derived CNA profiles in metastatic breast cancer, supporting the use of ctDNA for detecting CNAs [21, 22]. A recent study demonstrated the prognostic value of ctDNA-based CNAs derived from shallow whole-genome sequencing (sWGS) in patients with breast cancer [23]. Previous studies have also established ctDNA-based CNAs as a potential biomarker during immunotherapy for non-small cell lung cancer (NSCLC) and other cancer

types [24, 25]. However, the relationship between ctDNA-based CNAs and response to ICB in mTNBC remains largely unexplored. In this pilot study, we investigate the potential use of ctDNA-based CNAs for patients with mTNBC during treatment with ICB in a phase II clinical trial.

4.2. Results

Study design and patient characteristics

We conducted a pilot study in a subset of patients with mTNBC receiving nivolumab after induction treatment with low-dose chemotherapy or irradiation in the TONIC trial [26]. Thirty patients were selected taking all patients with clinical benefit (n=14) and a similar number of patients (n=16) without response to treatment. We performed ctDNA analysis from sWGS data of paired plasma samples at baseline and after 6 cycles (12 weeks) of nivolumab. Patient characteristics and study design are demonstrated in **Supplementary Table 4.1** and **Figure 4.1A**.

CNA profiles were derived from sWGS plasma samples and quantified using CPA scores

We applied a previously described bioinformatics pipeline [27] to the sWGS plasma sample data to obtain CNA profiles. Then, we used CPA scores to quantify the CNA profiles [29].

Each CPA score was calculated by summing the deviations across all segments between the CNA profile of a patient and the average CNA profiles of healthy samples (14 healthy samples were used as reference in our study), weighted by their lengths, and normalized by the total number of segments. Thus, a CPA score of zero signifies a “flat” CNA profile, while a higher CPA score reflects more genomic instability (representative examples in **Figure 4.1B**). CPA scores were all less than 1.5 (median = 0.80, range 0.53 to 1.45, **Supplementary Figure 4.3A**) in healthy donors. By contrast, patients with mTNBC have significantly higher CPA scores (median = 5.55, range 2.18 to 26.39, $p=0.0000001$, **Supplementary Figure 4.3A**), indicating that these CPA scores reflect copy number profiles of circulating tumor DNA rather than non-tumor DNA. Regarding ctDNA level (ng/mL), we measured the concentration of circulating DNA from the plasma samples.

Additionally, we compared patient baseline CPA scores with other metrics used in literature to quantify CNA levels, such as sums of total gains or losses [30], or percentages of genome affected by the CNAs [31, 32]. We found that they were highly correlated (**Supplementary Figure 4.3B**).

Concordance between ctDNA-based and tissue-based CNA profiles

4.2. Results

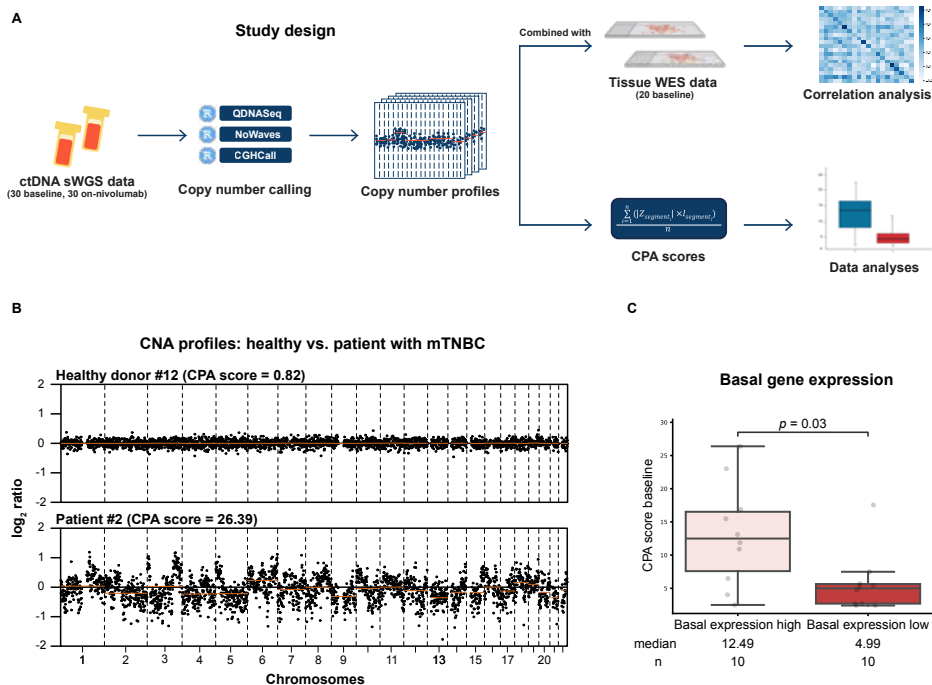


Figure 4.1: Study design, representative copy number profiles, and relationship between baseline CPA scores and basal gene expression. (A) Study design. The cohort included 60 (30 pairs, pre- and post-treatment) plasma sWGS data and 20 WES tissue data at baseline. Circulating tumor DNA (ctDNA)-based copy number alteration (CNA) profiles were generated using the bioinformatics pipeline by Deger et al. [27], while tissue CNA profiles were obtained from Sequenza [28]. Correlation analysis compared 20 paired ctDNA-based and tissue-based CNA profiles at baseline. All ctDNA-based CNA profiles were quantified using copy number abnormality (CPA) scores to explore the dynamics during anti-PD1 treatment for patients with mTNBC. (B) Representative copy number profiles and CPA scores from a healthy sample (Healthy donor #12) and a tumor sample (Patient #2). (C) Baseline CPA scores in patients with high (\geq median) versus low ($<$ median) basal gene expression; $n = 20$; median basal gene expression = 8.38. Box plot for (C) displays a minimum (Q0), a maximum (Q4), a median (Q2), and the interquartile range. p-value for (C) was determined using the two-sided Mann-Whitney U-test.

Next, we investigated the concordance between ctDNA-based and tissue-based CNA profiles. For 20 patients, we had access to both baseline sWGS data from plasma samples and corresponding whole exome sequencing (WES) data from tumor tissues. CNA profile segments from WES tissue samples were first log₂-transformed, and divided into 100 kb bins, matching the binning of WGS plasma samples. The transformed CNA profile segments from the WES tissue sample of each patient were then compared with the CNA profile segments from the corresponding WGS plasma sample. Significant correlations were observed across all patients between the matched ctDNA-based and tissue-based CNA profile segments, with a median correlation coefficient of 0.50 (0.27-0.87, $p < 0.05$ for all pairs). This underscores the potential

of using ctDNA-based CNA profiles to estimate the copy number tumor profiles in mTNBC.

Given the chromosomal instability in basal-like breast cancer [20, 32], we investigated the relationship between baseline CPA scores and the PAM50-based basal gene expression profiles (Nanostring [33]). Patients with higher baseline CPA scores had significantly higher basal gene expression ($p=0.03$, **Figure 4.1C**).

Baseline CPA scores and ctDNA levels in relation to clinical outcomes

Next, we analyzed whether CPA scores and ctDNA levels were associated with clinical outcomes. Baseline CPA scores showed no significant association with likelihood of response (objective response according to iRECIST [34]) to nivolumab ($p=0.27$, **Figure 4.2A**), OS (hazard ratio (HR)=1.31, 95% confidence interval (95%CI)=0.60-2.85, **Supplementary Figure 4.4A, Supplementary Table 4.2**), or PFS (HR=0.72, 95%CI=0.34-1.53, **Supplementary Figure 4.4B, Supplementary Table 4.2**). Similarly, baseline ctDNA levels also demonstrated no significant associations with response to nivolumab (**Figure 4.2B**), OS, or PFS (**Supplementary Figure 4.4C, Supplementary Figure 4.4D, and Supplementary Table 4.2**).

Dynamics of CPA scores and ctDNA levels in relation to clinical outcomes

Additionally, we explored the relationships between CPA score dynamics and important tumor-based parameters for TNBC, including sTIL levels, PD-L1 CPS, and CD8 counts at baseline. No associations were found (**Supplementary Figures 4.4G-I**).

Subsequently, we assessed CPA score dynamics from baseline to 12 weeks after nivolumab treatment and their association with clinical outcomes. Upon therapy, responders showed a significant decrease in CPA scores ($p=0.0004$, **Figure 4.2C**), while non-responders had a non-significant increase ($p=0.14$, **Figure 4.2D**). A decreased CPA score during immunotherapy was associated with improved OS (HR=2.25, 95%CI=1.00-5.05, $p=0.05$, **Figure 4.2E, Supplementary Table 4.2**) and PFS (HR=4.70, 95%CI=1.87-11.85, $p=0.001$, **Supplementary Figure 4.4E, Supplementary Table 4.2**). However, after adjusting for PD-L1 combined positive score (CPS) and disease-free interval (DFI), the associations were not significant for OS (HR=1.27, 95%CI=0.47-3.42, **Supplementary Table 4.2**) and PFS (HR=2.78, 95%CI=0.69-11.16, **Supplementary Table 4.2**) anymore.

ctDNA levels showed a non-significant decrease in responders ($p=0.39$, **Figure 4.2F**), whereas a significant increase in non-responders ($p=0.008$, **Figure 4.2G**) during nivolumab treatment. Decreased

Baseline CPA scores and ctDNA levels

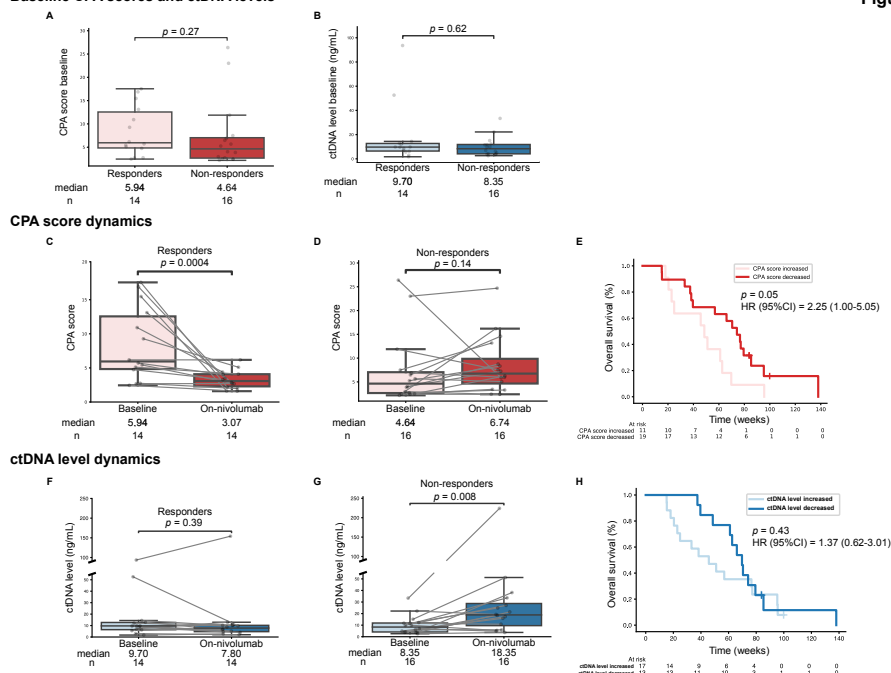


Figure 4.2: Baseline and dynamics of CPA scores and ctDNA levels in response to clinical outcomes. (A) Baseline CPA scores in responders and non-responders to nivolumab; $n = 30$. (B) Baseline ctDNA levels in responders and non-responders to nivolumab; $n = 30$. (C) CPA score dynamics during nivolumab treatment in responders; $n = 14$. (D) CPA score dynamics during nivolumab treatment in non-responders; $n = 16$. (E) Kaplan-Meier curve of overall survival in patients with increased (fold change > 1) CPA scores versus decreased (fold change < 1) CPA scores during nivolumab treatment; $n = 30$. No CPA score fold changes were equal to 1. (F) ctDNA level dynamics during nivolumab treatment in responders; $n = 14$. (G) ctDNA level dynamics during nivolumab treatment in non-responders; $n = 16$. (H) Kaplan-Meier curve of overall survival in patients with increased (fold change > 1) versus decreased (fold change < 1) ctDNA levels during nivolumab treatment; $n = 30$. No ctDNA level fold changes were equal to 1. Box plots in A-D, F, and G display a minimum (Q0), a maximum (Q4), a median (Q2), and the interquartile range. p-values for A and B were determined using the two-sided Mann-Whitney U-test, while p-values for C, D, F, and G were calculated using the two-sided Wilcoxon signed-rank paired test. p-values for E and H were obtained using the log-likelihood ratio test.

ctDNA levels during nivolumab were not associated with improved OS (HR=1.37, 95%CI=0.62-3.01, $p=0.43$, **Figure 4.2H, Supplementary Table 4.2**) or PFS (HR=1.16, 95%CI=0.55-2.42, $p=0.70$, **Figure 4.2F, Supplementary Table 4.2**).

4.3. Discussion

Here we present one of the first analyses on sWGS ctDNA-based CNAs in the context of ICB for patients with mTNBC. Our analyses indicate the

potential utility of using ctDNA-based CNAs to monitor response during ICB in addition to ctDNA levels, hereby providing a foundation for future studies on ctDNA-based CNA profiles as biomarker for ICB response for patients with mTNBC.

Molecular analysis of ctDNA offers an attractive non-invasive approach to obtain real-time tumor information. There are two main approaches: tumor-informed assays, which detect the presence of patient-specific mutations from tumor tissue, and tumor-agnostic assays [35, 36]. Studies on ctDNA indicate that ctDNA levels can serve as a surrogate for tumor burden in metastatic settings [37–39] and the presence of ctDNA can be used to detect minimal residual disease (MRD) in early-stage tumors [40, 41], as well as tumor mutational burden (TMB) [42], microsatellite instability (MSI) [43], mutational signatures [44], and driver mutations [45]. While most studies so far have focused on detecting mutations, here we present data on copy number analyses in liquid biopsies. Copy number alteration, a key cancer hallmark [46, 47], is particularly informative for tumors with lower mutational burden [48] and higher levels of chromosomal instability, such as TNBC. Previous studies have shown concordance between tissue-based and ctDNA-based CNA profiles [12, 22, 49], which is in line with our results. The inherent intra-tumor heterogeneity of TNBC and varying ctDNA fractions may account for the less than perfect alignment between ctDNA-based and tissue-based CNA profiles as also shown by others [50, 51]. Furthermore, we discovered that higher baseline CNA levels were associated with higher scores for basal gene expression according to PAM50, which is in line with studies showing that basal tumors have higher CNA levels than non-basal tumors [20, 32]. This indicates that ctDNA-based CNA profiles can reflect tumor subtype-specific biology in mTNBC, potentially identifying patients who might benefit from HRD-targeted therapies. The advantage of this approach is that it does not require profiling of the tumor and is relatively cheap.

Prior studies evaluating the prognostic value of baseline ctDNA levels to ICB response showed conflicting results, while ctDNA dynamics have shown to be prognostic among various cancer types including breast cancer [16, 25, 52–54]. Bratman et al. discovered an association between baseline ctDNA levels and OS and PFS in a multi-cohort clinical trial [16]. However, this association was not statistically significant in the subcohort of patients with TNBC (n=18), consistent with our findings, suggesting that the association between baseline ctDNA levels and survival could be tumor-type specific. In line with our study, they have demonstrated that an increase in ctDNA levels during immunotherapy was associated with disease progression and poor survival, whereas a decrease in ctDNA levels was associated with better clinical outcomes [16].

Previous studies have demonstrated the potential of tracking ctDNA-based CNA levels to monitor immunotherapy responses in various cancer types including one patient with TNBC [25, 52]. In our analysis, although baseline CPA scores did not differ between responders and non-responders, decreased CPA scores upon immunotherapy were associated with response to ICB and survival. This could suggest that either copy number tumor profiles could change during immunotherapy or that tumor clones with more CNA show a distinct response to ICB. Although prior research has shown tumors of patients with melanoma who do not respond to ICB have more CNAs compared to responding tumors [19, 55], it is largely unknown how copy number profiles change during the active phase of an anti-cancer immune response and upon the development of acquired resistance.

Our current study has certain limitations. First, the study was set up as a pilot study with a small sample size, making all analyses exploratory. Validation of our findings in larger cohorts of patients with mTNBC treated with ICB is needed. Second, we selected non-responders who had a plasma sample taken after 6 cycles of nivolumab (at 14 weeks). These non-responders likely had better outcomes than those who relapsed quickly after treatment initiation, indicating that our survival analysis primarily compared responders to non-responders with relatively favorable outcomes. Third, there is no standard method of detecting ctDNA and we did not perform additional steps to calculate the 'absolute' ctDNA level due to the low coverage nature of shallow whole genome sequencing, thus plasma samples might include both ctDNA and cell-free DNA. However, mTNBC tumors are known to have higher ctDNA levels than other breast cancer subtypes or other solid tumors [15, 16]. Also, we observed high levels of CNAs in the samples indicating that there were sufficient ctDNA present in the plasma.

We propose leveraging ctDNA-based CNA dynamics as a biomarker to monitor treatment response for patients with mTNBC receiving immunotherapy. The feasibility of prospective trials for this approach depends on available alternative treatments. A recent study, PADA-1 trial (NCT03079011) [56] showed that switching endocrine treatment upon detection or increase of ESR1 mutation in blood improves the PFS in patients with ER- positive, HER2-negative advanced breast cancer. Inspired by this and considering that antibody-drug conjugates (ADCs) like sacituzumab govitecan are promising second-line treatments for mTNBC [5, 57, 58], it might be worth evaluating ctDNA-based CNA dynamics for monitoring immunotherapy response in mTNBC. For instance, patients could be randomized to receive anti-PD-(L)1 therapy with a switch to an ADC upon clinical progression versus switching to ADCs if ctDNA-based CNA dynamics remain unaffected by anti-PD-(L)1 therapy.

In conclusion, this pilot study demonstrated that ctDNA-based CNA dynamics, assessed through sWGS, provide additional insights alongside ctDNA levels and other tumor-based parameters to monitor anti-PD1 treatment in mTNBC. Our work warrants further preclinical studies on the changes of CNAs during response or resistance to ICB and clinical studies on tracking ctDNA-based CNA dynamics and the option of timely treatment adjustment in the context of immunotherapy for mTNBC.

4.4. Methods

Clinical trial procedures

This paper included WGS data from blood samples (n=60) and WES data from tissue samples (n=20) of 30 patients with mTNBC in the stage 1 of the TONIC trial [26] (NCT02499367). The trial procedures were executed according to the previous publication [26]. Clinical benefit was defined as complete response, partial response, or stable disease for at least 26 weeks according to iRECIST, as described previously [29]. OS was determined by calculating the time period between the date of first nivolumab administration and the most recent follow-up or death date (data cut-off on 1 March 2021). DFI was defined as the time between the diagnosis of the primary tumor or locoregional recurrence and the date of diagnosis of metastatic disease. Tumor burden was measured as the sum of all target lesions in millimeters as described in the TONIC trial [26]. Plasma samples were taken at baseline and after 12 weeks of nivolumab treatment. All available paired samples were used for this study.

Immunohistochemistry and TIL scoring

Immunohistochemistry for CD8 (C8/144B, DAKO) and PD-L1 (22C3, DAKO) was performed on formalin-fixed paraffin-embedded tissue sections; the absolute CD8 count was scored manually by one pathologist. The percentages of sTILs on hematoxylin and eosin (H&E)-stained slides were assessed by pathologists trained for TIL assessment based on an accepted international standard from the International Immuno-Oncology Biomarker Working Group (visit www.tilsinbreastcancer.org for all guidelines on TIL assessment in solid tumors).

Blood processing and sequencing

Blood was collected in 10 ml K2-EDTA tubes, from which cell-free plasma was obtained within 4 hours by a two-step centrifugation: 20 minutes at 380 g followed by 10 minutes at 20,000 g. Cell-free plasma was stored in 1-4 ml aliquots at -80 °C. Cell-free DNA (cfDNA) isolation was performed using the QIAasympphony Circulating DNA kit (article number 1091063,

Qiagen, Dusseldorf, Germany) with the QIAasympy (Qiagen). No extraction blanks were used in this study. Elution volume was set to 60 μ l and samples were stored at 4 °C until use.

Maximum 50 μ l of eluate was used per sample for input into library preparation using the KAPA Hyperprep kit. Median cfDNA input per sample was 18.5 ng for baseline samples, 23.8 ng for on treatment samples, and 4.8 ng for samples from healthy donors. Library preparation failed for one sample on treatment, leading to exclusion of that patient (responder) from further analysis. Remaining 60 patient samples (baseline and on-treatment) were pooled and whole genome sequenced on a HiSeq 2500 in high output single-read mode, with a read length of 65 bp. 14 healthy age-matched female donor samples were sequenced on a separate lane with the same settings. Median number of generated reads per sample was 3.2 million for baseline samples, 3.4 million reads for on treatment samples, and 12.5 million reads for healthy donors.

ctDNA-based copy number profile derived from sWGS data

We employed an established bioinformatics pipeline [27] on sWGS plasma data to derive ctDNA-based copy number profiles. Briefly, QDNAseq R package [59] was used to remove problematic regions, correct for GC-content and mappability, and normalize the remaining bins. QDNAseq.hg38 was used for bin annotation. At a fixed bin size of 100 kilobases (Kb), the majority of data (24,888 out of 30,894 total bins) were retained with a low measured standard deviation. Subsequently, the NoWaves R package [60] with default settings was used to correct for wave bias. Finally, we generated copy number profiles using CGHcall [61]. The output of ctDNA-based CNA profile of each patient was binned into 100 kb bins across the genome and log2-transformed.

Tissue-based copy number profile obtained from whole-genome sequencing (WES) data

Tissue-based copy number profiles were generated using Sequenza [28] from 20 patients with tissue whole-exome sequencing (WES) data. The output of tissue-based CNA profile of each patient was binned with 100 kb bins across the genome and log2-transformed to make the data comparable with ctDNA-based CNA profiles.

Quantification of copy number profiles: CPA scores

CPA score was calculated as described previously [29]. Briefly, this could be summarized in two steps as shown in equations (4.1) and (4.2):

$$Z_{segment(n \rightarrow m)} = \frac{\mu(R_n, R_{...}, R_m) - \mu(\mu(r_{1,n}, r_{1,...}, r_{1,m}) \dots \mu(r_{p,n}, r_{p,...}, r_{p,m}))}{std(\mu(r_{1,n}, r_{1,...}, r_{1,m}) \dots \mu(r_{p,n}, r_{p,...}, r_{p,m}))} \quad (4.1)$$

$Z_{segment(n \rightarrow m)}$ denotes the Z-score encompassing the range from bin n to m within each segment. R_n indicates the read counts ratio of the patient sample at bin n , while $r_{1,n}$ represents the read counts ratio of the corresponding locus of the first healthy sample. Herein, p denotes healthy samples. The functions $\mu()$ and $std()$, correspondingly, compute the default mean and standard deviation. Note that the calculation of Z-score in our analysis used default mean calculation instead of weighted mean calculation described by Raman et al. [29] due to the use of different tools for copy number calling.

$$CPA = \frac{\sum_{i=1}^n (|Z_{segment_i}| \times l_{segment_i})}{n} \quad (4.2)$$

The Z-score and length for segment i are given as $Z_{segment_i}$ and $l_{segment_i}$, respectively. The number of segments per copy number profile is represented by n . The CPA score is expressed per 100 megabases (Mb), therefore, measurements were converted from Kb to Mb by dividing by 1,000.

NanoString gene expression analysis

The basal gene expression was obtained from nCounter technology provided by NanoString Technologies [33] using a PAM50 spike-in panel of 30 genes as calculated in TONIC trial [26].

Quantification and statistical analysis

All correlation analyses were calculated using Spearman's rank correlation. Non-parametric tests were used to compare different groups: Mann-Whitney U-test for two independent groups and Wilcoxon signed-rank test for paired samples. Kaplan-Meier curves and likelihood-ratio tests were used to compare the performance between the groups on OS and PFS. Cox proportional hazards regression model was used to evaluate the impact of CPA scores and ctDNA levels on OS and PFS. All tests were two-sided. Combined positive scores were calculated by dividing the number of PD-L1-staining cells (including tumor cells, lymphocytes, and macrophages) by the total number of viable tumor cells, multiplied by 100 [62]. PD-L1 expressed tumors were defined as CPS ≥ 10 . In the multivariate analysis, PD-L1 CPS and disease-free interval (DFI) were chosen as control variables because they are known to be associated with response in patients with mTNBC receiving immunotherapy [7, 26, 63].

4.5. Acknowledgements

We would like to thank the patients and their families for participating in the present study. We thank the NKI Core Facility of Molecular Pathology and Biobanking (NKI-CFMPB) for the storage and handling of human tumor material and to the NKI Genomics Core Facility (NKI-GCF) for DNA sequencing, in particular Annegien Broeks and Michiel de Maaker. The present study did not use specific funding, but we would like to thank Bristol-Myers-Squibb (BMS)/International Immuno-Oncology Network (II-ON) and the Dutch Cancer Society (NK12015-7710, 10653 ALPE) for funding the TONIC trial and a fellowship to M.K. (NK12015-7542). Research in the laboratory of M.K. is funded by the Netherlands Organization for Scientific Research (VIDI). The funders had no role in study design, data collection or analysis, decision to publish, or manuscript preparation.

4.6. Author contributions

A.Y.L. and O.I.I. performed and interpreted computational analyzes. A.Y.L., O.I.I. and M.K. wrote the manuscript. O.I.I. and M.K. conceptualized the study. T.D., M.S. and K.M. contributed to the bioinformatics analysis, under the supervision of J.W.M.M. V.C.M.G. and L.V. collected and interpreted clinical data. D.C.L.V. conducted blood sample preprocessing and analyses, supervised by D.v.d.B. P.v.d.L. contributed to blood sample data analysis. L.F.A.W. supervised the bioinformatics analyses. M.K. was the principal investigator of this study, supervised all the analyses presented in the manuscript and acquired funding. All authors edited and approved the manuscript.

4.7. Declaration of interests

A.Y.L., O.I.I., T.D., V.C.M.G., D.C.L.V., L.V., M.S., K.M., and P.v.d.L. have no competing interests to declare. L.F.A.W. received institute research funding from BMS. J.W.M.M. received personal fees from Novartis, other support from Roche, and grant from Pfizer, GSK, MLDS, Oncode, Eurostar, outside the submitted work. D.v.d.B. presented lectures and expert testimonies and participated on advisory boards for Roche and received support for research from DELFI diagnostics and the Dutch organization of Scientific research (NVO) outside the submitted work. M.K. reports research funding to the institute from BMS, Roche, and AstraZeneca/MedImmune and an advisory role/speakers' fee (all compensated to the institute) for Alderaan, BMS, Domain Therapeutics, Medscape, Roche, MSD, and Daiichi Sankyo, outside the submitted work.

4.8. Supplementary Information

Table 4.1: Baseline patient characteristics.

Characteristic		No. (%)
Age at inclusion, years	Median (range)	52 (29–70)
Location of metastasis	Lymph node only Visceral metastasis Other metastases ^a	4 (13) 17 (57) 9 (30)
Numbers of previous therapies ^b for metastatic disease	0 1 2–3	7 (23) 16 (53) 7 (23)
Germline BRCA 1/2	Mutation Wild type Unknown	3 (10) 23 (77) 4 (13)
PD-L1 CPS ^c	< 10 ≥ 10 Not available	14 (47) 15 (50) 1 (3)
sTILs ^d	< 10% ^e ≥ 10% Not available	14 (47) 14 (47) 2 (7)

^a bone, skin, and breast lesions;

^b palliative systemic chemotherapy before TONIC trial [1] inclusion;

^c combined positive score assessed using 22C3 clone (DAKO);

^d stromal tumor-infiltrating lymphocytes (International TILS Working Group, <https://www.tilsinbreastcancer.org/>);

^e median of sTILs in our cohort was 10%.

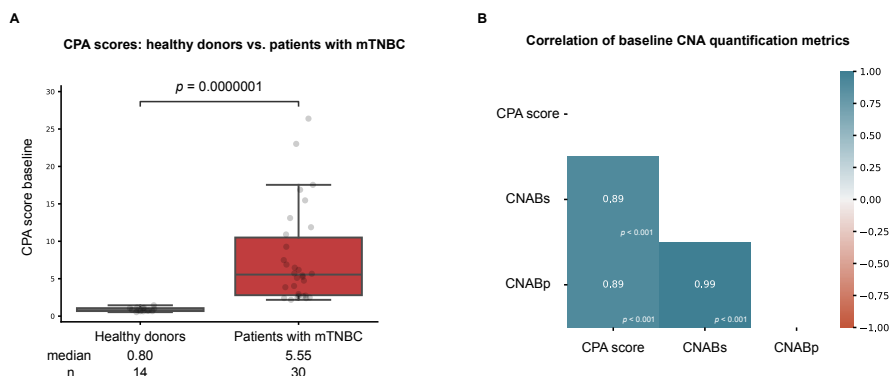


Figure 4.3: Baseline CPA scores in healthy donors vs. patients and correlations between different metrics for quantifying copy number profiles. **(A)** Baseline CPA scores in healthy donors (n=14) versus patients with mTNBC (n=30). **(B)** Correlation between CPA scores, CNABs, and CNABp at baseline; n = 30. The sum of copy number alteration burden (CNABs) was calculated by the total number of bins with gain or loss for each CNA profile. The percentage of copy number alteration burden (CNABp) was calculated by the percentage of genomes affected by the CNAs for each CNA profile. Box plot for **A** displays a minimum (Q0), a maximum (Q4), a median (Q2), and the interquartile range. P-value for **A** was determined using the two-sided Mann-Whitney U-test. The correlation coefficient (r) and p-value for **B** were determined by Spearman's rank correlation.

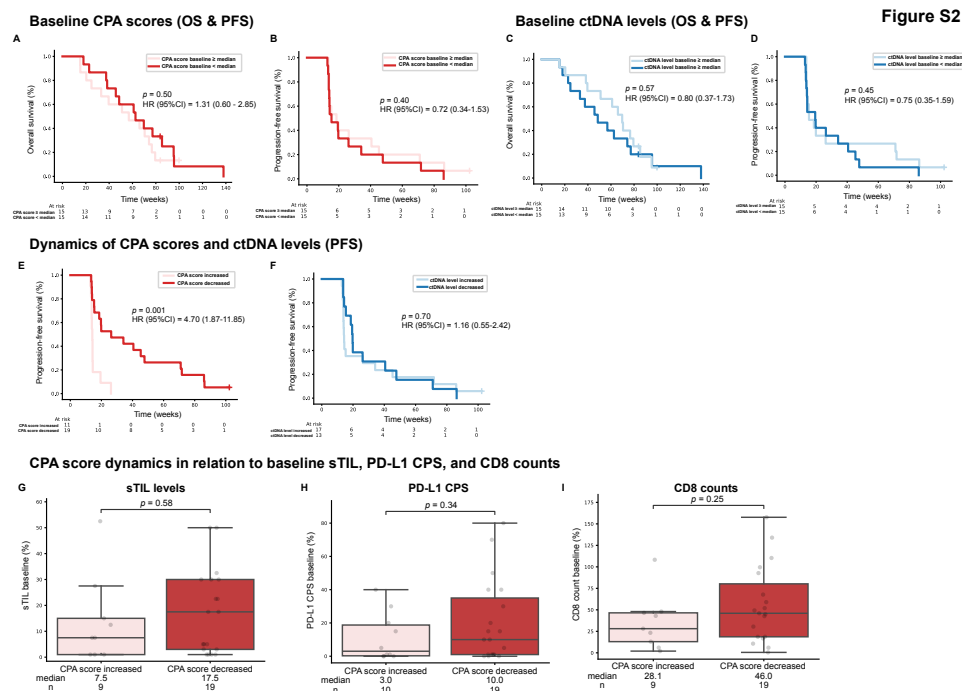


Figure 4.4: Baseline and dynamics of CPA scores and ctDNA levels in relation to overall survival, progression-free survival, and tumor-based parameters. (A) Kaplan-Meier curve of overall survival in patients with baseline CPA score high (\geq median) versus low ($<$ median); $n = 30$; median baseline CPA score = 5.55. (B) Kaplan-Meier curve of progression-free survival in patients with baseline CPA score high (\geq median) versus low ($<$ median); $n = 30$; median baseline CPA score = 5.55. (C) Kaplan-Meier curve of overall survival in patients with baseline ctDNA level high (\geq median) versus low ($<$ median) during nivolumab treatment; $n = 30$; median baseline ctDNA level = 9.70. (D) Kaplan-Meier curve of progression-free survival in patients with baseline ctDNA level high (\geq median) versus low ($<$ median) during nivolumab treatment; $n = 30$; median baseline ctDNA level = 9.70. (E) Kaplan-Meier curve of progression-free survival in patients with increased (fold change > 1) versus decreased (fold change < 1) CPA scores during nivolumab treatment; $n = 30$. No CPA score fold changes were equal to 1. (F) Kaplan-Meier curve of progression-free survival in patients with increased (fold change > 1) versus decreased (fold change < 1) ctDNA levels during nivolumab treatment; $n = 30$. No ctDNA level fold changes were equal to 1. (G) Baseline sTIL levels in patients with increased versus decreased CPA scores; $n=28$. (H) Baseline PD-L1 CPS in patients with increased versus decreased CPA scores; $n=29$. (I) Baseline CD8 counts in patients with increased versus decreased CPA scores; $n=28$. p-values for A-F were determined by the log-likelihood ratio test. Box plots for G-I display a minimum (Q0), a maximum (Q4), a median (Q2), and the interquartile range. p-values for G-I were determined using the two-sided Mann-Whitney U-test.

Table 4.2: Univariate analysis and multivariate analyses of baseline and dynamics of CPA scores and ctDNA levels in relation to OS and PFS in mTNBC.

	OS		PFS	
Univariate analysis				
Variables	HR (95% CI)	p-value	HR (95% CI)	p-value
Baseline CPA score ^a	1.31 (0.60–2.85)	0.50	0.72 (0.34–1.53)	0.40
Fold change ^b of CPA score	2.25 (1.00–5.05)	0.05	4.70 (1.87–11.85)	0.001
Baseline ctDNA level ^a	0.80 (0.37–1.73)	0.57	0.75 (0.35–1.59)	0.45
Fold change ^b of ctDNA level	1.37 (0.62–3.01)	0.43	1.16 (0.55–2.42)	0.70
Multivariate analysis				
Fold change ^b of CPA score	1.27 (0.47–3.42)	0.63	2.78 (0.69–11.16)	0.15
DFI ^c	0.28 (0.10–0.79)	0.02	0.47 (0.13–1.65)	0.24
PD-L1 CPS ^d	0.66 (0.28–1.57)	0.35	1.10 (0.48–2.51)	0.82

^a : \geq median vs. $<$ median;

^b > 1 (increased) vs. < 1 (decreased);

^c disease-free interval (≥ 1 vs. < 1 year);

^d combined positive score (≥ 10 vs. < 10).

References

- [1] R. Dent, M. Trudeau, K. I. Pritchard, W. M. Hanna, H. K. Kahn, C. A. Sawka, L. A. Lickley, E. Rawlinson, P. Sun, and S. A. Narod. "Triple-negative breast cancer: clinical features and patterns of recurrence". *Clin. Cancer Res.* 13.15 Pt 1 (Aug. 2007), pp. 4429–4434.
- [2] W. D. Foulkes, I. E. Smith, and J. S. Reis-Filho. "Triple-negative breast cancer". *N. Engl. J. Med.* 363.20 (Nov. 2010), pp. 1938–1948.
- [3] F. Kassam, K. Enright, R. Dent, G. Dranitsaris, J. Myers, C. Flynn, M. Fralick, R. Kumar, and M. Clemons. "Survival outcomes for patients with metastatic triple-negative breast cancer: implications for clinical practice and trial design". *Clin. Breast Cancer* 9.1 (Feb. 2009), pp. 29–33.
- [4] J. O'Shaughnessy, L. Schwartzberg, M. A. Danso, K. D. Miller, H. S. Rugo, M. Neubauer, N. Robert, B. Hellerstedt, M. Saleh, P. Richards, J. M. Specht, D. A. Yardley, R. W. Carlson, R. S. Finn, E. Charpentier, I. Garcia-Ribas, and E. P. Winer. "Phase III study of iniparib plus gemcitabine and carboplatin versus gemcitabine and carboplatin in patients with metastatic triple-negative breast cancer". *J. Clin. Oncol.* 32.34 (Dec. 2014), pp. 3840–3847.
- [5] A. Gennari, F. André, C. H. Barrios, J. Cortés, E. de Azambuja, A. DeMichele, R. Dent, D. Fenlon, J. Gligorov, S. A. Hurvitz, S.-A. Im, D. Krug, W. G. Kunz, S. Loi, F. Penault-Llorca, J. Ricke, M. Robson, H. S. Rugo, C. Saura, P. Schmid, C. F. Singer, T. Spanic, S. M. Tolaney, N. C. Turner, G. Curigliano, S. Loibl, S. Paluch-Shimon, N. Harbeck, and ESMO Guidelines Committee. Electronic address: clinicalguidelines@esmo.org. "ESMO Clinical Practice Guideline for the diagnosis, staging and treatment of patients with metastatic breast cancer". *Ann. Oncol.* 32.12 (Dec. 2021), pp. 1475–1495.
- [6] L. A. Emens, S. Adams, C. H. Barrios, V. Diéras, H. Iwata, S. Loi, H. S. Rugo, A. Schneeweiss, E. P. Winer, S. Patel, V. Henschel, A. Swat, M. Kaul, L. Molinero, S. Patel, S. Y. Chui, and P. Schmid. "First-line atezolizumab plus nab-paclitaxel for unresectable, locally advanced, or metastatic triple-negative breast cancer: IMpassion130 final overall survival analysis". *Ann. Oncol.* 32.8 (Aug. 2021), pp. 983–993.
- [7] J. Cortes, H. S. Rugo, D. W. Cescon, S.-A. Im, M. M. Yusof, C. Gallardo, O. Lipatov, C. H. Barrios, J. Perez-Garcia, H. Iwata, N. Masuda, M. Torregroza Otero, E. Gokmen, S. Loi, Z. Guo, X. Zhou, V. Karantza, W. Pan, P. Schmid, and KEYNOTE-355 Investigators. "Pembrolizumab plus chemotherapy in advanced triple-negative breast cancer". *N. Engl. J. Med.* 387.3 (July 2022), pp. 217–226.

- [8] P. Schmid, H. S. Rugo, S. Adams, A. Schneeweiss, C. H. Barrios, H. Iwata, V. Diéras, V. Henschel, L. Molinero, S. Y. Chui, V. Maiya, A. Husain, E. P. Winer, S. Loi, L. A. Emens, and IMpassion130 Investigators. "Atezolizumab plus nab-paclitaxel as first-line treatment for unresectable, locally advanced or metastatic triple-negative breast cancer (IMpassion130): updated efficacy results from a randomised, double-blind, placebo-controlled, phase 3 trial". *Lancet Oncol.* 21.1 (Jan. 2020), pp. 44–59.
- [9] P. Savas, R. Salgado, and S. Loi. "Seeing the forest and the tree: TILs and PD-L1 as immune biomarkers". *Breast Cancer Res. Treat.* 189.3 (Oct. 2021), pp. 599–606.
- [10] L. A. Emens, L. Molinero, S. Loi, H. S. Rugo, A. Schneeweiss, V. Diéras, H. Iwata, C. H. Barrios, M. Nechaeva, A. Nguyen-Duc, S. Y. Chui, A. Husain, E. P. Winer, S. Adams, and P. Schmid. "Atezolizumab and nab-paclitaxel in advanced triple-negative breast cancer: Biomarker evaluation of the IMpassion130 study". *J. Natl. Cancer Inst.* 113.8 (Aug. 2021), pp. 1005–1016.
- [11] P. I. Gonzalez-Ericsson, E. S. Stovgaard, L. F. Sua, E. Reisenbichler, Z. Kos, J. M. Carter, S. Michiels, J. Le Quesne, T. O. Nielsen, A.-V. Laenkhölm, S. B. Fox, J. Adam, J. M. Bartlett, D. L. Rimm, C. Quinn, D. Peeters, M. V. Dieci, A. Vincent-Salomon, I. Cree, A. I. Hida, J. M. Balko, H. R. Haynes, I. Frahm, G. Acosta-Haab, M. Balancin, E. Bellolio, W. Yang, P. Kirtani, T. Sugie, A. Ehinger, C. A. Castaneda, M. Kok, H. McArthur, K. Siziopikou, S. Badve, S. Fineberg, A. Gown, G. Viale, S. J. Schnitt, G. Pruner, F. Penault-Llorca, S. Hewitt, E. A. Thompson, K. H. Allison, W. F. Symmans, A. M. Bellizzi, E. Brogi, D. A. Moore, D. Larsimont, D. A. Dillon, A. Lazar, H. Lien, M. P. Goetz, G. Broeckx, K. El Bairi, N. Harbeck, A. Cimino-Mathews, C. Sotiriou, S. Adams, S.-W. Liu, S. Loibl, I.-C. Chen, S. R. Lakhani, J. W. Juco, C. Denkert, E. F. Blackley, S. Demaria, R. Leon-Ferre, O. Gluz, D. Zardavas, K. Emancipator, S. Ely, S. Loi, R. Salgado, M. Sanders, and International Immuno-Oncology Biomarker Working Group. "The path to a better biomarker: application of a risk management framework for the implementation of PD-L1 and TILs as immuno-oncology biomarkers in breast cancer clinical trials and daily practice". *J. Pathol.* 250.5 (Apr. 2020), pp. 667–684.
- [12] V. A. Adalsteinsson, G. Ha, S. S. Freeman, A. D. Choudhury, D. G. Stover, H. A. Parsons, G. Gydush, S. C. Reed, D. Rotem, J. Rhoades, D. Loginov, D. Livitz, D. Rosebrock, I. Leshchiner, J. Kim, C. Stewart, M. Rosenberg, J. M. Francis, C.-Z. Zhang, O. Cohen, C. Oh, H. Ding, P. Polak, M. Lloyd, S. Mahmud, K. Helvie, M. S. Merrill, R. A. Santiago, E. P. O'Connor, S. H. Jeong, R. Leeson, R. M. Barry, J. F. Kramkowski, Z. Zhang, L. Polacek, J. G. Lohr, M. Schleicher, E. Lipscomb, A. Saltzman, N. M. Oliver, L. Marini, A. G. Waks, L. C. Harshman, S. M. Tolaney, E. M. Van Allen, E. P. Winer, N. U. Lin, M. Nakabayashi, M.-E. Taplin, C. M. Johannessen, L. A. Garraway, T. R. Golub, J. S. Boehm, N. Wagle, G. Getz, J. C. Love, and M. Meyerson. "Scalable whole-exome sequencing of cell-free DNA reveals high concordance with metastatic tumors". *Nat. Commun.* 8.1 (Nov. 2017), p. 1324.

- [13] D. Chu, C. Paoletti, C. Gersch, D. A. VanDenBerg, D. J. Zabransky, R. L. Cochran, H. Y. Wong, P. V. Toro, J. Cidado, S. Croessmann, B. Erlanger, K. Cravero, K. Kyker-Snowman, B. Button, H. A. Parsons, W. B. Dalton, R. Gillani, A. Medford, K. Aung, N. Tokudome, A. M. Chinnaiyan, A. Schott, D. Robinson, K. S. Jacks, J. Lauring, P. J. Hurley, D. F. Hayes, J. M. Rae, and B. H. Park. "ESR1 mutations in circulating plasma tumor DNA from metastatic breast cancer patients". *Clin. Cancer Res.* 22.4 (Feb. 2016), pp. 993–999.
- [14] N. C. Turner, C. Swift, B. Jenkins, L. Kilburn, M. Coakley, M. Beaney, L. Fox, K. Goddard, I. Garcia-Murillas, P. Proszek, P. Hall, C. Harper-Wynne, T. Hickish, S. Kernaghan, I. R. Macpherson, A. F. C. Okines, C. Palmieri, S. Perry, K. Randle, C. Snowden, H. Stobart, A. M. Wardley, D. Wheatley, S. Waters, M. C. Winter, M. Hubank, S. D. Allen, J. M. Bliss, and c-TRAK TN investigators. "Results of the c-TRAK TN trial: a clinical trial utilising ctDNA mutation tracking to detect molecular residual disease and trigger intervention in patients with moderate- and high-risk early-stage triple-negative breast cancer". *Ann. Oncol.* 34.2 (Feb. 2023), pp. 200–211.
- [15] M. J. M. Magbanua, L. B. Swigart, H.-T. Wu, G. L. Hirst, C. Yau, D. M. Wolf, A. Tin, R. Salari, S. Shchegrova, H. Pawar, A. L. Delson, A. DeMichele, M. C. Liu, A. J. Chien, D. Tripathy, S. Asare, C.-H. J. Lin, P. Billings, A. Aleshin, H. Sethi, M. Louie, B. Zimmermann, L. J. Esserman, and L. J. van 't Veer. "Circulating tumor DNA in neoadjuvant-treated breast cancer reflects response and survival". *Ann. Oncol.* 32.2 (Feb. 2021), pp. 229–239.
- [16] S. V. Bratman, S. Y. C. Yang, M. A. J. Iaforla, Z. Liu, A. R. Hansen, P. L. Bedard, S. Lheureux, A. Spreafico, A. A. Razak, S. Shchegrova, M. Louie, P. Billings, B. Zimmermann, H. Sethi, A. Aleshin, D. Torti, K. Marsh, J. Eagles, I. Cirlan, Y. Hanna, D. L. Clouthier, S. C. Lien, P. S. Ohashi, W. Xu, L. L. Siu, and T. J. Pugh. "Personalized circulating tumor DNA analysis as a predictive biomarker in solid tumor patients treated with pembrolizumab". *Nat. Cancer* 1.9 (Sept. 2020), pp. 873–881.
- [17] P. Mondelo-Macía, J. García-González, L. León-Mateos, U. Anido, S. Aguín, I. Abdulkader, M. Sánchez-Ares, A. Abalo, A. Rodríguez-Casanova, Á. Díaz-Lagares, R. M. Lago-Lestón, L. Muinelo-Romay, R. López-López, and R. Díaz-Peña. "Clinical potential of circulating free DNA and circulating tumour cells in patients with metastatic non-small-cell lung cancer treated with pembrolizumab". *Mol. Oncol.* 15.11 (Nov. 2021), pp. 2923–2940.
- [18] Y. Bareche, D. Venet, M. Ignatiadis, P. Aftimos, M. Piccart, F. Rothe, and C. Sotiriou. "Unravelling triple-negative breast cancer molecular heterogeneity using an integrative multiomic analysis". *Ann. Oncol.* 29.4 (Apr. 2018), pp. 895–902.
- [19] T. Davoli, H. Uno, E. C. Wooten, and S. J. Elledge. "Tumor aneuploidy correlates with markers of immune evasion and with reduced response to immunotherapy". *Science* 355.6322 (Jan. 2017), eaaf8399.

- [20] Y. Bareche, L. Buisseret, T. Gruosso, E. Girard, D. Venet, F. Dupont, C. Desmedt, D. Larsimont, M. Park, F. Rothé, J. Stagg, and C. Sotiriou. "Unraveling triple-negative breast cancer tumor microenvironment heterogeneity: Towards an optimized treatment approach". *J. Natl. Cancer Inst.* 112.7 (July 2020), pp. 708–719.
- [21] D. G. Stover, H. A. Parsons, G. Ha, S. S. Freeman, W. T. Barry, H. Guo, A. D. Choudhury, G. Gydush, S. C. Reed, J. Rhoades, D. Rotem, M. E. Hughes, D. A. Dillon, A. H. Partridge, N. Wagle, I. E. Krop, G. Getz, T. R. Golub, J. C. Love, E. P. Winer, S. M. Tolaney, N. U. Lin, and V. A. Adalsteinsson. "Association of Cell-free DNA tumor fraction and somatic copy number alterations with survival in metastatic triple-negative breast cancer". *J. Clin. Oncol.* 36.6 (Feb. 2018), pp. 543–553.
- [22] A. Prat, F. Brasó-Maristany, O. Martínez-Sáez, E. Sanfeliu, Y. Xia, M. Bellet, P. Galván, D. Martínez, T. Pascual, M. Marín-Aguilera, A. Rodríguez, N. Chic, B. Adamo, L. Paré, M. Vidal, M. Margelí, E. Ballana, M. Gómez-Rey, M. Oliveira, E. Felip, J. Matito, R. Sánchez-Bayona, A. Suñol, C. Saura, E. Ciruelos, P. Tolosa, M. Muñoz, B. González-Farré, P. Villagrasa, J. S. Parker, C. M. Perou, and A. Vivancos. "Circulating tumor DNA reveals complex biological features with clinical relevance in metastatic breast cancer". *Nat. Commun.* 14.1 (Mar. 2023), p. 1157.
- [23] M. H. Kim, G. M. Kim, J. M. Ahn, W.-J. Ryu, S.-G. Kim, J. H. Kim, T. Y. Kim, H. J. Han, J. Y. Kim, H. S. Park, S. Park, B. W. Park, S. I. Kim, J. Jeong, J. Lee, S. Paik, S. Kim, K. H. Jung, E. H. Cho, and J. Sohn. "Copy number aberrations in circulating tumor DNA enables prognosis prediction and molecular characterization of breast cancer". *J. Natl. Cancer Inst.* 115.9 (Sept. 2023), pp. 1036–1049.
- [24] C. Carbonell, J. Frigola, N. Pardo, A. Callejo, P. Iranzo, A. Valdivia, I. Priano, S. Cedrés, A. Martínez-Martí, A. Navarro, L. Lenza, M. Soleda, J. Gonzalo-Ruiz, A. Vivancos, M. Sansó, E. Carcereny, T. Morán, R. Amat, and E. Felip. "Dynamic changes in circulating tumor DNA assessed by shallow whole-genome sequencing associate with clinical efficacy of checkpoint inhibitors in NSCLC". *Mol. Oncol.* 17.5 (May 2023), pp. 779–791.
- [25] T. J. Jensen, A. M. Goodman, S. Kato, C. K. Ellison, G. A. Daniels, L. Kim, P. Nakashe, E. McCarthy, A. R. Mazloom, G. McLennan, D. S. Grosu, M. Ehrich, and R. Kurzrock. "Genome-wide sequencing of cell-free DNA identifies copy-number alterations that can be used for monitoring response to immunotherapy in cancer patients". *Mol. Cancer Ther.* 18.2 (Feb. 2019), pp. 448–458.
- [26] L. Voorwerk, M. Slagter, H. M. Horlings, K. Sikorska, K. K. van de Vijver, M. de Maaker, I. Nederlof, R. J. C. Kluin, S. Warren, S. Ong, T. G. Wiersma, N. S. Russell, F. Lalezari, P. C. Schouten, N. A. M. Bakker, S. L. C. Ketelaars, D. Peters, C. A. H. Lange, E. van Werkhoven, H. van Tinteren, I. A. M. Mandjes, I. Kemper, S. Onderwater, M. Chalabi, S. Wilgenhof, J. B. A. G. Haanen, R. Salgado, K. E. de Visser, G. S. Sonke, L. F. A. Wessels, S. C. Linn, T. N. Schumacher, C. U. Blank, and M. Kok. "Immune induction strategies in metastatic triple-negative breast cancer

- to enhance the sensitivity to PD-1 blockade: the TONIC trial". *Nat. Med.* 25.6 (June 2019), pp. 920–928.
- [27] T. Deger, P. A. J. Mendelaar, J. Kraan, W. J. C. Prager-van der Smissen, M. van der Vlugt-Daane, E. M. J. Bindels, A. M. Sieuwerts, S. Sleijfer, S. M. Wilting, A. Hollestelle, and J. W. M. Martens. "A pipeline for copy number profiling of single circulating tumour cells to assess intrapatient tumour heterogeneity". *Mol. Oncol.* 16.16 (Aug. 2022), pp. 2981–3000.
- [28] F. Favero, T. Joshi, A. M. Marquard, N. J. Birkbak, M. Krzystanek, Q. Li, Z. Szallasi, and A. C. Eklund. "Sequenza: allele-specific copy number and mutation profiles from tumor sequencing data". *Ann. Oncol.* 26.1 (Jan. 2015), pp. 64–70.
- [29] L. Raman, M. Van der Linden, K. Van der Eecken, K. Vermaelen, I. Demedts, V. Surmont, U. Himpe, F. Dedeurwaerdere, L. Ferdinande, Y. Lievens, K. Claes, B. Menten, and J. Van Dorpe. "Shallow whole-genome sequencing of plasma cell-free DNA accurately differentiates small from non-small cell lung carcinoma". *Genome Med.* 12.1 (Apr. 2020), p. 35.
- [30] J. Budczies, A. Seidel, P. Christopoulos, V. Endris, M. Kloor, B. Györfy, B. Seliger, P. Schirmacher, A. Stenzinger, and C. Denkert. "Integrated analysis of the immunological and genetic status in and across cancer types: impact of mutational signatures beyond tumor mutational burden". *Oncoimmunology* 7.12 (Oct. 2018), e1526613.
- [31] L. Zhang, N. Feizi, C. Chi, and P. Hu. "Association analysis of somatic copy number alteration burden with breast cancer survival". *Front. Genet.* 9 (Oct. 2018), p. 421.
- [32] A. Bergamaschi, Y. H. Kim, P. Wang, T. Sørbye, T. Hernandez-Boussard, P. E. Lonning, R. Tibshirani, A.-L. Børresen-Dale, and J. R. Pollack. "Distinct patterns of DNA copy number alteration are associated with different clinicopathological features and gene-expression subtypes of breast cancer". *Genes Chromosomes Cancer* 45.11 (Nov. 2006), pp. 1033–1040.
- [33] G. K. Geiss, R. E. Bumgarner, B. Birditt, T. Dahl, N. Dowidar, D. L. Dunaway, H. P. Fell, S. Ferree, R. D. George, T. Grogan, J. J. James, M. Maysuria, J. D. Mitton, P. Oliveri, J. L. Osborn, T. Peng, A. L. Ratcliffe, P. J. Webster, E. H. Davidson, L. Hood, and K. Dimitrov. "Direct multiplexed measurement of gene expression with color-coded probe pairs". *Nat. Biotechnol.* 26.3 (Mar. 2008), pp. 317–325.
- [34] L. Seymour, J. Bogaerts, A. Perrone, R. Ford, L. H. Schwartz, S. Mandrekar, N. U. Lin, S. Litière, J. Dancey, A. Chen, F. S. Hodi, P. Therasse, O. S. Hoekstra, L. K. Shankar, J. D. Wolchok, M. Ballinger, C. Caramella, E. G. E. de Vries, and RECIST working group. "iRECIST: guidelines for response criteria for use in trials testing immunotherapeutics". *Lancet Oncol.* 18.3 (Mar. 2017), e143–e152.
- [35] M. J. M. Magbanua, O. Gumusay, R. Kurzrock, L. J. van 't Veer, and H. S. Rugo. "Immunotherapy in breast cancer and the potential role of liquid biopsy". *Front. Oncol.* 12 (Mar. 2022), p. 802579.

- [36] A. Santonja, W. N. Cooper, M. D. Eldridge, P. A. W. Edwards, J. A. Morris, A. R. Edwards, H. Zhao, K. Heider, D.-L. Couturier, A. Vijayaraghavan, P. Mennea, E.-J. Ditter, C. G. Smith, C. Boursnell, R. Manzano Garcia, O. M. Rueda, E. Beddowes, H. Biggs, S.-J. Sammut, N. Rosenfeld, C. Caldas, J. E. Abraham, and D. Gale. "Comparison of tumor-informed and tumor-naïve sequencing assays for ctDNA detection in breast cancer". *EMBO Mol. Med.* 15.6 (June 2023), e16505.
- [37] A. A. Davis, S. Jacob, L. Gerratana, A. N. Shah, F. Wehbe, N. Katam, Q. Zhang, L. Flaum, K. P. Siziopikou, L. C. Plataniias, W. J. Gradishar, A. Behdad, and M. Cristofanilli. "Landscape of circulating tumour DNA in metastatic breast cancer". *EBioMedicine* 58.102914 (Aug. 2020), p. 102914.
- [38] A. C. McEvoy, L. Warburton, Z. Al-Ogaili, L. Celliers, L. Calapre, M. R. Pereira, M. A. Khattak, T. M. Meniawy, M. Millward, M. Ziman, and E. S. Gray. "Correlation between circulating tumour DNA and metabolic tumour burden in metastatic melanoma patients". *BMC Cancer* 18.1 (Dec. 2018).
- [39] S.-J. Dawson, D. W. Y. Tsui, M. Murtaza, H. Biggs, O. M. Rueda, S.-F. Chin, M. J. Dunning, D. Gale, T. Forshew, B. Mahler-Araujo, S. Rajan, S. Humphray, J. Becq, D. Halsall, M. Wallis, D. Bentley, C. Caldas, and N. Rosenfeld. "Analysis of circulating tumor DNA to monitor metastatic breast cancer". *N. Engl. J. Med.* 368.13 (Mar. 2013), pp. 1199–1209.
- [40] I. Garcia-Murillas, G. Schiavon, B. Weigelt, C. Ng, S. Hrebien, R. J. Cutts, M. Cheang, P. Osin, A. Nerurkar, I. Kozarewa, J. A. Garrido, M. Dowsett, J. S. Reis-Filho, I. E. Smith, and N. C. Turner. "Mutation tracking in circulating tumor DNA predicts relapse in early breast cancer". *Sci. Transl. Med.* 7.302 (Aug. 2015), 302ra133.
- [41] J. Tie, Y. Wang, C. Tomasetti, L. Li, S. Springer, I. Kinde, N. Silliman, M. Tacey, H.-L. Wong, M. Christie, S. Kosmider, I. Skinner, R. Wong, M. Steel, B. Tran, J. Desai, I. Jones, A. Haydon, T. Hayes, T. J. Price, R. L. Strausberg, L. A. Diaz Jr, N. Papadopoulos, K. W. Kinzler, B. Vogelstein, and P. Gibbs. "Circulating tumor DNA analysis detects minimal residual disease and predicts recurrence in patients with stage II colon cancer". *Sci. Transl. Med.* 8.346 (July 2016), 346ra92–346ra92.
- [42] D. V. Araujo, A. Wang, D. Torti, A. Leon, K. Marsh, A. McCarthy, H. Berman, A. Spreafico, A. R. Hansen, A.-A. Razak, P. L. Bedard, L. Wang, E. Plackmann, H. Chow, H. Bao, X. Wu, T. J. Pugh, and L. L. Siu. "Applications of circulating tumor DNA in a cohort of phase I solid tumor patients treated with immunotherapy". *JNCI Cancer Spectr.* 5.3 (June 2021), kaa122.
- [43] M.-H. Stern, A. B. Silveira, I. Bieche, S. Melaabi, L. Cabel, B. Buecher, J.-Y. Pierga, F.-C. Bidard, and C. Proudhon. "Abstract 4599: Detecting MSI phenotype in circulating blood DNA". *Cancer Res.* 78.13_Supplement (July 2018), pp. 4599–4599.
- [44] J. C. M. Wan, D. Stephens, L. Luo, J. R. White, C. M. Stewart, B. Rousseau, D. W. Y. Tsui, and L. A. Diaz Jr. "Genome-wide mutational signatures in

- low-coverage whole genome sequencing of cell-free DNA". *Nat. Commun.* 13.1 (Aug. 2022), p. 4953.
- [45] P. C. Mack, K. C. Banks, C. R. Espenschied, R. A. Burich, O. A. Zill, C. E. Lee, J. W. Riess, S. A. Mortimer, A. Talasaz, R. B. Lanman, and D. R. Gandara. "Spectrum of driver mutations and clinical impact of circulating tumor DNA analysis in non-small cell lung cancer: Analysis of over 8000 cases". *Cancer* 126.14 (July 2020), pp. 3219–3228.
- [46] T. I. Zack, S. E. Schumacher, S. L. Carter, A. D. Cherniack, G. Saksena, B. Tabak, M. S. Lawrence, C.-Z. Zhsng, J. Wala, C. H. Mermel, C. Sougnez, S. B. Gabriel, B. Hernandez, H. Shen, P. W. Laird, G. Getz, M. Meyerson, and R. Beroukhim. "Pan-cancer patterns of somatic copy number alteration". *Nat. Genet.* 45.10 (Oct. 2013), pp. 1134–1140.
- [47] R. Beroukhim, C. H. Mermel, D. Porter, G. Wei, S. Raychaudhuri, J. Donovan, J. Barretina, J. S. Boehm, J. Dobson, M. Urashima, K. T. Mc Henry, R. M. Pinchback, A. H. Ligon, Y.-J. Cho, L. Haery, H. Greulich, M. Reich, W. Winckler, M. S. Lawrence, B. A. Weir, K. E. Tanaka, D. Y. Chiang, A. J. Bass, A. Loo, C. Hoffman, J. Prensner, T. Liefeld, Q. Gao, D. Yecies, S. Signoretti, E. Maher, F. J. Kaye, H. Sasaki, J. E. Tepper, J. A. Fletcher, J. Tabernero, J. Baselga, M.-S. Tsao, F. Demichelis, M. A. Rubin, P. A. Janne, M. J. Daly, C. Nucera, R. L. Levine, B. L. Ebert, S. Gabriel, A. K. Rustgi, C. R. Antonescu, M. Ladanyi, A. Letai, L. A. Garraway, M. Loda, D. G. Beer, L. D. True, A. Okamoto, S. L. Pomeroy, S. Singer, T. R. Golub, E. S. Lander, G. Getz, W. R. Sellers, and M. Meyerson. "The landscape of somatic copy-number alteration across human cancers". *Nature* 463.7283 (Feb. 2010), pp. 899–905.
- [48] L. B. Alexandrov, S. Nik-Zainal, D. C. Wedge, S. A. J. R. Aparicio, S. Behjati, A. V. Biankin, G. R. Bignell, N. Bolli, A. Borg, A.-L. Børresen-Dale, S. Boyault, B. Burkhardt, A. P. Butler, C. Caldas, H. R. Davies, C. Desmedt, R. Eils, J. E. Eyfjörd, J. A. Foekens, M. Greaves, F. Hosoda, B. Hutter, T. Illic, S. Imbeaud, M. Imielinski, N. Jäger, D. T. W. Jones, D. Jones, S. Knappskog, M. Kool, S. R. Lakhani, C. López-Otín, S. Martin, N. C. Munshi, H. Nakamura, P. A. Northcott, M. Pajic, E. Papaemmanuil, A. Paradiso, J. V. Pearson, X. S. Puente, K. Raine, M. Ramakrishna, A. L. Richardson, J. Richter, P. Rosenstiel, M. Schlesner, T. N. Schumacher, P. N. Span, J. W. Teague, Y. Totoki, A. N. J. Tutt, R. Valdés-Mas, M. M. van Buuren, L. van 't Veer, A. Vincent-Salomon, N. Waddell, L. R. Yates, Australian Pancreatic Cancer Genome Initiative, ICGC Breast Cancer Consortium, ICGC MMML-Seq Consortium, ICGC PedBrain, J. Zucman-Rossi, P. A. Futreal, U. McDermott, P. Lichter, M. Meyerson, S. M. Grimmond, R. Siebert, E. Campo, T. Shibata, S. M. Pfister, P. J. Campbell, and M. R. Stratton. "Signatures of mutational processes in human cancer". *Nature* 500.7463 (Aug. 2013), pp. 415–421.
- [49] M. Murtaza, S.-J. Dawson, D. W. Y. Tsui, D. Gale, T. Forshew, A. M. Piskorz, C. Parkinson, S.-F. Chin, Z. Kingsbury, A. S. C. Wong, F. Marass, S. Humphray, J. Hadfield, D. Bentley, T. M. Chin, J. D. Brenton, C. Caldas, and N. Rosenfeld. "Non-invasive analysis of acquired resistance to cancer

- therapy by sequencing of plasma DNA". *Nature* 497.7447 (May 2013), pp. 108–112.
- [50] L. R. Yates, M. Gerstung, S. Knappskog, C. Desmedt, G. Gundem, P. Van Loo, T. Aas, L. B. Alexandrov, D. Larsimont, H. Davies, Y. Li, Y. S. Ju, M. Ramakrishna, H. K. Haugland, P. K. Lilleng, S. Nik-Zainal, S. McLaren, A. Butler, S. Martin, D. Glodzik, A. Menzies, K. Raine, J. Hinton, D. Jones, L. J. Mudie, B. Jiang, D. Vincent, A. Greene-Colozzi, P.-Y. Adnet, A. Fatima, M. Maetens, M. Ignatiadis, M. R. Stratton, C. Sotiriou, A. L. Richardson, P. E. Lønning, D. C. Wedge, and P. J. Campbell. "Subclonal diversification of primary breast cancer revealed by multiregion sequencing". *Nat. Med.* 21.7 (July 2015), pp. 751–759.
- [51] M. Karaayvaz, S. Cristea, S. M. Gillespie, A. P. Patel, R. Mylvaganam, C. C. Luo, M. C. Specht, B. E. Bernstein, F. Michor, and L. W. Ellisen. "Unravelling subclonal heterogeneity and aggressive disease states in TNBC through single-cell RNA-seq". *Nat. Commun.* 9.1 (Sept. 2018), p. 3588.
- [52] G. J. Weiss, J. Beck, D. P. Braun, K. Bornemann-Kolatzki, H. Barilla, R. Cubello, W. Quan Jr, A. Sangal, V. Khemka, J. Waypa, W. M. Mitchell, H. Urnovitz, and E. Schütz. "Tumor cell-free DNA copy number instability predicts therapeutic response to immunotherapy". *Clin. Cancer Res.* 23.17 (Sept. 2017), pp. 5074–5081.
- [53] G. Marsavela, J. Lee, L. Calapre, S. Q. Wong, M. R. Pereira, A. C. McEvoy, A. L. Reid, C. Robinson, L. Warburton, A. Abed, M. A. Khattak, T. M. Meniawy, S.-J. Dawson, S. Sandhu, M. S. Carlino, A. M. Menzies, R. A. Scolyer, G. V. Long, B. Amanuel, M. Millward, M. R. Ziman, H. Rizos, and E. S. Gray. "Circulating tumor DNA predicts outcome from first-, but not second-line treatment and identifies melanoma patients who may benefit from combination immunotherapy". *Clin. Cancer Res.* 26.22 (Nov. 2020), pp. 5926–5933.
- [54] K. Patell, M. Kurian, B. Booker, M. Chung, A. Bennett, D. L. Bajor, A. M. R. Mohamed, A. Mahipal, S. Chakrabarti, and J. E. Selfridge. "Circulating tumor DNA (ctDNA) dynamics in response to checkpoint inhibitor immunotherapy in colorectal cancer". *J. Clin. Oncol.* 41.16_suppl (June 2023), e15540–e15540.
- [55] W. Roh, P.-L. Chen, A. Reuben, C. N. Spencer, P. A. Prieto, J. P. Miller, V. Gopalakrishnan, F. Wang, Z. A. Cooper, S. M. Reddy, C. Gumbs, L. Little, Q. Chang, W.-S. Chen, K. Wani, M. P. De Macedo, E. Chen, J. L. Austin-Breneman, H. Jiang, J. Roszik, M. T. Tetzlaff, M. A. Davies, J. E. Gershenwald, H. Tawbi, A. J. Lazar, P. Hwu, W.-J. Hwu, A. Diab, I. C. Glitza, S. P. Patel, S. E. Woodman, R. N. Amaria, V. G. Prieto, J. Hu, P. Sharma, J. P. Allison, L. Chin, J. Zhang, J. A. Wargo, and P. A. Futreal. "Integrated molecular analysis of tumor biopsies on sequential CTLA-4 and PD-1 blockade reveals markers of response and resistance". *Sci. Transl. Med.* 9.379 (Mar. 2017), eaah3560.
- [56] F.-C. Bidard, A.-C. Hardy-Bessard, F. Dalenc, T. Bachelot, J.-Y. Pierga, T. de la Motte Rouge, R. Sabatier, C. Dubot, J.-S. Frenel, J. M. Ferrero,

- S. Ladoire, C. Levy, M.-A. Mouret-Reynier, A. Lortholary, J. Grenier, C. Chakiba, L. Stefani, J. E. Plaza, F. Clatot, L. Teixeira, V. D'Hondt, H. Vegas, O. Derbel, C. Garnier-Tixidre, J.-L. Canon, B. Pistilli, F. André, L. Arnould, A. Pradines, I. Bièche, C. Callens, J. Lemonnier, F. Berger, S. Delaloge, and PADA-1 investigators. "Switch to fulvestrant and palbociclib versus no switch in advanced breast cancer with rising ESR1 mutation during aromatase inhibitor and palbociclib therapy (PADA-1): a randomised, open-label, multicentre, phase 3 trial". *Lancet Oncol.* 23.11 (Nov. 2022), pp. 1367–1377.
- [57] A. Bardia, S. A. Hurvitz, S. M. Tolaney, D. Loirat, K. Punie, M. Oliveira, A. Brufsky, S. D. Sardesai, K. Kalinsky, A. B. Zelnak, R. Weaver, T. Traina, F. Dalenc, P. Aftimos, F. Lynce, S. Diab, J. Cortés, J. O'Shaughnessy, V. Diéras, C. Ferrario, P. Schmid, L. A. Carey, L. Gianni, M. J. Piccart, S. Loibl, D. M. Goldenberg, Q. Hong, M. S. Olivo, L. M. Itri, H. S. Rugo, and ASCENT Clinical Trial Investigators. "Sacituzumab govitecan in metastatic triple-negative breast cancer". *N. Engl. J. Med.* 384.16 (Apr. 2021), pp. 1529–1541.
- [58] S. Modi, W. Jacot, T. Yamashita, J. Sohn, M. Vidal, E. Tokunaga, J. Tsurutani, N. T. Ueno, A. Prat, Y. S. Chae, K. S. Lee, N. Niikura, Y. H. Park, B. Xu, X. Wang, M. Gil-Gil, W. Li, J.-Y. Pierga, S.-A. Im, H. C. F. Moore, H. S. Rugo, R. Yerushalmi, F. Zagouri, A. Gombos, S.-B. Kim, Q. Liu, T. Luo, C. Saura, P. Schmid, T. Sun, D. Gambhire, L. Yung, Y. Wang, J. Singh, P. Vitazka, G. Meinhardt, N. Harbeck, D. A. Cameron, and DESTINY-Breast04 Trial Investigators. "Trastuzumab deruxtecan in previously treated HER2-low advanced breast cancer". *N. Engl. J. Med.* 387.1 (July 2022), pp. 9–20.
- [59] I. Scheinin, D. Sie, H. Bengtsson, M. A. van de Wiel, A. B. Olshen, H. F. van Thuijl, H. F. van Essen, P. P. Eijk, F. Rustenburg, G. A. Meijer, J. C. Reijneveld, P. Wesseling, D. Pinkel, D. G. Albertson, and B. Ylstra. "DNA copy number analysis of fresh and formalin-fixed specimens by shallow whole-genome sequencing with identification and exclusion of problematic regions in the genome assembly". *Genome Res.* 24.12 (Dec. 2014), pp. 2022–2032.
- [60] M. A. van de Wiel, R. Brosens, P. H. C. Eilers, C. Kumps, G. A. Meijer, B. Menten, E. Sistermans, F. Speleman, M. E. Timmerman, and B. Ylstra. "Smoothing waves in array CGH tumor profiles". *Bioinformatics* 25.9 (May 2009), pp. 1099–1104.
- [61] M. A. van de Wiel, K. I. Kim, S. J. Vosse, W. N. van Wieringen, S. M. Wilting, and B. Ylstra. "CGHcall: calling aberrations for array CGH tumor profiles". *Bioinformatics* 23.7 (Apr. 2007), pp. 892–894.
- [62] K. Kulangara, N. Zhang, E. Corigliano, L. Guerrero, S. Waldroup, D. Jaiswal, M. J. Ms, S. Shah, D. Hanks, J. Wang, J. Lunceford, M. J. Savage, J. Juco, and K. Emancipator. "Clinical utility of the combined positive score for programmed death ligand-1 expression and the approval of pembrolizumab for treatment of gastric cancer". *Arch. Pathol. Lab. Med.* 143.3 (Mar. 2019), pp. 330–337.

- [63] S. Adams, S. Loi, D. Toppmeyer, D. W. Cescon, M. De Laurentiis, R. Nanda, E. P. Winer, H. Mukai, K. Tamura, A. Armstrong, M. C. Liu, H. Iwata, L. Ryvo, P. Wimberger, H. S. Rugo, A. R. Tan, L. Jia, Y. Ding, V. Karantza, and P. Schmid. “Pembrolizumab monotherapy for previously untreated, PD-L1-positive, metastatic triple-negative breast cancer: cohort B of the phase II KEYNOTE-086 study”. *Ann. Oncol.* 30.3 (Mar. 2019), pp. 405–411.

5

Neoadjuvant nivolumab or nivolumab plus ipilimumab in early-stage triple negative breast cancer: a phase 2 adaptive BELLINI trial

Published in: *Nature Medicine*, 30:3223–3235, 2024.
DOI: 10.1038/s41591-024-03249-3

Iris Nederlof^{1,*}, **Olga I. Isaeva**^{1,*}, Manon de Graaf^{1,**}, Robbert C.A.M. Gielen^{1,**}, Noor A. M. Bakker^{1,2,**}, Adrienne L. Rolfes¹, Hannah Garner^{1,2}, Bram Boeckx^{3,4}, Joleen J.H. Traets¹, Ingrid A.M. Mandjes⁵, Michiel de Maaker⁶, Thomas van Brussel^{3,4}, Maksim Chelushkin¹, Elisa Champanhet¹, Marta Lopez-Yurda⁵, Koen van de Vijver^{7,8}, José G. van den Berg⁸, Ingrid Hofland⁶, Natasja Klioueva⁹, Ritse M. Mann¹⁰, Claudette E. Loo¹¹, Frederieke H. van Duijnhoven¹¹, Victoria Skinner¹¹, Sylvia Luykx¹², Emile Kerver¹³, Ekaterina Kalashnikova¹⁴, Marloes G. J. van Dongen¹⁵, Gabe S. Sonke¹⁵, Sabine C. Linn¹⁵, Christian U. Blank^{15,16}, Karin E. de Visser^{1,2,17}, Roberto Salgado^{18,19}, Lodewyk F.A. Wessels^{2,20}, Caroline A. Drukker¹¹, Ton N. Schumacher^{2,16,21}, Hugo M. Horlings⁸, Diether Lambrechts^{3,4}, Marleen Kok^{1,15}

*These authors contributed equally (shared co-first authors): Iris Nederlof, **Olga I. Isaeva**

**These authors contributed equally (shared co-second authors): Manon de Graaf, Robbert C.A.M. Gielen, Noor A.M. Bakker

5. Neoadjuvant nivolumab or nivolumab plus ipilimumab in early-stage triple negative breast cancer: a phase 2 adaptive BELLINI trial

- 1 Division of Tumor Biology and Immunology, The Netherlands Cancer Institute, Amsterdam, the Netherlands
- 2 Oncode Institute, Utrecht, the Netherlands
- 3 Laboratory for Translational Genetics, Department of Human Genetics, KU Leuven, Leuven, Belgium
- 4 VIB Center for Cancer Biology, Leuven, Belgium
- 5 Biometrics Department, The Netherlands Cancer Institute, Amsterdam, the Netherlands
- 6 Core Facility Molecular Pathology & Biobanking, The Netherlands Cancer Institute, Amsterdam, the Netherlands
- 7 Department of Pathology, UZ Gent - Universitair Ziekenhuis Gent, Gent, Belgium
- 8 Department of Pathology, The Netherlands Cancer Institute, Amsterdam, the Netherlands
- 9 Department of Pathology, OLVG Hospital, Amsterdam, Netherlands
- 10 Department of Radiology, The Netherlands Cancer Institute, Amsterdam, the Netherlands
- 11 Department of Surgical Oncology, The Netherlands Cancer Institute, Amsterdam, the Netherlands
- 12 Medical Oncology department, Tergooi Hospital - locatie Hilversum, Hilversum, the Netherlands
- 13 Department of Oncology, OLVG Hospital, Amsterdam, Netherlands
- 14 Natera, Natera Inc., San Carlos, CA, United States of America
- 15 Department of Medical Oncology, The Netherlands Cancer Institute, Amsterdam, the Netherlands
- 16 Division of Molecular Oncology and Immunology, The Netherlands Cancer Institute, Amsterdam, the Netherlands
- 17 Department of Immunology, Leiden University Medical Center, Leiden, the Netherlands
- 18 Department of Pathology, ZAS hospitals, Antwerp, Belgium
- 19 Division of Research, Peter MacCallum Cancer Centre, Melbourne, Victoria, Australia
- 20 Division of Molecular Carcinogenesis, The Netherlands Cancer Institute, Amsterdam, the Netherlands
- 21 Department of Hematology, Leiden University Medical Center, Leiden, the Netherlands

Immune checkpoint inhibition (ICI) with chemotherapy is now standard of care for stage II-III triple negative breast cancer (TNBC). However, it is largely unknown for which patients ICI without chemotherapy could be an option and what the benefit of combination ICI could be. The adaptive BELLINI trial explored whether short combination ICI induces immune activation (primary endpoint: two-fold increase in CD8+ T cells or IFNG), providing rationale for neoadjuvant ICI without chemotherapy.

In window of opportunity cohorts A (4 weeks anti-PD1) and B (4 weeks anti-PD1 + anti-CTLA4), we observed immune activation in 53% (8/15) and 60% (9/15) of patients, respectively. High tumor-infiltrating lymphocytes (TILs) correlated with response. Single-cell RNA

sequencing revealed that higher pretreatment tumor-reactive CD8+ T cells, follicular helper T cells and shorter distances between tumor and CD8+ T cells correlated with response. Higher levels of regulatory T cells post-treatment associated with non-response.

Based on these data, we opened cohort C for patients with high TILs ($\geq 50\%$) who received 6 weeks neoadjuvant anti-PD1 + anti-CTLA4 followed by surgery (primary endpoint: pathological complete response, pCR). 53% (8/15) of patients had major pathological response ($< 10\%$ viable tumor) at resection, with 33% (5/15) having pCR. All cohorts met Simon's two-stage threshold for expansion to stage II. We observed grade ≥ 3 adverse events for 17% of patients, and a high rate (57%) of immune-mediated endocrinopathies. In conclusion, neoadjuvant immunotherapy without chemotherapy demonstrates potential efficacy and warrants further investigation in patients with early TNBC. ClinicalTrials.gov Identifier: NCT03815890.

5.1. Introduction

The addition of programmed death (ligand) 1 blockade (anti-PD(L)1) to neoadjuvant chemotherapy has changed the treatment landscape for patients with early (stage II-III) triple negative breast cancer (TNBC) [1]. However, all trials evaluating the efficacy of anti-PD(L)1 in TNBC combined it with chemotherapy [1–4]. This chemotherapy backbone inevitably results in a high rate of adverse events, significantly affects quality of life and could diminish T cell activity [5, 6].

So far, no biomarkers have been established to predict which patients with early stage TNBC will benefit from anti-PD1. Therapy is currently given for a total duration of one year, while data in other tumor types have shown that a pCR can be reached after only a few weeks of treatment with immune checkpoint inhibitors (ICI) [7–11]. Overtreatment prevention is an increasingly important consideration due to the high number of patients needed to treat to prevent one recurrence and increasing toxicity with more intense and longer treatments. Therefore, there is an urgent clinical need to optimize treatment schedules and improve patient selection for specific treatments [12].

While numerous studies have integrated anti-PD(L)1 therapy with chemotherapy in early stage TNBC [1–3, 13], data on combination ICIs are limited. ICIs targeting CTLA4 have revolutionized treatment for non-small cell lung cancer (NSCLC) [8] and melanoma [14–16]. Additionally, neoadjuvant trials across various tumor types have shown impressive major pathological response rates when combining anti-PD(L)1 with low-dose anti-CTLA4 [7, 8, 10, 17]. A trial in metastatic breast cancer revealed long-lasting responses after combining low-dose anti-CTLA4 with anti-PD1 [18], which are infrequently observed with anti-PD(L)1 alone. These findings provide a rationale to test low-dose anti-CTLA4 in combination with anti-PD(L)1 in early TNBC.

Simultaneously with the advent of ICI, tumor-infiltrating lymphocytes (TILs) have emerged as a putative prognostic and predictive biomarker [19–22]. TNBC patients with high TIL levels have an excellent prognosis even without chemotherapy [19, 23], suggesting that TILs reflect an endogenous antitumor T cell response. Moreover, in metastatic TNBC, high TIL levels are associated with response to ICI [24, 25]. Collectively, these findings imply that TILs may serve as a tool for identifying TNBC patients who are more likely to benefit from ICI and have a favorable prognosis, paving the way for exploring chemotherapy de-escalation. The BELLINI trial is an adaptive platform trial exploring the effect of ICI without chemotherapy starting with window of opportunity cohorts with a biological endpoint followed by neoadjuvant cohorts with complete pathological response (pCR) endpoint. This adaptive platform trial consists of sequential, single-cohort, phase 2 studies, where new

cohorts can be opened based on signals obtained in prior cohorts. The first two cohorts evaluated whether four weeks of nivolumab (anti-PD1, cohort A) or nivolumab and low-dose ipilimumab (anti-PD1 and anti-CTLA4, cohort B) can lead to immune activation (primary endpoint). This four-week therapy regimen was scheduled before the start of regular therapy, and therefore the effect of ICI could be assessed independently of chemotherapy. Promising results in cohorts A and B among patients with high TILs ($\geq 50\%$) led to the initiation of cohort C. In cohort C, we used a neoadjuvant design with six weeks of nivolumab plus low-dose ipilimumab followed by surgery to assess the pCR rate [14, 26].

This is the first trial combining anti-PD1 with anti-CTLA4 in early breast cancer, as well as the first trial exploring what pCR rate could be achieved with ICI-only approaches and using TIL levels as an entry criterion to enrich for inflamed tumors.

5.2. Results

Design and patient characteristics

The BELLINI trial (NCT03815890; **Figure 5.1A,G, Supplementary Figure 5.5A**) is a pre-operative, window of opportunity (WOO), phase II, multiple-cohort non-randomized study in early (stage I-III) breast cancer utilizing an adaptive Simon's two-stage design [27]. Here, we report the initial results from the first two WOO cohorts exploring the immune-activating capacity of short-term neoadjuvant nivolumab \pm ipilimumab (cohorts A and B, $n=31$) in patients with $\geq 5\%$ TILs as well as the initial results of cohort C that was opened based on the results of cohorts A and B. The first patient was included on 19 September 2019 and the last patient on 24 January 2024.

Cohort A ($n=15$) received two cycles of nivolumab (240 mg) on days 1 and 15. Cohort B ($n=15$) received two cycles of nivolumab (240 mg) on days 1 and 15, plus one cycle of ipilimumab (1 mg/kg) on day 1. To exclude patients with a poor prognosis, less likely to respond to ICI and not suitable for chemotherapy de-escalation, we enrolled patients with $\geq 5\%$ TILs in cohorts A and B. Baseline characteristics were similar between cohorts A and B, except for a higher proportion of patients with positive lymph nodes in cohort B (**Table 5.1**).

The primary endpoint for cohorts A and B was immune activation, defined as at least a two-fold increase in CD8⁺ T cells (measured by immunohistochemistry (IHC), **Supplementary Figures 5.5B-F**) and/or increased interferon gamma (IFNG) gene expression. This endpoint was based on the observation that significant increases in intratumoral CD8⁺ T cells [25, 28] and higher IFNG signature scores [17, 29] in

5. Neoadjuvant nivolumab or nivolumab plus ipilimumab in early-stage triple negative breast cancer: a phase 2 adaptive BELLINI trial

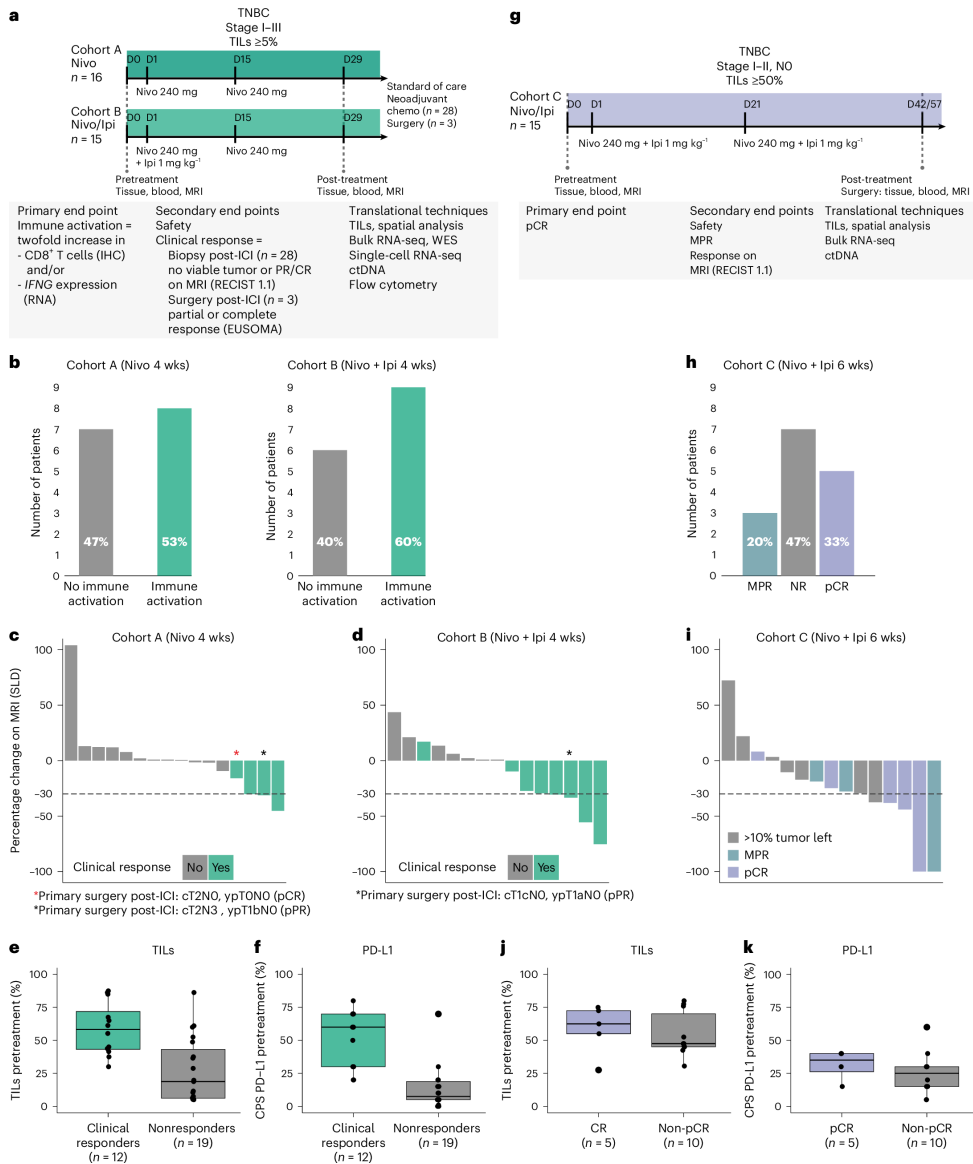


Figure 5.1: BELLINI trial design, efficacy data and baseline biomarkers. (A) Trial design for cohorts A and B. Cohort A received 2 cycles of nivolumab (anti-PD1). Cohort B received 2 cycles of nivolumab (anti-PD1) and one cycle of ipilimumab (anti-CTLA4). Biopsies and blood were taken pretreatment and after 4 weeks of treatment after which patients proceeded to standard of care: neoadjuvant chemotherapy (n=28) or primary surgery (n=3). (B) Numbers of patients reaching immune activation in cohorts A (n=15) and B (n=15). (C)-(D) Changes in tumor size according to the MRI for cohort A (C) and cohort B (D). The gray dashed line at -30%: radiological PR. The green bars indicate clinical responses (radiological PR and/or pathological response). Asterisks (*) represent patients with resection after ICI only (n=3). pPR: pathological partial response according to EUSOMA. (E) TILs in pretreatment biopsies of patients with and without clinical response in cohorts A and B. n=31 patients. (F) Combined positive PD-L1 score (CPS) in pretreatment biopsies of patients with and without clinical response in cohorts A and B. n=31 patients. (G) BELLINI trial design for cohort C. Cohort C (n=15) received 2 cycles of nivolumab and ipilimumab on days 1 and 21. Biopsies and blood were taken pretreatment and after 6 weeks. Patients proceeded to primary surgery (n=15). (H) pCR and MPR (<30% viable tumor left) rates in cohort C. (I) Changes in tumor size according to the MRI in cohort C. The gray dashed line at -30%: radiological PR. Dark blue bars: pCR. (J) TILs in pretreatment biopsies of patients according to pCR status in cohort C. n=15 patients. (K) CPS in pretreatment biopsies for patients according to pCR status in cohort C. n=15 patients. Figures A, G were created with BioRender.com. In E, J levels of TILs calculated as average from TIL levels at diagnostic- and pretreatment study. In E-F, J-K, boxplots display a minimum (Q0), a maximum (Q4), a median (Q2) and the interquartile range. P-values were derived using a two-sided Mann-Whitney test.

Table 5.1: Baseline patient characteristics.

Characteristic	A: Nivo (n=16)	B: Nivo-ipi 4 wks (n=15)	C: Nivo-ipi 6 wks (n=15)
Median age, years (IQR range)	48 (39.8- 53.2)	50 (42.5- 57.5)	51 (36.0- 56.5)
WHO PS ^a , n (%)			
0	16 (100)	14 (93.3)	15 (100)
1	0 (0.0)	1 (6.7)	0 (0.0)
Histological subtype, n (%)			
NST	16 (100)	13 (86.7)	14 (93.3)
Metaplastic	0 (0.0)	1 (6.7)	0 (0.0)
Lobular pleiomor- phic	0 (0.0)	1 (6.7)	1 (6.7)
Tumor stage, n (%)			
T1	5 (31.3)	5 (33.3%)	2 (13.3)
T2	10 (62.5)	9 (60.0)	13 (86.7)
T3	1 (6.2)	1 (6.7)	0 (0.0)
Nodal status, n (%)			
N0	13 (81.3)	5 (33.3)	15(100) ^d
N1	2 (12.5)	9 (60.0)	0 (0.0)
N3	1 (6.3)	1 (6.7)	0 (0.0)
Tumor grade ^b , n (%)			
2	1 (6.3)	4 (26.7)	0 (0.0)
3	15 (93.8)	11 (73.3)	15 (100)
Germline BRCA1/2 mutation, n (%)			
Yes	3 (18.8)	3 (20.0)	4 (26.7)
No	12 (75.0)	10 (66.7)	11 (0.0)
Unknown	1 (6.3)	2 (13.3)	0 (0.0)
TILS ^c , (%)			
Median (IQR)	40.8 (6.2, 60.3)	37.5 (23.8, 61.4)	52.5 (45.3,73.8)

^aWHO performance status.^bTumor grade according to Bloom Richardson.^cTILs were averaged between the diagnostic TILs score and the study pretreatment TILs score. sTILs were scored according to international guidelines [22] as a numerical variable. All samples were evaluated by at least two breast cancer pathologists and their score for each sample was averaged.^dCohort C only allowed inclusion of N0 patients. Abbreviations: NST, no special type; TILs, stromal tumor-infiltrating lymphocytes.

serially biopsied tumors are correlated with responses to anti-PD(L)1.

Clinical response (secondary endpoint) in cohorts A and B was defined as PR/CR on MRI (RECIST1.1) or no viable tumor in post-treatment biopsy for patients proceeding to neoadjuvant chemotherapy. For patients directly proceeding to surgery this was defined as partial or complete pathological response (EUSOMA). Other secondary endpoints included safety and translational analyses. MRI scans and biopsies were collected at baseline and after two ICI cycles.

Efficacy of short-term nivolumab and nivolumab+ipilimumab in early TNBC (window of opportunity)

Immune activation was achieved in 8 tumors (53.3%) in the nivolumab cohort (A) and 9 (60%) in the nivo-ipi cohort (B) (**Figure 5.1B**). Therefore, both cohorts met the Simon's two-stage [27] threshold for expansion to stage II. After four weeks, patients proceeded to standard neoadjuvant chemotherapy followed by surgery (n=28) or surgery without neoadjuvant chemotherapy (n=3). Clinical response was observed in 12/31 patients (38.7%, 95% CI 23.7%-56.2%) with 7/31 patients (22.6%, 95% CI 11.4%-39.8%) having a partial response (PR) according to RECIST 1.1 [30] (**Figures 5.1C,D**). 10/31 patients had no viable tumor in the biopsy and in the three patients who underwent surgery directly after ICI, two partial and one complete pathological response was seen. Despite these clear pathological responses, MRI showed modest downsizing, indicating MRI underestimates early ICI response (**Supplementary Figure 5.5H**), consistent with findings in early-stage melanoma [31], colorectal and gastroesophageal cancers [17, 32]. Strikingly, clinical response was only observed for patients with TILs $\geq 30\%$ (**Figure 5.1E**) and a CPS PDL1 $\geq 20\%$ (**Figure 5.1F**). Patients with lower pretreatment CD8+ T cell levels were more likely to achieve immune activation (**Figure 5.1G**), likely due to either less possibility for value doubling or to a very early immune response in highly inflamed tumors.

Short-term neoadjuvant nivolumab + ipilimumab can induce pathological responses in patients with high TILs

Both cohorts A and B met the predefined thresholds of the Simon's two-stage design [27], allowing expansion to stage II. However, given the promising clinical responses observed in cohorts A and B and the approval of neoadjuvant pembrolizumab plus chemotherapy [4], the study team decided not to proceed to stage II with the WOO design but to open cohort C with a true neoadjuvant design (n=15, **Figure 5.1G**). Since all patients with a clinical response in cohorts A and B had high TILs, cohort C was opened for patients with $\geq 50\%$ TILs and allowed only patients with node-negative disease since for this patient population chemotherapy de-escalation could be an option in the future. The

treatment schedule with combination ICI for cohort C was based on our data obtained in cohorts A and B as well as on the well established effective and tolerable combination ICI schedule in melanoma [14, 26].

Patients in cohort C underwent a 6-week treatment regimen of nivolumab and ipilimumab (administered on days 1 and 21), followed by surgery (**Figure 5.1G**). Five patients had a pCR, (33.3%, 95% CI 15.2%-58.3%, **Figure 5.1H**) with confirmed tumor-negative lymph nodes (ypT0N0). Less than 10% viable tumor remaining was seen in 3/15 patients (20%, 95% CI 4%-48%, **Figure 5.1H**), making major pathological response rate (MPR) $8/15=53\%$ (95% CI 27%-79%). Notably, of the 5 patients with a pCR only one had a complete radiological response (**Figure 5.1I**). Because of high TILs, N0 status and pCR which are all very favorable prognostic features, all 5 patients with a pCR were offered the option of omitting adjuvant chemotherapy and all chose not to undergo adjuvant chemotherapy (shared decision). Patients without pCR were advised adjuvant chemotherapy.

Safety data and follow-up

Toxicity data are summarized in **Table 5.2** (all events required steroids or persisted) and detailed in **Supplementary Table 5.3**. Neither neoadjuvant nivolumab nor nivolumab-ipilimumab resulted in previously unreported toxicities. All patients were monitored for (immune-related; IR) toxicities until one year post ICI-therapy. Treatment-related adverse events (AEs) of any grade occurred in 41/46 patients (89%). A total of 8 (17%) patients developed grade ≥ 3 treatment-related AEs, of which 6 were treated in cohort C. Except for the endocrinopathies all adverse events resolved. Notably, 19/46 patients (41%) developed treatment-related hypothyroidism. All patients with hypothyroidism remain dependent on replacement therapy. Six patients (13%) developed adrenal insufficiency and require ongoing corticoid replacement therapy. One patient developed a diabetic ketoacidosis and remains insulin-dependent.

All patients proceeded with tumor resection or neoadjuvant chemotherapy as scheduled. 44 patients received both ICI doses, and two patients only received one dose due to suspected immunotoxicity.

With a median follow-up duration of 32.5 months in cohorts A and B (interquartile range 28.1-40.3 months), one patient in cohort A (cT2N0; intermediate TILs) developed a second primary tumor, and one patient in cohort B (cT2N1; intermediate TILs) died from metastatic TNBC despite receiving standard of care (neo)adjuvant chemotherapy. Median follow-up for cohort C was 17.6 months (interquartile range 18.8-22.1 months). One patient (no response to ICI) refused adjuvant chemotherapy and radiotherapy and developed recurrent TNBC (pT1cNx, 80% TILs).

5. Neoadjuvant nivolumab or nivolumab plus ipilimumab in early-stage triple negative breast cancer: a phase 2 adaptive BELLINI trial

Table 5.2: Summary of adverse events.

	A: Nivolumab (N=16)		B: Nivo+Ipi 4 wks (N=15)		C: Nivo+Ipi 6 wks (N=15)	
	Number of patients (percent)					
Immune-mediated adverse events	Any grade	Grade ≥3	Any grade	Grade ≥3	Any grade	Grade ≥3
Hypothyroidism^	6 (38%)	0 (0%)	7 (47%)	0 (0%)	6 (40%)	0 (0%)
Adrenal insufficiency*	1 (6%)	0 (0%)	2 (13%)	1 (7%)	3 (20%)	1 (7%)
Diabetes Mellitus	0 (0%)	0 (0%)	1 (7%)	1 (7%)	0 (0%)	0 (0%)
Colitis	0 (0%)	0 (0%)	0 (0%)	0 (0%)	0 (0%)	1 (7%)
Hepatitis**	0 (0%)	0 (0%)	2 (13%)	0 (0%)	3 (20%)	3 (20%)
Polymyalgia rheumatica	0 (0%)	0 (0%)	0 (0%)	0 (0%)	1 (7%)	0 (0%)
Pneumonitis	0 (0%)	0 (0%)	0 (0%)	0 (0%)	2 (13%)	1 (7%)

Pretreatment composition of the tumor microenvironment is associated with ICI response

Due to limited sample size, we compared clinical responders versus non-responders from both cohorts (A+B) combined and not for the cohorts separately. Clinical responders in cohorts A and B had significantly higher pretreatment TILs ($p=0.0014$, Fig. **Figure 5.1E**) and PDL1 scores ($p=8.6e-05$, **Figure 5.1F**) compared to non-responders. CD8+ T cell density was not significantly associated with clinical response (**Figure 5.2A, Supplementary Figures 5.5B-F**). Spatial analysis showed that responders had significantly shorter distances from tumor cells to the nearest CD8+ T cells ($p=0.00001$, **Figure 5.2B**). Responders also exhibited a larger density of double-positive CD8+PD1+ cells ($p=0.02$, **Supplementary Figure 5.6A**) and PD1+ cells ($p=0.001$, IHC, **Supplementary Figure 5.6B**) pretreatment.

In cohort C, TILs were not different between responders and non-responders, probably due to the more homogeneous patient population with only patients with $\geq 50\%$ TILs (**Figure 5.1J**). In line with this, patients with pCR had similar PDL1 scores, CD8+ T cell density (cells/ μm^2) and distances from tumor to nearest CD8+ T cells as patients without pCR (**Figure 5.1K, Figures 5.2D-E**).

We found no association between tumor mutational burden and clinical response (**Supplementary Figures 5.6C-D**). There were no statistically

5.2. Results

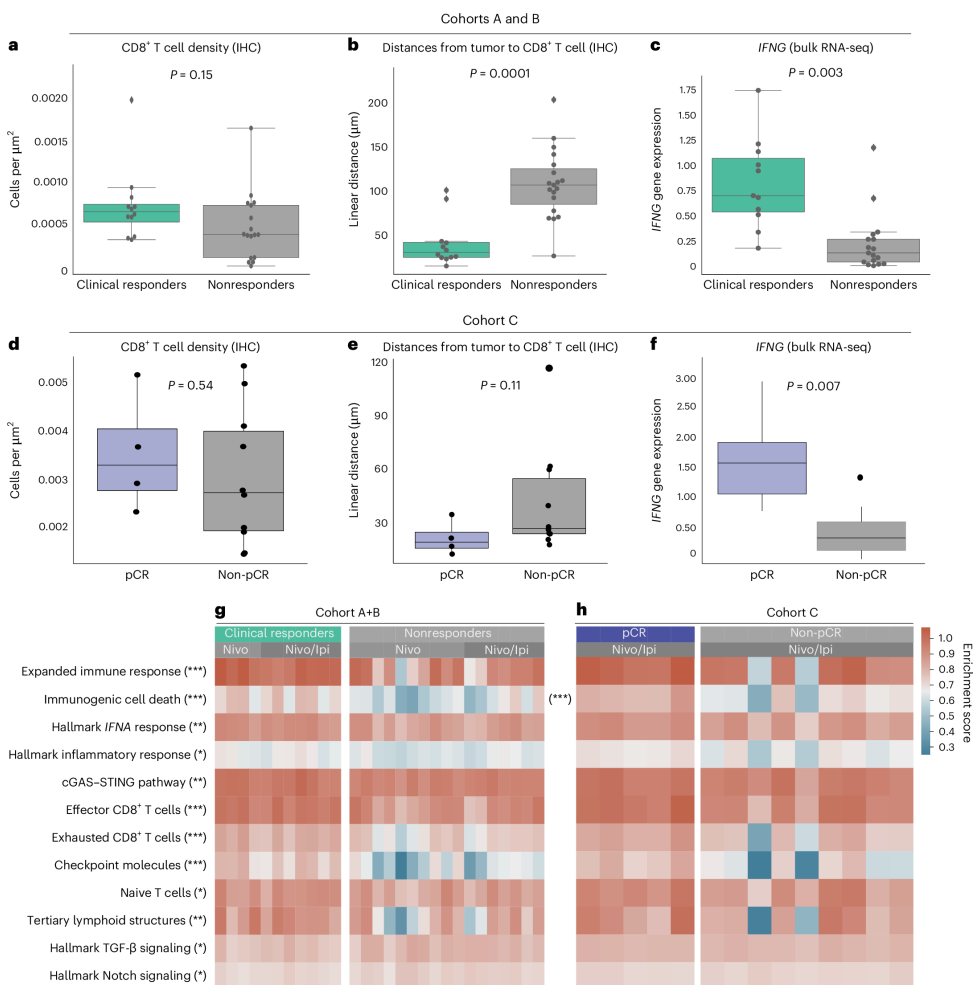


Figure 5.2: Pretreatment immune activation associated with clinical response. (A) CD8+ density (IHC) in pretreatment biopsies of patients with and without clinical response in cohorts A and B. $n=31$ patients. (B) Median distances (μm) from tumor cells to the nearest CD8+ T cells in pretreatment biopsies of patients with and without clinical response in cohorts A and B. $n=31$ patients. (C) IFNG gene expression scores in pretreatment biopsies of patients with and without clinical response in cohorts A and B. $n=28$ patients. (D) CD8+ density (IHC) in pretreatment biopsies of patients with and without pCR in cohort C. $n=14$ patients. (E) Median distances from tumor cells to the nearest CD8+ T cells in pretreatment biopsies of patients with and without pCR in cohort C. $n=14$ patients. (F) IFNG gene expression scores in pretreatment biopsies of patients with and without pCR in cohort C. $n=14$ patients. (G-H) Gene set enrichment expression scores in pretreatment biopsies of patients with and without clinical response in cohorts A and B (G), $n=28$ patients) or pCR (H), $n=14$ patients) in cohort C. Heatmaps include: Expanded immune signature [33], Immunogenic cell death signature [34], Hallmark IFNA response gene set, Hallmark inflammatory response gene set, cGAS-STING pathway gene set [35], Effector CD8+ T cell gene set [36], Exhausted T cell gene set [36], Checkpoint molecules gene set [36], Naive T cell gene set [37], Tertiary lymphoid structures gene set [38], Hallmark TGF-beta signaling gene set, Hallmark Notch signaling. Asterisks represent the p-value levels: " * ": $p \leq 0.05$, " * * ": $p \leq 0.01$, " * * * ": $p \leq 0.001$. Reported p-values were significant after Benjamini-Hochberg (FDR) correction at 10% significance level. In A-F, boxplots display a minimum (Q0), a maximum (Q4), a median (Q2) and the interquartile range. P-values were derived using a two-sided Mann-Whitney test.

significant differences between clinical responders and non-responders in TNBC subtypes [39] (**Supplementary Figure 5.6E**).

Tumors of clinical responders harbor preexisting inflammatory profiles and tumor-specific CD8+ T cells

We conducted in-depth analyses between clinical responders and non-responders using bulk RNA-Seq (all cohorts) and single-cell RNA-Seq and TCR sequencing (cohorts A and B) pre- and post-treatment. Bulk RNA-Seq revealed higher pretreatment levels of IFNG gene expression ($p=0.0003$, **Figure 5.2C**) and inflammatory gene signatures in clinical responders ($p<0.05$ for all, FDR 10%, **Figure 5.2G**, **Supplementary Figures 5.7A-E**). Clinical responders also exhibited higher gene signatures associated with immune infiltration ($p<0.05$ for all, FDR 10%, **Figure 5.2G**, **Supplementary Figures 5.7F-J**). Conversely, clinical non-responders displayed upregulation of TGF-beta and Notch signaling ($p<0.05$ for both, FDR 10%, **Figure 5.2D**, **Supplementary Figures 5.7L-M**). Though TIL levels and distances from tumor cells to CD8+ T cells were not different in responders versus non-responders in cohort C that included TIL high patients only, patients with pCR had significantly higher pretreatment IFNG gene expression (**Figure 5.2F**) and higher scores of gene signatures related to immune response and T cell infiltration (**Figure 5.2H**), consistent with our previous observations of a more inflammatory profile of the tumor microenvironment in clinical responders in cohorts A and B.

After single-cell RNA-Seq data preprocessing, we obtained 80 000 high quality T cells from 52 samples (29 patients). Following unsupervised clustering of the T cells, we identified various subpopulations (**Figures 5.3A-D**, **Supplementary Figures 5.8A-T**), including CD8+ effector T cells, CD8+ tissue resident memory (CD8+ TRM) T cells, proliferating CD8+ T cells, naive CD4+ T cells, follicular B helper T cells (Tfh), memory CD4+ T cells, regulatory T cells (Tregs), CD56bright and CD56dim NK cells. Intriguingly, we identified a cluster of CD8+ T cells with features of tumor-specific T cells. This cluster was characterized by the highest clonality and highest expression of tumor recognition signatures derived using functional tumor recognition experiments [40, 41] (**Figures 5.3C,D**). This CD8+ tumor-specific cluster was marked by high expression of tumor-reactive markers (CD39, CD103, PDCD1), IFNG, effector molecules (GZMB, NKG7, PRF1, GNLY), chemokines (CCL5, CCL4, CXCL13, CCL3) and exhaustion markers (LAG3, HAVCR2, TIGIT, TOX, CTLA4, **Figures 5.3C,D**). Clinical responders exhibited higher fractions of pretreatment CD8+ tumor-specific T cells (**Figure 5.3E**). This is a first report of tumor-specific T cell population identified using single-cell RNA-Seq in clinical trial data showing an association with response. Clinical responders also had higher fractions of CD4+ Tfh cells (**Figure 5.3F**). Presence of tumor-specific CD8+ T cells and Tfh in

pretreatment biopsies was correlated with tumor decrease on MRI, indicating a continuous association between the abundances of these cells pretreatment and the depth of the tumor response (**Supplementary Figures 5.8U,V**). Patients with different TIL levels had similar T cell subtypes pretreatment (**Supplementary Figure 5.8W**).

Flow cytometry of blood samples (19 markers, **Supplementary Table 5.4, Supplementary Figure 5.9A**) revealed increased Ki-67-positive cells within the PD1+ conventional CD4+ T cell population in clinical responders ($p=0.005$, **Figure 5.3G**). A similar trend was observed for CD8+ T cells (**Figure 5.3H**). The increased proliferation of PD1+CD4+ T cells observed in the blood could also be traced back to the tumor, with responders having higher levels of Ki67+ Tfh which was the CD4+ T cell cluster with the highest PDCD1 gene expression in the tumor single-cell RNA-Seq data (**Figures 5.3I,L**). In line with the blood data, the levels of PD1+ proliferating CD8+ T cells were not significantly different between clinical responders and non-responders (**Figures 5.3J-K**), suggesting a specific role for proliferating CD4+ T cells systemically as well as in the TME.

Dynamics and post-treatment composition of the tumor microenvironment are distinct in clinical responders and non-responders

Single-cell RNA-Seq analysis revealed that though the clinical responders had higher proportions of tumor-specific CD8+ T cells pretreatment, post-treatment their tumors included higher levels of effector CD8+ T cells compared to non-responders ($p=0.008$, **Figures 5.4A,B**). This suggests that effector CD8+ T cells contribute to ICI-induced tumor regression and underscore the ongoing antitumor CD8+ T cell response even four weeks after treatment initiation.

Conversely, non-responders had elevated memory CD4+ T cells ($p=0.05$, **Figures 5.4A,C**) and Tregs ($p=0.02$, **Figures 5.4A,D**) post-treatment, potentially suggesting the involvement of Tregs in mediating resistance to ICI, consistent with prior studies [42]. Intriguingly, we observed an association between the fraction of Tregs after treatment and the lack of response or in some patients even increase in tumor volume on MRI (**Figure 5.4E**). This correlation was specifically mediated by activated (CD137+) Tregs, rather than non-activated Tregs (**Supplementary Figures 5.9B-C**).

We also investigated whether the addition of anti-CTLA4 led to differential alterations in the TME compared to nivolumab monotherapy, though the study was not powered for cohort comparisons. Patients receiving nivolumab plus ipilimumab showed a reduced fold change in Tfh cells ($p=0.02$, **Figure 5.4F**), but an increased fold change in naive CD4+ T cells ($p=0.03$, **Figure 5.4G**). Additionally, the combination ICI resulted in a decreased fold change in Tregs ($p=0.01$, **Figure 5.4H**).

5. Neoadjuvant nivolumab or nivolumab plus ipilimumab in early-stage triple negative breast cancer: a phase 2 adaptive BELLINI trial

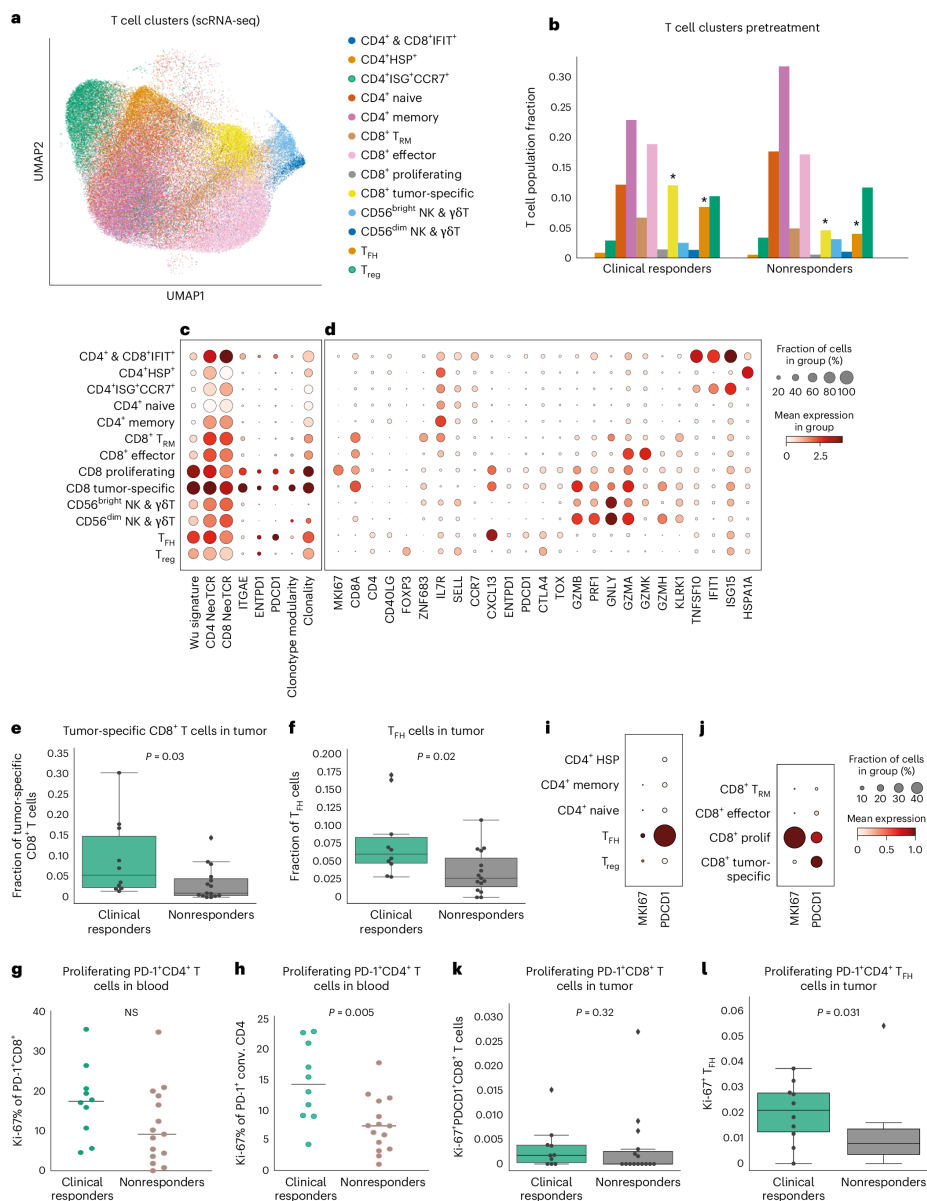


Figure 5.3: Pretreatment T cell profiles of the tumor microenvironment and peripheral blood associated with clinical response in cohorts A and B. (A) UMAP representation of the T cell clusters in the single-cell RNA-Seq dataset (cohorts A and B). n=52 samples from 29 patients, 80 000 cells. (B) Fractions of different T cell populations relative to all T cells in the pretreatment biopsies from clinical responders (left) and non responders (right) in cohorts A and B. (C) Dotplot illustrating differences in tumor reactivity markers in different T cell clusters based on single-cell RNA-Seq data (cohorts A and B). Wu signature: CD8+ T cell tumor specificity signature [41]; CD4 NeoTCR: CD4+ T cell tumor specificity signature [41]; CD8 NeoTCR: CD8+ T cell tumor specificity signature [41]. (E) Tumor-specific CD8+ T cell fractions relative to all T cells in pretreatment biopsies of patients with and without clinical response (cohorts A and B). n = 25 patients. (F) T_{FH} fractions relative to all T cells in pretreatment biopsies of patients with and without clinical response (cohorts A and B). n=25 patients. (G-H) Ki-67 expression on (G) PD1+ CD8+ T cells and (H) conventional CD4+ T cells pretreatment in peripheral blood of patients with and without clinical response in cohorts A and B. n = 25 patients (I) Dotplot for PDCD1 and MKI67 expression in CD4+ T cell clusters (tumoral, scRNA-Seq, cohorts A and B). (J) Dotplot for PDCD1 and MKI67 expression in CD8+ T cell clusters (tumoral, scRNA-Seq, cohorts A and B). (K) Fraction of Ki-67+ T_{FH} cells relative to all T cells in pretreatment biopsies of patients with and without clinical response (cohorts A and B). n=25 patients. (L) Fraction of proliferating PD1+ CD8+ T cells relative to all T cells in pretreatment biopsies of patients with and without clinical response based on single-cell RNA-Seq data (cohorts A and B). n=25 patients. In E-F, K-L boxplots display a minimum (Q0), a maximum (Q4), a median (Q2) and the interquartile range. P-values were derived using a two-sided Mann-Whitney test.

5.2. Results

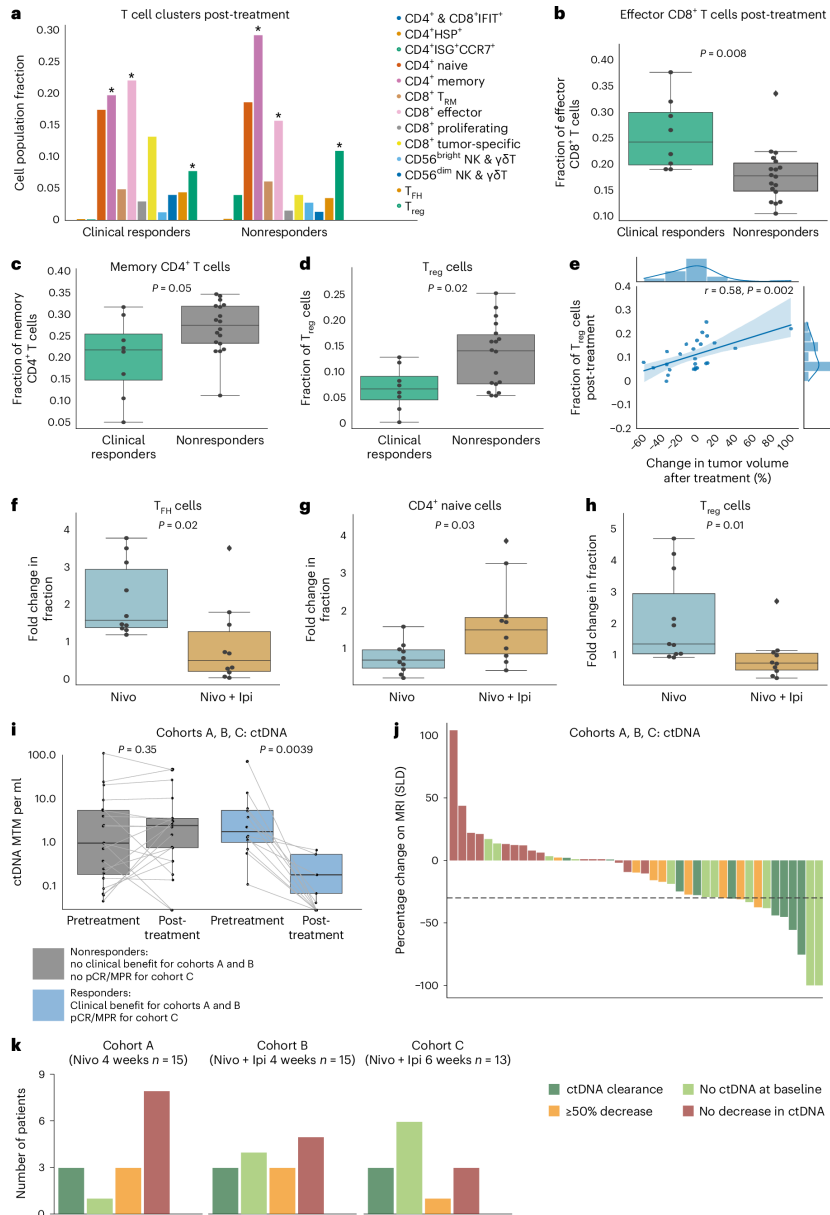


Figure 5.4: Effects of anti-PD1 ± anti-CTLA4 on the T cell profiles in the tumor microenvironment after treatment in cohorts A and B. ctDNA data for all cohorts. (A) Fractions of different T cell clusters relative to all T cells in post-treatment biopsies of patients who did (left) and did not (right) experience clinical response based on single-cell RNA-Seq data. (B) Effector CD8⁺ T cell fractions relative to all T cells in post-treatment biopsies versus response (cohorts A, B). n=26 patients. (C) Memory CD4⁺ T cell fractions relative to all T cells in post-treatment biopsies versus response (cohorts A and B). n=26 patients. (D) Regulatory T cell fractions relative to all T cells in post-treatment biopsies versus response (cohorts A, B). n=26 patients. (E) Fractions of regulatory T cells relative to all T cells in post-treatment biopsies of patients (cohorts A and B) in relation to the change in tumor volume after treatment assessed using MRI (RECIST 1.1). n=26 patients. (F-H) Fold changes in fractions of T cell populations relative to all T cells in cohort A and cohort B. n=22 patients. (F) Follicular B helper T cells. (G) Naive CD4⁺ T cells. (H) Regulatory T cells. (I) Changes in circulating tumor DNA (ctDNA) levels of responding and non-responding patients upon treatment. Patients from all cohorts (A, B, C) were included. (J) Waterfall plot of all patients (n=46, all cohorts) colored according to the fold change in ctDNA levels in blood upon treatment. The groups represent: ctDNA clearance; post-therapy decrease in ctDNA levels of 50% or more post therapy; no ctDNA at baseline; no decrease in ctDNA. The gray dashed line at -30%; radiological PR. (K) Barplots summarizing the number of patients for each ctDNA response category in each cohort (A, B, C). ctDNA at baseline was available for 43/46 patients. In B-D, F-I, boxplots display a minimum (Q0), a maximum (Q4), a median (Q2) and the interquartile range. P-values in B-D, F-H were derived using a two-sided Mann-Whitney test. P-values in I were derived using paired Wilcoxon test.

compared to monotherapy, including both activated and non-activated Tregs (**Supplementary Figures 5.9D-E**).

ctDNA dynamics during early response to ICI

To assess the impact of short-term ICI on circulating tumor DNA (ctDNA), we conducted ctDNA analysis pretreatment and after four weeks (cohorts A and B) or six weeks (cohort C) of ICI using a tumor-informed ctDNA assay (Signatera). Despite the early tumor stages included (mostly I-II), pretreatment ctDNA was detected in 32/43 (74%) patients. After treatment, 9 (21%) patients had complete ctDNA clearance, while additional seven patients had a reduction of $\geq 50\%$ in ctDNA load (MTM/mL, **Figures 5.4I-J**). All clinical responders in cohorts A+B and pCR/MPR patients (n=8) in cohort C demonstrated at least a 50% drop in ctDNA or were negative for ctDNA at baseline (**Figures 5.4I-K**).

5.3. Discussion

In this study, we demonstrate that neoadjuvant nivolumab, with or without ipilimumab, is a feasible chemotherapy-free regimen for patients with early stage TNBC. We show that nivolumab \pm ipilimumab induces immune activation in the majority of patients and can result in complete pathological responses and ctDNA clearance. Pre-existing inflammatory features such as higher TILs, shorter distances from CD8+ T cells to the tumor and higher baseline fractions of tumor-specific CD8+ T cells were associated with response. In contrast, higher fractions of Tregs post-treatment were associated with lack of response. While standard chemo-immunotherapy for TNBC with 4 chemotherapy agents plus anti-PD1 is a 5-month treatment regimen leading to a 63% pCR rate, our work suggests that with only six weeks of anti-PD1 plus low-dose anti-CTLA4 a 33% pCR rate may be obtained in TNBCs with high TILs. This suggests that for some patients a short-term immunotherapy-first approach may be an option if confirmed by future research in larger cohorts with more robust follow-up. However, a substantial group of patients still needs chemotherapy and/or longer treatment in order to obtain a pCR. Although we did not observe any unexpected toxicity, the rate of persisting endocrinopathies, in particular hypothyroidism, was high compared to reports in other tumor types or in breast cancer when anti-PD(L)1 is added to neoadjuvant chemotherapy. Although the 33% pCR rate would allow expansion of cohort C to stage II, with 40% grade 3-4 toxicity, 40% hypothyroidism and 20% adrenal gland insufficiencies, substantial toxicity is a serious concern, especially in light of the relatively good prognosis of TNBC patients with high TILs.

To our knowledge, the BELLINI trial is the first to investigate the

feasibility and potential efficacy of ICI without concurrent chemotherapy in early stage TNBC. Moreover, for the first time, the scoring of TILs is used as an inclusion criterion to select patients with a good prognosis for whom development of de-escalated treatment regimens is most promising. Larger clinical trials also using TILs according to this workflow when including patients have recently started (NCT05929768). In addition, ETNA trial (NCT06078384) will explore whether stage I TNBC patients with high TILs can forgo (neo)adjuvant chemotherapy or be treated with immunotherapy alone. The larger international OPTImaL patient preference study (NCT06476119) will also allow the option of no chemotherapy for this patient population. In addition, other studies use TILs as inclusion criteria for immunotherapy-first approaches: Pop-Durva (NCT05215106) and pan-cancer NEOASIS trial (NCT06279130). Further studies that are sufficiently powered to assess long-term outcomes are needed on the use of TILs or other immune-based biomarkers as entry criteria for immunotherapy or de-escalation studies, especially since patients with lower stage TNBC and high TILs can have an excellent outcome with local treatment alone [19, 43].

Immune-related endocrine disorders were the most common adverse events observed. Specifically, 41% of the patients developed hypothyroidism, which, though usually easy to manage, is a permanent condition, and 13% developed adrenal insufficiency, a serious long-term toxicity. Comparable neoadjuvant ICI-only studies with nivolumab + low-dose ipilimumab in head and neck squamous carcinoma, colorectal cancer, urothelial carcinoma and melanoma reported hypothyroidism in 4-8% of patients [9–11, 14] and adrenal insufficiency in 0-8% of patients [9–11, 14]. However, the recent largest phase III trial (stage III melanoma, n=423) reports substantial higher rates of endocrinopathies with 23.6% hypothyroidism and 9.9% adrenal gland insufficiency [26]. Importantly, for cancer types with poor prognosis such as stage III melanoma, high toxicity rates might be acceptable, while this is different for patient populations with more favorable outcomes. The higher rates of hypothyroidism and adrenal insufficiencies in BELLINI compared to these studies could stem from different patient demographics. Patients with TNBC are typically female and relatively young, potentially contributing to different systemic immunity and adverse event incidence [44]. In BELLINI, we reported all immune-mediated adverse events during the first year of follow-up, with 4/6 patients developing adrenal insufficiency >100 days since inclusion. Trials with shorter reporting periods may miss these late events, leading to underreported delayed toxicity, especially in centers not specialized in evaluating ICI regimens. When focusing on patients with similar demographics and disease, we still observe a higher rate of endocrine adverse events in BELLINI compared to neoadjuvant trials for TNBC evaluating ICI plus chemotherapy. The KEYNOTE-522 trial reported

thyroid dysfunction in 22% of patients treated with anti-PD1 plus chemotherapy [1]. Adrenal insufficiency/hypophysitis was reported for 4.5% of patients in the KEYNOTE-522 study. A recent study with an oncolytic virus without chemotherapy found that 3/6 breast cancer patients developed hypothyroidism [45], which is more in line with our observations. The lower hypothyroidism rate in the KEYNOTE-522 compared to the oncolytic virus study [45] and BELLINI could suggest that chemotherapy results in partial blunting of the immune response. Lastly, the preselection of patients with higher TILs in BELLINI may have resulted in patients that are more likely to develop immune-related adverse events due to a different systemic immunity. We also cannot rule out the influence of chemotherapy given after ICI, where steroids are used as antiemetics. Our cohort sizes are too small to compare toxicities induced by 4-week nivolumab versus 4-week nivo-ipi versus 6-week nivo-ipi. However, in the latter group, we observed more non-endocrinopathies such as colitis, hepatitis, and pneumonitis, while endocrinopathies were already remarkably high with nivolumab monotherapy. This potentially signifies that neoadjuvant ICI without chemotherapy could result in a higher rate of hypothyroidism in breast cancer patients. Of note, it was demonstrated that immunotherapy-related thyroid dysfunction and other immune-related adverse events are associated with improved survival in multiple cancer types [46–49]. Nevertheless, upfront prediction of risk of immunotherapy-related toxicity for individual patients is a large unmet clinical need and the burden of adverse events should be evaluated in light of the prognosis of each patient [50].

The advantage of WOO studies like BELLINI is the opportunity to evaluate promising drugs and drug combinations in an efficient manner and to analyze pre- and post-treatment tumor material that can provide insights into the therapy effects. Our primary endpoint, immune activation defined as doubling of CD8+ T cells and/or IFNG expression, was reached in 17/30 patients (57%). Although both cohorts reached the >30% immune activation rate, allowing cohort expansion, we observed more doubling of CD8+ T cells in patients with low pretreatment levels of these features. This could be due to the biopsy timing with deep responses at 4 weeks in tumors with high endogenous CD8+ T cells and/or a "saturation" of CD8+ T cells in patients with high pretreatment values. In contrast to CD8+ T cells, IFNG counts may double even with high pretreatment values, however, they could also be impacted by decreased antigen availability in case of tumor regression. This suggests that different biomarker approaches could apply to inflamed and non-inflamed tumors. Recent insights from the developments of personalized neoadjuvant immunotherapy in melanoma indicate that patients with high pre-existing IFNG levels or a significant increase in IFNG signature upon treatment were most likely to benefit [51]. The

disadvantage of WOO designs with short scheduled treatments is the non-guaranteed benefit for participating patients. Also, information on established endpoints such as pCR rate is needed before a novel treatment approach will be tested in larger trials. For this reason, the adaptive BELLINI trial allowed opening of new cohorts with established endpoints to bring therapies to the next step. Although allowed by the protocol and statistical analysis plan, reporting only stage I data of a Simon's 2-stage design comes with the risk of false-positive findings. Similarly to the cohorts A and B, cohort C also reached the threshold of sufficient responders to expand into stage II. However, given the relatively high rate of endocrinopathies, which are chronic, cohort C was not expanded to stage II. In this view, testing novel anti-CTLA4-targeting antibodies, such as botensilimab [52], intentionally designed to overcome the limitations of conventional ICI such as persisting endocrinopathies could be interesting for breast cancer patients.

When analyzing pretreatment tumor characteristics in high-TIL tumors only (cohort C), we found that the inflammatory phenotype and markers were still discriminative between responders and non-responders and remarkably similar to the clinical responders and non-responders in cohorts A+B. In cohort C, pathological complete responders had higher inflammatory gene expression profiles pretreatment, including signatures for IFNG response, checkpoint molecules, exhausted CD8+ T cells and immunogenic cell death. This suggests that, even in patients with high TILs, the profiling of baseline inflammatory status may facilitate early identification of (non)responders and should be considered in addition to TILs.

The recent publication of the tumor-specific T cell signatures [40, 41] enabled us to identify and follow tumor-specific CD8+ T cells in a clinical trial setting. Importantly, using these signatures as a proxy for the tumor reactivity, we demonstrate for the first time that the presence of tumor-specific CD8+ T cells pretreatment is linked to ICI response.

Additionally, we observed decreased fractions of Tregs in clinical responders compared to non-responders after treatment, in line with prior reports on the role of Tregs in resistance to ICI [53]. In a resistant mouse tumor model, anti-PDL1 therapy led to Treg activation, and Tregs were shown to be activated in the single-cell data of NSCLC and basal cell carcinoma patients not responding to anti-PD(L)1 ICI [42]. In this recent study, ICI treatment induced higher expression of genes involved in Treg-mediated immune suppression (PDCD1, CTLA4, CD38) and cell cycle (MKI67) in Tregs from the tumors of non-responders [42]. Together, these findings demonstrate that Treg cells might play a critical role in resistance to ICI.

To date, data on combining anti-PD(L)1 with low-dose anti-CTLA4 was

lacking in early stage breast cancer. Due to the non-comparative design and the small sample size, our data on the potential additive effect of ipilimumab should be considered exploratory. At the single-cell level, the addition of ipilimumab resulted in lower fold change in Tregs in the TME upon treatment. We also observed a correlation between higher levels of activated Tregs post-treatment and the lack of response or in some cases even slight increase in tumor volume on MRI. This suggests that activated Tregs play a role in resistance to immune checkpoint blockade and that depleting activated Tregs could be a promising strategy for TNBC patients unresponsive to anti-PD1-based treatments. Of note, we cannot exclude that the lack of response or the increase of tumor volume observed by imaging was in part due to pseudoprogression. A growing body of literature analyzing anti-CTLA4 using in-vivo models indicates that anti-CTLA4 can deplete Tregs [54]. However, whether anti-CTLA4 can deplete Tregs in human tumors remains a matter of debate [55]. A recent study by van der Leun et al. in head and neck squamous cell carcinoma also demonstrated an increase in transitional CD8+ T cells and a decrease in CD137+ Tregs in responders after treatment with anti-PD1 and anti-CTLA4 therapy [56], indicating that this might be a consistent pattern across multiple tumor types.

After the results of the landmark trials in early stage TNBC that added PD1 blockade to standard neoadjuvant chemotherapy [1, 3, 57, 58], our current data provide a rationale to further explore the following observations. First, we observed complete and near-complete pathological responses after only six weeks of treatment with ICI in patients with high TILs. This suggests that a subgroup of TNBC could be treated with chemo-free regimens if further research powered for long-term outcome analysis will confirm our results. More research is needed on the optimal selection strategy and treatment regimen, especially in view of the observed high endocrinopathy rate. It is tempting to speculate whether extending the six week treatment period could result in higher pCR rates and thereby reach responses similar to outcomes obtained with chemo+IO. This can only be done if accompanied toxicity would not increase. However, it remains unknown whether pCR after immunotherapy has the same prognostic value as pCR after chemotherapy. Therefore, larger trials are needed to validate the pCR rate after short-term ICI alone and to determine if this results in excellent survival rates, as seen in other cancers [59, 60]. Moreover, pCR might not be the optimal endpoint since KEYNOTE-522 and GeparNUEVO have indicated that the benefit of PD1-blockade is not exclusively seen in patients with pCR [57, 61]. Second, our exploratory clinical and translational data suggest that combination ICI is feasible and could potentially enhance the effects of PD1 blockade. However, the benefit-risk ratio of such combinations should always be carefully monitored. Third, establishing the feasibility of patient

inclusion based on TIL opens the door for more immune biomarker-driven trials, which is particularly important in diseases like TNBC that include both inflamed and non-inflamed subtypes. The potential integration of additional inflammation analyses, for example, using IFNG gene expression on top of TILs as suggested by our data, may optimize patient selection, increase pCR rates for ICI-only approaches and could help treatment personalization in the future. Lastly, a substantial fraction of patients achieved ctDNA clearance after short-term ICI. Given the strong prognostic value of early ctDNA decrease, as shown by the I-SPY trial [62], future studies are needed to investigate the feasibility and reliability of TILs-informed patient inclusion and the potential of ctDNA-informed therapy adjustments.

5.4. Methods

Patients

Patients in cohorts A and B were eligible for enrollment if they were at least 18 years of age and had stage I-III (clinical tumor stage T1c-3, nodal stage N0-3, according to the primary tumor regional lymph node staging criteria of the American Joint Committee on Cancer, 7th edition) triple negative breast cancer with confirmation of estrogen receptor and HER2 negativity (ER<10% and HER2 0, 1 or 2 in the absence of amplification as determined by in situ hybridization) on a biopsy from the primary tumor in the breast; newly diagnosed, previously untreated disease; a WHO performance status score [63] of 0 or 1 and adequate organ functions. The TILs percentage needed to be 5% or more. To ensure balanced enrollment based on TIL levels, each cohort included 5 patients with low (5-10%), 5 patients with intermediate (11-49%), and 5 patients with high ($\geq 50\%$) TIL levels. Patients with concurrent ipsilateral, bilateral, or multifocal primary tumors were also eligible for enrollment. For cohort C, patients had to meet the same criteria, but the nodal stage had to be N0, tumor stage T1c-T2, and TILs had to be 50% or more. The intention for cohort C was to explore the potential feasibility of chemotherapy de-escalation in patients with high TILs. Since withholding adjuvant capecitabine for high-risk patients and/or escalating locoregional treatment for patients with more extensive disease was undesired, cohort C included only LN-negative patients.

Exclusion criteria included history of immunodeficiency, autoimmune disease or conditions requiring immunosuppression (>10 mg daily prednisone or equivalent); other immunosuppressive medications intake within 28 days of study drug administration; chronic or recurring infections; occult breast cancer; fertility preservation due to breast cancer diagnosis; active hepatitis B virus or hepatitis C virus infection;

clinically significant cardiovascular disease; previous systemic anti-cancer treatment.

Trial design and treatments

The BELLINI trial (full title: Pre-operative Trial for Breast Cancer With Nivolumab in Combination With Novel IO; NCT03815890) is a single center, non-blinded, non-randomized, non-comparative phase II study designed to evaluate the feasibility and efficacy of checkpoint inhibition before regular neoadjuvant therapy or surgery in patients with primary breast cancer. Cohorts for prespecified breast cancer subgroups are opened in a sequential manner. Here we report the first three TNBC cohorts for patients who were treated with nivolumab (cohort A) or nivolumab + ipilimumab for four (cohort B) or six (cohort C) weeks. A: Nivolumab monotherapy, 240mg on D1 and D15. B: Nivolumab+ipilimumab 1 mg/kg on D1 and nivolumab 240mg on D15. C: Nivolumab+ ipilimumab 1 mg/kg on D1 and D21. Regular therapy, consisting of neoadjuvant chemotherapy or primary surgery, started on D29 and onwards. Given the poor prognosis of patients with low TIL levels and the hypothesis that these women will probably not be the super-responders to ICI, patients were only eligible with TILs \geq 5%. A threshold of 5% TILs was selected to exclude true immune-deserted tumors. Equal distribution of patients with different levels of tumor of infiltrating lymphocytes over the cohorts was ensured by inclusion of 5 patients with TILs-low (5-10%), 5 patients with TILs-intermediate (11-49%), and 5 patients with TILs-high (\geq 50%) scores per cohort.

After cohorts A (in the protocol defined as cohort 1B) and B (in the protocol defined as cohort 2B) the protocol was amended to open cohort C (in the protocol defined as cohort 3B). Cohort C had the same inclusion criteria as cohort A and B, except that only inclusion of patients with clinically node-negative disease and with TIL levels of 50% or higher was allowed. With the amendment to open cohort C, the window of opportunity design was changed into a true neoadjuvant design with all patients going to surgery after the immunotherapy. After completing the interim analysis of cohorts A and B an amendment was approved to use pathological complete response (pCR) as primary endpoint instead of immune activation for cohort C and subsequent cohorts (see details on **Endpoints** below).

Ethics statement

All patients provided written informed consent before enrollment. This investigator-initiated trial was designed by the Netherlands Cancer Institute (NKI).

The trial was conducted in accordance with the protocol, Good Clinical Practice standards and the Declaration of Helsinki. The full protocol,

amendments, and the informed consent form were approved by the medical ethical committee of the Netherlands Cancer Institute (NKI, Amsterdam).

Endpoints

Cohorts A and B:

The primary endpoint for cohorts A and B is immune activation following two cycles of neoadjuvant ICI, defined as a 2-fold increase in CD8+ T cells assessed via immunohistochemistry and/or an increase in IFNG gene expression. High-quality paired biopsies are necessary for the evaluability of this primary endpoint.

As a secondary endpoint for cohorts A and B, we evaluated the clinical response.

Clinical response was defined as:

Radiological signs of response: At least a 30% decrease on MRI (partial response (PR) according to RECIST 1.1, not confirmed). The target (or index) lesion is defined as the largest enhancing lesion. In case of multifocality or multicentricity the largest mass and/or non-mass enhancement was measured in the axial/sagittal or coronal plane and defined as target/index lesion. In these cases the total area occupied by the tumor (including all masses and non-mass enhancement) was also measured. The total tumor area was used for the RECIST measurements.

AND/OR

Pathological signs of response: Pathological response could be studied in biopsies from 28 patients due to the window of opportunity design. Absence of viable tumor after four weeks of therapy in the post-treatment biopsy was classified as a clinical response. For patients proceeding to surgery this was defined as partial or complete pathological response, according to the European Society of Mastology (EUSOMA criteria).

Cohort C:

The primary endpoint for cohort C is pathological complete response (pCR), defined as no viable tumor remaining in the breast and lymph nodes (ypT0N0) [64]. Major pathologic response (MPR, secondary endpoint) is a frequently used surrogate endpoint for efficacy in neoadjuvant trials evaluating immune checkpoint blockade across cancer types [8, 11, 26]. MPR was defined as $\leq 10\%$ of residual viable tumor in the surgical specimen [17, 65, 66] or no viable tumor in the breast but residual tumor cells in the lymph nodes.

All Cohorts (A, B, C):

Secondary endpoints included feasibility, safety, and radiological

response. Feasibility was determined based on any treatment-related complications that led to a delay in chemotherapy or primary surgery beyond six weeks from the start of therapy. All patients were closely monitored for adverse events (AEs) for 100 days after the administration of the last study treatment, following the Common Terminology Criteria for Adverse Events (CTCAE) v.5 [67]. In addition, we reported all immune-related adverse events in the first year of follow-up. Radiological response was assessed according to the RECIST 1.1 guidelines, but not confirmed.

Statistical analysis

For this exploratory, hypothesis-generating study, no formal sample size calculation was performed for efficacy because there was no data on the efficacy of neoadjuvant immunotherapy in breast cancer at the time of the design of this study. For cohorts A and B, the null hypothesis of a true immune activation in $\leq 30\%$ of patients was tested against a one-sided alternative. For cohort C, design was identical with the exception of null hypothesis being pCR in $\leq 30\%$ of patients tested against a one-sided alternative. For 80% power, at a one-sided significance level of 0.05, 15 patients were accrued per cohort to be evaluated in the first stage. If there were 5 or less responses among these 15 patients, the cohort was closed for futility. Otherwise, the cohort could be expanded with 31 additional patients, reaching a total of 46. We decided to publish after stage I, which was allowed by protocol, due to the observation that very early responses to ICI without chemotherapy are possible in TNBC, which warrants efforts to de-escalate therapy for a subset of patients, in contrast to the current therapy escalation for all TNBC patients. Median follow-up time was obtained using the reverse Kaplan-Meier method. Analyses were performed using R [68] v.4.2.1.

Pathology assessments and IHC analyses

All patients underwent baseline tumor staging, consisting of ultrasound of the breast, axilla and periclavicular region and MRI imaging of the breast. PET-CT imaging was performed in all participants to confirm the clinical stage. Pretreatment tumor histological biopsies (4 core biopsies, 14G needle) were taken for all patients, and post-treatment tissue was either obtained through a biopsy (3 core biopsies, 14G needle) for patients continuing neoadjuvant chemotherapy (n=28) and the surgical specimen was used for those undergoing surgery right after the ICI study treatment (n=3). Histopathological examination of biopsies and resection specimens was carried out by five experienced breast cancer pathologists (HMH, RS, KvdV, JvdB, NK). Resected tumors were examined in their entirety and regression of resected tumors was assessed by estimating the percentage of residual viable tumor of the macroscopically identifiable tumor bed, as identified

on routine hematoxylin and eosin (H&E) staining. Formalin-fixed paraffin-embedded tissue sections were used for H&E stainings and for immunohistochemical analysis of CD8 (C8/144B, DAKO), PDL1 (22C3, DAKO) and PD1 (NAT105, Roche Diagnostics). The percentage of tumor cells and TILs was assessed by pathologists trained for TILs assessment on H&E-stained slides according to the international standard from the International Immuno-Oncology Biomarker Working Group [22] (see www.tilsinbreastcancer.org for all guidelines on TILs assessment in solid tumors). After a pathologist provided an initial TILs score, an "expert TILs score" was generated as a consensus score from at least 2 out of 4 trained pathologists using slidescore.com for online scoring [69]. TILs scores for inclusion were scored on the diagnostic biopsy of the patient to allow for stratification of patients (low $\geq 5\%$ -10%, intermediate 11-49%, high $\geq 50\%$).

Immunohistochemistry

Immunohistochemistry of the FFPE tumor samples was performed on a BenchMark Ultra autostainer (Ventana Medical Systems). The double stain was performed on a Discovery Ultra autostainer. Briefly, paraffin sections were cut at 3 μm , heated at 75°C for 28 minutes and deparaffinized in the instrument with EZ prep solution (Ventana Medical Systems). Heat-induced antigen retrieval was carried out using Cell Conditioning 1 (CC1, Ventana Medical Systems) for 48 minutes at 95°C (PDL1) or 64 minutes at 95°C. (PD1/CD8 double). PDL1 was detected using clone 22C3 (1/40 dilution, 1 hour at RT, Agilent/DAKO, Lot11654144). Bound antibody was detected using the OptiView DAB Detection Kit (Ventana Medical Systems). Slides were counterstained with Hematoxylin and Bluing Reagent (Ventana Medical Systems).

For the double staining PD1 (Yellow) followed by CD8 (Purple), the PD1 was detected in the first sequence using clone NAT5 (Ready-to-Use, 32 minutes at 37°C, Roche Diagnostics, Lot11654144). The PD1-bound antibody was visualized using Anti-Mouse NP (Ventana Medical systems, Ready to Use dispenser, LotK09956) for 12 minutes at 37°C followed by Anti-NP AP (Ventana Medical systems, Ready to Use dispenser, LotJ23971) for 12 minutes at 37°C, followed by the Discovery Yellow detection kit (Ventana Medical Systems). In the second sequence of the double staining procedure, CD8 was detected using clone C8/144B (1/200 dilution, 32 minutes at 37°C, Agilent, Lot41527763). CD8 was visualized using Anti-Mouse HQ (Ventana Medical systems, Ready to Use dispenser, LotK20711) for 12 minutes at 37°C followed by Anti-HQ HRP (Ventana Medical systems, Ready to Use dispenser, LotK22062) for 12 minutes at 37°C, followed by the Discovery Purple Detection Kit (Ventana Medical Systems). Slides were counterstained with Hematoxylin and Bluing Reagent (Ventana Medical Systems). A PANNORAMIC 1000 scanner from 3DHISTECH was used to scan the

slides at a 40x magnification.

Distance analysis between tumor and CD8+ T cells

Spatial analysis was performed on the pretreatment biopsies of all included patients. The stained slides were scanned, and image analysis was performed with the HALO image analysis software from Indica Labs, v3.4.2986.185 (cohorts A and B) and v.3.6.4134 (cohort C). Within HALO, the multiplex IHC module was used to phenotype and quantify CD8-positive cells. Cell segmentation was performed by the detection of hematoxylin (detection weight = 1) and PD1 (detection weights 0.045 for cohorts A&B; 0.5 for cohort C) and CD8 for cohort C (detection weight = 0.5) staining, utilizing a nuclear segmentation aggressiveness of 0.045. Minimal intensity thresholds to consider a cell positive for a marker were set for hematoxylin (0), PD1 (0.25 for cohorts A&B, 0.1 for cohort C), and CD8 (0.1) separately. Biopsies were analyzed in total, while for resection specimens the analysis was restricted to representative tumor beds as annotated by a breast cancer pathologist. The quantified levels of CD8+ and PD1+CD8+ cells were corrected for the analyzed tissue area (cells/ μm^2).

Artificial intelligence tumor classifiers (Object Phenotyper, HALO AI) were developed to discriminate between tumor and non-tumor cells in cohorts A&B and in cohort C. Individual cells were segmented (nuclei seg BF v.1.0.0), and the classifiers were trained by annotating single cells as tumor or non-tumor. The annotations were guided by marked tumor regions on H&E-stained slides by a trained BC pathologist. The classifiers were finalized with 20.000 iterations and a cross-entropy of 0.009 (cohort A&B) and >10.000 iterations and cross-entropy of 0.021 (cohort C).

Merging the results of the multiplex IHC and tumor classifier enabled the visualization of the spatial distribution of tumor and CD8+ cells (**Supplementary Figures 5.5B-F**). Using the nearest neighborhood analysis, the average distance between the tumor and immune cells was quantified by taking the mean of the distances between every tumor cell and its nearest cell of the above-mentioned immune phenotypes in the pretreatment biopsies (**Supplementary Figure 5.5F**). Distances from tumor cells to the nearest CD8+ T cells were taken as a measure of proximity of CD8+ T cells to the tumor.

DNA and RNA isolation

DNA and RNA were extracted from fresh-frozen, pre- and post-treatment tumor material using the AllPrep DNA/RNA Kit (QIAGEN) for frozen material, following the manufacturer's protocol, in a QIAcube (QIAGEN). Germline DNA was isolated from patient peripheral blood mononuclear cells using the DNeasy Blood&Tissue Kit (QIAGEN).

Bulk RNA sequencing

Total RNA Quality Control

Quality and quantity of the total RNA was assessed by the 2100 Bioanalyzer using a Nano chip (Agilent, Santa Clara, CA). Total RNA samples having RIN>8 were subjected to library generation.

TruSeq Stranded mRNA library generation

Strand-specific libraries were generated using the TruSeq Stranded mRNA sample preparation kit (Illumina Inc., San Diego, RS-122-2101/2) according to the manufacturer's instructions (Illumina, Document # 1000000040498 v00). Briefly, polyadenylated RNA from intact total RNA was purified using oligo-dT beads. Following purification, the RNA was fragmented, random primed and reverse transcribed using SuperScript II Reverse Transcriptase (Invitrogen, part #18064-014) with the addition of Actinomycin D. Second strand synthesis was performed using Polymerase I and RNaseH with replacement of dTTP for dUTP. The generated cDNA fragments were 3' end adenylated and ligated to IDT xGen UDI(10bp)-UMI(9bp) paired-end sequencing adapters (Integrated DNA Technologies, Inc., Coralville) and subsequently amplified by 12 cycles of PCR. The libraries were analyzed on a 2100 Bioanalyzer using a 7500 chip (Agilent, Santa Clara, CA), diluted and pooled equimolar into a multiplex sequencing pool.

Sequencing

The libraries were sequenced with 54 paired-end reads on a NovaSeq6000 using a S1 Reagent Kit v1.5 (100cycles) (Illumina Inc., San Diego).

Data analysis

RNA sequencing data were aligned to GRCh38 with STAR [70] 2.7.1a, with the twopassMode='Basic'. FPKM were obtained with RSeQC [71] 4.0.0 FPKM_count.py and subsequently normalized to transcripts per million. Data quality was assessed with FastQC [72] 0.11.5, FastQ Screen [73] 0.14.0, the Picard CollectRnaSeqMetrics [74, 75] and RSeQC [71] 4.0.0 read_distribution.py and read_duplication.py and were found to be suitable for the downstream analysis. TNBCtype [76] was used for the Lehmann subtype classification [77]. The Gseapy [78] 1.0.3 ssgsea tool with the sample_norm_method='rank' was used for gene set signature scoring. For the signature analysis, p-values were significant after FDR correction (Benjamini-Hochberg) at 10% significance level. Data were analyzed with Python [79] 3.10.5. Pandas [80, 81] 2.0.0 and numpy [82] 1.22.4 were used for data handling. Matplotlib [74] 3.5.2, seaborn [83] 0.12.2 and statannotations [84] 0.5.0 were used for plotting.

Whole exome sequencing

For each sample the amount of double stranded DNA was quantified by using the Qubit dsDNA HS Assay Kit (Invitrogen, cat no Q32851). A maximum amount of 2 μ g of double stranded genomic DNA was fragmented by covaris AFA technology to obtain fragment sizes of 200-300 bp. Samples were purified using Agencourt AMPure XP Reagent (Beckman Coulter, cat no A63881) in a 2x reaction volume settings according to manufacturer's instructions. The fragmented DNA was quantified and qualified on a BioAnalyzer system using the DNA7500 assay kit (Agilent Technologies cat no. 5067-1506). With a maximum input amount of 1 μ g fragmented DNA, NGS library preparation for Illumina sequencing was performed using the KAPA HTP Prep Kit (KAPA Biosystems, KK8234) in combination with xGen UDI-UMI Adapters of IDT (Integrated DNA Technologies). During the library amplification step, 4 cycles of PCR were performed to obtain enough yield for the exome enrichment assay. All DNA libraries were quantified on a BioAnalyzer system using the DNA7500 assay kit. Exome enrichment was performed on library pools of 6 unique dual indexed libraries, 500 ng each, using the xGen Exome Hyb Panel v2 (IDT, cat no 10005152) and xGen Hybridization Capture Core Reagents according to manufacturer's protocol, with hybridization time adjusted to 16 hours and 10 cycles of PCR performed during post-capture PCR. All exome enriched library pools were quantified on a BioAnalyzer system using the DNA7500 assay kit, pooled equimolar to a final concentration of 10nM and subjected to paired-end 100 bp sequencing on an Illumina Novaseq 6000 instrument using a NovaSeq 6000 S4 Reagent Kit v1.5 (Illumina, 20028313), according to manufacturer's instructions.

Data analysis

Sequencing reads were aligned to the human reference GRCh38 (Ensemble, v. 105) using BWA [85] 0.7.17. Duplicated reads were marked using Picard [75] MarkDuplicates 2.25.0, after which quality scores were recalibrated using GATK4 [86] BaseRecalibrator 4.2.2.0. Single-nucleotide variants (SNVs) and short insertions and deletions (indels) were called using GATK4 [86] Mutect2 4.2.2.0 on the tumor samples matched with germline samples. Subsequently, variants were filtered by the PASS filter, and annotated using Ensembl Variant Effect Predictor. maftools [87] 2.10.5 package was used for the analysis. Tumor mutational burden (TMB) was calculated by summarizing the total number of non-synonymous somatic mutations with a minimal variant allele frequency of 20%. Data were analyzed with Python [79] 3.10.5 and R [88] 4.1.3. Pandas [80, 81] 2.0.0 was used for data handling. maftools [87] 2.10.5, Matplotlib [74] 3.5.2, seaborn [83] 0.12.2, and statannotations [84] 0.5.0 were used for plotting.

Single cell RNA sequencing and TCR sequencing

Preparation of the single cell suspension

Following biopsy or obtaining resection specimens, samples were rapidly processed for single-cell RNA sequencing (scRNA-seq). Samples from cohort A were minced on ice and frozen in 10% DMSO FCS in the -80°C degrees. Within 4 weeks after freezing, samples were defrosted in 37°C degrees medium. Samples from cohort B were minced on ice and immediately processed for single cell sequencing (not frozen), which did not result in a batch effect.

Samples were transferred to a tube containing 1mL digestion medium containing collagenase P (2 mg/ml, ThermoFisher Scientific) and DNase 1 (10 U/ μ L, Sigma) in RPMI (ThermoFisher Scientific). Samples were incubated for 20 min at 37°C degrees and were pipetted up and down every 5 minutes for 30 seconds. Next, samples were filtered on a 40 micron nylon mesh (ThermoFisher Scientific) and directly after the same volume of ice cold PBS containing 0.04% BSA was added. Following centrifugation at 300 g and 4°C degrees for 5 min, the supernatant was removed and discarded, and the cell pellet was resuspended in red cell blood lysis buffer for 5 minutes at room temperature and then centrifuged again at 300 g at 4°C degrees for 5 min. The supernatant was removed and discarded and the pellet was resuspended in PBS containing 0.04% BSA. Next, 10 μ L of this cell suspension was counted using an automated cell counter (ChemoMetec NucleoCounter NC-200) to determine the concentration of live cells. The entire procedure was usually completed within 1h and 15 minutes.

Single cell RNA-seq data acquisition and preprocessing

Libraries for scRNA-seq were generated using the Chromium Single Cell 5' library and Gel Bead & Multiplex Kit from 10x Genomics. We aimed to profile 10 000 cells per library if a sufficient number of cells was retained during dissociation. All libraries were sequenced on a HiSeq4000 or NovaSeq6000 until sufficient saturation was reached.

Data analysis

After quality control, raw sequencing reads were aligned to the human reference genome GRCh38 and processed to a matrix representing the UMI's per cell barcode per gene using CellRanger (10x Genomics, v2.0). The data were analyzed with scanpy [89] 1.9.3 and Seurat [90] v3. Cellbender [91] 0.3.0 was used for eliminating technical artifacts, and cells above the quality cutoff of 0.5 were filtered out. Cells with mitochondrial RNA content >0.25, the number of genes <200 or >6000 and <400 counts were filtered out. After normalization, regression for the number of UMIs, percentage mt-RNA, sample ID, cell cycle, hypoxia, interferon content and cell stress was performed on the 2000 most

variable genes followed by a principal component analysis. Next a UMAP was generated and clustering was performed at resolution 0.2 using the 30 most informative components. Major cell types were identified based on canonical marker genes.

For the T cell subclustering, the T cells were selected from the full Seurat object and the analysis described above was repeated with 10 principal components based on the elbow plot and clusters were identified at a resolution of 0.6 and were annotated based on breast cancer tissue-specific marker genes [92]. Cells expressing markers of other cell types (immunoglobulins, hemoglobin) were filtered out. PCA was calculated on highly variable genes with $k=30$. Clustering was performed with Phenograph [93] with $k=30$. Cluster identification was performed based on canonical marker genes. Signature scores were calculated with `sc.tl.score_genes`. Groups were compared with `sc.tl.rank_genes_groups`, with `method='wilcoxon'` and `use_raw=True`. EnrichR [94, 95] was used for the pathway enrichment analysis. Activated Tregs were defined based on the level of CD137 gene expression >0.5 in the Treg cell population. PD1+Ki67+CD4+ cells were defined based on the level of MKI67 gene expression >0 in the Tfh cell population. Scirpy [96] 0.11.2 was used for the TCR analysis. Clonotypes were defined based on the amino acid structure. Clonality was calculated as $(1 - \text{normalized Shannon entropy})$. Data were analyzed with Python [79] 3.10.5. Pandas [80, 81] 2.0.0 and numpy [82] 1.22.4 were used for data handling. Matplotlib [74] 3.5.2, seaborn [83] 0.12.2, sc-toolbox [97] 0.12.3 and statannotations [84] 0.5.0 were used for plotting.

ctDNA analysis

A proprietary bioinformatics tissue variant calling pipeline was used to select a set of 16 high-ranked, patient-specific, somatic, clonal single nucleotide variants (SNVs) from WES. The Signatera amplicon design pipeline was used to generate mPCR primer pairs for the given set of 16 variants. For cfDNA library preparation, up to 20 000 genome equivalents of cfDNA from each plasma sample were used. The cfDNA was end-repaired, A-tailed, and ligated with custom adapters, followed by amplification (20 cycles) and purified using Ampure XP beads (Agencourt/Beckman Coulter). A proprietary multiplex PCR (mPCR) methodology was used to run patient-specific assays. Sequencing was performed on these mPCR products on an Illumina HiSeq 2500 Rapid Run (50 cycles) using the Illumina Paired End v2 kit with an average read depth of $>100000\times$ per amplicon. All paired-end reads were merged using Pear 0.9.8 software and mapped to the hg19 reference genome with Novoalign version 2.3.4 (<http://www.novocraft.com/>). Plasma samples with at least 2 variants with a confidence score above a predefined algorithm threshold were defined as ctDNA-positive.

Flow cytometry of fresh blood

The flow cytometry was performed as previously described [98]. In short, fresh blood samples were processed and analyzed within 24 hours after blood draw. Peripheral blood was collected in EDTA vacutainers (BD) and subjected to red blood cell lysis (lysis buffer: dH₂O, NH₄Cl, NaHCO₃, EDTA). Cells were suspended in PBS containing 0.5% BSA and 2mM EDTA and counted using the NucleoCounter NC-200 (Chemometec) automated cell counter. To obtain absolute white blood cell (WBC) counts per mL of human blood, the total amount of post-lysis cells was divided by the volume (mL) of blood obtained from the patient. For surface antigen staining, cells were first incubated with human FcR Blocking Reagent (1:100 Miltenyi) for 15 min at 4°C and then incubated with fluorochrome-conjugated antibodies for 30 min at 4°C. For intracellular antigen staining, cells were fixed with Fixation/Permeabilization solution 1X (Foxp3/Transcription Factor Staining Buffer Set, eBioscience) for 30 min at 4°C and stained with fluorochrome-conjugated antibodies in Permeabilization buffer 1X (eBioscience) for 30 min at room temperature. Viability was assessed by staining with either 7AAD staining solution (1:10; eBioscience) or Zombie Red Fixable Viability Kit (1:800, BioLegend). Data acquisition was performed on an LSRII SORP flow cytometer (BD Biosciences) using Diva software and data analysis was performed using FlowJo 10.6.2. Gating strategy is displayed in **Supplementary Figure 5.9A**.

5.5. Data availability

DNA and RNA sequencing data is stored in the European Genome-Phenome Archive ((EGAS50000000567 (RNA-Seq) and EGAS50000000568 (WES))). Sequencing data and source data supporting the findings of this study will be made available from the corresponding author (m.kok@nki.nl) for academic use, within limitations of the provided informed consent. Data will not be made available for commercial use. A first response to the request will be sent in <4 weeks. Data requests will be reviewed by the corresponding author and Institutional Review Board of the NKI, and, after approval, applying researchers will have to sign a data transfer agreement with the NKI.

5.6. Acknowledgements

We are grateful to the participants and their families for participating in the trial. We thank all supporting clinical trial staff, in particular nurse specialists and the Departments of Medical Oncology, Surgery,

Radiology and Pathology of the participating centers. We thank the NKI trial lab for handling incoming blood samples. We are grateful to Annegien Broeks and the Core Facility of Molecular Pathology and Biobanking for the storage and handling of human tumor material and to the Genomics Core Facility for DNA and RNA sequencing. We acknowledge the supporting staff of the clinical trials of the Departments of Medical Oncology and the Triallab. We thank Chris Klaver and Maxime Duijst for blood sample experiments and the Flow Cytometry Facility the AKL for support in these experiments. We thank Bauke Stegenga from Bristol Myers Squibb for trial support and arranging supply of nivolumab and ipilimumab. R.S. is supported by the Breast Cancer Research Foundation (grant number 17-194). Research at the NKI is supported by institutional grants of the Dutch Cancer Society and of the Dutch Ministry of Health, Welfare and Sport. Research in the laboratory of M.K. is funded by the Netherlands Organization for Scientific Research (VIDI 09150172010043) and Victoria's Secret Global Fund for Women's Cancers Rising Innovator Research Grant, in Partnership with Pelotonia & AACR (23-30-73-KOK). Trial costs were supported by Bristol Myers Squibb. The funders had no role in study design, data collection or analysis, decision to publish or preparation of the manuscript.

5.7. Author Contributions

I.N. and O.I.I. contributed equally to this work as shared co-first authors. M.d.G., R.C.A.M.G. and N.A.M.B. contributed equally to this work as shared co-second authors. I.N. wrote the study protocol, coordinated trial procedures, performed wet lab experiments for single-cell RNA-Seq analyses, analyzed and interpreted clinical and translational data of the trial. O.I.I. designed, performed and interpreted computational analyses of the DNA, bulk and single-cell RNA sequencing data, analyzed and interpreted translational data. I.N., O.I.I., and M.K. wrote the paper. N.A.M.B., E.C. and H.G. were responsible for blood sample processing and analysis, supervised by K.E.d.V. and M.K., and H.G. designed the flow cytometry panel. M.d.G. performed the spatial analyses and helped with collection and analysis of clinical data. R.C.A.M.G. and A.L.R. coordinated trial procedures and collected clinical data for cohort C. B.B., J.G.H.T and M.C. performed bioinformatics analyses and contributed to their design. I.A.M.M. was the clinical projects manager. M.d.M. processed FFPE for IHC and isolated DNA and RNA from tissue biopsies. T.v.B. performed wet lab experiments for single-cell RNA-Seq analyses. M.L.-Y. performed the statistical analysis of the trial data. J.G.v.d.B., N.K., H.M.H., K.v.d.V. and R.S. performed the TILs and histological scoring of the pathology slides. I.H. developed and performed double CD8-PD1 staining. R.M.M. and C.E.L. revised MRI scans and, together with colleagues, were involved in

taking biopsies. Ek.K. organized the ctDNA experiments. Em.K., F.H.v.D., V.S., S.L., C.A.D., M.G.J.v.D., G.S.S., S.C.L. and M.K. were the main treating physicians. I.N., I.A.M.M., G.S.S., T.N.S., C.U.B., S.C.L. and M.K. wrote the trial protocol. H.M.H supervised the computational pathology analyses. L.F.A.W. and D.L. supervised computational analyses. M.K. was the principal investigator of the trial, supervised all the analyses presented in the paper and acquired funding. All authors edited and approved the paper.

5.8. Competing interests

I.N., O.I.I., M.d.G, R.C.A.M.G., N.A.M.B., A.L.R., H.G., B.B., J.G.H.T., I.A.M.M., M.d.M, T.v.B., M.C., E.C., M.L.-Y., K.v.d.V., J.G.v.d.B., I.H., N.K., C.E.L., F.H.v.D., V.S., S.L., Em.K., C.A.D., M.G.J.v.D., H.M.H. and D.L. have no competing interests to declare. R.M.M. reports research grants from Siemens Healhtineers, Bayer Healthcare, Screenpoint Medical, Beckton & Dickinson, PA Imaging, Lunit and Koning, and is an advisory board member for Screenpoint, Bayer, Siemens and Guerbet, all outside the scope of this work. Ek.K. is an employee of Natera, Inc. G.S.S. reports research funding to the institute from Merck, Agendia, AstraZeneca, Roche and Novartis and a consulting role for Novartis, Seattle Genetics and Biovica, outside the submitted work. S.C.L. reports research funding to the institute from Roche/Genentech, AstraZeneca, BMS, Tesaro, Merck, Immunomedics, Eurocept Pharmaceuticals, Agendia and Novartis and a consulting role and travel grant from Daiichi Sankyo, outside this work. C.U.B. has received research grants from Novartis, BMS and NanoString, is a paid advisory board member for BMS, MSD, Roche, Novartis, GlaxoSmithKline, AstraZeneca, Pfizer, Lilly, GenMab and Pierre Fabre and holds ownership interest in Uniti Card, Neon Therapeutics and Forty Seven, all outside this submitted work. K.E.d.V. reports research funding from Roche and is a consultant for Macomics, outside the scope of this work. R.S. reports non-financial support from Merck and Bristol Myers Squibb (BMS), research support from Merck, Puma Biotechnology and Roche and personal fees from Roche, BMS and Exact Sciences for advisory boards, all outside the scope of this paper. L.F.A.W. reports funding to the institute from Genmab BV. T.N.S. is advisor for Allogene Therapeutics, Asher Bio, Merus, Neogene Therapeutics, and Scenic Biotech; is a stockholder in Allogene Therapeutics, Asher Bio, Cell Control, Celsius, Merus, and Scenic Biotech; and is venture partner at Third Rock Ventures, all outside of the current work. M.K. reports research funding to the institute from BMS, Roche and AstraZeneca/MedImmune and an advisory role/speakers' fee (all compensated to the institute) for Alderaan, BMS, Domain Therapeutics, Medscape, Roche, MSD and Daiichi Sankyo, outside the submitted work.

Natera provided non-financial support to this study.

5.9. Supplementary Information

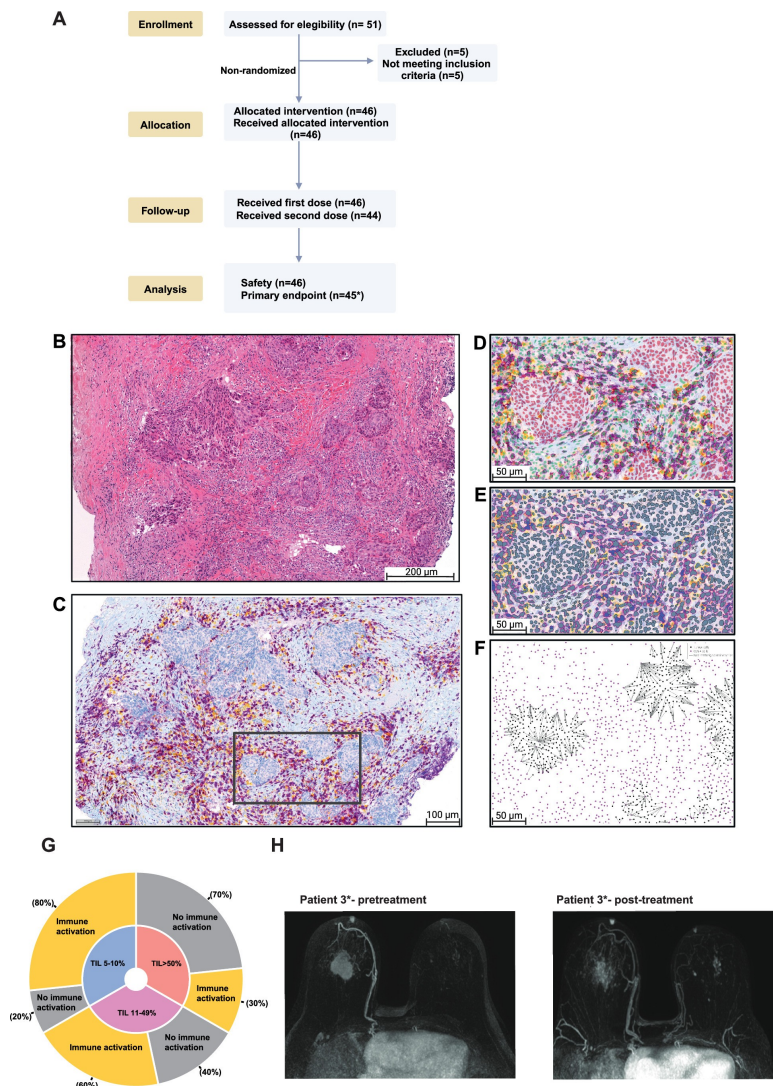


Figure 5.5: IHC CD8+ T cell analysis. (A) H&E-stained image, corresponding to CD8/PD1 stained tissue under (B). (B) Representative example of a CD8/PD1 double-stained tissue (haematoxylin = blue, PD1 = yellow, CD8 = purple). (C) Representative example of the performance of the AI-based tumor cell classifier (Tumor classification (red) and non-tumor cells (green)). (D) Example of cell segmentation and tumor phenotype assignment. Cell with purple border = CD8+ cell, yellow border = PD1+ cell, orange border = PD1+CD8+ cell. (E) Corresponding distance analysis in the same tissue area as under (C) and (D). The grey lines represent the shortest distance from a tumor cell to its nearest CD8+ T cell (F) Proportions of patients reaching immune activation stratified according to TIL levels at inclusion in cohorts A and B. 10 patients had 5-10% TILs, 10 patients 11-49% TILs and 10 patients had 50% or more TILs. (G) Pretreatment and post-treatment MRI images of patient #3 with a pathological complete response (pCR) at surgery after ICI only (cT2N0, ypT0N0).

5.9. Supplementary Information

Table 5.3: Adverse Events

	A: Nivolumab (N=16)			B: Nivo+Ipi 4 wks (N=15)			Nivo+Ipi 6 wks (N=15)		
Adverse event	Grade 1-2	Grade 3	Grade 4	Grade 1-2	Grade 3	Grade 4	Grade 1-2	Grade 3	Grade 4
Worst grade adverse event per patient	12 (75%)	1 (6%)	0 (0%)	13 (86.6%)	1 (7%)	1 (7%)	9 (60%)	5 (33%)	1 (7%)
Endocrine disorders									
Thyroid dysfunction	7 (44%)	1 (6%) ^a	0 (0%)	9 (60%)	0 (0%)	0 (0%)	9 (60%)	0 (0%)	0 (0%)
Hypothyroidism	6 (38%)	0 (0%)	0 (0%)	7 (47%)	0 (0%)	0 (0%)	8 (40%)	0 (0%)	0 (0%)
Hyperthyroidism	4 (25%)	1 (6%)	0 (0%)	8 (53%)	0 (0%)	0 (0%)	9 (60%)	0 (0%)	0 (0%)
Adrenal insufficiency*	1 (6%)	0 (0%)	0 (0%)	1 (7%)	1 (7%) ^b	0 (0%)	2 (13%)	1 (7%) ^f	0 (0%)
Diabetes Mellitus (immune mediated)	0 (0%)	0 (0%)	0 (0%)	0 (0%)	0 (0%)	1 (7%) ^b	0 (0%)	0 (0%)	0 (0%)
Gastro-intestinal									
Abdominal pain	0 (0%)	0 (0%)	0 (0%)	1 (7%)	0 (0%)	0 (0%)	0 (0%)	0 (0%)	0 (0%)
Diarrhea	0 (0%)	0 (0%)	0 (0%)	1 (7%)	0 (0%)	0 (0%)	1 (7%)	0 (0%)	0 (0%)
Nausea	1 (6%)	0 (0%)	0 (0%)	0 (0%)	0 (0%)	0 (0%)	2 (13%)	0 (0%)	0 (0%)
Colitis	0 (0%)	0 (0%)	0 (0%)	0 (0%)	0 (0%)	0 (0%)	0 (0%)	1 (7%) ^g	0 (0%)
Rectal ulcer	0 (0%)	0 (0%)	0 (0%)	1 (7%)	0 (0%)	0 (0%)	0 (0%)	0 (0%)	0 (0%)
Laboratory test									
Elevated liver function tests	0 (0%)	0 (0%)	0 (0%)	1 (7%)	0 (0%)	0 (0%)	7 (47%)	0 (0%)	0 (0%)
Hyperphosphatemia	0 (0%)	0 (0%)	0 (0%)	0 (0%)	0 (0%)	0 (0%)	1 (7%)	0 (0%)	0 (0%)
Hypophosphatemia	0 (0%)	0 (0%)	0 (0%)	0 (0%)	0 (0%)	0 (0%)	1 (7%)	0 (0%)	0 (0%)
Lymphocyte count decreased	0 (0%)	0 (0%)	0 (0%)	0 (0%)	0 (0%)	0 (0%)	1 (7%)	0 (0%)	0 (0%)
Troponine T increased	0 (0%)	0 (0%)	0 (0%)	0 (0%)	0 (0%)	0 (0%)	1 (7%)	0 (0%)	0 (0%)
Immune related hepatitis	0 (0%)	0 (0%)	0 (0%)	2 (13%)	0 (0%)	0 (0%)	0 (0%)	2 (13%) ^{e,d}	1 (7%) ^h
Musculo-skeletal									
Arthralgia	3 (19%)	0 (0%)	0 (0%)	0 (0%)	0 (0%)	0 (0%)	0 (0%)	0 (0%)	0 (0%)
Myalgia	2 (12%)	0 (0%)	0 (0%)	0 (0%)	0 (0%)	0 (0%)	0 (0%)	0 (0%)	0 (0%)
Back pain	1 (6%)	0 (0%)	0 (0%)	0 (0%)	0 (0%)	0 (0%)	0 (0%)	0 (0%)	0 (0%)
Immune mediated polymyalgia rheumatica	0 (0%)	0 (0%)	0 (0%)	0 (0%)	0 (0%)	0 (0%)	1 (7%)	0 (0%)	0 (0%)
Cardiopulmonary									
Chest pain	0 (0%)	0 (0%)	1 (6%) ^a	0 (0%)	0 (0%)	0 (0%)	0 (0%)	0 (0%)	0 (0%)
Ejection fraction decreased #	1 (6%)	0 (0%)	0 (0%)	0 (0%)	0 (0%)	0 (0%)	0 (0%)	0 (0%)	0 (0%)
Pneumonitis	0 (0%)	0 (0%)	0 (0%)	0 (0%)	0 (0%)	0 (0%)	1 (7%)	1 (7%) ^e	0 (0%)
Upper respiratory infection	0 (0%)	0 (0%)	0 (0%)	1 (7%)	0 (0%)	0 (0%)	0 (0%)	0 (0%)	0 (0%)
Cough	0 (0%)	0 (0%)	0 (0%)	1 (7%)	0 (0%)	0 (0%)	0 (0%)	0 (0%)	0 (0%)
Other									
Allergic reaction	1 (6%)	0 (0%)	0 (0%)	0 (0%)	0 (0%)	0 (0%)	0 (0%)	0 (0%)	0 (0%)
Anemia	0 (0%)	0 (0%)	0 (0%)	0 (0%)	0 (0%)	0 (0%)	3 (20%)	0 (0%)	0 (0%)
Dry eye	1 (6%)	0 (0%)	0 (0%)	0 (0%)	0 (0%)	0 (0%)	1 (7%)	0 (0%)	0 (0%)
Dry mouth	2 (12%)	0 (0%)	0 (0%)	0 (0%)	0 (0%)	0 (0%)	4 (27%)	0 (0%)	0 (0%)
Dry skin	1 (6%)	0 (0%)	0 (0%)	2 (13%)	0 (0%)	0 (0%)	1 (7%)	0 (0%)	0 (0%)
Fatigue	1 (6%)	0 (0%)	0 (0%)	1 (7%)	0 (0%)	0 (0%)	1 (7%)	0 (0%)	0 (0%)
Flu-like symptoms	2 (12%)	0 (0%)	0 (0%)	0 (0%)	0 (0%)	0 (0%)	1 (7%)	0 (0%)	0 (0%)
Headache	2 (12%)	0 (0%)	0 (0%)	1 (7%)	0 (0%)	0 (0%)	0 (0%)	0 (0%)	0 (0%)
Infusion-related reaction	2 (12%)	0 (0%)	0 (0%)	1 (7%)	0 (0%)	0 (0%)	1 (7%)	0 (0%)	0 (0%)
Skin rash	2 (12%)	0 (0%)	0 (0%)	1 (7%)	0 (0%)	0 (0%)	4 (27%)	0 (0%)	0 (0%)
Photosensitivity	1 (6%)	0 (0%)	0 (0%)	0 (0%)	0 (0%)	0 (0%)	0 (0%)	0 (0%)	0 (0%)
Itching	0 (0%)	0 (0%)	0 (0%)	1 (7%)	0 (0%)	0 (0%)	1 (7%)	0 (0%)	0 (0%)
Cervical lymphadenopathy	0 (0%)	0 (0%)	0 (0%)	0 (0%)	0 (0%)	0 (0%)	1 (7%)	0 (0%)	0 (0%)

* All patients were classified as having secondary adrenal insufficiencies and all patients are still dependent on corticosteroid replacement. # Ejection fraction decreased during ddAC treatment, however IR-myocarditis could not be ruled out. A total of 8 patients from cohorts A, B and C developed grade 3/4 treatment-related adverse events.

a) ID 14 (Cohort A) - Hyperthyroidism (grade 3) and chest pain (grade 3). Patient was diagnosed with hyperthyroidism leading to an orthostatic tremor requiring hospitalization of the patient. Symptoms were treated with beta-blockers. b) ID 36 (Cohort B) - Hyperglycemia with diabetic ketoacidosis (grade 4) and adrenal insufficiency (grade 3). The patient remains insulin-dependent and dependent on corticosteroid replacement therapy. c) ID 44 (Cohort C) - IR hepatitis (grade 3) with primary biliary cholangitis, treated with corticosteroids. d) ID 47 (Cohort C) - IR hepatitis (grade 3), patient did not receive corticosteroid treatment. e) ID 55 (Cohort C) - Pneumonitis (grade 3) with suspicion of pulmonary sarcoidosis, treated with corticosteroids. f) ID 59 (Cohort C) - Adrenal insufficiency (grade 3), still dependent on corticosteroid replacement therapy. g) ID 65 (Cohort C) - Colitis (grade 3), treated with corticosteroids. h) ID 66 (Cohort C) - IR hepatitis (grade 4), treated with corticosteroids.

5. Neoadjuvant nivolumab or nivolumab plus ipilimumab in early-stage triple negative breast cancer: a phase 2 adaptive BELLINI trial

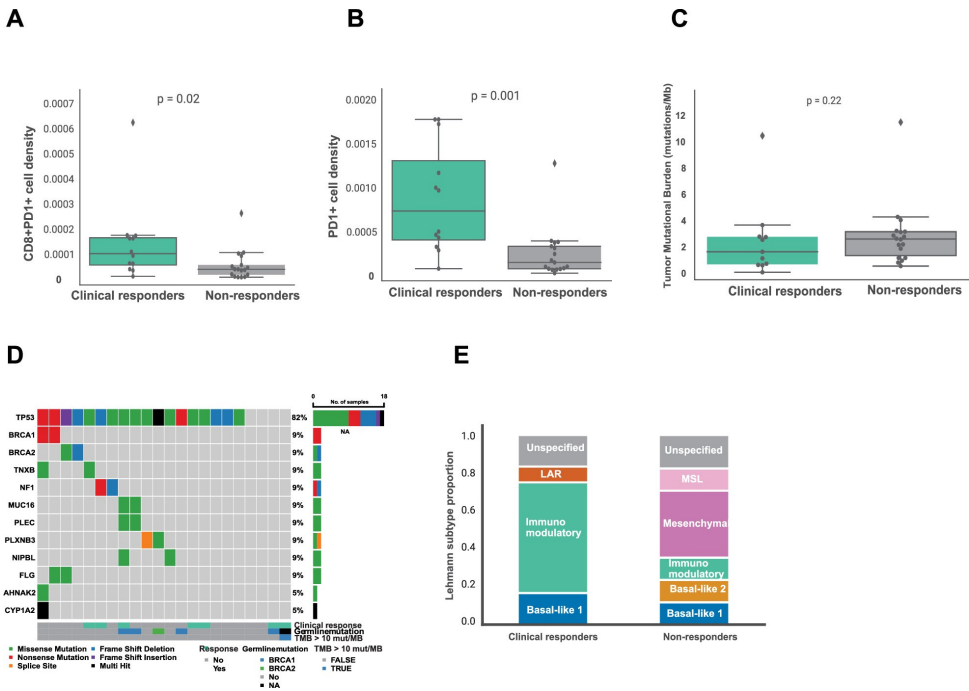


Figure 5.6: Baseline tumor microenvironment features and genomic profile of cohorts A and B (A) PD1+ CD8+ T cell density in pretreatment biopsies of patients who did and did not experience clinical response in cohorts A and B. (B) PD1+ cell density in pretreatment biopsies of patients who did and did not experience clinical response in cohorts A and B. (C) Tumor mutational burden (TMB) in pretreatment biopsies of patients with and without clinical response in cohorts A and B. Boxplots display a minimum (Q0), a maximum (Q4), a median (Q2) and the interquartile range. Data were analyzed by a two-sided Mann-Whitney test. (D) Oncoplot of TMB (mutations per megabase (Mb)) and top mutated genes in cohorts A and B. (E) Proportions of Lehmann et al. subtypes [39] in patients with and without clinical response in cohorts A and B. MSL, mesenchymal stem-like; LAR, luminal androgen receptor.

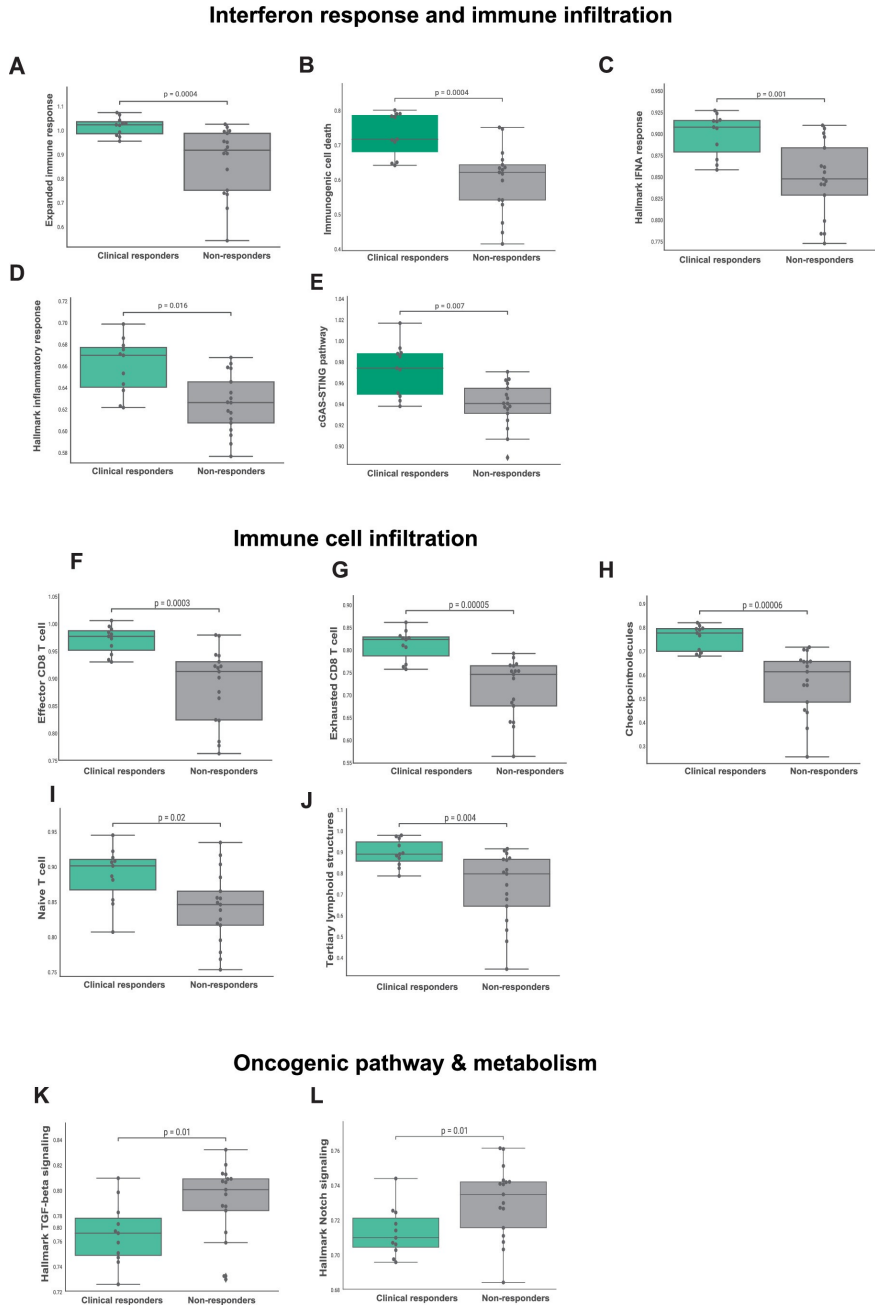
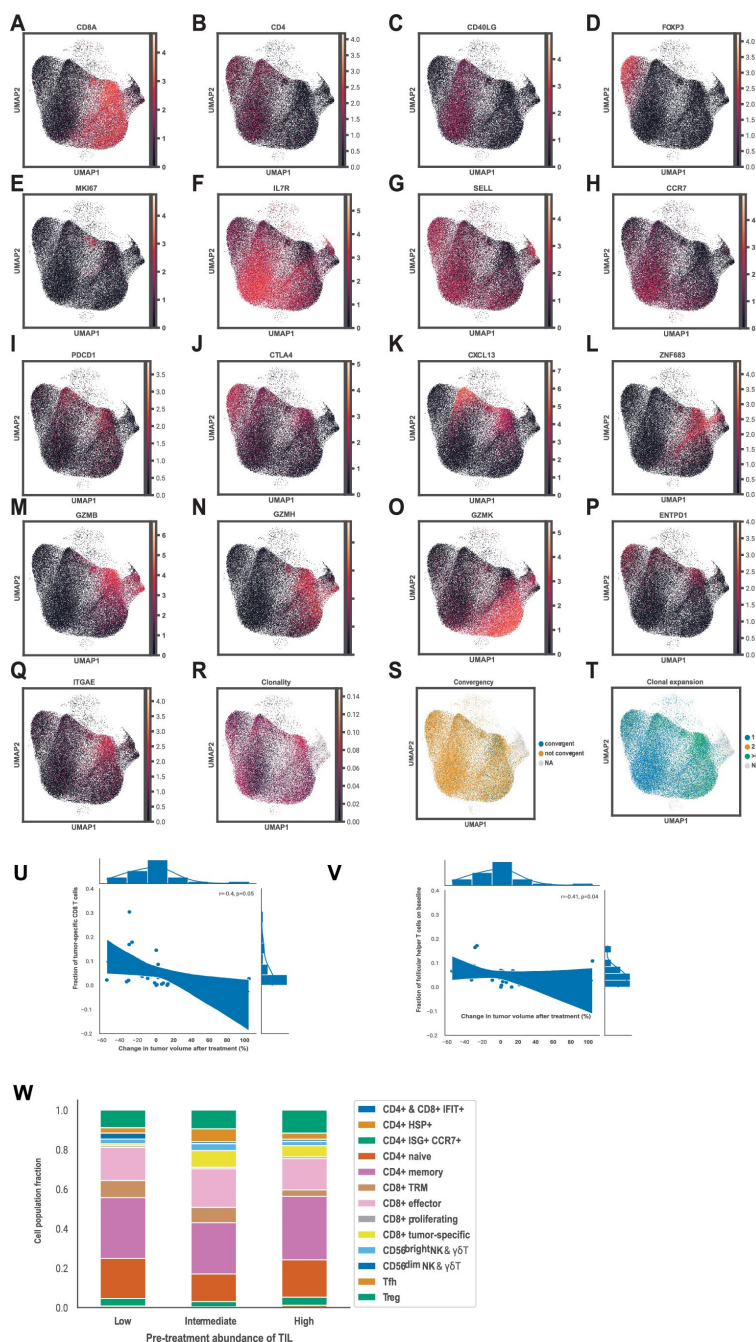


Figure 5.7: Gene signatures in pretreatment biopsies associated with clinical response in cohorts A and B (A-L) Gene set expression scores in pretreatment biopsies of patients with and without clinical response in cohorts A and B. (A) Expanded immune signature from Ayers et al. [33] (B) Immunogenic cell death signature [34]. (C) Hallmark IFNA response gene set. (D) Hallmark inflammatory response gene set. (E) cGAS-STING pathway gene set [35]. (F) Effector CD8+ T cell gene set [36]. (G) Exhausted T cell gene set [36]. (H) Checkpoint molecules gene set [36]. (I) Naive T cell gene set [37]. (J) Tertiary lymphoid structures gene set [38]. (K) Hallmark TGF-beta signaling gene set. (L) Hallmark Notch signaling. In A-L, boxplots display a minimum (Q0), a maximum (Q4), a median (Q2) and the interquartile range. P-values were derived using a two-sided Mann-Whitney test. Reported p-values were significant after Benjamini-Hochberg (FDR) correction at 10% significance level.

5. Neoadjuvant nivolumab or nivolumab plus ipilimumab in early-stage triple negative breast cancer: a phase 2 adaptive BELLINI trial



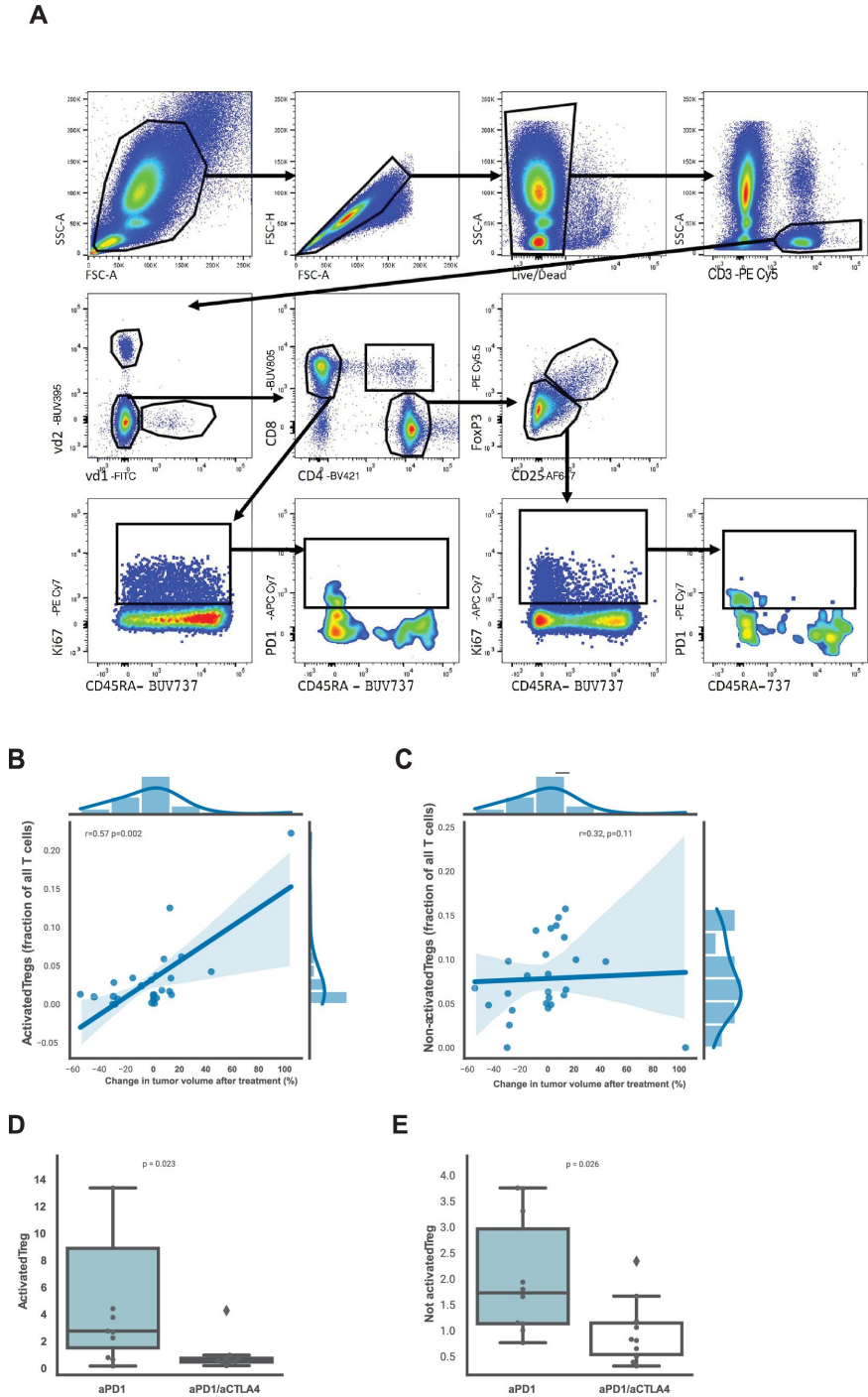


Figure 5.9: Gating strategy used for the flow cytometry data analysis and activated and non-activated Tregs in cohorts A and B. (A) Gating strategy used for the flow cytometry data analysis. **(B)** Spearman correlation between fraction of activated Tregs and the change in tumor size on MRI (%). **(C)** Spearman correlation between fraction of non-activated Tregs and the change in tumor size on MRI (%). Activated Tregs were defined as activated by the expression of CD137. **(D-E)** Fold change in activated **(D)** and non-activated **(E)** Tregs after anti-PD1 or anti-PD1/anti-CTLA4 therapy.

Table 5.4: Antibody overview

Human flow cytometry antibodies					
Antigen	Fluorochrome	Clone	Dilution	Company	Catalog number
CD3	PE Cy5	UCHT1	1:200	1	555334
CD4	BV421	RPA-T4	1:100	1	562424
CD8	BUV805	SK1	1:200	1	612754
Pan $\gamma\delta$ TCR	PE	11F2	1:100	1	555717
V δ 1	FITC	TS8.2	1:100	2	TCR2730
V δ 2	BUV395	B6	1:100	1	748582
FoxP3	PE Cy5.5	FJK-16s	1:50	2	35-5773-82
CCR7	APC R700	150503	1:50	1	565868
CD45RA	BUV737	HI100	1:400	1	612846
CD25	AF647	BC96	1:100	3	302618
PD-1	APC Cy7	EH12.2H7	1:100	3	329922
CTLA-4	PE CF594	BN13	1:200	1	562742
IL-17	PerCP Cy5.5	N49-653	1:50	1	560799
IFN γ	BV785	4S.B3	1:200	3	502542
TNF α	PE Cy7	Mab11	1:400	3	502930
CD27	BV786	L128	1:100	1	563327
TIGIT	PerCP Cy5.5	A151536	1:100	3	372718
Ki-67	PE Cy7	B56	1:50	1	561283
CTLA-4	PE CF594	PE/Dazzle594	1:200	3	369616

1 BD Bioscience;

2 Thermofisher;

3 BioLegend.

References

- [1] P. Schmid, J. Cortes, R. Dent, L. Pusztai, H. McArthur, S. Kümmel, J. Bergh, C. Denkert, Y. H. Park, R. Hui, N. Harbeck, M. Takahashi, M. Untch, P. A. Fasching, F. Cardoso, J. Andersen, D. Patt, M. Danso, M. Ferreira, M.-A. Mouret-Reynier, S.-A. Im, J.-H. Ahn, M. Gion, S. Baron-Hay, J.-F. Boileau, Y. Ding, K. Tryfonidis, G. Aktan, V. Karantza, J. O'Shaughnessy, and KEYNOTE-522 Investigators. "Event-free survival with pembrolizumab in early triple-negative breast cancer". *N. Engl. J. Med.* 386.6 (Feb. 2022), pp. 556–567.
- [2] S. Loibl, M. Untch, N. Burchardi, J. Huober, B. V. Sinn, J.-U. Blohmer, E.-M. Grischke, J. Furlanetto, H. Tesch, C. Hanusch, K. Engels, M. Rezai, C. Jackisch, W. D. Schmitt, G. von Minckwitz, J. Thomalla, S. Kümmel, B. Rautenberg, P. A. Fasching, K. Weber, K. Rhiem, C. Denkert, and A. Schneeweiss. "A randomised phase II study investigating durvalumab in addition to an anthracycline taxane-based neoadjuvant therapy in early triple-negative breast cancer: clinical results and biomarker analysis of GeparNuevo study". *Ann. Oncol.* 30.8 (Aug. 2019), pp. 1279–1288.
- [3] E. A. Mittendorf, H. Zhang, C. H. Barrios, S. Saji, K. H. Jung, R. Hegg, A. Koehler, J. Sohn, H. Iwata, M. L. Telli, C. Ferrario, K. Punie, F. Penault-Llorca, S. Patel, A. N. Duc, M. Liste-Hermoso, V. Maiya, L. Molinero, S. Y. Chui, and N. Harbeck. "Neoadjuvant atezolizumab in combination with sequential nab-paclitaxel and anthracycline-based chemotherapy versus placebo and chemotherapy in patients with early-stage triple-negative breast cancer (IMpassion031): a randomised, double-blind, phase 3 trial". *Lancet* 396.10257 (Oct. 2020), pp. 1090–1100.
- [4] P. Schmid, J. Cortes, L. Pusztai, H. McArthur, S. Kümmel, J. Bergh, C. Denkert, Y. H. Park, R. Hui, N. Harbeck, M. Takahashi, T. Foukakis, P. A. Fasching, F. Cardoso, M. Untch, L. Jia, V. Karantza, J. Zhao, G. Aktan, R. Dent, J. O'Shaughnessy, and KEYNOTE-522 Investigators. "Pembrolizumab for early triple-negative breast cancer". *N. Engl. J. Med.* 382.9 (Feb. 2020), pp. 810–821.
- [5] C. E. Gustafson, R. Jadhav, W. Cao, Q. Qi, M. Pegram, L. Tian, C. M. Weyand, and J. J. Goronzy. "Immune cell repertoires in breast cancer patients after adjuvant chemotherapy". *JCI Insight* 5.4 (Feb. 2020).
- [6] A. Mariniello, T. H. Nasti, D. Y. Chang, M. Hashimoto, S. Malik, D. T. McManus, J. Lee, D. J. McGuire, M. A. Cardenas, P. Umana, V. Nicolini, R. Antia, A. Saha, Z. Buchwald, H. Kissick, E. Ghorani, S. Novello, D. Sangiolo, G. V. Scagliotti, S. S. Ramalingam, and R. Ahmed. "Platinum-based chemotherapy attenuates the effector response of CD8 T cells

- to concomitant PD-1 blockade". *Clin. Cancer Res.* 30.9 (May 2024), pp. 1833–1845.
- [7] C. U. Blank, E. A. Rozeman, L. F. Fanchi, K. Sikorska, B. van de Wiel, P. Kvistborg, O. Krijgsman, M. van den Braber, D. Philips, A. Broeks, J. V. van Thienen, H. A. Mallo, S. Adriaansz, S. Ter Meulen, L. M. Pronk, L. G. Grijpink-Ongering, A. Bruining, R. M. Gittelman, S. Warren, H. van Tinteren, D. S. Peeper, J. B. A. G. Haanen, A. C. J. van Akkooi, and T. N. Schumacher. "Neoadjuvant versus adjuvant ipilimumab plus nivolumab in macroscopic stage III melanoma". *Nat. Med.* 24.11 (Nov. 2018), pp. 1655–1661.
- [8] T. Cascone, W. N. William Jr, A. Weissferdt, C. H. Leung, H. Y. Lin, A. Pataer, M. C. B. Godoy, B. W. Carter, L. Federico, A. Reuben, M. A. W. Khan, H. Dejima, A. Francisco-Cruz, E. R. Parra, L. M. Solis, J. Fujimoto, H. T. Tran, N. Kalhor, F. V. Fossella, F. E. Mott, A. S. Tsao, G. Blumenschein Jr, X. Le, J. Zhang, F. Skoulidis, J. M. Kurie, M. Altan, C. Lu, B. S. Glisson, L. A. Byers, Y. Y. Elamin, R. J. Mehran, D. C. Rice, G. L. Walsh, W. L. Hofstetter, J. A. Roth, M. B. Antonoff, H. Kadara, C. Haymaker, C. Bernatchez, N. J. Ajami, R. R. Jenq, P. Sharma, J. P. Allison, A. Futreal, J. A. Wargo, I. I. Wistuba, S. G. Swisher, J. J. Lee, D. L. Gibbons, A. A. Vaporciyan, J. V. Heymach, and B. Sepesi. "Neoadjuvant nivolumab or nivolumab plus ipilimumab in operable non-small cell lung cancer: the phase 2 randomized NEOSTAR trial". *Nat. Med.* 27.3 (Mar. 2021), pp. 504–514.
- [9] J. L. Vos, J. B. W. Elbers, O. Krijgsman, J. J. H. Traets, X. Qiao, A. M. van der Leun, Y. Lubeck, I. M. Seignette, L. A. Smit, S. M. Willems, M. W. M. van den Brekel, R. Dirven, M. Baris Karakullukcu, L. Karssemakers, W. M. C. Klop, P. J. F. M. Lohuis, W. H. Schreuder, L. E. Smeele, L.-A. van der Velden, I. Bing Tan, S. Onderwater, B. Jasperse, W. V. Vogel, A. Al-Mamgani, A. Keijser, V. van der Noort, A. Broeks, E. Hooijberg, D. S. Peeper, T. N. Schumacher, C. U. Blank, J. P. de Boer, J. B. A. G. Haanen, and C. L. Zuur. "Neoadjuvant immunotherapy with nivolumab and ipilimumab induces major pathological responses in patients with head and neck squamous cell carcinoma". *Nat. Commun.* 12.1 (Dec. 2021), p. 7348.
- [10] N. van Dijk, A. Gil-Jimenez, K. Silina, K. Hendricksen, L. A. Smit, J. M. de Feijter, M. L. van Montfoort, C. van Rooijen, D. Peters, A. Broeks, H. G. van der Poel, A. Bruining, Y. Lubeck, K. Sikorska, T. N. Boellaard, P. Kvistborg, D. J. Vis, E. Hooijberg, T. N. Schumacher, M. van den Broek, L. F. A. Wessels, C. U. Blank, B. W. van Rhijn, and M. S. van der Heijden. "Preoperative ipilimumab plus nivolumab in locoregionally advanced urothelial cancer: the NABUCCO trial". *Nat. Med.* 26.12 (Dec. 2020), pp. 1839–1844.
- [11] M. Chalabi, Y. L. Verschoor, P. B. Tan, S. Balduzzi, A. U. Van Lent, C. Grootsholten, S. Dokter, N. V. Büller, B. A. Grotenhuis, K. Kuhlmann, J. W. Burger, I. L. Huibregtse, T. S. Aukema, E. R. Hendriks, S. J. Oosterling, P. Snaebjornsson, E. E. Voest, L. F. Wessels, R. G. Beets-Tan, M. E. Van Leerdam, T. N. Schumacher, J. G. van den Berg, G. L. Beets, and J. B. Haanen. "Neoadjuvant immunotherapy in locally advanced

- mismatch repair-deficient colon cancer". *N. Engl. J. Med.* 390.21 (June 2024), pp. 1949–1958.
- [12] G. Bianchini, C. De Angelis, L. Licata, and L. Gianni. "Treatment landscape of triple-negative breast cancer - expanded options, evolving needs". *Nat. Rev. Clin. Oncol.* 19.2 (Feb. 2022), pp. 91–113.
- [13] L. Gianni, C. Huang, D. Egle, B. Bermejo, C. Zamagni, M. Thill, A. Anton Torres, G. Bianchini, E. Sevillano Fernandez, S. Russo, E. M. Ciruelos, R. Greil, V. Semiglazov, M. A. Colleoni, C. M. Kelly, G. Mariani, L. Del Mastro, R. Spezia, H. Ali, and G. Viale. "LBA19 Event-free survival (EFS) analysis of neoadjuvant taxane/carboplatin with or without atezolizumab followed by an adjuvant anthracycline regimen in high-risk triple negative breast cancer (TNBC): NeoTRIP Michelangelo randomized study". *Ann. Oncol.* 34 (Oct. 2023), S1258–S1259.
- [14] E. A. Rozeman, A. M. Menzies, A. C. J. van Akkooi, C. Adhikari, C. Bierman, B. A. van de Wiel, R. A. Scolyer, O. Krijgsman, K. Sikorska, H. Eriksson, A. Broeks, J. V. van Thienen, A. D. Guminski, A. T. Acosta, S. Ter Meulen, A. M. Koenen, L. J. W. Bosch, K. Shannon, L. M. Pronk, M. Gonzalez, S. Ch'ng, L. G. Grijpink-Ongering, J. Stretch, S. Heijmink, H. van Tinteren, J. B. A. G. Haanen, O. E. Nieweg, W. M. C. Klop, C. L. Zuur, R. P. M. Saw, W. J. van Houdt, D. S. Peeper, A. J. Spillane, J. Hansson, T. N. Schumacher, G. V. Long, and C. U. Blank. "Identification of the optimal combination dosing schedule of neoadjuvant ipilimumab plus nivolumab in macroscopic stage III melanoma (OpACIN-neo): a multicentre, phase 2, randomised, controlled trial". *Lancet Oncol.* 20.7 (July 2019), pp. 948–960.
- [15] C. Robert, L. Thomas, I. Bondarenko, S. O'Day, J. Weber, C. Garbe, C. Lebbe, J.-F. Baurain, A. Testori, J.-J. Grob, N. Davidson, J. Richards, M. Maio, A. Hauschild, W. H. Miller Jr, P. Gascon, M. Lotem, K. Harmankaya, R. Ibrahim, S. Francis, T.-T. Chen, R. Humphrey, A. Hoos, and J. D. Wolchok. "Ipilimumab plus dacarbazine for previously untreated metastatic melanoma". *N. Engl. J. Med.* 364.26 (June 2011), pp. 2517–2526.
- [16] F. S. Hodi, S. J. O'Day, D. F. McDermott, R. W. Weber, J. A. Sosman, J. B. Haanen, R. Gonzalez, C. Robert, D. Schadendorf, J. C. Hassel, W. Akerley, A. J. M. van den Eertwegh, J. Lutzky, P. Lorigan, J. M. Vaubel, G. P. Linette, D. Hogg, C. H. Ottensmeier, C. Lebbé, C. Peschel, I. Quirt, J. I. Clark, J. D. Wolchok, J. S. Weber, J. Tian, M. J. Yellin, G. M. Nichol, A. Hoos, and W. J. Urba. "Improved survival with ipilimumab in patients with metastatic melanoma". *N. Engl. J. Med.* 363.8 (Aug. 2010), pp. 711–723.
- [17] M. Chalabi, L. F. Fanchi, K. K. Dijkstra, J. G. Van den Berg, A. G. Aalbers, K. Sikorska, M. Lopez-Yurda, C. Grootsholten, G. L. Beets, P. Snaebjornsson, M. Maas, M. Mertz, V. Veninga, G. Bounova, A. Broeks, R. G. Beets-Tan, T. R. de Wijkerslooth, A. U. van Lent, H. A. Marsman, E. Nuijten, N. F. Kok, M. Kuiper, W. H. Verbeek, M. Kok, M. E. Van Leerdam, T. N. Schumacher, E. E. Voest, and J. B. Haanen. "Neoadjuvant immunotherapy leads to pathological responses in MMR-proficient and MMR-deficient early-stage colon cancers". *Nat. Med.* 26.4 (Apr. 2020), pp. 566–576.

- [18] S. Adams, M. Othus, S. P. Patel, K. D. Miller, R. Chugh, S. M. Schuetze, M. D. Chamberlin, B. J. Haley, A. M. V. Storniolo, M. P. Reddy, S. A. Anderson, C. T. Zimmerman, A. P. O'Dea, H. R. Mirshahidi, J. R. Ahnert, F. J. Brescia, O. Hahn, J. M. Raymond, D. D. Biggs, R. M. Connolly, E. Sharon, L. A. Korde, R. J. Gray, E. Mayerson, M. Plets, C. D. Blanke, Y. K. Chae, and R. Kurzrock. "A multicenter phase II trial of ipilimumab and nivolumab in unresectable or metastatic metaplastic breast cancer: Cohort 36 of dual anti-CTLA-4 and anti-PD-1 blockade in rare tumors (DART, SWOG S1609)". *Clin. Cancer Res.* 28.2 (Jan. 2022), pp. 271–278.
- [19] V. M. T. de Jong, Y. Wang, N. D. Ter Hoeve, M. Opdam, N. Stathonikos, K. Jóźwiak, M. Hauptmann, S. Cornelissen, W. Vreuls, E. H. Rosenberg, E. A. Koop, Z. Varga, C. H. M. van Deurzen, A. L. Mooyaart, A. Córdoba, E. J. Groen, J. Bart, S. M. Willems, V. Zolota, J. Wesseling, A. Sapino, E. Chmielik, A. Ryska, A. Broeks, A. C. Voogd, S. Loi, S. Michiels, G. S. Sonke, E. van der Wall, S. Siesling, P. J. van Diest, M. K. Schmidt, M. Kok, G. M. H. E. Dackus, R. Salgado, and S. C. Linn. "Prognostic value of stromal tumor-infiltrating lymphocytes in young, node-negative, triple-negative breast cancer patients who did not receive (neo)adjuvant systemic therapy". *J. Clin. Oncol.* 40.21 (July 2022), pp. 2361–2374.
- [20] S. Loi, D. Drubay, S. Adams, G. Pruneri, P. A. Francis, M. Lacroix-Triki, H. Joensuu, M. V. Dieci, S. Badve, S. Demaria, R. Gray, E. Munzone, J. Lemonnier, C. Sotiriou, M. J. Piccart, P.-L. Kellokumpu-Lehtinen, A. Vingiani, K. Gray, F. Andre, C. Denkert, R. Salgado, and S. Michiels. "Tumor-infiltrating lymphocytes and prognosis: A pooled individual patient analysis of early-stage triple-negative breast cancers". *J. Clin. Oncol.* 37.7 (Mar. 2019), pp. 559–569.
- [21] C. Denkert, G. von Minckwitz, S. Darb-Esfahani, B. Lederer, B. I. Heppner, K. E. Weber, J. Budczies, J. Huober, F. Klauschen, J. Furlanetto, W. D. Schmitt, J.-U. Blohmer, T. Karn, B. M. Pfitzner, S. Kümmel, K. Engels, A. Schneeweiss, A. Hartmann, A. Noske, P. A. Fasching, C. Jackisch, M. van Mackelenbergh, P. Sinn, C. Schem, C. Hanusch, M. Untch, and S. Loibl. "Tumour-infiltrating lymphocytes and prognosis in different subtypes of breast cancer: a pooled analysis of 3771 patients treated with neoadjuvant therapy". *Lancet Oncol.* 19.1 (Jan. 2018), pp. 40–50.
- [22] R. Salgado, C. Denkert, S. Demaria, N. Sirtaine, F. Klauschen, G. Pruneri, S. Wienert, G. Van den Eynden, F. L. Baehner, F. Penault-Llorca, E. A. Perez, E. A. Thompson, W. F. Symmans, A. L. Richardson, J. Brock, C. Criscitiello, H. Bailey, M. Ignatiadis, G. Floris, J. Sparano, Z. Kos, T. Nielsen, D. L. Rimm, K. H. Allison, J. S. Reis-Filho, S. Loibl, C. Sotiriou, G. Viale, S. Badve, S. Adams, K. Willard-Gallo, and S. Loi. "The evaluation of tumor-infiltrating lymphocytes (TILs) in breast cancer: recommendations by an International TILs Working Group 2014". *Ann. Oncol.* 26.2 (Feb. 2015), pp. 259–271.
- [23] J. H. Park, S. F. Jonas, G. Bataillon, C. Criscitiello, R. Salgado, S. Loi, G. Viale, H. J. Lee, M. V. Dieci, S.-B. Kim, A. Vincent-Salomon, G. Curigliano, F. André, and S. Michiels. "Prognostic value of tumor-infiltrating lymphocytes in patients with early-stage triple-negative breast cancers (TNBC) who

- did not receive adjuvant chemotherapy". *Ann. Oncol.* 30.12 (Dec. 2019), pp. 1941–1949.
- [24] S. Loi, R. Salgado, P. Schmid, J. Cortes, D. W. Cescon, E. P. Winer, D. L. Toppmeyer, H. S. Rugo, M. De Laurentiis, R. Nanda, H. Iwata, A. Awada, A. R. Tan, Y. Sun, V. Karantz, A. Wang, L. Huang, A. Saadatpour, R. Cristescu, J. Yearley, J. Lunceford, P. Jelinic, and S. Adams. "Association between biomarkers and clinical outcomes of pembrolizumab monotherapy in patients with metastatic triple-negative breast cancer: KEYNOTE-086 exploratory analysis". *JCO Precis. Oncol.* 7 (Apr. 2023), e2200317.
- [25] L. Voorwerk, M. Slagter, H. M. Horlings, K. Sikorska, K. K. van de Vijver, M. de Maaker, I. Nederlof, R. J. C. Kluin, S. Warren, S. Ong, T. G. Wiersma, N. S. Russell, F. Lalezari, P. C. Schouten, N. A. M. Bakker, S. L. C. Ketelaars, D. Peters, C. A. H. Lange, E. van Werkhoven, H. van Tinteren, I. A. M. Mandjes, I. Kemper, S. Onderwater, M. Chalabi, S. Wilgenhof, J. B. A. G. Haanen, R. Salgado, K. E. de Visser, G. S. Sonke, L. F. A. Wessels, S. C. Linn, T. N. Schumacher, C. U. Blank, and M. Kok. "Immune induction strategies in metastatic triple-negative breast cancer to enhance the sensitivity to PD-1 blockade: the TONIC trial". *Nat. Med.* 25.6 (June 2019), pp. 920–928.
- [26] C. U. Blank, M. W. Lucas, R. A. Scolyer, B. A. van de Wiel, A. M. Menzies, M. Lopez-Yurda, L. L. Hoeijmakers, R. P. M. Saw, J. M. Lijnsvelt, N. G. Maher, S. M. Pulleman, M. Gonzalez, A. Torres Acosta, W. J. van Houdt, S. N. Lo, A. M. J. Kuijpers, A. Spillane, W. M. C. Klop, T. E. Pennington, C. L. Zuur, K. F. Shannon, B. A. Seinstr, R. V. Rawson, J. B. A. G. Haanen, S. Ch'ng, K. A. T. Naipal, J. Stretch, J. V. van Thienen, M. A. Rtshiladze, S. Wilgenhof, R. Kapoor, A. Meerveld-Eggink, L. G. Griepink-Ongering, A. C. J. van Akkooi, I. L. M. Reijers, D. E. Gyorki, D. J. Grünhagen, F. M. Speetjens, S. B. Vliek, J. Placzke, L. Spain, R. C. Stassen, M. Amini-Adle, C. Lebbé, M. B. Faries, C. Robert, P. A. Ascierto, R. van Rijn, F. W. P. J. van den Bergmortal, D. Piersma, A. van der Westhuizen, G. Vreugdenhil, M. J. B. Aarts, M. A. M. Stevense-den Boer, V. Atkinson, M. Khattak, M. C. Andrews, A. J. M. van den Eertwegh, M. J. Boers-Sonderen, G. A. P. Hospers, M. S. Carlino, J.-W. B. de Groot, E. Kapiteijn, K. P. M. Suijkerbuijk, P. Rutkowski, S. Sandhu, A. A. M. van der Veldt, and G. V. Long. "Neoadjuvant nivolumab and ipilimumab in resectable stage III melanoma". *N. Engl. J. Med.* 391.18 (Nov. 2024), pp. 1696–1708.
- [27] R. Simon. "Optimal two-stage designs for phase II clinical trials". *Control. Clin. Trials* 10.1 (Mar. 1989), pp. 1–10.
- [28] P. C. Tume, C. L. Harview, J. H. Yearley, I. P. Shintaku, E. J. M. Taylor, L. Robert, B. Chmielowski, M. Spasic, G. Henry, V. Ciobanu, A. N. West, M. Carmona, C. Kivork, E. Seja, G. Cherry, A. J. Gutierrez, T. R. Grogan, C. Mateus, G. Tomasic, J. A. Glaspy, R. O. Emerson, H. Robins, R. H. Pierce, D. A. Elashoff, C. Robert, and A. Ribas. "PD-1 blockade induces responses by inhibiting adaptive immune resistance". *Nature* 515.7528 (Nov. 2014), pp. 568–571.

- [29] B. W. Higgs, C. A. Morehouse, K. Streicher, P. Z. Brohawn, F. Pilataxi, A. Gupta, and K. Ranade. "Interferon gamma messenger RNA signature in tumor biopsies predicts outcomes in patients with non-small cell lung carcinoma or urothelial cancer treated with durvalumab". *Clin. Cancer Res.* 24.16 (Aug. 2018), pp. 3857–3866.
- [30] E. A. Eisenhauer, P. Therasse, J. Bogaerts, L. H. Schwartz, D. Sargent, R. Ford, J. Dancey, S. Arbuck, S. Gwyther, M. Mooney, L. Rubinstein, L. Shankar, L. Dodd, R. Kaplan, D. Lacombe, and J. Verweij. "New response evaluation criteria in solid tumours: revised RECIST guideline (version 1.1)". *Eur. J. Cancer* 45.2 (Jan. 2009), pp. 228–247.
- [31] A. M. Menzies, R. N. Amaria, E. A. Rozeman, A. C. Huang, M. T. Tetzlaff, B. A. van de Wiel, S. Lo, A. A. Tarhini, E. M. Burton, T. E. Pennington, R. P. M. Saw, X. Xu, G. C. Karakousis, P. A. Ascierto, A. J. Spillane, A. C. J. van Akkooi, M. A. Davies, T. C. Mitchell, H. A. Tawbi, R. A. Scolyer, J. A. Wargo, C. U. Blank, and G. V. Long. "Pathological response and survival with neoadjuvant therapy in melanoma: a pooled analysis from the International Neoadjuvant Melanoma Consortium (INMC)". *Nat. Med.* 27.2 (Feb. 2021), pp. 301–309.
- [32] Y. L. Verschoor, J. van de Haar, J. G. van den Berg, J. W. van Sandick, L. L. Kodach, J. M. van Dieren, S. Balduzzi, C. Grootscholten, M. E. IJsselsteijn, A. A. F. A. Veenhof, K. J. Hartemink, M. A. Vollebergh, A. Jurdi, S. Sharma, E. Spickard, E. C. Owers, A. Bartels-Rutten, P. den Hartog, N. F. C. C. de Miranda, M. E. van Leerdam, J. B. A. G. Haanen, T. N. Schumacher, E. E. Voest, and M. Chalabi. "Neoadjuvant atezolizumab plus chemotherapy in gastric and gastroesophageal junction adenocarcinoma: the phase 2 PANDA trial". *Nat. Med.* 30.2 (Feb. 2024), pp. 519–530.
- [33] M. Ayers, J. Lunceford, M. Nebozhyn, E. Murphy, A. Loboda, D. R. Kaufman, A. Albright, J. D. Cheng, S. P. Kang, V. Shankaran, S. A. Piha-Paul, J. Yearley, T. Y. Seiwert, A. Ribas, and T. K. McClanahan. "IFN- γ -related mRNA profile predicts clinical response to PD-1 blockade". *J. Clin. Invest.* 127.8 (Aug. 2017), pp. 2930–2940.
- [34] A. D. Garg, D. De Ruyscher, and P. Agostinis. "Immunological metagene signatures derived from immunogenic cancer cell death associate with improved survival of patients with lung, breast or ovarian malignancies: A large-scale meta-analysis". *Oncoimmunology* 5.2 (Feb. 2016), e1069938.
- [35] X. E. Hu, P. Yang, S. Chen, G. Wei, L. Yuan, Z. Yang, L. Gong, L. He, L. Yang, S. Peng, Y. Dong, X. He, and G. Bao. "Clinical and biological heterogeneities in triple-negative breast cancer reveals a non-negligible role of HER2-low". *Breast Cancer Res.* 25.1 (Mar. 2023), p. 34.
- [36] A. Bagaev, N. Kotlov, K. Nomie, V. Svekolkina, A. Gafurov, O. Isaeva, N. Osokin, I. Kozlov, F. Frenkel, O. Gancharova, N. Almog, M. Tsiper, R. Ataullakhanov, and N. Fowler. "Conserved pan-cancer microenvironment subtypes predict response to immunotherapy". *Cancer Cell* 39.6 (June 2021), 845–865.e7.
- [37] A. Gangaev, S. L. C. Ketelaars, O. I. Isaeva, S. Patiwaal, A. Dopler, K. Hoefakker, S. De Biasi, L. Gibellini, C. Mussini, G. Guaraldi, M. Girardis,

- C. M. P. T. Ormeno, P. J. M. Hekking, N. M. Lardy, M. Toebe, R. Balderas, T. N. Schumacher, H. Ovaa, A. Cossarizza, and P. Kvistborg. "Identification and characterization of a SARS-CoV-2 specific CD8+ T cell response with immunodominant features". *Nat. Commun.* 12.1 (May 2021), p. 2593.
- [38] R. Cabrita, M. Lauss, A. Sanna, M. Donia, M. Skaarup Larsen, S. Mitra, I. Johansson, B. Phung, K. Harbst, J. Vallon-Christersson, A. van Schoiack, K. Lövgren, S. Warren, K. Jirström, H. Olsson, K. Pietras, C. Ingvar, K. Isaksson, D. Schadendorf, H. Schmidt, L. Bastholt, A. Carneiro, J. A. Wargo, I. M. Svane, and G. Jönsson. "Tertiary lymphoid structures improve immunotherapy and survival in melanoma". *Nature* 577.7791 (Jan. 2020), pp. 561–565.
- [39] B. D. Lehmann, B. Jovanović, X. Chen, M. V. Estrada, K. N. Johnson, Y. Shyr, H. L. Moses, M. E. Sanders, and J. A. Pietenpol. "Refinement of triple-negative breast cancer molecular subtypes: Implications for neoadjuvant chemotherapy selection". *PLoS One* 11.6 (June 2016), e0157368.
- [40] G. Oliveira, K. Stromhaug, S. Klaeger, T. Kula, D. T. Frederick, P. M. Le, J. Forman, T. Huang, S. Li, W. Zhang, Q. Xu, N. Cieri, K. R. Clauser, S. A. Shukla, D. Neuberger, S. Justesen, G. MacBeath, S. A. Carr, E. F. Fritsch, N. Hacohen, M. Sade-Feldman, K. J. Livak, G. M. Boland, P. A. Ott, D. B. Keskin, and C. J. Wu. "Phenotype, specificity and avidity of antitumour CD8+ T cells in melanoma". *Nature* 596.7870 (Aug. 2021), pp. 119–125.
- [41] F. J. Lowery, S. Krishna, R. Yossef, N. B. Parikh, P. D. Chatani, N. Zacharakis, M. R. Parkhurst, N. Levin, S. Sindiri, A. Sachs, K. J. Hitscherich, Z. Yu, N. R. Vale, Y.-C. Lu, Z. Zheng, L. Jia, J. J. Gartner, V. K. Hill, A. R. Copeland, S. K. Nah, R. V. Masi, B. Gasmi, S. Kivitz, B. C. Paria, M. Florentin, S. P. Kim, K.-I. Hanada, Y. F. Li, L. T. Ngo, S. Ray, M. L. Shindorf, S. T. Levi, R. Shepherd, C. Toy, A. Y. Parikh, T. D. Prickett, M. C. Kelly, R. Beyer, S. L. Goff, J. C. Yang, P. F. Robbins, and S. A. Rosenberg. "Molecular signatures of antitumor neoantigen-reactive T cells from metastatic human cancers". *Science* 375.6583 (Feb. 2022), pp. 877–884.
- [42] M. van Gulijk, A. van Krimpen, S. Schetters, M. Eterman, M. van Elsas, J. Mankor, L. Klaase, M. de Bruijn, M. van Nimwegen, T. van Tienhoven, W. van Ijcken, L. Boon, J. van der Schoot, M. Verdoes, F. Scheeren, S. H. van der Burg, B. N. Lambrecht, R. Stadhouders, F. Dammeijer, J. Aerts, and T. van Hall. "PD-L1 checkpoint blockade promotes regulatory T cell activity that underlies therapy resistance". *Sci. Immunol.* 8.83 (May 2023), eabn6173.
- [43] V. C. M. Geurts, S. Balduzzi, T. G. Steenbruggen, S. C. Linn, S. Siesling, S. S. Badve, A. DeMichele, M. Ignatiadis, R. A. Leon-Ferre, M. P. Goetz, A. C. Wolff, N. Klar, S. Michiels, S. Loi, S. Adams, H. M. Horlings, G. S. Sonke, R. Salgado, and M. Kok. "Tumor-infiltrating lymphocytes in patients with stage I triple-negative breast cancer untreated with chemotherapy". *JAMA Oncol.* 10.8 (Aug. 2024), pp. 1077–1086.
- [44] J. M. Unger, R. Vaidya, K. S. Albain, M. LeBlanc, L. M. Minasian, C. C. Gotay, N. L. Henry, M. J. Fisch, S. M. Lee, C. D. Blanke, and D. L.

- Hershman. "Sex differences in risk of severe Adverse Events in patients receiving immunotherapy, targeted therapy, or chemotherapy in cancer clinical trials". *J. Clin. Oncol.* 40.13 (May 2022), pp. 1474–1486.
- [45] V. P. Nguyen, K. M. Campbell, T. S. Nowicki, N. Elumalai, E. Medina, I. Baselga-Carretero, M. L. DiNome, H. R. Chang, D. K. Oseguera, A. Ribas, and J. A. Glaspy. "A pilot study of neoadjuvant nivolumab, ipilimumab, and intralesional oncolytic virotherapy for HER2-negative breast cancer". *Cancer Res. Commun.* 3.8 (Aug. 2023), pp. 1628–1637.
- [46] V. E. Maher, L. L. Fernandes, C. Weinstock, S. Tang, S. Agarwal, M. Brave, Y.-M. Ning, H. Singh, D. Suzman, J. Xu, K. B. Goldberg, R. Sridhara, A. Ibrahim, M. Theoret, J. A. Beaver, and R. Pazdur. "Analysis of the association between adverse events and outcome in patients receiving a programmed death protein 1 or programmed death ligand 1 antibody". *J. Clin. Oncol.* 37.30 (Oct. 2019), pp. 2730–2737.
- [47] A. M. M. Eggermont, M. Kicinski, C. U. Blank, M. Mandala, G. V. Long, V. Atkinson, S. Dalle, A. Haydon, A. Khattak, M. S. Carlino, S. Sandhu, J. Larkin, S. Puig, P. A. Ascierto, P. Rutkowski, D. Schadendorf, R. Koornstra, L. Hernandez-Aya, A. M. Di Giacomo, A. J. M. van den Eertwegh, J.-J. Grob, R. Gutzmer, R. Jamal, P. C. Lorigan, C. Krepler, N. Ibrahim, S. Marreaud, A. van Akkooi, C. Robert, and S. Suciu. "Association between immune-related adverse events and recurrence-free survival among patients with stage III melanoma randomized to receive pembrolizumab or placebo: A secondary analysis of a randomized clinical trial". *JAMA Oncol.* 6.4 (Apr. 2020), pp. 519–527.
- [48] M. Beaufils, V. Amodru, M. Tejada, J. M. Boher, C. Zemmour, B. Chanez, A. S. Chrétien, L. Gorvel, G. Gravis, D. Bruyat, R. Mari, A. Madroszyk, T. Cuny, A. Gonçalves, A. E. Lisberg, D. Olive, L. Tassy, F. Castinetti, and P. Rochigneux. "Dysthyroidism during immune checkpoint inhibitors is associated with improved overall survival in adult cancers: data mining of 1385 electronic patient records". *J. Immunother. Cancer* 11.8 (Aug. 2023), e006786.
- [49] S. Street, D. Chute, I. Strohbehn, S. Zhao, M. Rengarajan, A. Faje, H. Seethapathy, M. Lee, R. Seethapathy, Z. Drobni, O. Rahma, T. G. Neilan, R. J. Sullivan, A. C. Villani, L. Zubiri, M. J. Mooradian, K. L. Reynolds, and M. E. Sise. "The positive effect of immune checkpoint inhibitor-induced thyroiditis on overall survival accounting for immortal time bias: a retrospective cohort study of 6596 patients". *Ann. Oncol.* 32.8 (Aug. 2021), pp. 1050–1051.
- [50] S. Groha, S. A. Alaiwi, W. Xu, V. Naranbhai, A. H. Nassar, Z. Bakouny, T. El Zarif, R. M. Saliby, G. Wan, A. Rajeh, E. Adib, P. V. Nuzzo, A. L. Schmidt, C. Labaki, B. Ricciuti, J. V. Alessi, D. A. Braun, S. A. Shukla, T. E. Keenan, E. Van Allen, M. M. Awad, M. Manos, O. Rahma, L. Zubiri, A.-C. Villani, B. Fairfax, C. Hammer, Z. Khan, K. Reynolds, Y. Semenov, D. Schrag, K. L. Kehl, M. L. Freedman, T. K. Choueiri, and A. Gusev. "Germline variants associated with toxicity to immune checkpoint blockade". *Nat. Med.* 28.12 (Dec. 2022), pp. 2584–2591.

- [51] I. L. M. Reijers, D. Rao, J. M. Versluis, A. M. Menzies, P. Dimitriadis, M. W. Wouters, A. J. Spillane, W. M. C. Klop, A. Broeks, L. J. W. Bosch, M. Lopez-Yurda, W. J. van Houdt, R. V. Rawson, L. G. Griepink-Ongering, M. Gonzalez, S. Cornelissen, J. Bouwman, J. Sanders, E. Plasmeijer, Y. S. Elshot, R. A. Scolyer, B. A. van de Wiel, D. S. Peeper, A. C. J. van Akkooi, G. V. Long, and C. U. Blank. "IFN- γ signature enables selection of neoadjuvant treatment in patients with stage III melanoma". *J. Exp. Med.* 220.5 (May 2023).
- [52] A. J. Bullock, B. L. Schlechter, M. G. Fakih, A. M. Tsimberidou, J. E. Grossman, M. S. Gordon, B. A. Wilky, A. Pimentel, D. Mahadevan, A. S. Balmanoukian, R. E. Sanborn, G. K. Schwartz, G. K. Abou-Alfa, N. H. Segal, B. Bockorny, J. C. Moser, S. Sharma, J. M. Patel, W. Wu, D. Chand, K. Rosenthal, G. Mednick, C. Delepine, T. J. Curiel, J. Stebbing, H.-J. Lenz, S. J. O'Day, and A. B. El-Khoueiry. "Botensilimab plus balstilimab in relapsed/refractory microsatellite stable metastatic colorectal cancer: a phase 1 trial". *Nat. Med.* 30.9 (Sept. 2024), pp. 2558–2567.
- [53] O. S. Blomberg, K. Kos, L. Spagnuolo, O. I. Isaeva, H. Garner, M. D. Wellenstein, N. Bakker, D. E. M. Duits, K. Kersten, S. Klarenbeek, C.-S. Hau, D. Kaldenbach, E. A. M. Raeven, K. Vrijland, M. Kok, and K. E. de Visser. "Neoadjuvant immune checkpoint blockade triggers persistent and systemic Treg activation which blunts therapeutic efficacy against metastatic spread of breast tumors". *Oncoimmunology* 12.1 (Apr. 2023), p. 2201147.
- [54] T. R. Simpson, F. Li, W. Montalvo-Ortiz, M. A. Sepulveda, K. Bergerhoff, F. Arce, C. Roddie, J. Y. Henry, H. Yagita, J. D. Wolchok, K. S. Peggs, J. V. Ravetch, J. P. Allison, and S. A. Quezada. "Fc-dependent depletion of tumor-infiltrating regulatory T cells co-defines the efficacy of anti-CTLA-4 therapy against melanoma". *J. Exp. Med.* 210.9 (Aug. 2013), pp. 1695–1710.
- [55] A. Sharma, S. K. Subudhi, J. Blando, J. Scutti, L. Vence, J. Wargo, J. P. Allison, A. Ribas, and P. Sharma. "Anti-CTLA-4 immunotherapy does not deplete FOXP3+ regulatory T cells (tregs) in human cancers". *Clin. Cancer Res.* 25.4 (Feb. 2019), pp. 1233–1238.
- [56] A. M. van der Leun, J. J. H. Traets, J. L. Vos, J. B. W. Elbers, S. Patiwaal, X. Qiao, M. Machuca-Ostos, D. S. Thommen, J. B. A. G. Haanen, T. N. M. Schumacher, and C. L. Zuur. "Dual immune checkpoint blockade induces analogous alterations in the dysfunctional CD8+ T-cell and activated Treg compartment". *Cancer Discov.* 13.10 (Oct. 2023), pp. 2212–2227.
- [57] S. Loibl, A. Schneeweiss, J. Huober, M. Braun, J. Rey, J.-U. Blohmer, J. Furlanetto, D.-M. Zahm, C. Hanusch, J. Thomalla, C. Jackisch, P. Staib, T. Link, K. Rhiem, C. Solbach, P. A. Fasching, V. Nekljudova, C. Denkert, M. Untch, and GBG and AGO-B. "Neoadjuvant durvalumab improves survival in early triple-negative breast cancer independent of pathological complete response". *Ann. Oncol.* 33.11 (Nov. 2022), pp. 1149–1158.
- [58] L. Gianni, C. S. Huang, D. Egle, B. Bermejo, C. Zamagni, M. Thill, A. Anton, S. Zambelli, G. Bianchini, S. Russo, E. M. Ciruelos, R. Greil,

- V. Semiglazov, M. Colleoni, C. Kelly, G. Mariani, L. Del Mastro, I. Maffei, P. Valagussa, and G. Viale. "Pathologic complete response (pCR) to neoadjuvant treatment with or without atezolizumab in triple-negative, early high-risk and locally advanced breast cancer: NeoTRIP Michelangelo randomized study". *Ann. Oncol.* 33.5 (May 2022), pp. 534–543.
- [59] M. Chalabi, Y. L. Verschoor, J. van den Berg, K. Sikorska, G. Beets, A. V. Lent, M. C. Grootsholten, A. Aalbers, N. Buller, H. Marsman, E. Hendriks, P. W. A. Burger, T. Aukema, S. Oosterling, R. Beets-Tan, T. N. Schumacher, M. van Leerdam, E. E. Voest, and J. B. A. G. Haanen. "LBA7 Neoadjuvant immune checkpoint inhibition in locally advanced MMR-deficient colon cancer: The NICHE-2 study". *Ann. Oncol.* 33 (Sept. 2022), S1389.
- [60] E. A. Rozeman, E. P. Hoefsmit, I. L. M. Reijers, R. P. M. Saw, J. M. Versluis, O. Krijgsman, P. Dimitriadis, K. Sikorska, B. A. van de Wiel, H. Eriksson, M. Gonzalez, A. Torres Acosta, L. G. Grijpink-Ongering, K. Shannon, J. B. A. G. Haanen, J. Stretch, S. Ch'ng, O. E. Nieweg, H. A. Mallo, S. Adriaansz, R. M. Kerkhoven, S. Cornelissen, A. Broeks, W. M. C. Klop, C. L. Zuur, W. J. van Houdt, D. S. Peeper, A. J. Spillane, A. C. J. van Akkooi, R. A. Scolyer, T. N. M. Schumacher, A. M. Menzies, G. V. Long, and C. U. Blank. "Survival and biomarker analyses from the OpACIN-neo and OpACIN neoadjuvant immunotherapy trials in stage III melanoma". *Nat. Med.* 27.2 (Feb. 2021), pp. 256–263.
- [61] L. Pusztai, C. Denkert, J. O'Shaughnessy, J. Cortes, R. Dent, H. McArthur, S. Kümmel, J. Bergh, Y. H. Park, R. Hui, N. Harbeck, M. Takahashi, M. Untch, P. A. Fasching, F. Cardoso, Y. Zhu, W. Pan, K. Tryfonidis, and P. Schmid. "Event-free survival by residual cancer burden with pembrolizumab in early-stage TNBC: exploratory analysis from KEYNOTE-522". *Ann. Oncol.* 35.5 (May 2024), pp. 429–436.
- [62] M. J. M. Magbanua, L. B. Swigart, H.-T. Wu, G. L. Hirst, C. Yau, D. M. Wolf, A. Tin, R. Salari, S. Shchegrova, H. Pawar, A. L. Delson, A. DeMichele, M. C. Liu, A. J. Chien, D. Tripathy, S. Asare, C.-H. J. Lin, P. Billings, A. Aleshin, H. Sethi, M. Louie, B. Zimmermann, L. J. Esserman, and L. J. van 't Veer. "Circulating tumor DNA in neoadjuvant-treated breast cancer reflects response and survival". *Ann. Oncol.* 32.2 (Feb. 2021), pp. 229–239.
- [63] M. M. Oken, R. H. Creech, and D. C. Tormey. "Toxicity and response criteria of the Eastern Cooperative Oncology Group". *Am J Clin Oncol* 5.6 (1982), pp. 649–655.
- [64] J. K. Litton, M. M. Regan, L. Pusztai, H. S. Rugo, S. M. Tolaney, E. Garrett-Mayer, L. Amiri-Kordestani, R. K. Basho, A. F. Best, J.-F. Boileau, C. Denkert, J. C. Foster, N. Harbeck, H. A. Jacene, T. A. King, G. Mason, C. C. O'Sullivan, T. M. Prowell, A. L. Richardson, K. A. Sepulveda, M. L. Smith, J. A. Tjoe, G. Turashvili, W. A. Woodward, L. P. Butler, E. I. Schwartz, and L. A. Korde. "Standardized Definitions for Efficacy End Points in neoadjuvant breast cancer clinical trials: NeoSTEEP". *J. Clin. Oncol.* 41.27 (Sept. 2023), pp. 4433–4442.

- [65] C. M. Blakely and C. E. McCoach. "Role of MPR as an early signal for efficacy in neoadjuvant studies". *Clin. Cancer Res.* 26.14 (July 2020), pp. 3499–3500.
- [66] T. Cascone, B. Sepesi, H. Y. Lin, N. Kalhor, E. R. Parra, M. Jiang, M. C. B. Godoy, J. Zhang, F. V. Fossella, A. S. Tsao, V. K. Lam, C. Lu, F. E. Mott, G. R. Simon, M. B. Antonoff, R. J. Mehran, D. C. Rice, C. Behrens, A. Weissferdt, C. Moran, A. A. Vaporciyan, J. J. Lee, S. G. Swisher, D. L. Gibbons, I. I. Wistuba, W. N. William Jr, and J. V. Heymach. "A phase I/II study of neoadjuvant cisplatin, docetaxel, and nintedanib for resectable non-small cell lung cancer". *Clin. Cancer Res.* 26.14 (July 2020), pp. 3525–3536.
- [67] U.S. Departments of Health and Human Services. *Common Terminology Criteria for Adverse Events (CTCAE). Version 5.0*. <https://dctd.cancer.gov/research/ctep-trials/for-sites/adverse-events/ctcae-v5-5x7.pdf>. 2017.
- [68] R Core Team. *R: A language and environment for statistical computing*. <https://www.R-project.org/>. 2023.
- [69] J. Hudeček, L. Voorwerk, M. van Seijen, I. Nederlof, M. de Maaker, J. van den Berg, K. K. van de Vijver, K. Sikorska, S. Adams, S. Demaria, G. Viale, T. O. Nielsen, S. S. Badve, S. Michiels, W. F. Symmans, C. Sotiriou, D. L. Rimm, S. M. Hewitt, C. Denkert, S. Loibl, S. Loi, J. M. S. Bartlett, G. Pruneri, D. A. Dillon, M. C. U. Cheang, A. Tutt, J. A. Hall, Z. Kos, R. Salgado, M. Kok, H. M. Horlings, and International Immuno-Oncology Biomarker Working Group. "Application of a risk-management framework for integration of stromal tumor-infiltrating lymphocytes in clinical trials". *NPJ Breast Cancer* 6.1 (May 2020), p. 15.
- [70] A. Dobin, C. A. Davis, F. Schlesinger, J. Drenkow, C. Zaleski, S. Jha, P. Batut, M. Chaisson, and T. R. Gingeras. "STAR: ultrafast universal RNA-seq aligner". *Bioinformatics* 29.1 (Jan. 2013), pp. 15–21.
- [71] L. Wang, S. Wang, and W. Li. "RSeQC: quality control of RNA-seq experiments". *Bioinformatics* 28.16 (Aug. 2012), pp. 2184–2185.
- [72] Andrews, Simon. *A quality control tool for high throughput sequence data*. 2016.
- [73] S. W. Wingett and S. Andrews. "FastQ Screen: A tool for multi-genome mapping and quality control". *F1000Res.* 7 (Aug. 2018), p. 1338.
- [74] J. D. Hunter. "Matplotlib: A 2D Graphics Environment". *Computing in Science & Engineering* 9.3 (2007), pp. 90–95.
- [75] B. Institute. *Picard toolkit*. <https://broadinstitute.github.io/picard/>. 2019.
- [76] X. Chen, J. Li, W. H. Gray, B. D. Lehmann, J. A. Bauer, Y. Shyr, and J. A. Pietenpol. "TNBCtype: A subtyping tool for triple-negative breast cancer". *Cancer Inform.* 11 (July 2012), pp. 147–156.
- [77] B. D. Lehmann, J. A. Bauer, X. Chen, M. E. Sanders, A. B. Chakravarthy, Y. Shyr, and J. A. Pietenpol. "Identification of human triple-negative

- breast cancer subtypes and preclinical models for selection of targeted therapies". *J. Clin. Invest.* 121.7 (July 2011), pp. 2750–2767.
- [78] Z. Fang, X. Liu, and G. Peltz. "GSEAPy: a comprehensive package for performing gene set enrichment analysis in Python". *Bioinformatics* 39.1 (Jan. 2023).
- [79] The Python Software Foundation. *The Python Language Reference. Python documentation*. <https://docs.python.org/3/reference/index.html>.
- [80] The pandas development team. *pandas-dev/pandas: Pandas*. Zenodo. <https://doi.org/10.5281/zenodo.7549438>. 2023.
- [81] W. McKinney. "Data Structures for Statistical Computing in Python". *Proceedings of the Python in Science Conference*. Austin, Texas: SciPy, 2010, pp. 56–61.
- [82] C. R. Harris, K. J. Millman, S. J. van der Walt, R. Gommers, P. Virtanen, D. Cournapeau, E. Wieser, J. Taylor, S. Berg, N. J. Smith, R. Kern, M. Picus, S. Hoyer, M. H. van Kerkwijk, M. Brett, A. Haldane, J. F. Del Río, M. Wiebe, P. Peterson, P. Gérard-Marchant, K. Sheppard, T. Reddy, W. Weckesser, H. Abbasi, C. Gohlke, and T. E. Oliphant. "Array programming with NumPy". *Nature* 585.7825 (Sept. 2020), pp. 357–362.
- [83] M. L. Waskom. "seaborn: statistical data visualization". *Journal of Open Source Software* 6.60 (2021), p. 3021. url: <https://doi.org/10.21105/joss.03021>.
- [84] F. Charlier, M. Weber, D. Izak, E. Harkin, M. Magnus, J. Lalli, L. Fresnais, M. Chan, N. Markov, O. Amsalem, S. Proost, A. Krasoulis, getzze, and S. Repplinger. *Statannotations*. Version v0.6. Oct. 2022. doi: 10.5281/zenodo.7213391. url: <https://doi.org/10.5281/zenodo.7213391>.
- [85] H. Li and R. Durbin. "Fast and accurate short read alignment with Burrows-Wheeler transform". *Bioinformatics* 25.14 (July 2009), pp. 1754–1760.
- [86] G. Auwera and B. D. Van Der. *Genomics in the Cloud : Using Docker, GATK, and WDL in Terra*. O'Reilly Media, 2020.
- [87] A. Mayakonda, D.-C. Lin, Y. Assenov, C. Plass, and H. P. Koeffler. "Maftools: efficient and comprehensive analysis of somatic variants in cancer". *Genome Res.* 28.11 (Nov. 2018), pp. 1747–1756.
- [88] R Core Team. *R: A language and environment for statistical computing*. <https://www.R-project.org/>. 2023.
- [89] F. A. Wolf, P. Angerer, and F. J. Theis. "SCANPY: large-scale single-cell gene expression data analysis". *Genome Biol.* 19.1 (Dec. 2018).
- [90] Y. Hao, T. Stuart, M. H. Kowalski, S. Choudhary, P. Hoffman, A. Hartman, A. Srivastava, G. Molla, S. Madad, C. Fernandez-Granda, and R. Satija. "Dictionary learning for integrative, multimodal and scalable single-cell analysis". *Nat. Biotechnol.* 42.2 (Feb. 2024), pp. 293–304.

- [91] S. J. Fleming, M. D. Chaffin, A. Arduini, A.-D. Akkad, E. Banks, J. C. Marioni, A. A. Philippakis, P. T. Ellinor, and M. Babadi. "Unsupervised removal of systematic background noise from droplet-based single-cell experiments using CellBender". *Nat. Methods* 20.9 (Sept. 2023), pp. 1323–1335.
- [92] A. Bassez, H. Vos, L. Van Dyck, G. Floris, I. Arijs, C. Desmedt, B. Boeckx, M. Vanden Bempt, I. Nevelsteen, K. Lambein, K. Punie, P. Neven, A. D. Garg, H. Wildiers, J. Qian, A. Smeets, and D. Lambrechts. "A single-cell map of intratumoral changes during anti-PD1 treatment of patients with breast cancer". *Nat. Med.* 27.5 (May 2021), pp. 820–832.
- [93] J. H. Levine, E. F. Simonds, S. C. Bendall, K. L. Davis, E.-A. D. Amir, M. D. Tadmor, O. Litvin, H. G. Fienberg, A. Jager, E. R. Zunder, R. Finck, A. L. Gedman, I. Radtke, J. R. Downing, D. Pe'er, and G. P. Nolan. "Data-driven phenotypic dissection of AML reveals progenitor-like cells that correlate with prognosis". *Cell* 162.1 (July 2015), pp. 184–197.
- [94] E. Y. Chen, C. M. Tan, Y. Kou, Q. Duan, Z. Wang, G. V. Meirelles, N. R. Clark, and A. Ma'ayan. "Enrichr: interactive and collaborative HTML5 gene list enrichment analysis tool". *BMC Bioinformatics* 14.1 (Apr. 2013), p. 128.
- [95] M. V. Kuleshov, M. R. Jones, A. D. Rouillard, N. F. Fernandez, Q. Duan, Z. Wang, S. Koplev, S. L. Jenkins, K. M. Jagodnik, A. Lachmann, M. G. McDermott, C. D. Monteiro, G. W. Gundersen, and A. Ma'ayan. "Enrichr: a comprehensive gene set enrichment analysis web server 2016 update". *Nucleic Acids Res.* 44.W1 (July 2016), W90–W97.
- [96] G. Sturm, T. Szabo, G. Fotakis, M. Haider, D. Rieder, Z. Trajanoski, and F. Finotello. "Scirpy: a Scanpy extension for analyzing single-cell T-cell receptor-sequencing data". *Bioinformatics* 36.18 (Sept. 2020), pp. 4817–4818.
- [97] Ansari, Meshal and Heumos, Lukas. *GitHub - schillerlab/sc-toolbox: A collection of project templates and useful functions for single-cell data analysis with Scanpy.* <https://github.com/schillerlab/sc-toolbox>. 2023.
- [98] O. S. Blomberg, L. Spagnuolo, H. Garner, L. Voorwerk, O. I. Isaeva, E. van Dyk, N. Bakker, M. Chalabi, C. Klaver, M. Duijst, K. Kersten, M. Brüggemann, D. Pastoors, C.-S. Hau, K. Vrijland, E. A. M. Raeven, D. Kaldenbach, K. Kos, I. S. Afonina, P. Kaptein, L. Hoes, W. S. M. E. Theelen, P. Baas, E. E. Voest, R. Beyaert, D. S. Thommen, L. F. A. Wessels, K. E. de Visser, and M. Kok. "IL-5-producing CD4+ T cells and eosinophils cooperate to enhance response to immune checkpoint blockade in breast cancer". *Cancer Cell* 41.1 (Jan. 2023), 106–123.e10.

6

Discussion

This thesis leverages the power of high-throughput sequencing to understand the biology of disease and combat it. In Part 1, including **Chapter 2**, the disease of interest is COVID-19, and in Part 2, containing the rest of the chapters, it is breast cancer. We hope that this work paves the way for applying similar approaches to other diseases, which, hopefully, would be more common in the future with the rising affordability of sequencing.

The opportunity to actively use sequencing data in translational and clinical research allows the research community to leverage this data to find biomarkers of treatment response and better survival. It is particularly important in the field of immunotherapy, as many patients do not benefit from treatments, and as adverse events may be severe. In this thesis, we describe the following contributions to the field:

- In **Chapter 2**, we used the publicly available SARS-CoV-2 genomic data to predict the degree of protection against the novel SARS-CoV-2 variants provided by prior vaccination or infection by the original SARS-CoV-2 strain.
- In **Chapter 3**, we used bulk RNA sequencing to demonstrate that treatment with anti-PDL1 in combination with carboplatin leads to increased T cell infiltration and checkpoint molecule expression in metastatic lobular breast cancer.
- In **Chapter 4**, we used shallow whole genome sequencing of circulating tumor DNA to calculate a genome-wide copy number alteration score and demonstrated that change in this score upon treatment is associated with response to anti-PD1 in metastatic triple-negative breast cancer.
- Finally, in **Chapter 5**, we used bulk and single-cell RNA sequencing to dissect the biology of the tumor microenvironment in early triple-negative breast cancer upon treatment with anti-PD1 +/- anti-CTLA4 checkpoint blockade. We described profound differences in the tumor microenvironment of responders and non-responders to checkpoint blockade in this setting which might be helpful to select patients more likely to benefit from this treatment in future clinical trials.

In this discussion, we will focus on the topics related to breast cancer presented in this thesis.

6.1. Breast cancer immunotherapy: successes and challenges

Until the last decade, breast cancer was mostly treated with chemotherapy, radiation, surgery, hormone and targeted therapy [1]. In particular, the therapies targeting the estrogen, progesterone and HER2 receptors proved to be beneficial for the patients who had overexpression or amplification of the corresponding genes, even though these therapies may lead to molecular resistance [2]. Breast cancer was not considered a promising cancer type for immunotherapy approaches, as breast cancers are not typically highly immune infiltrated [3] and have low TMB [4].

However, it was demonstrated that TNBC tumors, that are typically higher infiltrated than hormone-positive breast tumors, benefit from the addition of anti-PD1 to chemotherapy [5]. Nowadays, anti-PD1 in combination with chemotherapy is the standard of care for metastatic PDL1+ TNBC [6]. The combination of anti-PD1 with neoadjuvant chemotherapy is also approved by the FDA and the EMA for treatment of early TNBC, and this regimen is currently the standard of care in the Netherlands [7].

Though TNBC tumors benefit from immunotherapy, only a minority of patients respond to the therapy [5, 6]. Therefore, it is essential to modify the current regimens to improve the patient outcomes. The investigation of the biology of the TNBC in context of the tumor microenvironment helps to understand which features may be used as biomarkers to personalize treatment and to come up with new therapeutic options or combination approaches for TNBC. Bioinformatics approaches, as demonstrated in this thesis, allow to conduct this investigation in detail.

6.2. Biomarkers for breast cancer immunotherapy

Several biomarkers have been approved for use in the context of checkpoint blockade therapy in metastatic breast cancer. In particular, it is the case for mismatch-repair deficiency, present in 1-2% of breast tumors [8], as well as for tumor mutational burden higher than 10 mutations per Mb [9]. Additionally, PDL1 expression (combined positive score ≥ 10) is also an approved biomarker which was used in the metastatic TNBC setting in the KEYNOTE-355 study [6], a randomized phase III trial of pembrolizumab with chemotherapy in advanced TNBC, and in the early TNBC setting in the KEYNOTE-522 study [7], a randomized phase III trial of neoadjuvant pembrolizumab with chemotherapy in stage II-III TNBC. However, these biomarkers have limitations, as mismatch-repair deficiency and high TMB are rare

in breast cancer, and PDL1 expression demonstrates different staining patterns for different antibody clones and low concordance between pathologists, as well as differences per biological site and tumor stage.

Other well-known biomarkers for immunotherapy in TNBC include stromal tumor infiltrating lymphocytes (TILs), CD8+ T cell infiltration and presence of particular CD8+ T cell subsets. The presence of TILs has a strong prognostic value in early TNBC [10] and a predictive value for immune checkpoint blockade treatment in metastatic TNBC [11].

The presence of effector CD8+ T cells in the tumor before therapy has also been shown to be associated with response to checkpoint blockade in metastatic TNBC [12–14]. In **Chapter 5**, we demonstrate that the presence of the CD8+ T cells, as well as the presence of TILs, is also associated with response to ICB in early triple-negative breast cancer.

Not only the general abundance of intratumoral CD8+ T cells but also the presence of particular functional CD8+ T cell phenotypes may be associated with response to checkpoint blockade in TNBC. The discovery of these populations is made possible by the use of high-throughput sequencing methods, allowing to examine the tumor microenvironment at single-cell resolution. In particular, CD8+ T cells with tissue-resident phenotype have been shown to be associated with response in the Gepar-Nuevo clinical trial [15], a randomized phase II trial of neoadjuvant treatment with anti-PDL1 agent durvalumab in combination with chemotherapy in early TNBC. In **Chapter 5**, we used single-cell RNA sequencing to describe another CD8+ T cell population associated with response to immune checkpoint blockade: a population of potentially tumor-reactive CD8+ T cells, possessing different traits of tumor reactivity: high clonality and high expression of tumor reactivity markers and tumor recognition signatures derived using functional tumor recognition experiments.

As the adverse events associated with modern cancer treatment regimens may be very severe and long-lasting, it is also important to find biomarkers associated with high likelihood of high treatment toxicity and find patient populations that might achieve good clinical outcomes with less treatment exposure. In particular, in early TNBC the combination of neoadjuvant immunotherapy with chemotherapy leads to a high rate of chemotherapy-related adverse events, affects quality of life and could limit T cell functionality [16, 17]. In **Chapter 5**, we demonstrated that early TNBC patients with high tumor-infiltrating lymphocyte levels may achieve pathological complete responses after immunotherapy only, without neoadjuvant chemotherapy. This finding needs to be further evaluated in larger studies. Genomic and transcriptomic data insights may help to define such groups of potential excellent responders better.

The biomarkers linked with good clinical outcomes also may be used to preselect patients for particular treatments in order to limit or prevent the unnecessary adverse events in patients that are not likely to benefit from the treatment. This was also achieved in the BELLINI trial. As discussed in **Chapter 5**, to exclude patients with a poor prognosis, less likely to respond to ICI and not suitable for chemotherapy de-escalation, only patients with TIL > 5% were recruited in cohorts A and B. As cohorts A and B revealed that the most promising results were observed in patients with high TIL, only patients with TIL > 50% were recruited in cohort C. The future BELLINI cohorts will further explore the optimal TIL threshold in the context of preselecting early TNBC patients for checkpoint blockade treatment. Of course, these findings would also need to be evaluated in larger randomized studies.

6.3. Combining treatments for breast cancer immunotherapy

The breakthrough success of using checkpoint inhibitors in cancer makes it attractive to combine checkpoint inhibitors with other therapies, or to combine different checkpoint blockade agents to achieve better responses. The use of bulk and single-cell RNA-Seq, as well as TCR sequencing, allows to examine the differences in the tumor microenvironment of the patients that received different treatments and to select the treatment that demonstrates higher biological activity in the translational setting.

In both metastatic and early TNBC, the current standard of care includes combining checkpoint blockade therapy with chemotherapy. Chemotherapy agents used include paclitaxel, carboplatin, doxorubicin, epirubicin, cyclophosphamide and gemcitabine [6, 7]. It would be beneficial if selected chemotherapies would synergize with checkpoint blockade treatment. An attempt to find such combinations was made in the first stage of the TONIC trial, where anti-PD1 treatment was given to patients with metastatic TNBC after two-week induction treatment with chemotherapy or irradiation, with three chemotherapies tested in separate arms: doxorubicin, cisplatin and cyclophosphamide [13]. Though the study was not powered to compare doxorubicin and cisplatin showed higher response rates and signs of biological activity in the TME. These findings emphasize the importance of testing the combinations of different chemotherapies with immunotherapy. This investigation is currently being continued in the follow-up larger TONIC2 study.

In **Chapter 3**, we explored the similar induction concept in the context of metastatic lobular breast cancer in the GELATO trial. In this study,

patients received carboplatin for 12 weeks with anti-PDL1 added from the third week until progression. Therefore, patients also had a two-week induction window when carboplatin could prime their TME for the subsequent action of the checkpoint blockade treatment. Previous preclinical studies suggested that carboplatin could induce cGAS-STING signalling [18] and immunogenic cell death [19] which could improve the recognition of the tumor by the immune system following anti-PDL1 treatment. However, we did not observe major changes in the TME upon carboplatin treatment, and only a combination treatment with carboplatin and anti-PDL1 led to an enrichment in the biological activity in the TME. This demonstrates that though preclinical findings may provide indications of the potential synergy between some agents, this synergy might not present in the clinical trial.

It is also an attractive possibility to combine anti-PD1 or anti-PDL1 regimens with other immunotherapies. In **Chapter 5**, we compared the post-treatment T cell profiles in the tumor microenvironment of patients with early TNBC treated with nivolumab and a combination of nivolumab and ipilimumab in the context of the BELLINI trial. Surprisingly, we did not observe major differences upon addition of ipilimumab, though it led to a lower fold change in frequency of tumor-infiltrating Tregs post-treatment. In the next cohorts of the BELLINI trial, anti-PD1 treatment would be combined with other immunotherapies, targeting LAG3 and TIGIT. Such approaches seem promising, as they would allow to target multiple T cell checkpoint pathways simultaneously, and hopefully with the growing number of immunotherapy agents successful combinations would be discovered soon.

6.4. Treating particular breast cancer patient populations

The impact of immunotherapy, and in particular checkpoint inhibitors, may vary in different patient populations. The use of high-throughput sequencing methods allows to select subgroups of patients most likely to benefit from treatment and to validate whether particular groups indeed have a specific profile of response to checkpoint inhibitors.

To date, there are many classifications of breast tumors, with the most well-known being the division into the luminal A, luminal B, HER2-positive and basal-like subtypes [20]. There is also a histological classification that divides breast tumors into ductal, lobular, tubular, cribriform, mucinous, medullary, papillary, micropapillary, metaplastic, lipid-rich, secretory, oncocytic, adenoid cystic, acinic cell carcinomas and carcinoma of no special type, as well as apocrine and neuroendocrine

tumors [21].

TNBC is also a heterogeneous disease which can be viewed as a compendium of subtypes, in particular using computational approaches. Lehmann et al. described six TNBC subtypes: two basal-like subtypes, an immunomodulatory, a mesenchymal, a mesenchymal stem-like, and a luminal androgen receptor subtype [22]. Burnstein et al. described four TNBC subtypes: luminal androgen receptor, mesenchymal, basal-like immunosuppressed and basal-like immune-activated [23]. Others have also proposed subtypes associated with PTEN loss [24], APOBEC signature [25], homologous recombination deficiency [25], expression of particular long non-coding RNAs [26] and other features.

It is also possible to classify the tumors based on the activity of the immune and transformed cells in the tumour microenvironment. Our work with Bagaev et al. suggested that there are pancancer tumor microenvironment profiles that are associated with response to immunotherapy [27]. Similarly, Sanchez-Vega et al. described ten canonical oncogenic pathways that can be used to classify tumors in the pancancer approach using The Cancer Genome Atlas [28].

All these classifications were made possible by the use of high-throughput sequencing and bioinformatic approaches. The prior knowledge on the subtypes and functional profiles may allow clinicians to choose suitable treatment options for the individual patients based on their tumor characteristics. It also allows the creation of clinical trials specific for particular patient populations.

In **Chapter 3**, we discussed the GELATO trial, where patients with metastatic lobular breast cancer received immune checkpoint blockade treatment in combination with carboplatin. This study was motivated by previous work that demonstrated that some lobular breast tumors belong to an immune-enriched subtype that might benefit from immunotherapy treatment. Additionally, two of the three responders in the KEYNOTE-028 study of pembrolizumab in ER+/HER2- advanced breast cancer, had ILC [29], and the synergy between platinum agents and immune checkpoint blockade was suggested in preclinical studies [19]. Though we did not observe a particular pattern of response in lobular breast cancer in the context of GELATO, the trial revealed that most responding patients in fact had TNBC, which emphasized the importance of molecular classification in breast cancer immunotherapy.

In **Chapter 5**, in the context of the BELLINI trial, we demonstrated that early TNBC patients with high tumor-infiltrating lymphocyte levels and high IFNG expression before treatment were more likely to benefit from immune checkpoint blockade. These patients may form an “immune-activated” subgroup that needs to be more deeply characterized in future studies.

6.5. Limitations of the studies presented in the thesis

The studies presented in this thesis have several limitations. In **Chapters 3-5**, we present the data based on clinical trials with relatively small patient numbers per cohort, as these trials are signal-finding, proof-of-concept trials. GELATO, discussed in **Chapter 3**, included 23 patients; subset of the TONIC trial used for the ctDNA analysis in **Chapter 4** was comprised of 30 patients; and cohorts A, B and C of the BELLINI trial presented in **Chapter 5** consisted of 15 patients each. These numbers are substantial for the clinical context. For example, the accrual of GELATO, first trial ever performed that focused on invasive lobular breast cancer, took more than three years. However, for the translational analysis the statistical power of these datasets is limited and the findings need to be validated in larger, independent cohorts.

The trial cohorts in the BELLINI trial presented in **Chapter 5** were not randomized. This allowed the study team to achieve the similar distribution of the clinical and demographic features in the cohorts and to include the same numbers of patients with various levels of TILs in each cohort. However, the non-randomized design of the trial might impact the results of the translational findings. Similarly, patient populations included in the clinical studies discussed in this thesis are heterogeneous by age, molecular characteristics of the tumor, prior treatment, lifestyle and other variables, which also might have an impact on the study results.

In **Chapter 3**, the tumor microenvironment composition was assessed using bulk RNA-Seq, with the presence of specific cell populations and phenotypes estimated using cell deconvolution and previously published immune signatures. While these approaches allowed us to understand the general phenotype of the tumor microenvironment, they lack the single-cell resolution and spatial dimension. The use of single-cell RNA-Seq might have allowed us to uncover smaller cell populations and rarer phenotypes, and the use of spatial omics technologies would have made it possible to analyse the differences in immune composition in different tumor and stromal compartments.

In **Chapter 4**, we worked with shallow whole-genome ctDNA data. Shallow whole-genome sequencing is a cost-effective approach which allows to determine large-scale copy number alterations in ctDNA and track them in time. However, the resulting genome coverage did not allow us to track the copy number alterations in particular genes or loci of interest, which might have shedded more light on the clonal dynamics in the tumors of the patients. Also, the approach we used was not tumor-informed.

In **Chapter 5**, we analysed both bulk and single-cell RNA-Seq for cohorts A and B but only performed bulk RNA-Seq analyses for cohort C due to the manuscript timeline. We also focused only on the T cell compartment in the single-cell RNA-Seq analysis of the cohorts A and B, which limited the amount of insights we could get from the data. Analysis of the other cell populations in the cohorts A and B and of the single-cell RNA-Seq data of the cohort C would be performed in the future and published separately by the members of the Kok group team.

Finally, the tumor microenvironment profiling in **Chapters 3** and **Chapters 5** was performed based on RNA sequencing under the assumption that RNA expression corresponds to the functional state of the cell. This is a widely accepted assumption which is true to a certain degree, as translation and posttranslational modifications also impact the protein abundance and functionality. Combining RNA-Seq with proteomic approaches might have allowed us to test this assumption and describe the functionality of the tumor microenvironment in GELATO and BELLINI in more detail.

6.6. Improving biomarkers in breast cancer

To be useful for clinical practice, biomarkers identified with the use of high-throughput sequencing methods should be easy to evaluate, scalable and cost-effective. They also need to be identified in a reliable manner and tested in independent large cohorts, ideally in the prospective clinical trial setting. It is also beneficial for the biomarkers to be easily interpretable and be linked to the well-understood processes in tumor biology.

The presence of stromal TILs in the tumor biopsy appears to be a promising biomarker that meets several of the criteria listed above. It can be evaluated by a trained pathologist according to the established guidelines, which fits well into the routine clinical practice, and is cost-effective and interpretable. The presence of TILs has been shown to be highly prognostic in early TNBC [10, 30], and a large international OPTIMAL trial is going to investigate whether chemotherapy may be safely omitted in stage I TNBC patients with highest TIL scores [31]. In **Chapter 5**, we also demonstrated that all patients with early TNBC in cohorts A and B of the BELLINI trial who responded to checkpoint blockade treatment had TILs $\geq 30\%$, which motivated the study team to only include patients with TILs $\geq 50\%$ to the cohort C of the trial. This illustrates the important role of TILs as a biomarker of response to immune checkpoint blockade in addition to its role as a prognostic biomarker in early TNBC.

As also discussed in **Chapter 5**, IFNG gene expression levels may also be explored as a promising biomarker for immune checkpoint blockade response in early TNBC. Gene expression of a single gene can be estimated in a timely and cost-effective manner and is easy to interpret, which makes this biomarker attractive for use in the clinic. Also, IFNG activity has been demonstrated to be associated with immune checkpoint blockade response in other cancer types, e.g. in melanoma [32, 33], non-small cell lung cancer [33, 34], gastric cancer and head and neck squamous cell carcinoma [35]. In **Chapter 5**, we demonstrate that early TNBC patients who benefit from immune checkpoint blockade treatment have higher IFNG than non-responders, and that the difference between responders and non-responders in IFNG expression is conserved in the group of patients with high TILs. Of course, this observation would need to be tested in larger independent cohorts.

Using liquid biopsies to track residual disease is also a cost-effective and feasible approach. ctDNA abundance has been shown to be prognostic in metastatic TNBC, and in early TNBC it can be used as a marker of the residual disease [36]. ctDNA has also been shown to be prognostic in TNBC patients having a non-PCR after neoadjuvant systemic therapy [37]. In **Chapters 4** and **5** we showed that ctDNA abundance and copy number alteration profile may be used to predict response to immune checkpoint blockade in TNBC, which should also be explored further in larger studies.

In summary, breast cancer immunotherapy would highly benefit from biomarker-driven prospective clinical trials, and biomarkers that are cost-effective and feasible to use in the clinical practice should be given particular attention.

6.7. Outlook

In this thesis, we made contributions to the field of immuno-oncology in breast cancer. Currently, it becomes clear that immunotherapy has an important place in the breast cancer treatment landscape, even though initially this idea was met with more scepticism than the use of immunotherapy in other malignancies, e.g. melanoma or non-small cell lung cancer. Nevertheless, it is crucial to continue improving immunotherapy outcomes by combining therapeutic agents, selecting appropriate patient populations and using biomarkers, and bioinformatic approaches may help to achieve all these goals.

Routine use of high-throughput sequencing became an integral part of translational research in oncology. In the future, it may also become an

integral part of clinical practice. This would highly raise the amount of information available for personalisation of treatment, but also would require adaptations of the clinical workflows and infrastructure.

Clinical teams would have to become even more interdisciplinary and to include bioinformaticians and data specialists. Hospital infrastructures would need to be adjusted to allow for efficient data collection, processing, storage and biobanking, and many other adjustments will need to be made. Nevertheless, the power of information that would become available after this transition will be enormous. The optimal use of this information, possibly involving artificial intelligence, would hopefully help to reduce the global disease burden of cancer.

References

- [1] G. W. Sledge, E. P. Mamounas, G. N. Hortobagyi, H. J. Burstein, P. J. Goodwin, and A. C. Wolff. "Past, present, and future challenges in breast cancer treatment". *J. Clin. Oncol.* 32.19 (July 2014), pp. 1979–1986.
- [2] V. Masoud and G. Pagès. "Targeted therapies in breast cancer: New challenges to fight against resistance". *World J. Clin. Oncol.* 8.2 (Apr. 2017), pp. 120–134.
- [3] H. R. Ali, E. Provenzano, S.-J. Dawson, F. M. Blows, B. Liu, M. Shah, H. M. Earl, C. J. Poole, L. Hiller, J. A. Dunn, S. J. Bowden, C. Twelves, J. M. S. Bartlett, S. M. A. Mahmoud, E. Rakha, I. O. Ellis, S. Liu, D. Gao, T. O. Nielsen, P. D. P. Pharoah, and C. Caldas. "Association between CD8+ T-cell infiltration and breast cancer survival in 12,439 patients". *Ann. Oncol.* 25.8 (Aug. 2014), pp. 1536–1543.
- [4] R. Barroso-Sousa, E. Jain, O. Cohen, D. Kim, J. Buendia-Buendia, E. Winer, N. Lin, S. M. Tolaney, and N. Wagle. "Prevalence and mutational determinants of high tumor mutation burden in breast cancer". *Ann. Oncol.* 31.3 (Mar. 2020), pp. 387–394.
- [5] P. Schmid, J. Cortes, L. Pusztai, H. McArthur, S. Kümmel, J. Bergh, C. Denkert, Y. H. Park, R. Hui, N. Harbeck, M. Takahashi, T. Foukakis, P. A. Fasching, F. Cardoso, M. Untch, L. Jia, V. Karantza, J. Zhao, G. Aktan, R. Dent, J. O'Shaughnessy, and KEYNOTE-522 Investigators. "Pembrolizumab for early triple-negative breast cancer". *N. Engl. J. Med.* 382.9 (Feb. 2020), pp. 810–821.
- [6] J. Cortes, H. S. Rugo, D. W. Cescon, S.-A. Im, M. M. Yusof, C. Gallardo, O. Lipatov, C. H. Barrios, J. Perez-Garcia, H. Iwata, N. Masuda, M. Torregroza Otero, E. Gokmen, S. Loi, Z. Guo, X. Zhou, V. Karantza, W. Pan, P. Schmid, and KEYNOTE-355 Investigators. "Pembrolizumab plus chemotherapy in advanced triple-negative breast cancer". *N. Engl. J. Med.* 387.3 (July 2022), pp. 217–226.
- [7] P. Schmid, J. Cortes, R. Dent, L. Pusztai, H. McArthur, S. Kümmel, J. Bergh, C. Denkert, Y. H. Park, R. Hui, N. Harbeck, M. Takahashi, M. Untch, P. A. Fasching, F. Cardoso, J. Andersen, D. Patt, M. Danso, M. Ferreira, M.-A. Mouret-Reynier, S.-A. Im, J.-H. Ahn, M. Gion, S. Baron-Hay, J.-F. Boileau, Y. Ding, K. Tryfonidis, G. Aktan, V. Karantza, J. O'Shaughnessy, and KEYNOTE-522 Investigators. "Event-free survival with pembrolizumab in early triple-negative breast cancer". *N. Engl. J. Med.* 386.6 (Feb. 2022), pp. 556–567.
- [8] H. Davies, S. Morganella, C. A. Purdie, S. J. Jang, E. Borgen, H. Russnes, D. Glodzik, X. Zou, A. Viari, A. L. Richardson, A.-L. Børresen-Dale,

- A. Thompson, J. E. Eyfjord, G. Kong, M. R. Stratton, and S. Nik-Zainal. "Whole-genome sequencing reveals breast cancers with mismatch repair deficiency". *Cancer Res.* 77.18 (Sept. 2017), pp. 4755–4762.
- [9] A. Marabelle, D. T. Le, P. A. Ascierto, A. M. Di Giacomo, A. De Jesus-Acosta, J.-P. Delord, R. Geva, M. Gottfried, N. Penel, A. R. Hansen, S. A. Piha-Paul, T. Doi, B. Gao, H. C. Chung, J. Lopez-Martin, Y.-J. Bang, R. S. Frommer, M. Shah, R. Gori, A. K. Joe, S. K. Pruitt, and L. A. Diaz Jr. "Efficacy of pembrolizumab in patients with noncolorectal high microsatellite instability/mismatch repair-deficient cancer: Results from the phase II KEYNOTE-158 study". *J. Clin. Oncol.* 38.1 (Jan. 2020), pp. 1–10.
- [10] V. M. T. de Jong, Y. Wang, N. D. Ter Hoeve, M. Opdam, N. Stathonikos, K. Jóźwiak, M. Hauptmann, S. Cornelissen, W. Vreuls, E. H. Rosenberg, E. A. Koop, Z. Varga, C. H. M. van Deurzen, A. L. Mooyaart, A. Córdoba, E. J. Groen, J. Bart, S. M. Willems, V. Zolota, J. Wesseling, A. Sapino, E. Chmielik, A. Ryska, A. Broeks, A. C. Voogd, S. Loi, S. Michiels, G. S. Sonke, E. van der Wall, S. Siesling, P. J. van Diest, M. K. Schmidt, M. Kok, G. M. H. E. Dackus, R. Salgado, and S. C. Linn. "Prognostic value of stromal tumor-infiltrating lymphocytes in young, node-negative, triple-negative breast cancer patients who did not receive (neo)adjuvant systemic therapy". *J. Clin. Oncol.* 40.21 (July 2022), pp. 2361–2374.
- [11] S. Loi, R. Salgado, S. Adams, G. Pruneri, P. A. Francis, M. Lacroix-Triki, H. Joensuu, M. V. Dieci, S. Badve, S. Demaria, R. Gray, E. Munzone, D. Drubay, J. Lemonnier, C. Sotiriou, P. L. Kellokumpu-Lehtinen, A. Vingiani, K. Gray, F. André, C. Denkert, M. Piccart, E. Roblin, and S. Michiels. "Tumor infiltrating lymphocyte stratification of prognostic staging of early-stage triple negative breast cancer". *NPJ Breast Cancer* 8.1 (Jan. 2022), p. 3.
- [12] S. Loi, R. Salgado, P. Schmid, J. Cortes, D. W. Cescon, E. P. Winer, D. L. Toppmeyer, H. S. Rugo, M. De Laurentiis, R. Nanda, H. Iwata, A. Awada, A. R. Tan, Y. Sun, V. Karantza, A. Wang, L. Huang, A. Saadatpour, R. Cristescu, J. Yearley, J. Lunceford, P. Jelinic, and S. Adams. "Association between biomarkers and clinical outcomes of pembrolizumab monotherapy in patients with metastatic triple-negative breast cancer: KEYNOTE-086 exploratory analysis". *JCO Precis. Oncol.* 7 (Apr. 2023), e2200317.
- [13] L. Voorwerk, M. Slagter, H. M. Horlings, K. Sikorska, K. K. van de Vijver, M. de Maaker, I. Nederlof, R. J. C. Kluin, S. Warren, S. Ong, T. G. Wiersma, N. S. Russell, F. Lalezari, P. C. Schouten, N. A. M. Bakker, S. L. C. Ketelaars, D. Peters, C. A. H. Lange, E. van Werkhoven, H. van Tinteren, I. A. M. Mandjes, I. Kemper, S. Onderwater, M. Chalabi, S. Wilgenhof, J. B. A. G. Haanen, R. Salgado, K. E. de Visser, G. S. Sonke, L. F. A. Wessels, S. C. Linn, T. N. Schumacher, C. U. Blank, and M. Kok. "Immune induction strategies in metastatic triple-negative breast cancer to enhance the sensitivity to PD-1 blockade: the TONIC trial". *Nat. Med.* 25.6 (June 2019), pp. 920–928.
- [14] L. A. Emens, L. Molinero, S. Loi, H. S. Rugo, A. Schneeweiss, V. Diéras, H. Iwata, C. H. Barrios, M. Nechaeva, A. Nguyen-Duc, S. Y. Chui, A. Husain, E. P. Winer, S. Adams, and P. Schmid. "Atezolizumab and

- nab-paclitaxel in advanced triple-negative breast cancer: Biomarker evaluation of the IMpassion130 study". *J. Natl. Cancer Inst.* 113.8 (Aug. 2021), pp. 1005–1016.
- [15] B. Virassamy, F. Caramia, P. Savas, S. Sant, J. Wang, S. N. Christo, A. Byrne, K. Clarke, E. Brown, Z. L. Teo, B. von Scheidt, D. Freestone, L. C. Gandolfo, K. Weber, J. Teply-Szymanski, R. Li, S. J. Luen, C. Denkert, S. Loibl, O. Lucas, C. Swanton, T. P. Speed, P. K. Darcy, P. J. Neeson, L. K. Mackay, and S. Loi. "Intratumoral CD8+ T cells with a tissue-resident memory phenotype mediate local immunity and immune checkpoint responses in breast cancer". *Cancer Cell* 41.3 (Mar. 2023), 585–601.e8.
- [16] C. E. Gustafson, R. Jadhav, W. Cao, Q. Qi, M. Pegram, L. Tian, C. M. Weyand, and J. J. Goronzy. "Immune cell repertoires in breast cancer patients after adjuvant chemotherapy". *JCI Insight* 5.4 (Feb. 2020).
- [17] R. Rotolo, V. Leuci, C. Donini, F. Galvagno, A. Massa, M. C. De Santis, S. Peirone, G. Medico, M. Sanlorenzo, I. Vujic, L. Gammaitoni, M. Basirico, L. Righi, C. Riganti, I. C. Salaroglio, F. Napoli, F. Tabbò, A. Mariniello, E. Vigna, C. Modica, L. D'Ambrosio, G. Grignani, R. Taulli, E. Hirsch, M. Cereda, M. Aglietta, G. V. Scagliotti, S. Novello, P. Bironzo, and D. Sangiolo. "Novel lymphocyte-independent antitumor activity by PD-1 blocking antibody against PD-1+ chemoresistant lung cancer cells". *Clin. Cancer Res.* 29.3 (Feb. 2023), pp. 621–634.
- [18] L. Schadt, C. Sparano, N. A. Schweiger, K. Silina, V. Cecconi, G. Lucchiari, H. Yagita, E. Guggisberg, S. Saba, Z. Nascakova, W. Barchet, and M. van den Broek. "Cancer-cell-intrinsic cGAS expression mediates tumor immunogenicity". *Cell Rep.* 29.5 (Oct. 2019), 1236–1248.e7.
- [19] O. S. Blomberg, L. Spagnuolo, H. Garner, L. Voorwerk, O. I. Isaeva, E. van Dyk, N. Bakker, M. Chalabi, C. Klaver, M. Duijst, K. Kersten, M. Brüggemann, D. Pastoors, C.-S. Hau, K. Vrijland, E. A. M. Raeven, D. Kaldenbach, K. Kos, I. S. Afonina, P. Kaptein, L. Hoes, W. S. M. E. Theelen, P. Baas, E. E. Voest, R. Beyaert, D. S. Thommen, L. F. A. Wessels, K. E. de Visser, and M. Kok. "IL-5-producing CD4+ T cells and eosinophils cooperate to enhance response to immune checkpoint blockade in breast cancer". *Cancer Cell* 41.1 (Jan. 2023), 106–123.e10.
- [20] O. Yersal and S. Barutca. "Biological subtypes of breast cancer: Prognostic and therapeutic implications". *World J. Clin. Oncol.* 5.3 (Aug. 2014), pp. 412–424.
- [21] J. Makki. "Diversity of breast carcinoma: Histological subtypes and clinical relevance". *Clin. Med. Insights Pathol.* 8 (Dec. 2015), pp. 23–31.
- [22] B. D. Lehmann, J. A. Bauer, X. Chen, M. E. Sanders, A. B. Chakravarthy, Y. Shyr, and J. A. Pietersen. "Identification of human triple-negative breast cancer subtypes and preclinical models for selection of targeted therapies". *J. Clin. Invest.* 121.7 (July 2011), pp. 2750–2767.
- [23] M. D. Burstein, A. Tsimelzon, G. M. Poage, K. R. Covington, A. Contreras, S. A. W. Fuqua, M. I. Savage, C. K. Osborne, S. G. Hilsenbeck, J. C. Chang, G. B. Mills, C. C. Lau, and P. H. Brown. "Comprehensive genomic analysis

- identifies novel subtypes and targets of triple-negative breast cancer". *Clin. Cancer Res.* 21.7 (Apr. 2015), pp. 1688–1698.
- [24] D.-Y. Wang, Z. Jiang, Y. Ben-David, J. R. Woodgett, and E. Zacksenhaus. "Molecular stratification within triple-negative breast cancer subtypes". *Sci. Rep.* 9.1 (Dec. 2019), p. 19107.
- [25] Y.-Z. Jiang, D. Ma, C. Suo, J. Shi, M. Xue, X. Hu, Y. Xiao, K.-D. Yu, Y.-R. Liu, Y. Yu, Y. Zheng, X. Li, C. Zhang, P. Hu, J. Zhang, Q. Hua, J. Zhang, W. Hou, L. Ren, D. Bao, B. Li, J. Yang, L. Yao, W.-J. Zuo, S. Zhao, Y. Gong, Y.-X. Ren, Y.-X. Zhao, Y.-S. Yang, Z. Niu, Z.-G. Cao, D. G. Stover, C. Verschraegen, V. Kaklamani, A. Daemen, J. R. Benson, K. Takabe, F. Bai, D.-Q. Li, P. Wang, L. Shi, W. Huang, and Z.-M. Shao. "Genomic and transcriptomic landscape of triple-negative breast cancers: Subtypes and treatment strategies". *Cancer Cell* 35.3 (Mar. 2019), 428–440.e5.
- [26] Y.-R. Liu, Y.-Z. Jiang, X.-E. Xu, K.-D. Yu, X. Jin, X. Hu, W.-J. Zuo, S. Hao, J. Wu, G.-Y. Liu, G.-H. Di, D.-Q. Li, X.-H. He, W.-G. Hu, and Z.-M. Shao. "Comprehensive transcriptome analysis identifies novel molecular subtypes and subtype-specific RNAs of triple-negative breast cancer". *Breast Cancer Res.* 18.1 (Mar. 2016), p. 33.
- [27] A. Bagaev, N. Kotlov, K. Nomie, V. Svekolkina, A. Gafurov, O. Isaeva, N. Osokin, I. Kozlov, F. Frenkel, O. Gancharova, N. Almog, M. Tsiper, R. Ataulkhanov, and N. Fowler. "Conserved pan-cancer microenvironment subtypes predict response to immunotherapy". *Cancer Cell* 39.6 (June 2021), 845–865.e7.
- [28] F. Sanchez-Vega, M. Mina, J. Armenia, W. K. Chatila, A. Luna, K. C. La, S. Dimitriadou, D. L. Liu, H. S. Kantheti, S. Saghafein, D. Chakravarty, F. Daian, Q. Gao, M. H. Bailey, W.-W. Liang, S. M. Foltz, I. Shmulevich, L. Ding, Z. Heins, A. Ochoa, B. Gross, J. Gao, H. Zhang, R. Kundra, C. Kandoth, I. Bahceci, L. Dervishi, U. Dogrusoz, W. Zhou, H. Shen, P. W. Laird, G. P. Way, C. S. Greene, H. Liang, Y. Xiao, C. Wang, A. Iavarone, A. H. Berger, T. G. Bivona, A. J. Lazar, G. D. Hammer, T. Giordano, L. N. Kwong, G. McArthur, C. Huang, A. D. Tward, M. J. Frederick, F. McCormick, M. Meyerson, Cancer Genome Atlas Research Network, E. M. Van Allen, A. D. Cherniack, G. Ciriello, C. Sander, and N. Schultz. "Oncogenic signaling pathways in The Cancer Genome Atlas". *Cell* 173.2 (Apr. 2018), 321–337.e10.
- [29] H. S. Rugo, J.-P. Delord, S.-A. Im, P. A. Ott, S. A. Piha-Paul, P. L. Bedard, J. Sachdev, C. L. Tourneau, E. M. J. van Brummelen, A. Varga, R. Salgado, S. Loi, S. Saraf, D. Pietrangelo, V. Karantza, and A. R. Tan. "Safety and antitumor activity of pembrolizumab in patients with estrogen receptor-positive/human epidermal growth factor receptor 2-negative advanced breast cancer". *Clin. Cancer Res.* 24.12 (June 2018), pp. 2804–2811.
- [30] R. A. Leon-Ferre, S. F. Jonas, R. Salgado, S. Loi, V. de Jong, J. M. Carter, T. O. Nielsen, S. Leung, N. Riaz, S. Chia, G. Jules-Clément, G. Curigliano, C. Criscitiello, V. Cckenpot, M. Lambertini, V. J. Suman, B. Linderholm, J. W. M. Martens, C. H. M. van Deurzen, A. M. Timmermans, T. Shimoi, S. Yazaki, M. Yoshida, S.-B. Kim, H. J. Lee, M. V. Dieci, G. Bataillon,

- A. Vincent-Salomon, F. André, M. Kok, S. C. Linn, M. P. Goetz, S. Michiels, and International Immuno-Oncology Biomarker Working Group. "Tumor-infiltrating lymphocytes in triple-negative breast cancer". *JAMA* 331.13 (Apr. 2024), pp. 1135–1144.
- [31] *OPTImaL: Optimisation of treatment for patients with low stage triple-negative breast cancer with high sTIL*. <https://onderzoekmetmensen.nl/en/trial/57045>.
- [32] J. M. Versluis, S. A. Blankenstein, P. Dimitriadis, J. S. Wilmott, R. Elens, W. A. M. Blokk, W. van Houdt, A. M. Menzies, Y. M. Schrage, M. W. J. M. Wouters, J. Sanders, A. Broeks, R. A. Scolyer, K. P. M. Suijkerbuijk, G. V. Long, A. C. J. van Akkooi, and C. U. Blank. "Interferon-gamma signature as prognostic and predictive marker in macroscopic stage III melanoma". *J. Immunother. Cancer* 12.4 (Apr. 2024).
- [33] N. Karachaliou, M. Gonzalez-Cao, G. Crespo, A. Drozdowskyj, E. Aldeguer, A. Gimenez-Capitan, C. Teixido, M. A. Molina-Vila, S. Viteri, M. De Los Llanos Gil, S. M. Algarra, E. Perez-Ruiz, I. Marquez-Rodas, D. Rodriguez-Abreu, R. Blanco, T. Puertolas, M. A. Royo, and R. Rosell. "Interferon gamma, an important marker of response to immune checkpoint blockade in non-small cell lung cancer and melanoma patients". *Ther. Adv. Med. Oncol.* 10 (Jan. 2018), p. 1758834017749748.
- [34] T. Kanai, H. Suzuki, H. Yoshida, A. Matsushita, H. Kawasumi, Y. Samejima, Y. Noda, S. Nasu, A. Tanaka, N. Morishita, S. Hashimoto, K. Kawahara, Y. Tamura, N. Okamoto, T. Tanaka, and T. Hirashima. "Significance of quantitative interferon-gamma levels in non-small-cell lung cancer patients' response to immune checkpoint inhibitors". *Anticancer Res.* 40.5 (May 2020), pp. 2787–2793.
- [35] M. Ayers, J. Lunceford, M. Nebozhyn, E. Murphy, A. Loboda, D. R. Kaufman, A. Albright, J. D. Cheng, S. P. Kang, V. Shankaran, S. A. Piha-Paul, J. Yearley, T. Y. Seiwert, A. Ribas, and T. K. McClanahan. "IFN- γ -related mRNA profile predicts clinical response to PD-1 blockade". *J. Clin. Invest.* 127.8 (Aug. 2017), pp. 2930–2940.
- [36] R. Mazzeo, J. Sears, L. Palmero, S. Bolzonello, A. A. Davis, L. Gerratana, and F. Puglisi. "Liquid biopsy in triple-negative breast cancer: unlocking the potential of precision oncology". *ESMO Open* 9.10 (Oct. 2024), p. 103700.
- [37] S. R. Stecklein, B. F. Kimler, R. Yoder, K. Schwensen, J. M. Staley, Q. J. Khan, A. P. O'Dea, L. E. Nye, M. Elia, J. Heldstab, T. Home, S. Hyter, K. Isakova, H. B. Pathak, A. K. Godwin, and P. Sharma. "ctDNA and residual cancer burden are prognostic in triple-negative breast cancer patients with residual disease". *NPJ Breast Cancer* 9.1 (Mar. 2023), p. 10.

Curriculum Vitæ

Olga Igorevna Isaeva was born on December 31, 1992 in Khimki, Moscow region, Russia. She started studying biology and conducting research projects in 2004 while attending a scientific summer camp, 'Summer Ecology School'. In 2006, she was admitted to a specialized boarding school, "Intellectual", where she fulfilled the requirements both for the biology & chemistry and the humanities tracks upon graduation. She was a winner of multiple national and international competitions for high school students in biology and chemistry and research project competitions.

In 2012, Olga was accepted to the Faculty of Biology of the Lomonosov Moscow State University without entrance exams as a winner of a national competition in biology. She specialized in Cell Biology and received her BSc in Biology in 2016 with a GPA of 4.4/5. Her BSc thesis work focusing on the role of PHF10 in cell cycle and proliferation was performed at the N.N.Blokhin Russian Cancer Research Center under the supervision of Dr. Viktor Tatarskii.

Throughout her studies, Olga worked as a private tutor in biology and chemistry, organized competitions in biology for high school students, and was a lab assistant helping with administrative tasks. In 2017, she received a Master I degree in History from the Collège universitaire français de Moscou, a French-taught MSc program, for a thesis on early soviet TV series pursued as a hobby.

In 2016-2019, Olga worked as a lead immunologist for BostonGene, a tumor immunology start-up company. She managed a team of two people and developed a core product of the company, a Tumor Portrait™ test (US patent 11984200).

In 2017-2019, Olga followed an English-taught MSc program in Life Sciences at Skolkovo Institute of Science and Technology with a specialization in Bioinformatics which she finished in 2019 with a GPA of 5/5. She wrote her MSc thesis, "Influence of immunotherapy and prognostic significance of lymphocyte subsets in tumor microenvironment" under the supervision of Dr. Dmitry Chudakov. In 2019, Olga won a travel grant that allowed her to do an MSc internship in the laboratory of Dr. Alexander Rudensky at Memorial Sloan Kettering Cancer Center where she worked on Treg phenotypes in various settings.

In September 2019, Olga started as a computational tumor immunology PhD student in the laboratories of Dr. Pia Kvistborg and Dr. Marleen Kok at the Netherlands Cancer Institute under co-supervision of Dr. Lodewyk Wessels. She was a part of the institute Diversity, Equity, and Inclusion committee. After Dr. Kvistborg left the institute in 2022, Olga continued her PhD in the laboratory of Dr. Kok. During her PhD, Olga participated in > 30 research projects and co-authored 14 publications.

List of Publications

Included in this thesis:

1. **O. I. Isaeva**[#], S. L. C. Ketelaars[#], and P. Kvistborg. “In silico analysis predicts a limited impact of SARS-CoV-2 variants on CD8 T cell recognition”. *Front. Immunol.* 13 (Apr. 2022), p. 891524
2. L. Voorwerk^{*}, **O. I. Isaeva**^{*}, H. M. Horlings, S. Balduzzi, M. Chelushkin, N. A. M. Bakker, E. Champanhet, H. Garner, K. Sikorska, C. E. Loo, I. Kemper, I. A. M. Mandjes, M. de Maaker, J. J. L. van Geel, J. Boers, M. de Boer, R. Salgado, M. G. J. van Dongen, G. S. Sonke, K. E. de Visser, T. N. Schumacher, C. U. Blank, L. F. A. Wessels, A. Jager, V. C. G. Tjan-Heijnen, C. P. Schröder, S. C. Linn, and M. Kok. “PD-L1 blockade in combination with carboplatin as immune induction in metastatic lobular breast cancer: the GELATO trial”. *Nat. Cancer* 4.4 (Apr. 2023), pp. 535–549
3. A. Y. Lin^{*}, **O. I. Isaeva**^{*}, T. Deger, V. C. M. Geurts, D. C. L. Vessies, L. Voorwerk, M. Slagter, K. Moore, P. Van Der Leest, L. F. A. Wessels, J. Martens, D. Van Den Broek, and M. Kok. “ctDNA-based copy number dynamics during anti-PD-1 treatment in metastatic triple negative breast cancer”. *Cell Reports Medicine*, accepted for publication. (2025)
4. I. Nederlof^{*}, **O. I. Isaeva**^{*}, M. de Graaf^{**}, R. C. A. M. Gielen^{**}, N. A. M. Bakker^{**}, A. L. Rolfes, H. Garner, B. Boeckx, J. J. H. Traets, I. A. M. Mandjes, M. de Maaker, T. van Brussel, M. Chelushkin, E. Champanhet, M. Lopez-Yurda, K. van de Vijver, J. G. van den Berg, I. Hofland, N. Klioueva, R. M. Mann, C. E. Loo, F. H. van Duijnhoven, V. Skinner, S. Luykx, E. Kerver, E. Kalashnikova, M. G. J. van Dongen, G. S. Sonke, S. C. Linn, C. U. Blank, K. E. de Visser, R. Salgado, L. F. A. Wessels, C. A. Drukker, T. N. Schumacher, H. M. Horlings, D. Lambrechts, and M. Kok. “Neoadjuvant nivolumab or nivolumab plus ipilimumab in early-stage triple-negative breast cancer: a phase 2 adaptive trial”. *Nat. Med.* 30.11 (Nov. 2024), pp. 3223–3235

Other works:

1. **O. I. Isaeva**, G. V. Sharonov, E. O. Serebrovskaya, M. A. Turchaninova, A. R. Zaretsky, M. Shugay, and D. M. Chudakov. “Intratumoral immunoglobulin isotypes predict survival in lung adenocarcinoma subtypes”. *J. Immunother. Cancer* 7.1 (Oct. 2019), p. 279
2. V. C. M. Geurts^{*}, **O. I. Isaeva**^{*}, M. De Graaf^{**}, M. Chelushkin^{**}, K. Moore, L. Voorwerk, I. Nederlof, M. De Maaker, S. Balduzzi, N. Abbott, K. K. Van De Vijver, I. Kemper, R. Salgado, H. M. Horlings, T. N. Schumacher, L. F. A. Wessels, and M. Kok. *Dissecting immunomodulatory capacity of low dose doxorubicin or cisplatin to enhance sensitivity to anti*. Manuscript in prepa-

ration.

3. A. Gangaev*, S. L. C. Ketelaars*, **O. I. Isaeva**, S. Patiwaal, A. Dopler, K. Hoefakker, S. De Biasi, L. Gibellini, C. Mussini, G. Guaraldi, M. Girardis, C. M. P. T. Ormeno, P. J. M. Hekking, N. M. Lardy, M. Toebes, R. Balderas, T. N. Schumacher, H. Ovaa, A. Cossarizza, and P. Kvistborg. "Identification and characterization of a SARS-CoV-2 specific CD8+ T cell response with immunodominant features". *Nat. Commun.* 12.1 (May 2021), p. 2593
4. A. Gangaev, E. A. Rozeman*, M. W. Rohaan*, D. **O. I. Isaeva*** and Philips, S. Patiwaal, J. H. van den Berg, A. Ribas, D. Schadendorf, B. Schilling, T. N. Schumacher, C. U. Blank, J. B. A. G. Haanen, and P. Kvistborg. "Differential effects of PD-1 and CTLA-4 blockade on the melanoma-reactive CD8 T cell response". *Proc. Natl. Acad. Sci. U. S. A.* 118.43 (Oct. 2021)
5. O. S. Blomberg*, L. Spagnuolo*, H. Garner*, L. Voorwerk*, **O. I. Isaeva****, E. van Dyk**, N. Bakker**, M. Chalabi, C. Klaver, M. Duijst, K. Kersten, M. Brüggemann, D. Pastoors, C.-S. Hau, K. Vrijland, E. A. M. Raeven, D. Kaldenbach, K. Kos, I. S. Afonina, P. Kaptein, L. Hoes, W. S. M. E. Theelen, P. Baas, E. E. Voest, R. Beyaert, D. S. Thommen, L. F. A. Wessels, K. E. de Visser, and M. Kok. "IL-5-producing CD4+ T cells and eosinophils cooperate to enhance response to immune checkpoint blockade in breast cancer". *Cancer Cell* 41.1 (Jan. 2023), 106–123.e10
6. O. S. Blomberg*, K. Kos*, L. Spagnuolo*, **O. I. Isaeva**, H. Garner, M. D. Wellenstein, N. Bakker, D. E. M. Duits, K. Kersten, S. Klarenbeek, C.-S. Hau, D. Kaldenbach, E. A. M. Raeven, K. Vrijland, M. Kok***, and K. E. de Visser***. "Neoadjuvant immune checkpoint blockade triggers persistent and systemic Treg activation which blunts therapeutic efficacy against metastatic spread of breast tumors". *Oncoimmunology* 12.1 (Apr. 2023), p. 2201147
7. O. Zolotareva, S. Khakabimamaghani, **O. I. Isaeva**, Z. Chervontseva, A. Savchik, and M. Ester. "Identification of differentially expressed gene modules in heterogeneous diseases". *Bioinformatics* 37.12 (July 2021), pp. 1691–1698
8. C. Campbell, P. T. McKenney, D. Konstantinovskiy, **O.I. Isaeva**, M. Schizas, J. Verter, C. Mai, W.-B. Jin, C.-J. Guo, S. Violante, R. J. Ramos, J. R. Cross, K. Kadaveru, J. Hambor, and A. Y. Rudensky. "Bacterial metabolism of bile acids promotes generation of peripheral regulatory T cells". *Nature* 581.7809 (May 2020), pp. 475–479
9. A. Bagaev, N. Kotlov, K. Nomie, V. Svekolkin, A. Gafurov, **O. I. Isaeva**, N. Osokin, I. Kozlov, F. Frenkel, O. Gancharova, N. Almog, M. Tsiper, R. Ataullakhanov, and N. Fowler. "Conserved pan-cancer microenvironment subtypes predict response to immunotherapy". *Cancer Cell* 39.6 (June 2021), 845–865.e7
10. A. Bagaev, F. Frenkel, N. Kotlov, R. Ataullakhanov, and **O. Isaeva**. "Systems and methods for generating, visualizing and classifying molecular functional profiles." Patent US11984200 (US). 2024
11. M. Hartung, A. Maier, F. Delgado-Chaves, Y. Burankova, **O. I. Isaeva**, F. M.

de Sá Patroni, D. He, C. Shannon, K. Kaufmann, J. Lohmann, A. Savchik, A. Hartebrodt, Z. Chervontseva, F. Firoozbakht, N. Probul, E. Zotova, O. Tsoy, D. B. Blumenthal, M. Ester, T. Laske, J. Baumbach^{***}, and O. Zolotareva^{**}. *UnPaSt: unsupervised patient stratification by differentially expressed bi-clusters in omics data*. 2024. arXiv: 2408.00200. url: <https://arxiv.org/abs/2408.00200>

12. D. Hammerl, J. W. M. Martens, M. Timmermans, M. Smid, A. M. Trapman-Jansen, R. Foekens, **O. I. Isaeva**, L. Voorwerk, H. E. Balcioglu, R. Wijers, I. Nederlof, R. Salgado, H. Horlings, M. Kok, and R. Debets. "Spatial immunophenotypes predict response to anti-PD1 treatment and capture distinct paths of T cell evasion in triple negative breast cancer". *Nat. Commun.* 12.1 (Sept. 2021), p. 5668
13. A. Dopler, F. Alkan, Y. Malka, R. van der Kammen, K. Hoefakker, D. Taranto, N. Kocabay, I. Mimpfen, C. Ramirez, E. Malzer, **O. I. Isaeva**, M. Kerkhoff, A. Gangaev, J. Silva, S. Ramalho, L. Hoekman, M. Altelaar, R. Beijersbergen, L. Akkari, J. W. Yewdell, P. Kvistborg, and W. J. Faller. "P-stalk ribosomes act as master regulators of cytokine-mediated processes". *Cell* 187.24 (Nov. 2024), 6981–6993.e23
14. Y. Wang, G. M. H. E. Dackus, E. H. Rosenberg, S. Cornelissen, L. W. de Boo, A. Broeks, W. Brugman, T. W. S. Chan, P. J. van Diest, M. Hauptmann, N. D. Ter Hoeve, **O. I. Isaeva**, V. M. T. de Jong, K. Jóźwiak, R. J. C. Kluin, M. Kok, E. Koop, P. M. Nederlof, M. Opdam, P. C. Schouten, S. Siesling, C. van Steenis, A. C. Voogd, W. Vreuls, R. F. Salgado, S. C. Linn, and M. K. Schmidt. "Long-term outcomes of young, node-negative, chemotherapy-naïve, triple-negative breast cancer patients according to BRCA1 status". *BMC Med.* 22.1 (Jan. 2024), p. 9

These authors contributed equally as co-shared first authors and are listed in alphabetical order.

* These authors contributed equally, co-shared first authors.

** These authors contributed equally, co-shared second authors.

*** These authors contributed equally, co-corresponding authors.

Acknowledgements

This thesis brings me a Doctor of Philosophy title, which confirms my skills as a scientist. Many wonderful people helped me to become a scientist in the last twenty years, and I am deeply grateful for their help, support and presence in my life. I cannot acknowledge every one here personally, as it would be hundreds of people, but I cherish everyone in my heart.

I would like to thank my thesis committee members for taking the time to evaluate my thesis. I am also grateful to my supervisors, Lodewyk Wessels, Marleen Kok and Pia Kvistborg. Thank you for your clear vision, your brilliant scientific thinking and your desire to help and approachability.

I would like to thank all my colleagues from the Wessels, Kok and Kvistborg groups at the NKI, as well as all my collaborators from other groups. Thank you for being great teammates and always being available for a chat or a work discussion. To all other colleagues from B3, B6, B7 and other departments, thank you for creating a great scientific atmosphere, for all discussions, feedback and ideas.

I would also like to thank all my previous teachers, instructors and research advisors. You always believed in me and perceived me as a scientist, and all the knowledge I have received from you is what forms me today. I am forever grateful to you.

To my friends and people who had been my friends through the years, thank you for making my life fuller and brighter and for all the inspiration you brought me. You helped me on the dark days and celebrated with me on the good days. Even when we were not in touch, your support made me stronger. I appreciate it so much.

To everyone in the Armed Forces of Ukraine, thank you for your service and sacrifice. I think of you every day. For everyone who volunteers or donates for Ukraine, thank you for your contributions. The victory is closer with each small step.

To all my family, thank you for your support. You thought of me as a scientist since I was a kid and helped me along the way.

Uncle Sasha, thank you for your trust and all your help. It is a privilege to become a member of your family.

Aunt Natasha, thank you for your kindness and openness. You are an ex-

ample of a beautiful and energetic woman that I would like to be. Thank you for being there for me.

To my father, Igor Isaev, thank you for being there for me. It's so sad that you did not live to see me defend my thesis. I know you would be proud. I miss you.

To my mother, Elena Fadeeva, thank you for always trying to develop me intellectually and loving me unconditionally.

To my husband, Serhii Volosheniuk, thank you for always being there for me. I am so grateful to share my life with you. It was very special to live through our PhD journeys together; thank you for moving to the Netherlands and making it possible. You always support and protect me, and it changes my life every day. I love you.

To Shchek, I am so glad to share a part of my PhD journey with you. I will tell you all about it one day.

And of course to my bunnies Quentin, Gertrud, Taras, Alaya, Rosa, Agatha, Hidde, Fedya, Tasya and Petunia. Thank you for sharing your lives with me. I know you could not care less that I am a scientist, but you still accept and love me even if your meals are delayed due to my work. Thank you for this understanding and for reminding me that life is more than work.

